Aus dem CharitéCentrum für Herz-, Kreislauf- und Gefäßmedizin
Klinik für Kardiologie und Angiologie
Direktor: Prof. Dr. Karl Stangl

Habilitationsschrift

G_q/G_{11}- und G_{12}/G_{13}-Protein-vermittelte Signaltransduktion im Kontext kardiovaskulärer Erkrankungsprozesse

zur Erlangung der Lehrbefähigung
für das Fach Innere Medizin

vorgelegt dem Fakultätsrat der Medizinischen Fakultät
Charité - Universitätsmedizin Berlin

von

Dr. med. Till Peter Friedrich Althoff

Eingereicht: August 2020

Dekan: Prof. Dr. med. Axel R. Pries

1. Gutachter/in: Prof. Dr. med. Stephanie Dimmeler

2. Gutachter/in: Prof. Dr. med. Thomas Eschenhagen

Inhalt

Abkürzungsverzeichnis

GPCR	G-Protein-gekoppelter Rezeptor
AT1	Angiotensin II-Rezeptor Typ 1
ET	Endothelin-1-Rezeptor
IP3	Inositol-1,4,5-Tris-Phosphat
RhoGEF	Rho-Guanin-Nukleotid-Austausch-Faktor
LARG	leukaemia-associated RhoGEF
RGS-Proteine	Regulatoren der G-Protein-vermittelten Signaltransduktion
GRK	GPCR-Kinase
MLC	Myosin-Leichtketten
MLCK	MLC-Kinase
MLCP	MLC-Phosphatase

1 Einleitung

1.1 G-Protein-gekoppelte Rezeptoren in der kardiovaskulären Pharmakotherapie

Kardiovaskuläre Erkrankungen sind nach wie vor die führende Todesursache in Europa (Nichols, Townsend, Scarborough, & Rayner, 2014). Ein Großteil der verfügbaren Pharmako-Therapien von Bluthochdruck, Koronarer Herzerkrankung, Herzinsuffizienz oder pulmonaler Hypertonie greift an G-Protein-gekoppelten Rezeptoren (GPCRs) an. Dabei bieten diese Membran-ständigen GPCRs als pharmakologische Zielstrukturen zahlreiche Vorteile, beispielsweise gegenüber intrazellulären Molekülen. Insbesondere die Gewebe- und Kontext-spezifische Expression der GPCRs sowie die lokale und temporale Regulation ihrer endogenen Liganden, ermöglichen spezifischere pharmakologische Interventionen mit höherer Effektivität bei geringeren Nebenwirkungen. Diese Vorteile mögen den anhaltenden Erfolg klassischer GPCR-Agonisten und –Antagonisten erklären, die nach wie vor über 30 Prozent aller zugelassenen Medikamente sowie einen erheblichen Anteil der Neuentwicklungen ausmachen (Garland, 2013).

Einige der erfolgreichsten kardiovaskulären Therapien wirken über eine direkte oder indirekte Inhibition von GPCRs wie dem Angiotensin II-Rezeptor Typ 1 (AT1-Antagonisten und ACE-Hemmer), dem Endothelin-1-Rezeptor (Endothelin-Rezeptor-Antagonisten) oder dem Thromboxan-Rezeptor (Acetylsalicylsäure). Diese und andere kardiovaskuläre Rezeptoren haben gemein, dass sie dual an G-Proteine der Familien G_q/G_{11} und G_{12}/G_{13} koppeln (Galie et al., 2009; Schiffrin, 2002; Schmieder, 2005). Die entsprechend aktivierten G_q/G_{11}- und G_{12}/G_{13}-abhängigen Signalwege und Ihre Rolle im Rahmen kardiovaskulärer Erkrankungen und deren Therapie stellen den Fokus dieser Arbeit dar.

1.2 Heterotrimere G-Proteine

1.2.1 Hintergrund

Die Kommunikation zwischen Zellen und deren Wahrnehmung bzw. Verarbeitung extrazellulärer Signale (Signaltransduktion) basiert in aller Regel auf zwei Komponenten; einem Rezeptor, der den extrazellulären Stimulus wahrnimmt und einen Effektor-Signalweg, der durch den Rezeptor aktiviert wird. G-Protein-gekoppelte Rezeptoren stellen ein weit verbreitetes Signaltransduktionssystem dar, bestehend aus dem genannten Rezeptor (GPCR) und einem heterotrimeren G-Protein als Effektor. Dabei können heterotrimere G-Proteine sowohl durch unterschiedliche GPCRs aktiviert werden als auch ihrerseits eine Vielzahl nachgeschalteter Effektoren und entsprechender Signalwege induzieren.(Wettschureck & Offermanns, 2005).

1.2.2 Grundlegende Prinzipien der G-Protein-vermittelten Signaltransduktion

Als Reaktion auf die Aktivierung eines GPCR, etwa durch Bindung dessen endogener Liganden, wird die Kopplung des Rezeptors mit heterotrimeren G-Proteinen induziert. Heterotrimere G-Proteine bestehen aus einer GTP-hydrolysierenden α-Untereinheit sowie einer β- und einer γ-Unterheit. Wie in Kapitel 1.2.3 erläutert gibt es zahlreiche unterschiedliche Isoformen von α-, β- und γ-Unterheiten.

Die Aktivierung und Inaktivierung von G-Proteinen basiert auf der Bindung von GDP bzw. GTP an der α-Untereinheit. So begünstigt die Rekrutierung des Heterotrimers aus βγ-Komplex und der GDP-gebundenen α-Untereinheit durch einen aktivierten Rezeptor den Austausch von GDP für GTP an der α-Untereinheit und damit dessen Aktivierung. Daraufhin dissoziiert die GTP-gebundene α-Untereinheit vom aktivierten Rezeptor und dem βγ-Komplex. So können sowohl die α-Untereinheit als auch der βγ-Komplex unabhängig voneinander Effektoren rekrutieren und entsprechende Signalwege aktivieren. Diese G-Protein-vermittelte Signaltransduktion wird durch die Hydrolyse von GTP zu GDP durch die intrinsische GTPase-Aktivität der α-Untereinheit beendet und ist folglich selbstlimitierend. Die inaktivierte GDP-gebundene α-Untereinheit bildet mit dem βγ-Komplex wieder ein Heterotrimer – bis es zur erneuten Rekrutierung durch einen aktivierten Rezeptor kommt (Worzfeld, Wettschureck, & Offermanns, 2008).

1.2.3 G-Protein-Familien

Die funktionelle Einteilung der G-Proteine in unterschiedliche Familien basiert auf den spezifischen Isoformen ihrer α-Untereinheiten. Anhand dieser Isoformen definieren sich die G-Protein-Familien G_s ($G\alpha_s$), G_i/G_o ($G\alpha_i$ u. $G\alpha_o$), G_q/G_{11} ($G\alpha_q$ u. $G\alpha_{11}$) und G_{12}/G_{13} ($G\alpha_{12}$ u. $G\alpha_{13}$). Die unterschiedlichen Isoformen einer G-Protein-Familie haben mitunter sehr spezifische Expressionsmuster, sind strukturell verwandt und teilen in vielen Fällen ihre funktionellen Eigenschaften. Während das humane Genom hunderte von GPCRs kodiert, werden deren Effekte lediglich durch diese vier verschiedenen Familien heterotrimerer G-Proteine vermittelt. Die meisten Rezeptoren können mehr als eine G-Protein-Familie aktivieren, haben aber klare Präferenzen bezüglich der einzelnen G-Protein-Familien. Im Kontext dieser Arbeit ist insbesondere zu erwähnen, dass Rezeptoren, die G-Proteine der Familie G_{12}/G_{13} aktivieren, meist auch G_q/G_{11} aktivieren. Während G-Proteine der G_s-Familie (Isoformen $G\alpha_s$ und $G\alpha_{olf}$) eine GPCR-abhängige Aktivierung der Adenylat-Zyklase und somit einen Anstieg der intrazellulären cAMP-Konzentration vermitteln, inhibieren G-Proteine der G_i/G_o-Familie die Adenylat-Zyklase. G-Proteine der Familie G_q/G_{11} rekrutieren entsprechende Rezeptoren an β-Isoformen der Phospholipase C, deren Aktivierung zur Bildung von Inositol-1,4,5-Tris-Phosphat (IP3) und der Freisetzung von intrazellulär gespeichertem Calcium führt. Die

Erforschung der G_{12}/G_{13}-Familie von G-Proteinen verlief gegenüber den anderen G-Protein-Familien deutlich verzögert und ihre Effektoren blieben über viele Jahre unbekannt, da spezifische Inhibitoren und Analyse-Methoden fehlten. Erst im Jahr 1990 wurden die entsprechenden Isoformen, die α-Untereinheiten G_{12} und G_{13} entdeckt (Strathmann & Simon, 1990). Mit der Entwicklung entsprechender Analyse-Methoden in den letzten Jahren wurde zunächst deutlich, dass die $G\alpha_{12}/G\alpha_{13}$ –vermittelte Signaltransduktion zu einer Aktivierung der kleinen GTPase RhoA führt. Diese wird durch $G\alpha_{12}/G\alpha_{13}$-abhängige Rho-Guanin-Nukleotid-Austausch-Faktoren (RhoGEFs) aktiviert. Mittlerweile wissen wir, dass auch die $G\alpha_{12}/G\alpha_{13}$-vermittelte Signaltransduktion deutlich komplexer ist als zunächst angenommen. So werden noch weitere Signalwege durch G_{12}/G_{13} auf die hier aber nicht näher eingegangen werden soll. (Worzfeld et al., 2008)

1.2.4 Regulation von G-Proteinen

Der Aktivierungs/Deaktivierungs-Zyklus von G-Proteinen kann auf unterschiedlichen Ebenen reguliert werden. Dabei hat die Entdeckung sogenannter „Regulatoren der G-Protein-vermittelten Signaltransduktion“ (RGS-Proteine), die die intrinsische GTPase-Aktivität der G-Protein α-Untereinheiten steigern, erheblich zum besseren Verständnis dieser Prozesse beigetragen. So sind mittlerweile über 30 RGS-Proteine mit unterschiedlichen Präferenzen für bestimmte Isoformen der α-Untereinheiten bekannt.

1.2.5 G-Protein-unabhängige Signaltransduktion (β-Arrestine)

Neben heterotrimeren G-Proteinen gibt es noch zwei weitere Protein-Familien, die spezifisch mit GPCRs interagieren, GPCR-Kinasen (GRKs) und β-Arrestine (Reiter, Ahn, Shukla, & Lefkowitz, 2012). Gemeinsam spielen GRKs und β-Arrestine eine wichtige Rolle bei der Desensibilisierung, Internalisierung und Wiederverwertung von GPCRs. So iniziiert die Phosphorylierung des Rezeptor C-Terminus durch GRKs eine Rekrutierung von β-Arrestinen. Diese wiederum unterbinden physikalisch die Kopplung von GPCR und G-Protein und bewirken letztlich die Internalisierung des Rezeptors durch Clathrin-abhängige Endozytose. Darüber hinaus weiß man mittlerweile, das GRKs und β-Arrestine auch als G-Protein-unabhängige Signal-Transduktoren fungieren. So vermögen insbesondere β-Arrestine unterschiedliche Effektoren wie beispielsweise die MAP-Kinase ERK1/2 oder die kleine GTPase RhoA zu aktivieren (Reiter et al., 2012).

1.3 G_q/G_{11}- und G_{12}/G_{13}-vermittelte Signaltransduktion in glatten Gefäßmuskelzellen

Eine wesentliche Funktion von glatten Gefäßmuskelzellen ist die Kontraktion und damit Etablierung des Gefäßtonus, über den letztlich Blutdruck und Organperfusion reguliert werden. Dabei stellt die Phosphorylierung von Myosin-Leichtketten (MLC) einen zentralen Regulations-

Mechanismus dar. So führt eine MLC-Phosphorylierung durch die Ca^{2+}-Calmodulin-aktivierte MLC-Kinase zu einer verstärkten Interaktion von Myosin und Aktin und einem erhöhten Gefäßtonus, während eine Dephosphorylierung durch die MLC-Phosphatase (MLCP) den Gefäßtonus senkt. Im Gegensatz zur Ca^{2+}-abhängigen Regulation der MLCK, wird die MLCP Ca^{2+}-unabhängig reguliert (Althoff & Offermanns, 2015b; Wirth et al., 2008).

Klassische Vasokonstriktoren, wie Endothelin-1, Angiotensin II oder Vasopressin vermitteln ihre Effekte über GPCRs, die überwiegend an G-Proteine der Familien G_q/G_{11} und G_{12}/G_{13} koppeln. So führt die G_q/G_{11}-abhängige Signaltransduktion zur Freisetzung von intrazellulär gespeichertem Ca^{2+} und einer Calmodulin-vermittelten Aktivierung der MLCK, was wiederum eine gesteigerte MLC-Phosphorylierung und Kontraktion bewirkt. Die Aktivierung von G_{12}/G_{13} bewirkt steigert ebenfalls den Gefäßtonus, allerdings Ca^{2+}-unabhängig über eine durch RhoA und die Rho-assoziierte Proteinkinase (Luscher et al.) vermittelte Inhibition der MLCP. Somit wirken G_q/G_{11}- und G_{12}/G_{13}-vermittelte Signaltransduktion in glatten Gefäßmuskelzellen synergistisch im Sinne einer Steigerung des Gefäßtonus (Althoff & Offermanns, 2015b). Die Rolle dieser Signalwege im Kontext von Gefäßumbauprozessen oder Gefäßerkrankungen wie der Atherosklerose war bis dato unbekannt.

1.4 G_q/G_{11}- und G_{12}/G_{13}-vermittelte Signaltransduktion in Endothelzellen

Neben der Regulation durch Vasopressoren und G_q/G_{11}- bzw. G_{12}/G_{13}-vermittelte prokontraktile Signaltransduktion in glatten Muskelzellen, unterliegt der Gefäßtonus auch autoregulatorischen Mechanismen. Ein fundamentaler Prozess dieser Autoregulation ist die Fluss-induzierte Vasorelaxation. So sezernieren Endothelzellen als Reaktion auf Blutfluss-abhängige Scherkräfte zahlreiche vasoaktive Faktoren, von denen Stickstoff-Monoxid (NO) die führende Rolle bei der Fluss-induzierten Vasorelaxation spielt. Aktuelle Daten deuten darauf hin, dass G_q/G_{11} nicht aber G_{12}/G_{13} an der Wahrnehmung und intrazellulären Verarbeitung Fluss-induzierter Scherkräfte durch Endothelzellen zentral beteiligt sind (Wang et al., 2015). So scheinen G-Proteine der Familie G_q/G_{11} für diese sogenannte endotheliale Mechanotransduktion und resultierende NO-Freisetzung essenziell. Obwohl die endotheliale Mechanotransduktion Fluss-induzierter Scherkräfte ein wesentlicher Mechanismus bei der Pathogenese der Atherosklerose ist, war die Rolle endothelialer G-Proteine der Familien G_q/G_{11} und G_{12}/G_{13} in diesem Kontext bis dato unbekannt.

Beiden G-Protein-Familien - G_q/G_{11} und G_{12}/G_{13} – wird eine wesentliche Rolle bei der endothelialen Regulation der VEGF-induzierten Tumor-Angiogenese zugeschrieben (Sivaraj et al., 2015; Sivaraj et al., 2013). Schließlich scheint die G_q/G_{11}-vermittelte Signaltransduktion für die pathologische Gefäßpermeabilität im Rahmen eines anaphylaktischen Schocks verantwortlich zu sein (Korhonen et al., 2009).

1.5 G_q/G_{11}- und G_{12}/G_{13}-vermittelte Signaltransduktion in Kardiomyozyten

Liganden kardialer G_q/G_{11}- und G_{12}/G_{13}-gekoppelter Rezeptoren wie Endothelin-1 oder Angiotensin II haben wesentlichen Einfluss auf Erkrankungen des Herzmuskels und spielen eine zentrale Rolle bei der Pathogenese unterschiedlicher Kardiomyopathien. Insbesondere induzieren sie sowohl in vitro als auch in vivo einen hypertrophen Phänotyp von Kardiomyozyten. Im Mausmodell einer kardialen Druckbelastung zeigte sich Entwicklung einer Herzmuskel-Hypertrophie gänzlich abhängig von G_q/G_{11} (Wettschureck et al., 2001). Interessanterweise wirkt sich das Fehlen dieses G_q/G_{11}-vermittelten Kompensationsmechanismus im Langzeitverlauf nicht negativ auf die Herzfunktion aus. Darüber deutet einiges darauf hin, dass die G_q/G_{11}-vermittelte Signaltransduktion eine wesentliche Rolle bei der Entstehung der Diabetischen Kardiomyopathie spielt (Harris et al., 2004). Während die Rolle der G_q/G_{11}-vermittelten Signaltransduktion in Kardiomyozyten im Rahmen von Hermuskelerkrankungen also gut untersucht ist, blieb die Funktion von G_{12}/G_{13} in diesem Kontext bis dato ungeklärt.

1.6 G_q/G_{11}- und G_{12}/G_{13}-vermittelte Signaltransduktion in Thrombozyten

Die Adhäsion, Aktivierung und schließlich Aggregation von Thrombozyten im Bereich von Gefäßverletzungen ist ein wichtiger Bestandteil der primären Hämostase, spielt aber auch eine zentrale Rolle im Rahmen von Gefäßerkrankungen. Dabei vermitteln Thrombozyten nicht nur unmittelbar die Entstehung atherothrombotischer Komplikationen wie den Myokardinfarkt als Folge eines thrombotischen Gefäßverschlusses im Bereich von Plaque-Rupturen. Sie unterhalten auch den chronisch-inflammatorischen Prozess der Atherosklerose und begünstigen so die Entwicklung und Progression der Erkrankung.

Die Thrombozyten-Aktivierung wird unter anderem durch extrazelluläre Stimuli wie ADP, Thrombin oder Thromboxan A2 induziert. Diese binden an entsprechende GPCRs, die die Aktivierung von Thrombozyten im Wesentlichen über drei nachgeschaltete G-Protein-abhängige Signalwege vermitteln: Während ADP über seine Rezeptoren P2Y1 und P2Y12 G_q/G_{11}- bzw. G_i-abhängige Signalwege aktiviert, wirken Thromboxan A2 und Thrombin über G_q/G_{11}- und G_{12}/G_{13}-gekoppelte Rezeptoren - den Thromboxan A2-Rezeptor bzw. die Protease-Aktivierten Rezeptoren PAR1/PAR4 oder PAR3/PAR4. Was die G-Protein-Familie G_q/G_{11} angeht, stellen Thrombozyten eine Ausnahme dar. Während die meisten Zelltypen sowohl die Isoform G_q als auch die Isoform G_{11} exprimieren, enthalten Thrombozyten lediglich die Isoform G_q.

Wesentliche Thrombozyten-Funktionen und Bestandteile der Thrombozyten-Aktivierung werden über G_q/G_{11}- und G_{12}/G_{13}-abhängige Signal-Wege vermittelt. So lässt sich die

charakteristische Formveränderung aktivierter Thrombozyten über diese G-Protein-Familien induzieren, nicht aber über die G-Protein-Familie G_i. Dabei scheinen die Ca^{2+}- und Rho/ROCK-vermittelte MLC-Phosphorylierung als Folge einer Aktivierung von $G\alpha_q$ bzw. $G\alpha_{13}$ eine zentrale Rolle zu spielen. Auch für die $\alpha_{IIb}\beta_3$–abhängige Thrombozyten-Aggregation sind G-Proteine-vermittelte Signalwege notwendig. So führt die Thrombozyten-Aktivierung über G-Protein-abhängige Signalwege zu einer „inside-out-Aktivierung“ von $\alpha_{IIb}\beta_3$–Integrinen und einer Fibrinogen- und von Willebrand-Faktor-vermittelten Brückenbildung zwischen Thrombozyten und damit zur Aggregation. Hinsichtlich dieser „inside-out-Aktivierung“ von $\alpha_{IIb}\beta_3$ wirken Gq-, G13- und Gi-vermittelte Signalwege synergistisch, wobei die G_q-vermittelte Ca^{2+}-Freisetzung essenziell zu sein scheint. In Abwesenheit einer der drei Signalwege, kommt es zwar weiterhin zur Thrombozytenaggregation, allerdings in reduzierter Form.

Thrombozyten-Aggregationshemmer sind essenzieller Bestandteil der Atherosklerose-Therapie und verringern zuverlässig das Myokardinfarkt-Risiko bei Patienten mit Koronarer Herzerkrankung. Insbesondere nach Behandlung von Koronar-Stenosen oder –Verschlüssen durch Implantation sogenannter Stents (metallene Gefäßstützten) ist eine intensivierte antithrombozytäre Therapie unerlässlich, um Stent-Thrombosen und Myokardinfarkte zu verhindern. Dabei stellen Aspirin (Acetylsalicylsäure), das die Bildung von Thromboxan A2 unterbindet sowie Antagonisten des P2Y12-Rezeptors derzeit die Standard-Therapie dar, während die Antagonisten des Thrombin-Rezeptors PAR1 wie Voraxapar klinisch wenig etabliert sind.

1.7 Rationale

Obwohl G_q/G_{11}- und G_{12}/G_{13}-gekoppelte Rezeptoren im Rahmen kardiovaskulärer Erkrankungen eine zentrale Rolle spielen und pharmakologische Zielstrukturen für zahlreiche Medikamente darstellen, sind die entsprechenden G-Protein-vermittelten Signalwege in diesem Zusammenhang nur unvollständig untersucht. So war die Funktion von G_q/G_{11} und G_{12}/G_{13} in Gefäßständigen Zellen bei vaskulären Umbauprozessen und Gefäßerkrankungen wie der Atherosklerose oder dem essenziellen Bluthochdruck bis zum Beginn der unten vorgestellten Arbeiten gänzlich unbekannt. Wir haben nun unterschiedliche in vitro- und in vivo-Modelle für atherogenen Blutfluss sowie Fluss-induzierten Gefäßumbau und Atherosklerose etabliert, um die Rolle dieser G-Proteine in diesem Kontext zu untersuchen. Während der Einfluss G_q/G_{11}-vermittelter Signaltransduktion auf kardiale Umbauprozesse und Hypertrophie zum Beginn unserer Arbeiten bereits gut definiert war, war die Rolle von G_{12}/G_{13} in diesem Kontext noch nicht untersucht worden. Auch hier etablierten wir entsprechende in vitro und in vivo Modelle.

Diese Arbeiten beruhen ganz wesentlich auf transgenen Mausmodellen auf Basis Cre/loxP-vermittelter Mutagenese. Um die einzelnen G-Protein-Familien zu untersuchen haben wir Doppel-Knockout-Modelle generiert, bei denen konditional beide relevanten Isoformen der jeweiligen Familie inaktiviert werden können ($G\alpha_q$ und $G\alpha_{11}$ für die G_q/G_{11}-Familie bzw. $G\alpha_{12}$ und $G\alpha_{13}$ für die G_{12}/G_{13}-Familie). Nur so kann verhindert werden, dass bei Inaktivierung nur einer der beiden Isoformen, die jeweils andere, funktionell teilweise redundante Isoform, für den Ausfall kompensiert. Die Kombination von Zelltyp-spezifisch exprimierten Cre-Rekombinasen mit den jeweiligen loxP-flankierten Allelen ermöglichte dabei eine selektive Inaktivierung in glatten Muskelzellen, Endothelzellen oder Kardiomyozyten. So konnten differenzielle Zelltyp-spezifische Funktionen definiert werden.

Die Rolle G_q/G_{11}- und G_{12}/G_{13}-vermittelter Signaltransduktion war in keinem Bereich so gut definiert wie bei der Thrombozyten-Aktivierung und –Aggregation, und sämtliche Standard-Ansätze der therapeutischen Thrombozyten-Aggregationshemmung (Acetylsalicylsäure und P2Y12-Inhibitoren) basieren letztlich auf der Inhibition G-Protein-vermittelter Signalwege. Allerdings kamen in den letzten Jahren erhebliche Zweifel an der zuverlässigen Wirksamkeit dieser Medikamente auf. So wurden vor dem Hintergrund einer erheblichen interindividuellen Variabilität der Wirkung die Begriffe Aspirin- bzw. Clopidogrel-Resistenz geprägt, die letztlich ein nicht adäquates Ansprechen auf die jeweilige Therapie beschreiben. Für Patienten mit einer solchen Aspirin- oder Clopidogrel-Resistenz konnte ein deutlich erhöhtes Risiko für kardiovaskuläre Ereignisse wie Myokardinfarkt oder Stentthrombosen nachgewiesen werden. Unsere Arbeit in diesem Zusammenhang beruhte nun auf der Hypothese, dass das Ansprechen auf Aspirin und Clopidogrel im Zeitraum nach einem akuten Myokardinfarkt per se eingeschränkt ist und a priori eine intensivierte Inhibition der thrombozytären G-Protein-vermittelten Signaltransduktion erfordert.

2 Ergebnisse

2.1 Prokontraktile G-Protein-vermittelte Signalwege regulieren die Differenzierung glatter Muskelzellen im Kontext vaskulärer Umbauprozesse antagonistisch

Procontractile G protein–mediated signaling pathways antagonistically regulate smooth muscle differentiation in vascular remodeling. **Althoff TF**, Albarrán Juárez J, Troidl K, Tang C, Wang S, Wirth A, Takefuji M, Wettschureck N, Offermanns S. *J Exp Med* (2012), Nov:209(12), 2277-90.

https://doi.org/10.1084/jem.20120350

„Glatte Muskelzellen sind äußerst plastisch. Der Differenzierungsstatus glatter Muskelzellen wird durch Serum Response Factor (SRF) reguliert; dieser aktiviert Gene, die an der Differenzierung und Proliferation glatter Muskelzellen beteiligt sind, indem er Co-Faktoren, beispielsweise aus der Myokardin-Familie oder der Familie der Ternary Complex Factors, rekrutiert. Allerdings sind die extrazellulären Signale und übergeordneten Signaltransduktionsmechanismen, die die SRF-abhängige Differenzierung glatter Muskelzellen unter in vivo-Bedingungen regulieren, bislang kaum verstanden. In dieser Studie zeigen wir, dass prokontraktile Signalwege, die durch die G-Proteine G_{12}/G_{13} and G_q/G_{11} vermittelt werden, die Plastizität glatter Muskelzellen in unterschiedlichen Modellen für Gefäßumbau antagonistisch regulieren. In Mäusen in denen $G\alpha_{12}/G\alpha_{13}$ oder deren Effektor LARG inaktiviert wurde, war die RhoA-abhängige SRF-Regulation blockiert und die Herab-Regulation von glattmuskulären Markergenen verstärkt. Dies war mit einem exzessiven Gefäßumbau und exazerbierter Atherosklerose assoziiert. Im Gegensatz dazu verhinderte eine glattmuskelspezifische $G\alpha_q/G\alpha_{11}$-Defizienz die Aktivierung der Extracellular Signal Regulated Kinase 1/2 (ERK1/2) und des Ternary Complex Factors ELK-1, was eine reduzierte Differenzierung glatter Muskelzellen infolge Unterbrechung des Blutflusses oder Gefäßverletzung zur Folge hatte. Diese Daten zeigen, dass eine ausgewogene Aktivität beider G-Protein-vermittelter Signalwege in glatten Muskelzellen für eine angemessene Gefäßantwort im Rahmen vaskulärer Erkrankungen erforderlich ist und suggeriert neue Ansätze, die Differenzierung glatter Muskelzellen im Kontext von Gefäßpathologien zu modulieren.“ Übersetzung durch den Autor.

Published November 5, 2012

Procontractile G protein–mediated signaling pathways antagonistically regulate smooth muscle differentiation in vascular remodeling

Till F. Althoff,[1] Julián Albarrán Juárez,[1] Kerstin Troidl,[1,2] Cong Tang,[1] Shengpeng Wang,[1] Angela Wirth,[1,3] Mikito Takefuji,[1] Nina Wettschureck,[1,2] and Stefan Offermanns[1,2]

[1]Department of Pharmacology, Max-Planck-Institute for Heart and Lung Research, 61231 Bad Nauheim, Germany
[2]Medical Faculty, Johann Wolfgang Goethe University Frankfurt, 60590 Frankfurt am Main, Germany
[3]Institute of Pharmacology, University of Heidelberg, 69120 Heidelberg, Germany

Vascular smooth muscle (Sm) cells (VSMCs) are highly plastic. Their differentiation state can be regulated by serum response factor (SRF), which activates genes involved in Sm differentiation and proliferation by recruiting cofactors, such as members of the myocardin family and ternary complex factors (TCFs), respectively. However, the extracellular cues and upstream signaling mechanisms regulating SRF-dependent VSMC differentiation under in vivo conditions are poorly understood. In this study, we show that the procontractile signaling pathways mediated by the G proteins G_{12}/G_{13} and G_q/G_{11} antagonistically regulate VSMC plasticity in different models of vascular remodeling. In mice lacking $G\alpha_{12}/G\alpha_{13}$ or their effector, the RhoGEF protein LARG, RhoA-dependent SRF-regulation was blocked and downregulation of VSMC differentiation marker genes was enhanced. This was accompanied by an excessive vascular remodeling and exacerbation of atherosclerosis. In contrast, Sm-specific $G\alpha_q/G\alpha_{11}$ deficiency blocked activation of extracellular signal-regulated kinase 1/2 and the TCF Elk-1, resulting in a reduced VSMC dedifferentiation in response to flow cessation or vascular injury. These data show that the balanced activity of both G protein–mediated pathways in VSMCs is required for an appropriate vessel remodeling response in vascular diseases and suggest new approaches to modulate Sm differentiation in vascular pathologies.

CORRESPONDENCE
Stefan Offermanns:
stefan.offermanns@mpi-bn.mpg.de

Abbreviations used: GPCR, G protein–coupled receptor; MRTF, myocardin-related transcription factor; qRT-PCR, quantitative RT-PCR; RhoGEF, Rho guanine nucleotide exchange factor; Sm, smooth muscle; SMC, Sm cell; SRF, serum response factor; TCF, ternary complex factor; VSMC, vascular SMC.

Unlike skeletal or cardiac muscle cells, which are terminally differentiated, vascular smooth muscle (Sm) cells (SMCs [VSMCs]) retain a remarkable degree of plasticity throughout their lives. They can switch between a quiescent contractile state and phenotypes of increased proliferation, migration, and synthetic capacity (Owens, 1995). Dedifferentiation and redifferentiation of VSMCs are believed to be involved in vascular remodeling processes that physiologically enable vascular development and repair, as well as adaptation to chronically altered hemodynamics. However, dysregulation of VSMC plasticity also plays a role in the pathogenesis of vascular diseases such as atherosclerosis, restenosis after percutaneous interventions, and systemic as well as pulmonary hypertension (Owens et al., 2004).

The differentiation state of VSMCs is under the control of transcriptional regulators. Many genes involved in the regulation of SMC contractility are controlled by serum response factor (SRF), a widely expressed transcription factor which is believed to play a key role in the regulation of Sm differentiation (Miano et al., 2007; Owens, 2007). However, SRF can also induce the transcription of growth-related genes involved in Sm proliferation and dedifferentiation, and it is now well established that two families of transcriptional cofactors, the myocardin family (Pipes et al., 2006; Parmacek, 2007) and the ternary complex factor (TCF) family of Ets domain proteins (Treisman, 1994), differentially modulate the transcription of these distinct SRF target genes through their mutually exclusive binding to SRF (Wang et al., 2004). Whereas coactivators of the myocardin family,

The Rockefeller University Press $30.00
J. Exp. Med. 2012
www.jem.org/cgi/doi/10.1084/jem.20120350

Published November 5, 2012

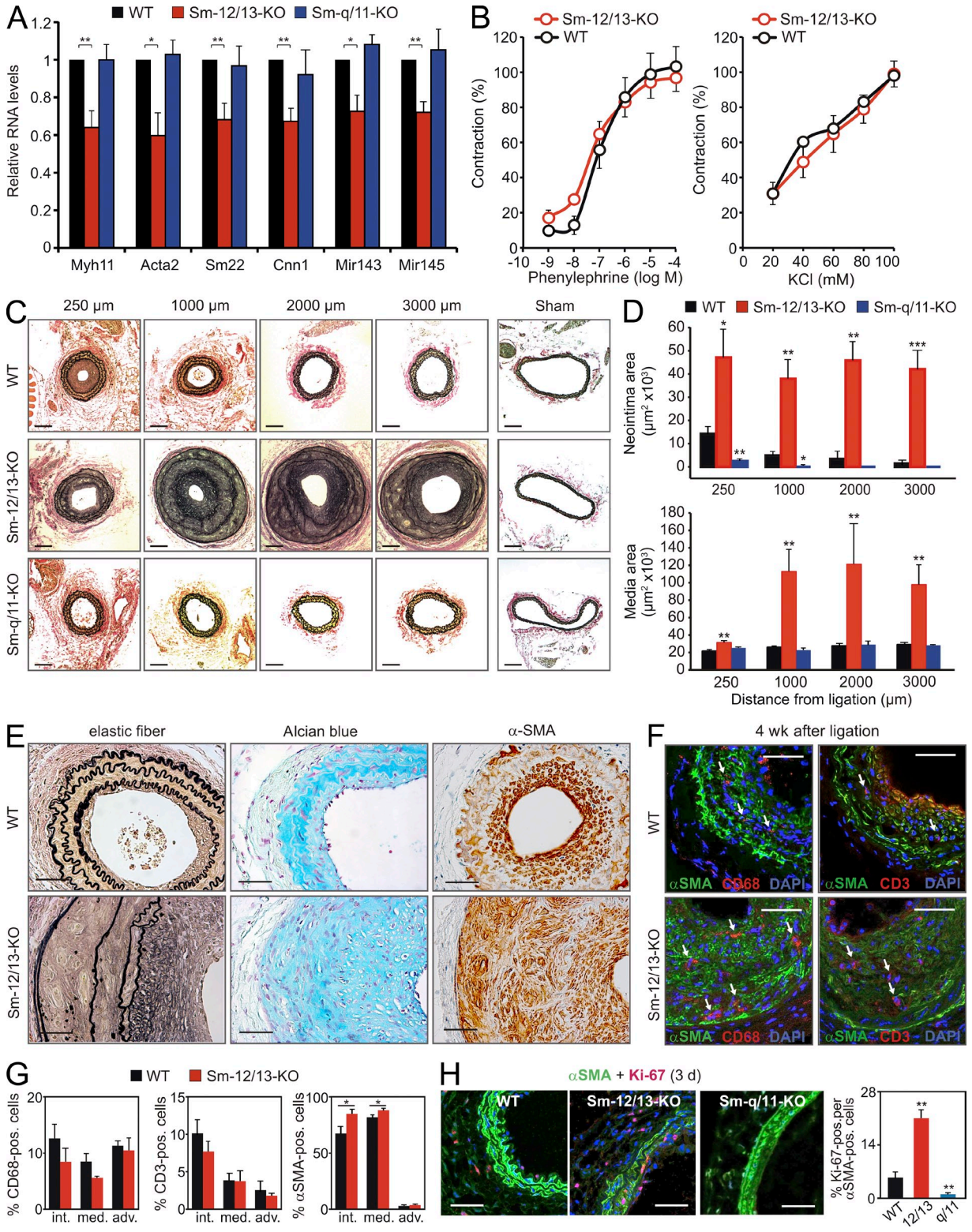

Figure 1. Differential effects of G_q/G_{11} and G_{12}/G_{13} on neointima formation. (A) Relative levels of mRNAs encoding Sm differentiation markers normalized against 18S and of miR143/miR145 normalized against 4.5S RNA in the media of carotid arteries from WT, Sm-Gα_{12}/Gα_{13}-KO (Sm-12/13-KO), or Sm-Gα_q/Gα_{11}-KO (Sm-q/11-KO) mice (the data are representative for five to six males and three independent experiments per group). Levels in the media of WT mice were set as 100%. (B) Effect of increasing concentration of phenylephrine or KCl on the vascular tone of carotid arteries from WT or Sm-12/13-KO mice in percentage of maximal response (the data are representative for four males and two independent experiments per group). (C and D) Analysis of carotid artery remodeling after ligation. (C) Shown are sections of the carotid arteries from WT, Sm-12/13-KO, and Sm-q/11-KO

Published November 5, 2012

consisting of myocardin itself and myocardin-related transcription factors (MRTFs) A and B, promote VSMC differentiation, competitive binding of TCFs induces decreased expression of SMC-selective marker genes and VSMC proliferation (Mack, 2011). TCFs are phosphorylated and activated through the Ras/MAPK pathway (Posern and Treisman, 2006), whereas RhoA-mediated signaling has been shown to promote nuclear translocation of MRTFs and to induce Sm differentiation (Lu et al., 2001; Mack et al., 2001; Olson and Nordheim, 2010). However, the extracellular cues and upstream signaling mechanisms regulating SRF-dependent VSMC differentiation under in vivo conditions have remained poorly understood.

Most of the extracellular stimuli that regulate vascular Sm tone and increase contractility exert their effects via G protein–coupled receptors (GPCRs), which regulate two major pathways involving the heterotrimeric G proteins G_q/G_{11} and G_{12}/G_{13}. Whereas G_q/G_{11} mediates the activation of phospholipase C β-isoforms and subsequent Ca^{2+}/calmodulin-dependent activation of myosin light chain kinase, the G_{12}/G_{13} family of G proteins couples to Rho guanine nucleotide exchange factor (RhoGEF) proteins to activate RhoA and thereby induces a Ca^{2+}-independent VSMC contraction via inhibition of myosin phosphatase (Gohla et al., 2000; Somlyo and Somlyo, 2003; Maguire and Davenport, 2005). G_q/G_{11}-mediated signaling in VSMCs is required for basal vascular tone induced by vasoactive mediators, whereas both G_q/G_{11} and G_{12}/G_{13} need to be activated for pathological increases in vascular tone like in hypertension (Wirth et al., 2008).

Here we report that the procontractile signaling pathways mediated by the G proteins G_{12}/G_{13} and G_q/G_{11} antagonistically regulate SRF-dependent VSMC differentiation. Whereas G_{12}/G_{13} promotes differentiation, G_q/G_{11} reduces SMC-selective marker gene expression and stimulates proliferation. Our data indicate that the balanced activities of both procontractile G protein–mediated signaling pathways control VSMC plasticity under basal conditions as well as after vascular injury or in response to changes in blood flow.

RESULTS

Reduced expression of Sm differentiation marker genes in $G\alpha_{12}/G\alpha_{13}$- but not in $G\alpha_q/G\alpha_{11}$–deficient vascular Sm

Using quantitative RT-PCR (qRT-PCR) analysis, we evaluated the effect of Sm-specific $G\alpha_q/G\alpha_{11}$ and $G\alpha_{12}/G\alpha_{13}$ deficiency on vascular gene expression in the media of arterial vessels using SMMHC-CreER^{T2};$G\alpha_q^{flox/flox}$;$G\alpha_{11}^{-/-}$ mice (Sm-$G\alpha_q$/$G\alpha_{11}$-KO) and SMMHC-CreER^{T2};$G\alpha_{12}^{-/-}$;$G\alpha_{13}^{flox/flox}$ mice (Sm-$G\alpha_{12}/G\alpha_{13}$-KO; Wirth et al., 2008). In different vessels from Sm-$G\alpha_{12}/G\alpha_{13}$-KO mice, we detected decreased mRNA levels of Sm differentiation marker genes such as Acta2 (α-Sm actin [α-SMA]), Myh11 (Sm myosin heavy chain [SMMHC]), Cnn1 (calponin-1), or Tagln (SM22), as well as of the Sm-enriched microRNAs 143 and 145, compared with WT and Sm-$G\alpha_q/G\alpha_{11}$-KO mice (Fig. 1 A and not depicted). Despite the down-regulation of genes encoding proteins of the contractile apparatus of SMCs, myometric experiments of agonist-induced contraction in carotid arteries did not reveal any functional defect in Sm-$G\alpha_{12}/G\alpha_{13}$-KO mice (Fig. 1 B). These results are in line with our previous finding that Sm-$G\alpha_{12}$/$G\alpha_{13}$-KO mice display a normal blood pressure profile (Wirth et al., 2008), suggesting that the observed subtle but significant changes in expression pattern are of no functional relevance.

G_q/G_{11} and G_{12}/G_{13} antagonistically regulate VSMC differentiation

As vascular remodeling processes such as neointima formation in response to vascular injury or flow cessation are often accompanied by decreased expression of SMC differentiation marker genes, we tested the response of Sm-specific $G\alpha_q$/$G\alpha_{11}$- and $G\alpha_{12}/G\alpha_{13}$-deficient mice to flow cessation in the carotid artery ligation model. In WT vessels, carotid artery ligation results in neointimal hyperplasia, adjacent to the ligation site. Histological evaluation 4 wk after ligation revealed a severely exaggerated response to flow cessation in Sm-$G\alpha_{12}/G\alpha_{13}$-KO mice, with excessive neointimal as well as medial hyperplasia (Fig. 1, C–E). By morphometric analysis, Sm-specific deletion of $G\alpha_{12}/G\alpha_{13}$ increased neointima and media thickness several fold compared with WT animals.

A closer analysis of the expanded media of ligated vessels from Sm-$G\alpha_{12}/G\alpha_{13}$-KO mice showed a disarray of elastic lamina and the presence of proteoglycans stained with Alcian blue (Fig. 1 E). Although the number of α-SMA–positive cells in the vessels of Sm-$G\alpha_{12}/G\alpha_{13}$-KO mice was increased compared with WT animals 4 wk after ligation, the proportion of CD68- and CD3-positive cells was indistinguishable between both genotypes (Fig. 1, F and G). VSMCs in the absence of $G\alpha_{12}/G\alpha_{13}$ showed an increased acute proliferative response to vascular injury as indicated by the strongly increased number

mice at a distance of 250, 1,000, 2,000, and 3,000 µm from the ligation site as well as sections of the contralateral vessel 4 wk after ligation. (D) The neointima and media areas in sections at the indicated distances from the ligation site were determined (the data are representative for five to seven males and three independent experiments per group). (E) Carotid arteries from WT and Sm-12/13-KO animals 4 wk after ligation were stained for elastic fibers (left), proteoglycans (middle), and α-SMA (right). Shown are representative sections (the data are representative for four to six males and two independent experiments per group). (F and G) Carotid arteries from WT and Sm-12/13-KO mice were immunostained 4 wk after ligation for CD68 and α-SMA or CD3 and α-SMA. Nuclei were counterstained with DAPI. Shown are representative images of stained sections (F) as well as the proportions of CD3-, α-SMA–, or CD68-positive cells in the intima (int.), media (media.), or adventitia (adv.; G; the data are representative for four to five males and two independent experiments per group). Arrows in F indicate CD68 (left)- or CD3 (right)-positive cells. (H) Carotid arteries from WT, Sm-12/13-KO (12/13), or Sm-q/11-KO mice (q/11) were stained 3 d after ligation for α-SMA and Ki-67. Shown are representative images as well as a statistical analysis of the percentage of Ki-67–positive cells among α-SMA–positive cells (the data are representative for four males and two independent experiments per group). Shown are mean values ± SEM; *, $P < 0.05$; **, $P < 0.01$; ***, $P < 0.001$ (compared with WT). Bars: (C) 100 µm; (E, F, and H) 50 µm.

Published November 5, 2012

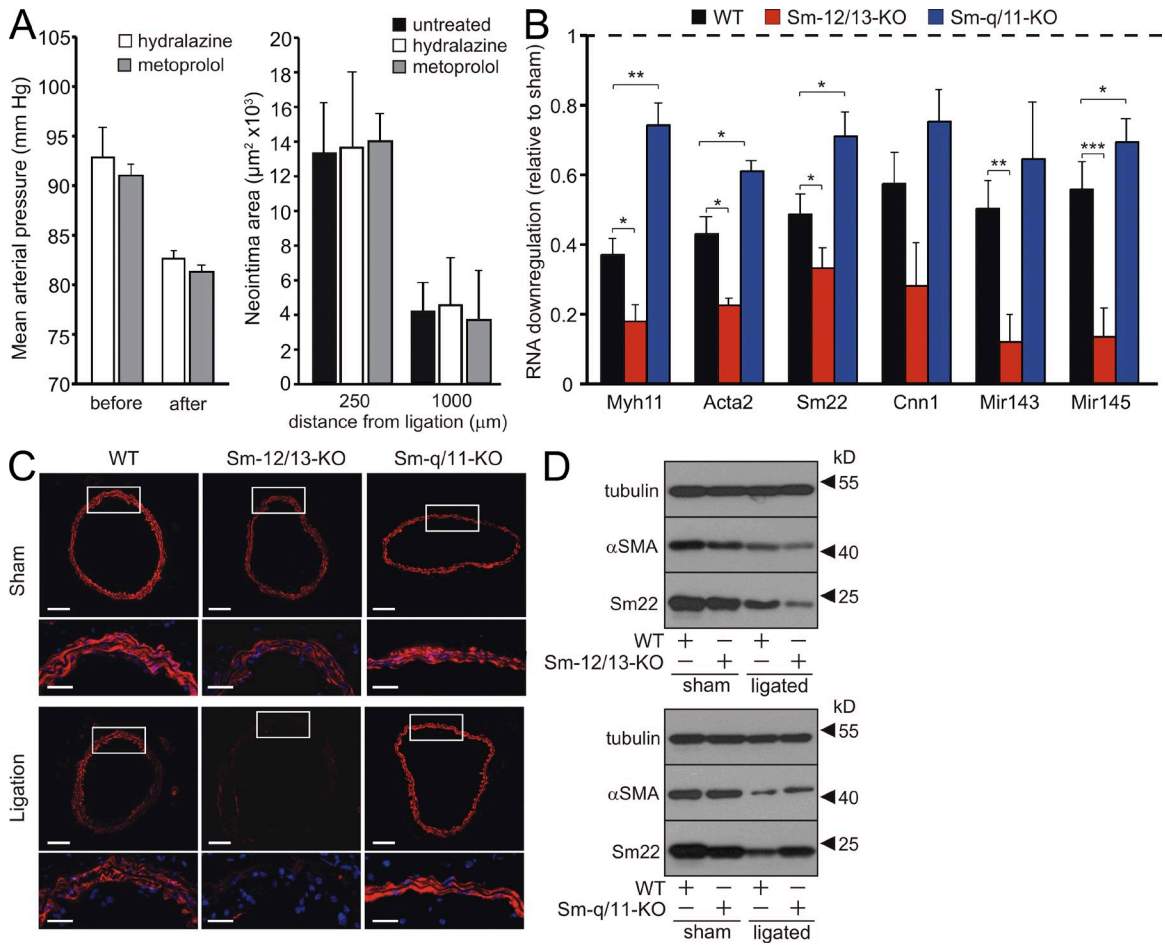

Figure 2. Effects of $G\alpha_q/G\alpha_{11}$ and $G\alpha_{12}/G\alpha_{13}$ deficiency on SMC differentiation marker gene expression. (A) Effect of hydralazine- and metoprolol-induced hypotension on neointima formation after carotid ligation. WT mice were treated without or with 500 mg/liter hydralazine or 2.5 g/liter metoprolol in the drinking water resulting in a 10–15% reduction of the mean arterial blood pressure in the treated group compared with untreated animals. Shown are the mean arterial blood pressure values during 2 d before treatment (before) and during days 3 and 4 after the start of treatment (after) and an evaluation of the neointima areas in sections from untreated and treated animals at the indicated distances from the ligation site ($n = 3$). (B) Relative levels of mRNAs encoding Sm differentiation markers as well as of miR143/miR145 in the media of carotid arteries from WT, Sm-12/13-KO, and Sm-q/11-KO mice 3 d after carotid artery ligation relative to the levels in the media of the sham-operated contralateral vessel ($n = 5–6$). (C) Carotid artery sections at a distance of 1,000 µm from the ligation site from WT, Sm-12/13-KO, and Sm-q/11-KO mice 7 d after sham operation (sham) or carotid artery ligation stained with an anti–α-SMA antibody. White boxes indicate enlarged areas at the bottom of each image. (D) 3 d after sham operation or ligation, carotid arteries of WT, Sm-$G\alpha_{12}/G\alpha_{13}$-KO (Sm-12/13-KO), or Sm-$G\alpha_q/G\alpha_{11}$-KO (Sm-q/11-KO) were prepared free of adventitia and intima, and lysates were analyzed by immunoblotting using antibodies against α-SMA, Sm22, and tubulin. (A–D) Shown is one representative of at least three experiments. Shown are mean values ± SEM; *, $P < 0.05$; **, $P < 0.01$; ***, $P < 0.001$ (compared with WT). Bars: (C, bottom) 40 µm; (C, top) 100 µm.

of Ki-67 and α-SMA double-positive cells in the media 3 d after ligation (Fig. 1 H).

Surprisingly, an opposite phenotype was observed in Sm-$G\alpha_q/G\alpha_{11}$-KO mice, in which neointimal size was reduced compared with WT mice (Fig. 1, C and D). In most sections from Sm-$G\alpha_q/G\alpha_{11}$-KO mice, no neointima formation could be detected. This correlated with a reduced proliferative response to vascular injury compared with WT mice (Fig. 1 H). Because systemic blood pressure is reduced by 10–15% in $G\alpha_q/G\alpha_{11}$- deficient mice (Wirth et al., 2008), we tested whether the observed phenotype in Sm-$G\alpha_q/G\alpha_{11}$-KO animals was caused by hypotensive hemodynamics. In mice treated with the antihypertensives hydralazine or metoprolol in concentrations that reduced blood pressure to a level comparable with that in Sm-$G\alpha_q/G\alpha_{11}$-KO mice, the extent of neointima formation equaled that in untreated littermates (Fig. 2 A), suggesting that the reduced response of Sm-q/11-KO mice to flow cessation was unlikely to be a consequence of a reduced blood pressure.

3 d after carotid artery ligation, RNA levels of Sm differentiation marker genes were significantly decreased in the media of operated WT vessels compared with contralateral control vessels (Fig. 2 B). In addition to the reduced basal expression of Sm differentiation marker genes, carotid artery ligation resulted in an exaggerated down-regulation of the genes in Sm-$G\alpha_{12}/G\alpha_{13}$-KO vessels (Fig. 2 B). In contrast,

Published November 5, 2012

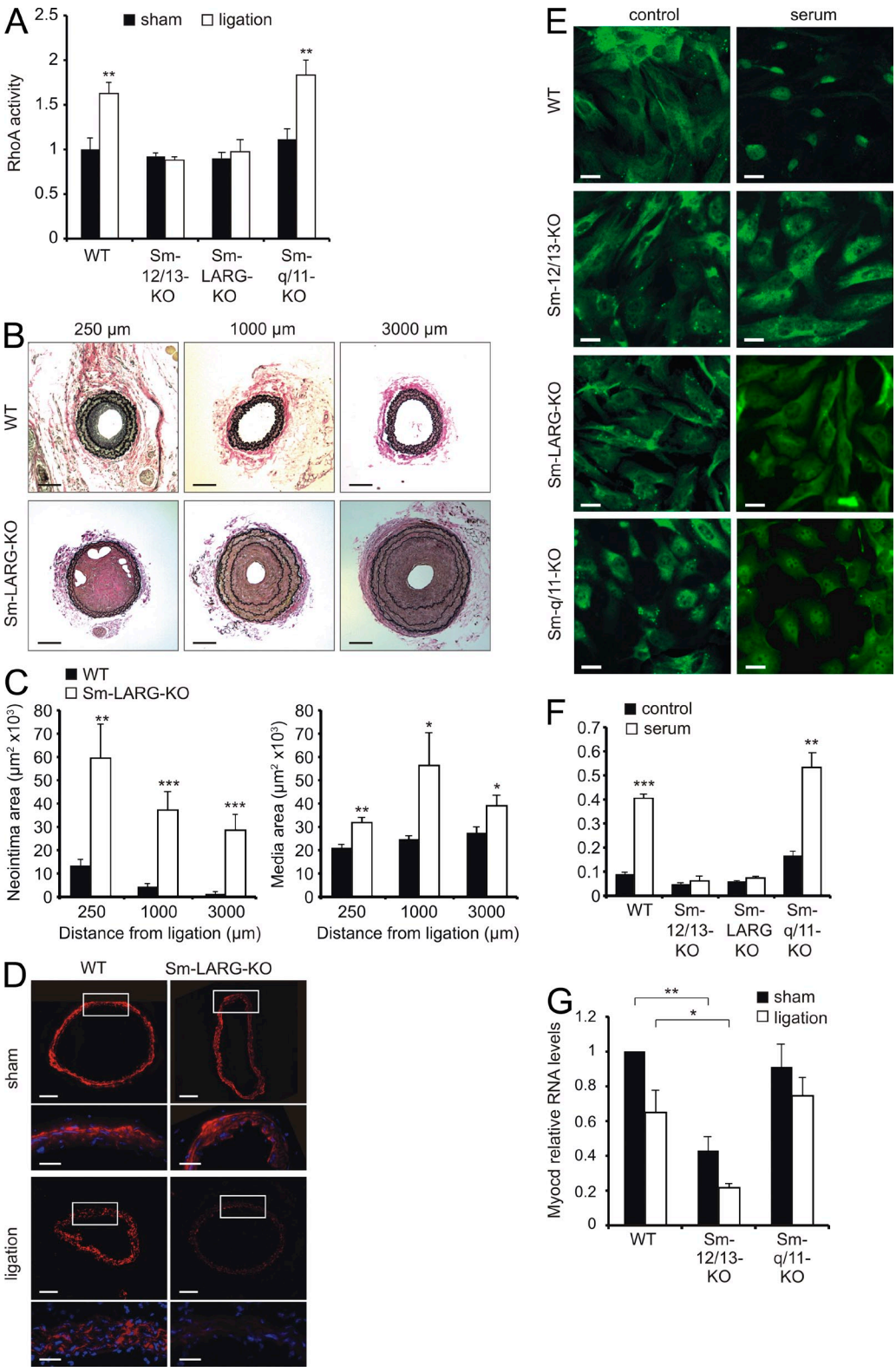

Figure 3. VSMC differentiation via RhoA/LARG. (A) Relative RhoA activity in the media of carotid arteries from WT, Sm-12/13-KO, Sm-LARG-KO, and Sm-q/11-KO mice 24 h after sham operation or carotid artery ligation (the data are representative for four to six males and three independent experiments per group). (B and C) The left common carotid artery of WT and Sm-LARG-KO mice was ligated and analyzed. Shown are sections of the vessel (B) as well as the determination of the neointima and media areas (C) at a distance of 250, 1,000, and 3,000 µm from the ligation site (the data are representative for six males and three independent experiments per group). (D) Carotid arteries from WT or Sm-LARG-KO mice were

Published November 5, 2012

down-regulation of Sm differentiation marker genes was significantly reduced in Sm-$G\alpha_q/G\alpha_{11}$-KO compared with WT vessels. Consistent with the results from qRT-PCR, immunohistochemistry revealed a decreased α-SMA expression in response to carotid artery ligation in WT VSMCs. However, although α-SMA expression in $G\alpha_{12}/G\alpha_{13}$-deficient VSMCs was reduced after ligation to almost undetectable levels, no significant down-regulation was apparent in $G\alpha_q/G\alpha_{11}$-deficient VSMCs (Fig. 2 C). Similarly, immunoblotting of lysates of the media from sham-operated and ligated WT, Sm-$G\alpha_{12}/G\alpha_{13}$-KO, and Sm-$G\alpha_q/G\alpha_{11}$-KO vessels showed reduced levels of α-SMA and Sm22 in sham-operated Sm-$G\alpha_{12}/G\alpha_{13}$-KO media compared with WT (Fig. 2 D). 3 d after ligation, protein levels were more reduced in media from Sm-specific $G\alpha_{12}/G\alpha_{13}$-deficient vessels compared with WT media, whereas the reduction was less pronounced in media from ligated Sm-q/11-KO vessels when compared with WT (Fig. 2 D).

G_{12}/G_{13} promotes VSMC differentiation through LARG-mediated activation of RhoA

As G_{12}/G_{13} link GPCRs to activation of RhoA, we assessed whether RhoA is activated upon carotid artery ligation. Indeed, RhoA activity significantly increased upon carotid artery ligation in the media of WT and Sm-$G\alpha_q/G\alpha_{11}$-KO mice (Fig. 3 A). However, Sm-specific deletion of $G\alpha_{12}/G\alpha_{13}$ blocked activation of RhoA. G_{12}/G_{13} activates RhoA through a subfamily of RhoGEFs consisting of p115-RhoGEF (Arhgef1), PDZ-RhoGEF (Arhgef11), and LARG (Arhgef12). Because LARG is the predominant RhoGEF effector of G_{12}/G_{13} in VSMCs (Wirth et al., 2008), we analyzed mice with Sm-specific LARG deficiency (SMMHC-CreER^{T2};Arhgef12$^{flox/flox}$ [Sm-LARG-KO]). Sm-LARG-KO mice also lacked RhoA activation after carotid artery ligation (Fig. 3 A), and as in $G\alpha_{12}/G\alpha_{13}$-deficient mice, ligation resulted in excessive neointima and media hyperplasia, accompanied by a disarray of elastic lamina (Fig. 3, B and C) and enhanced down-regulation of α-SMA (Fig. 3 D). Thus, Sm-specific LARG-deficient mice phenocopy Sm-12/13-KO mice, indicating that the G_{12}/G_{13}-dependent differentiation of VSMCs in vivo involves LARG-dependent activation of RhoA.

Cell-based studies have suggested that RhoA can induce SRF-dependent transcription of Sm marker genes through two mechanisms, up-regulation of myocardin expression (Wamhoff et al., 2004; Yoshida et al., 2004) and facilitation of MRTF nuclear translocation (Miralles et al., 2003; Lockman et al., 2004; Jeon et al., 2008). We therefore tested the effect of Sm-specific $G\alpha_{12}/G\alpha_{13}$ and LARG deficiency on nuclear translocation of MRTF-A in primary VSMCs. Serum-induced nuclear translocation of MRTF-A was absent in $G\alpha_{12}/G\alpha_{13}$- and LARG-deficient VSMCs (Fig. 3, E and F). In contrast, nuclear translocation of MRTF-A in $G\alpha_q/G\alpha_{11}$-deficient VSMCs was comparable with WT VSMCs (Fig. 3, E and F). We also investigated expression levels of myocardin and found reduced levels in the media of carotid arteries from sham-operated and operated Sm-$G\alpha_{12}/G\alpha_{13}$-KO mice compared with WT animals or animals with Sm-specific $G\alpha_q/G\alpha_{11}$ deficiency (Fig. 3 G).

G_q/G_{11} regulates MAPK-dependent induction of early response genes

To determine the mechanism that underlies the Sm-$G\alpha_q/G\alpha_{11}$-KO phenotype of reduced neointima formation, we analyzed the phosphorylation of the MAPK Erk1/2 as well as of the TCF Elk-1, which have been shown to mediate an inhibition of Sm differentiation (Mack, 2011). 24 h after ligation, we observed a significant increase of anti–phospho-Erk1/2 staining in the media of WT and Sm-$G\alpha_{12}/G\alpha_{13}$-KO mice but not in that of Sm-$G\alpha_q/G\alpha_{11}$-KO mice (Fig. 4, A and B). Similarly, the Erk1/2 substrate Elk-1 showed increased phosphorylation in WT and Sm-specific $G\alpha_{12}/G\alpha_{13}$-deficient mice compared with the media of Sm-$G\alpha_q/G\alpha_{11}$-KO animals 24 h after carotid artery ligation (Fig. 4, C and D). Finally, the ligation-induced and TCF-mediated up-regulation of early response genes such as Fos, Egr1, and Ets1 was blocked by Sm-specific $G\alpha_q/G\alpha_{11}$ deficiency, whereas their up-regulation was not affected in Sm-$G\alpha_{12}/G\alpha_{13}$-KO mice (Fig. 4, E–G).

G_{12}/G_{13} and G_q/G_{11} antagonistically regulate the VSMC response to injury

Having uncovered an antagonistic role of G_{12}/G_{13}- and G_q/G_{11}-mediated signaling in the regulation of SRF cofactors and neointima formation in the carotid artery ligation model, we wondered whether our findings apply analogously to other vascular remodeling processes. This prompted us to use a femoral artery injury model for restenosis. Our observations 4 wk after femoral artery injury paralleled those from the carotid artery ligation model. Sm-$G\alpha_{12}/G\alpha_{13}$-KO mice displayed excessive neointimal and medial hyperplasia, whereas Sm-specific deficiency of $G\alpha_q/G\alpha_{11}$ significantly attenuated the response to injury compared with WT animals (Fig. 5, A and B). Moreover, down-regulation of VSMC

analyzed 7 d after sham operation or carotid artery ligation, and sections at ∼1,000 µm from the ligation site were stained with an anti–α-SMA antibody. White boxes indicate enlarged areas at the bottom of each panel. (E and F) VSMCs from carotid arteries of WT, Sm-12/13-KO, Sm-LARG-KO, or Sm-q/11-KO mice were isolated, starved for 48 h, and then incubated in the absence or presence of 20% FBS for 1 h. Cells were fixed and stained with an anti–MRTF-A antibody (E), and the fraction of cells with nuclear MRTF-A staining was determined (F; the data are representative for four to six males and three independent experiments per group). (G) Relative levels of mRNA encoding myocardin (myocd) in the media of carotid arteries in WT, Sm-12/13-KO, and Sm-q/11-KO mice 3 d after sham operation carotid artery ligation (the data are representative for three to six males and twp independent experiments per group). Shown are mean values ± SEM; *, $P < 0.05$; **, $P < 0.01$; ***, $P < 0.001$ (compared with WT, sham, or –serum conditions, respectively). Bars: (B and D [top]) 100 µm; (D, bottom) 40 µm; (E) 5 µm.

Published November 5, 2012

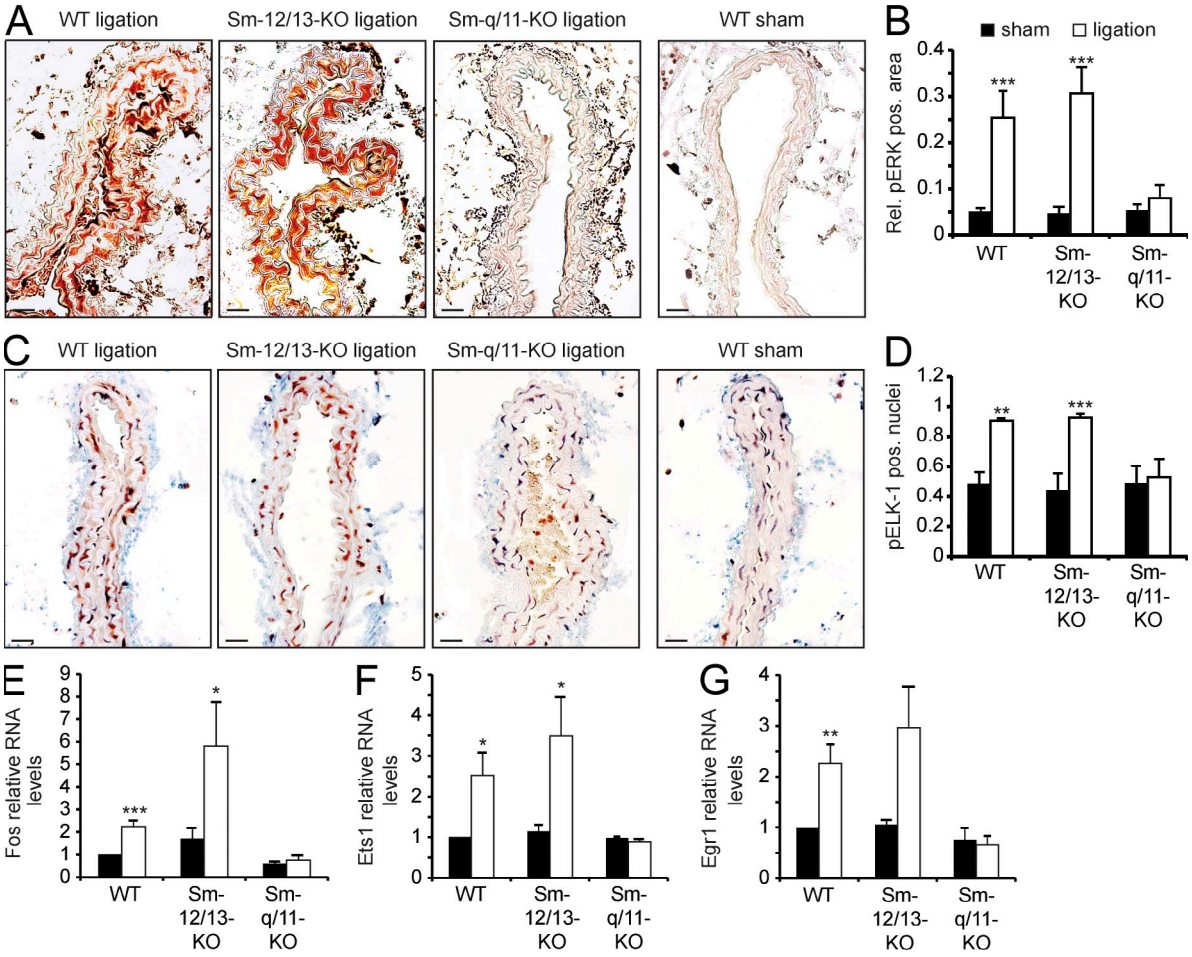

Figure 4. G_q/G_{11}-mediated signaling in VSMCs after carotid artery ligation. (A and B) 24 h after carotid artery ligation or sham operation, carotid arteries of WT, Sm-12/13-KO, or Sm-q/11-KO mice were isolated and sectioned. Shown are sections at a distance of 250–500 µm from the ligation site stained with an anti-phospho-Erk1/2 antibody (A), and the relative pERK-positive area was determined (n = 3–4; B). (C and D) 24 h after carotid artery ligation or sham operation, carotid arteries from WT, Sm-12/13-KO, or Sm-q/11-KO mice were isolated and sectioned. Shown are sections at a distance of 250–500 µm from the ligation site stained with an anti-phospho-Elk1 (pElk1) antibody and counterstained with hematoxylin (n = 3–4; C). (D) The percentage of pElk1-positive nuclei is shown. (E–G) 3 d after carotid artery ligation or sham operation of WT, Sm-12/13-KO, or Sm-q/11-KO mice, the media of carotid arteries was isolated, and the levels of mRNAs encoding Fos, Ets1, or Egr1 were determined. (A–G) Shown are mean values ± SEM (n = 3–6); *, $P < 0.05$; **, $P < 0.01$; ***, $P < 0.001$ (compared with sham). Shown is one representative of at least three experiments. Bars, 20 µm.

differentiation marker genes as determined by α-SMA staining was pronounced in $G\alpha_{12}/G\alpha_{13}$-deficient but not in $G\alpha_q/G\alpha_{11}$-deficient VSMCs (Fig. 5 C). This further indicates a critical role of G_q/G_{11} and G_{12}/G_{13} signaling in the regulation of vascular Sm differentiation.

Sm-specific deficiency of $G\alpha_{12}/G\alpha_{13}$ promotes atherosclerotic plaque progression

As changes in vascular Sm differentiation may be involved in the pathogenesis of atherosclerosis (Dzau et al., 2002; Owens et al., 2004), we crossed Sm-$G\alpha_{12}/G\alpha_{13}$-KO mice with atherosclerosis-prone $ApoE^{-/-}$ mice. We did not analyze the effect of Sm-specific $G\alpha_q/G\alpha_{11}$ deficiency on atherosclerosis as any result would be confounded by the reduced vascular tone and blood pressure in Sm-$G\alpha_q/G\alpha_{11}$-KO mice (Wirth et al., 2008). After 12 wk of a high-fat diet, atherosclerotic lesions in ApoE-deficient Sm-$G\alpha_{12}/G\alpha_{13}$-KO mice compared with ApoE-deficient control mice were far more pronounced in terms of intimal plaque and media area (Fig. 6, A and B). In addition, we found total occlusions of the right common carotid artery in about a quarter of ApoE-deficient Sm-$G\alpha_{12}/G\alpha_{13}$-KO mice compared with none in the ApoE-deficient control mice. Consistent with the results obtained from carotid artery ligation and femoral artery injury, we observed a reduced α-SMA staining of the media in atherosclerotic vessels of Sm-12/13-KO mice (Fig. 6 C).

Immunostaining of atherosclerotic lesions of ApoE-deficient control mice and mice lacking $G\alpha_{12}/G\alpha_{13}$ in VSMCs with antibodies against α-SMA and against the proliferation marker Ki-67 revealed that the number of α-SMA–positive cells as well as the number of proliferating α-SMA–positive cells (Ki-67 and α-SMA double-positive cells) were significantly increased

Published November 5, 2012

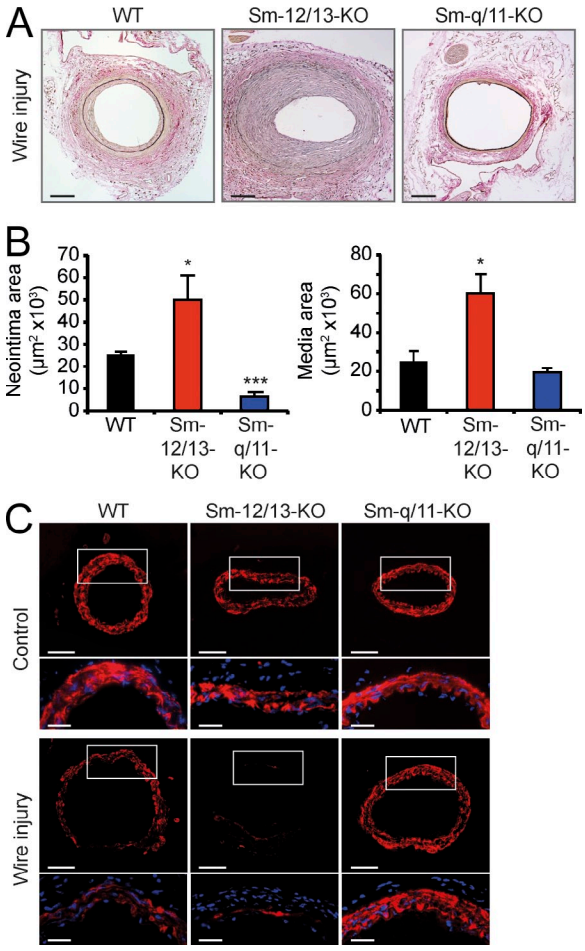

Figure 5. Effect of Sm-specific Gα deficiencies on vascular response to femoral artery injury. (A and B) 4 wk after femoral artery injury, femoral arteries from WT, Sm-12/13-KO, or Sm-q/11-KO mice were isolated and sectioned as described in Materials and methods. Shown are representative sections (A) and an evaluation of the neointima and media areas ($n = 4$; B). Shown are mean values ± SEM; *, $P < 0.05$; ***, $P < 0.001$ (compared with WT). (C) 7 d after femoral artery injury, femoral arteries from WT, Sm-12/13-KO, or Sm-q/11-KO mice were isolated. Shown are immunohistochemical analyses performed with an antibody against α-SMA. Boxes indicate magnified areas at the bottom of each panel. (A–C) Shown is one representative of at least three experiments. Bars: (A and C [top]) 100 µm; (C, bottom) 40 µm.

in lesions from Sm-specific $G\alpha_{12}/G\alpha_{13}$-deficient mice (Fig. 6, C and D). This suggests that lack of $G\alpha_{12}/G\alpha_{13}$ in VSMCs results in an increased propensity of α-SMA–positive cells in the atherosclerotic lesion to proliferate. Immunostaining with anti-CD68 antibodies revealed no significant differences in numbers of macrophages per plaque area in lesions from mice with Sm-specific $G\alpha_{12}/G\alpha_{13}$ deficiency compared with WT animals (Fig. 6 E).

DISCUSSION

VSMCs are highly plastic, and their dedifferentiation as well as their redifferentiation are thought to underlie many vascular remodeling processes. In this study, we show that the G proteins G_{12}/G_{13} and G_q/G_{11} antagonistically regulate VSMC plasticity in different models of vascular remodeling. Our data from mice lacking $G\alpha_{12}/G\alpha_{13}$ or their effector, the RhoGEF protein LARG, specifically in SMCs reveal the dramatic consequences of an imbalance in the activity of the two G protein–mediated pathways. The predominance of G_q/G_{11}- over G_{12}/G_{13}-LARG–mediated signaling promoted down-regulation of SMC differentiation marker genes and resulted in a highly abnormal phenotype of excessive vascular remodeling and exacerbation of atherosclerosis. In contrast, Sm-specific $G\alpha_q/G\alpha_{11}$ deficiency protected mice from neointimal hyperplasia in response to flow cessation or femoral artery injury.

Based on these findings, we conclude that G_{12}/G_{13}-mediated signaling is required to maintain VSMCs in a fully differentiated state and to prevent their unrestrained dedifferentiation in response to extracellular cues. Consistent with our observations, various vasoconstrictors acting through receptors coupled to both G_{12}/G_{13} and G_q/G_{11} such as thrombin, lysophosphatidic acid, thromboxane A_2, angiotensin-II, sphingosine-1-phosphate (S1P), or endothelin-1 have been reported to be capable of promoting the expression of Sm differentiation marker genes in vitro (Andrawis et al., 1996; Yoshida et al., 2004; Kim et al., 2009; Martin et al., 2009; Medlin et al., 2010). Our data from mice lacking $G\alpha_{12}/G\alpha_{13}$ or LARG specifically in SMCs suggest that $G\alpha_{12}/G\alpha_{13}$ promotes VSMC differentiation through LARG-mediated activation of RhoA. This is supported by in vitro data indicating that RhoA and LARG can mediate SMC differentiation (Lu et al., 2001; Mack et al., 2001; Gorenne et al., 2006; Medlin et al., 2010). In addition, evidence from cell-based studies shows that RhoA can induce SRF-dependent transcription of Sm differentiation marker genes through two distinct mechanisms, up-regulation of myocardin expression (Wamhoff et al., 2004; Yoshida et al., 2004; Martin et al., 2009) and facilitation of MRTF-A nuclear translocation (Miralles et al., 2003; Lockman et al., 2004; Jeon et al., 2008). Concordant with these data, we observed a down-regulation of myocardin expression in response to $G\alpha_{12}/G\alpha_{13}$ deletion in VSMCs in vivo. Moreover, our data show that G_{12}/G_{13}-LARG–mediated signaling is required for serum-induced nuclear translocation of MRTF-A. A precise analysis of the involvement of individual myocardin factors in the regulation of SMC differentiation has been difficult because of their overlapping expression and potential heterodimerization. Studies in mice lacking individual factors clearly indicate considerable functional redundancy in most types of VSMCs (Li et al., 2005; Oh et al., 2005; Pipes et al., 2005; Li et al., 2006; Sun et al., 2006). There are several effectors downstream of RhoA that can link RhoA to MRTFs such as Rho-kinase or mammalian homologue of diaphanous (mDia; Olson and Nordheim, 2010). A study using bone marrow chimeras has provided evidence that at least Rho-kinase subtype 1 in non-SMCs is involved in neointima formation (Noma et al., 2008); however, this study could not rule out a function of Rho-kinases in VSMCs. It is also possible that the RhoA-regulated actin nucleating protein mDia links G_{12}/G_{13}-RhoA to the regulation of

Published November 5, 2012

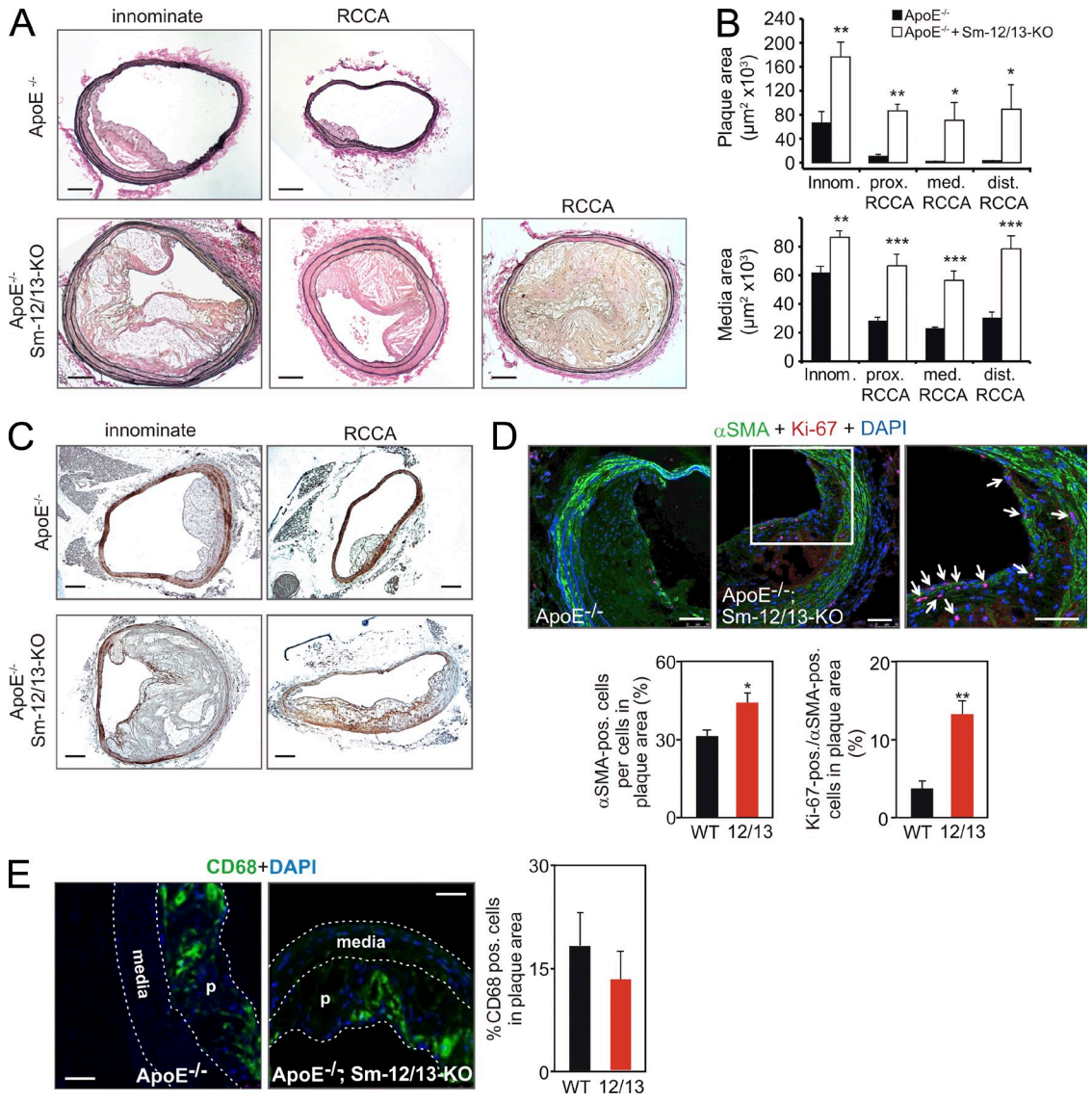

Figure 6. Increased plaque size in Sm-specific $G\alpha_{12}/G\alpha_{13}$-deficient mice lacking ApoE. (A and B) After 12 wk of a high-fat diet, the innominate and right common carotid arteries of $ApoE^{-/-}$ or $ApoE^{-/-}$;SMMHC-$CreER^{T2}$;$G\alpha_{12}{}^{-/-}$;$G\alpha_{13}{}^{flox/flox}$ ($ApoE^{-/-}$;Sm-12/13-KO) mice were isolated and analyzed histologically. (A) Shown are representative sections. (B) The plaque and media areas in animals of both genotypes were determined in innominate arteries at a distance of 1,000 µm from the aortic arch (innom.), in the right common carotid artery at a distance of 1,000 µm from the bifurcation of the innominate artery (prox. RCCA), at a distance of 1,000 µm from the bifurcation of the common carotid artery (dist. RCCA), or in between (med. RCCA; the data are representative for nine males and two independent experiments per group). (C) The innominate artery or right common carotid artery (RCCA) of $ApoE^{-/-}$ or $ApoE^{-/-}$;Sm-12/13-KO mice was isolated and stained with an anti–α-SMA antibody. (D) Atherosclerotic plaques from $ApoE^{-/-}$ or $ApoE^{-/-}$;Sm-12/13-KO mice were immunostained with antibodies against α-SMA and Ki-67. Shown are representative images. The right image is a magnification of the area indicated by the white box, and arrows point to α-SMA and Ki-67 double-positive cells. The bar graphs show a statistical evaluation of the number of α-SMA–positive cells per cells in the plaque area and the percentage of Ki-67–positive cells per α-SMA–positive cells in plaques from $ApoE^{-/-}$ (WT) and $ApoE^{-/-}$;Sm-12/13-KO mice (12/13; the data are representative for four males and two independent experiments per group). (E) Sections of atherosclerotic plaques from $ApoE^{-/-}$ or $ApoE^{-/-}$;Sm-12/13-KO mice were immunostained with antibodies against CD68. Shown are individual images counterstained with DAPI (media and plaques [p] are marked) as well as a bar graph showing the statistical evaluation of the percentage of CD68-positive cells in plaques of both groups of animals (the data are representative for six males and two independent experiments per group). Shown are mean values ± SEM; *, $P < 0.05$; **, $P < 0.01$; ***, $P < 0.001$. Bars: (A and C) 100 µm; (D and E) 50 µm.

SRF-mediated transcriptional events via MRTFs as it has been shown to promote actin polymerization and SMC-specific gene expression (Copeland and Treisman, 2002; Staus et al., 2007).

We found that the G_q/G_{11}-mediated signaling pathway in VSMCs mediates the expression of early response genes and the suppression of SMC differentiation marker gene expression, as well as proliferation in response to flow cessation and

Published November 5, 2012

vascular injury. In addition, our data indicate that this pathway involves activation of Erk1/2 as well as of its effector, the TCF Elk-1. This is consistent with earlier studies showing a central role for Erk in the regulation of TCFs (Treisman, 1994; Xi et al., 1997; Lockman et al., 2004). How G_q/G_{11} regulates Erk1/2 in VSMCs is not fully clear. In vitro studies and studies in other organ systems suggest that G_q/G_{11} can mediate Erk1/2 activation through transactivation of receptor tyrosine kinases (Hsieh et al., 2009) or by direct regulation of Erk1/2 through βγ-subunits released from G_q/G_{11} (Lorenz et al., 2009). In SMCs, several mechanisms have been described that link G_q/G_{11}-mediated signaling to the activation of RhoA (Guilluy et al., 2010; Wuertz et al., 2010; Momotani et al., 2011). However, $G\alpha_q/G\alpha_{11}$ deletion in VSMCs did not affect RhoA activity in our in vivo experiments, indicating that RhoA activation via G_q/G_{11} is not critically involved in vascular remodeling.

G_q/G_{11}- and G_{12}/G_{13}-mediated signaling pathways are able to increase myosin light chain phosphorylation and Sm tone through different mechanisms (Gohla et al., 2000; Somlyo and Somlyo, 2003; Maguire and Davenport, 2005; Wirth et al., 2008). In contrast to their synergistic function in vascular tone regulation, our data show that G_q/G_{11}- and G_{12}/G_{13}-mediated signaling pathways antagonistically regulate the differentiation state of VSMCs at sites of vascular dysfunction or injury. Interestingly, both the G_q/G_{11}-Erk1/2–mediated pathway mediating suppression of SMC-selective marker gene expression and proliferation as well as the G_{12}/G_{13}-Rho-mediated pathway, which promotes Sm differentiation, are activated in parallel in VSMCs shortly after induction of vascular injury. The net response of the vessel, which is also affected by other upstream signaling mechanisms involving integrins or receptor tyrosine kinases such as PDGFR-β (Ferns et al., 1991; Raines, 2000), is a dedifferentiation, which obviously requires intact G_q/G_{11}-mediated signaling. The parallel activation of the G_{12}/G_{13}-mediated pathway, which promotes Sm differentiation, therefore appears counterintuitive. However, activation of the G_{12}/G_{13}-RhoA–mediated pathway prevented excessive loss of SMC-selective marker gene expression and proliferation of VSMCs in the course of vascular remodeling and may facilitate the redifferentiation of VSMCs, once the influence of proliferative stimuli declines. Thus, a well-balanced parallel activation of antagonistic pathways promoting differentiation and dedifferentiation of VSMCs appears to be required for the adaptive response to vascular injury or to changing hemodynamics. Alternatively or in addition, the balance of G_q/G_{11}- and G_{12}/G_{13}-mediated signaling may be modulated in VSMCs during vascular remodeling by other factors such as regulators of G protein signaling, which have been shown to specifically affect G protein–mediated signaling in VSMCs (Heximer et al., 2003; Tang et al., 2003; Cho et al., 2008; Gunaje et al., 2011).

The receptors of most vasocontractile stimuli including angiotensin-II, S1P, thrombin, thromboxane A_2, or endothelin-1 are dually coupled to G_q/G_{11} and G_{12}/G_{13}, albeit some receptors show a certain preference (Maguire and Davenport, 2005). The question therefore arises as to whether receptor ligands can be used to modulate Sm differentiation under pathological conditions. Pharmacological approaches indicate that individual S1P receptor subtypes play antagonistic roles in the regulation of neointima formation (Wamhoff et al., 2008), and global loss of the S1P-receptor $S1P_2$, which efficiently couples to G_{12}/G_{13} (Chun et al., 2010), increases susceptibility to injury-induced neointima formation (Shimizu et al., 2007). Thus, activation or blockade of receptor subtypes preferentially coupled to either of the two G protein families may promote VSMC differentiation and dedifferentiation, respectively. To efficiently reduce vascular remodeling by preferential inhibition of G_q/G_{11}-mediated signaling, it may also be of interest to interfere directly with G_q/G_{11} or downstream signaling components. In addition, a preferential inhibition of G_q/G_{11}- or activation of G_{12}/G_{13}-mediated signaling in VSMCs could be achieved by receptor ligands, which act as allosteric modulators or biased agonists (Reiter et al., 2012; Valant et al., 2012) on procontractile GPCRs.

Our data show that G_q/G_{11} and G_{12}/G_{13}, which both mediate effects of procontractile stimuli in VSMCs, antagonistically regulate VSMC differentiation by controlling the recruitment of transcriptional cofactors by SRF. Our in vivo experiments in different models of vascular disorders indicate that the balanced activity of both pathways in VSMCs controls the remodeling response of the vessel in vascular diseases. The opposite regulation of SMC differentiation marker gene expression by the two pathways may allow for modulation of VSMC differentiation under pathological conditions by biased GPCR ligands or by inhibitors of G protein–mediated signaling processes.

MATERIALS AND METHODS

Materials. Phenylephrine, hydralazine, metoprolol, Alcian blue, and Accustain Elastic Stain were purchased from Sigma-Aldrich, DAPI was purchased from Invitrogen, and collagenases were purchased from Worthington Biochemical Corporation.

Genetic mouse models. The generation of SMMHC-CreER^{T2} mice as well as genotyping procedures and induction of Cre activity by tamoxifen have been described previously (Wirth et al., 2008). The generation of floxed or null alleles of genes encoding G protein α-subunits $G\alpha_q$ (Gnaq), $G\alpha_{11}$ (Gna11), $G\alpha_{12}$ (Gna12), $G\alpha_{13}$ (Gna13), or LARG (Arhgef12) as well as genotyping procedures have been described previously (Wettschureck et al., 2001; Moers et al., 2003; Herroeder et al., 2009). All animals were on a C57BL/6 background, and care and experimental procedures in this study were approved by the local authorities (Regierungspräsidia Darmstadt and Karlsruhe).

qRT-PCR. Snap-frozen carotid media samples, isolated 3 d after ligation and sham operation, respectively, were disrupted and homogenized at 4°C using a mixer bead mill. RNA was then extracted using the RNeasy Micro kit (QIAGEN) for mRNA and the miRNeasy kit (QIAGEN) for microRNA according to the manufacturer's instructions. 250 ng of total RNA was reverse transcribed using the Transcriptor High Fidelity kit (Roche). For microRNA, we used the NCode Vilo miRNA cDNA Synthesis kit (Invitrogen). Quantitative real-time PCR was performed with LightCycler 480 Probe Master (Roche) for mRNA analyses and LightCycler 480 SYBR Green Master (Roche) for microRNA analyses. Gene-specific RT-PCR primers were selected using the Roche ProbeFinder software. The relative

Published November 5, 2012

amount of target mRNA normalized to 18S and of microRNA normalized to S4.5 RNA was calculated as previously described (Pfaffl et al., 2001). Primer sequences are as follows: 18s, forward 5′-GCAATTATTCCCCATGAACG-3′, reverse 5′-GGGACTTAATCAACGCAAGC-3′, probe #48; Myh11, forward 5′-TGGAGGCCAAGATTGCAC-3′, reverse 5′-GGCCGCCTGTTTCTCTCT-3′, probe #68; Acta2, forward 5′-CCAGCACCATGAAGATCAAG-3′, reverse 5′-TGGAAGGTAGACAGCGAAGC-3′, probe #58; SM22-α, forward 5′-GCAGTGTGGCCCTGATGTA-3′, reverse 5′-TCACCAATTTGCTCAGAATCA-3′, probe #5; Cnn1, forward 5′-GAAGGTCAATGAGTCAACTCAGAA-3′, reverse 5′-CCATACTTGGTAATGGCTTTGA-3′, probe #78; Myocd, forward 5′-AGGCTCCTCTGGACACAATC-3′, reverse 5′-TCCCAGGGTCTGACTGGTT-3′, probe #20; Elk1, forward 5′-GCTCCCCACACATACCTTGA-3′, reverse 5′-GGGTGCAATTGGACTCAGA-3′, probe #50; Fos, forward 5′-GAAGGGGCAAAGTAGAGCAG-3′, reverse 5′-CAGCTCCCTCCTCCGATT-3′, probe #46; Ets1, forward 5′-ACTGTGTGCCCTGGGTAAAG-3′, reverse 5′-CCTGATATGGTTTCACATCCTCT-3′, probe #50; Egr1, forward 5′-CCTATGAGCACCTGACCACA-3′, reverse 5′-TCGTTTGGCTGGGATAACTC-3′, probe #22; 4.5s, universal forward 5′-GTACTGCGCGTGGAGAGGAATT-3′, reverse 5′-GTCCAAACTCTTGGGAAGCAGA-3′; miR-143, universal forward 5′-GTACTGCGCGTGGAGAGGAATT-3′, reverse 5′-TGAGATGAAGCACTGTAGCTCA-3′; and miR-145, universal forward 5′-GTACTGCGCGTGGAGAGGAATT-3′, reverse 5′-CAGTTTTCCCAGGAATCCCTT-3′.

Western blotting. Snap-frozen carotid media samples, isolated 3 d after ligation and sham operation, respectively, were homogenized on ice in lysis buffer, pH 8.0 containing 0.1 M Tris/HCl, 0.01 M EDTA, 10% SDS, 1× protease, and phosphatase inhibitor cocktail (Roche) using a handheld rotor–stator homogenizer (MM300; Retsch) and 3-mm stainless steel beads. The homogenates were centrifuged for 20 min at 10,000 *g* at 4°C to remove debris, and aliquots of the supernatants were assayed for total protein content by the BCA method (Thermo Fisher Scientific). Equal amounts of protein (10 µg per lane) were separated by 13% SDS-PAGE gels and transferred onto nitrocellulose membranes (Whatman; GE Healthcare). Immunoblotting was performed by using specific antibodies. In brief, polyclonal antisera against α-SM22 (Abcam), α-SMA (Abcam), and monoclonal antibody against α-tubulin (Sigma-Aldrich) were used. All primary antibodies were used at 1:200 dilutions, except for anti–α-tubulin, which was used at 1:3,000 dilutions. Secondary antibodies (1:3,000 dilutions) were from Cell Signaling Technology (goat anti–rabbit HRP and goat anti–mouse HRP). Immunoreactive proteins were visualized with corresponding HRP-conjugated secondary antibodies using a commercially available kit (Immobilon Western; Millipore) and developed through exposure to x-ray film.

Determination of RhoA activity. Snap-frozen carotid media samples, isolated 24 h after ligation or sham operation, respectively, were disrupted and homogenized at 4°C using a mixer bead mill. Total protein concentrations where measured and equalized with lysis buffer. RhoA activity, determined by the amount of GTP-loaded RhoA, was then assessed using an absorbance-based ELISA-kit (G-LISA RhoA Activation Assay; Cytoskeleton) according to the manufacturer's instructions. RhoA activity was expressed in relative units with the absorbance of sham-operated WT vessels serving as reference.

Carotid artery ligation. Male mice at 12 wk of age were anesthetized, and left and right common carotid arteries were dissected after a midline incision of the neck. Distal ligation of the left common carotid artery was performed with a 7/0 silk thread (Serag-Wiessner).

Wire injury. Male mice underwent femoral artery dilation at the age of 12 wk. After induction of anesthesia, a medial skin incision of the hind limb thigh was performed, and the femoral as well as the profunda femoris artery were dissected. Using 6/0 silk thread (Fine Science Tools) a loop was placed at the proximal femoral artery, and tension was applied to disrupt blood flow. A straight spring wire (diameter 0.38 mm; Cook) was introduced into the femoral artery via transverse arteriotomy of the profunda femoris artery. The wire was advanced ∼5 mm proximally and left in place for 1 min to dilate the femoral artery. After removal of the wire and ligation of the profunda femoris branch, blood flow was reconstituted.

Atherosclerosis. To obtain Sm-specific Gα deficiency in ApoE$^{-/-}$ mice, ApoE$^{-/-}$ animals were crossed with tamoxifen-inducible Sm-Gα_{12}/Gα_{13}-KO mice. The offspring were then intercrossed. ApoE$^{-/-}$ mice without or with inducible Sm-specific Gα_{12}/Gα_{13} deficiency were treated with tamoxifen at an age of 6 wk. At the age of 8 wk, a high-fat diet was started and continued for 12 wk. Thereafter, animals were sacrificed, and atherosclerotic lesions were analyzed as described under Histology and immunohistochemistry.

Telemetric blood pressure measurements and myography. Telemetry experiments were performed as described previously (Wirth et al., 2008). A 10–15% decrease in mean arterial blood pressure was induced pharmacologically by application of 500 mg/liter hydralazine or 2.5 g/liter metoprolol in the drinking water. Treatment was started 7 d before and continued throughout the experiments. For isometric tension recordings, common carotid arteries were isolated after euthanization and PBS perfusion of mice. 3-mm-long carotid segments were prepared, mounted on a conventional myograph setup (610-M; Danish Myo Technology), and myography was performed as described previously (Wirth et al., 2008). Individual experiments were performed at least three times.

Histology and immunohistochemistry. For histology, vessels were perfused and fixed in 4% PFA overnight. Vessels were then dehydrated using increasing concentrations of ethanol and embedded in paraffin. Paraffin-embedded arteries were cut in 5-µm serial cross sections, and predefined sections (see below) were mounted on slides and stained with Accustain Elastic Stain according to the manufacturer's instructions. In ligated left common carotid arteries, cross sections from four predefined proximal distances from the ligation site (250, 1,000, 2,000, and 3,000 µm) were analyzed. In sham-operated right common carotid arteries, sections from within ∼1,000-µm distance to the bifurcation of internal and external carotid artery were analyzed. Femoral arteries were analyzed 4 wk after injury. Within the injured distal region (5,000 µm) of the left femoral artery, cross sections were analyzed in regular intervals of 1,000 µm to calculate a vessel mean for each parameter. Sections from the distal part of the contralateral right femoral artery (i.e., within ≈1,000 µm distance to the branching of the profunda femoris artery) were analyzed as an internal control. For the analysis of atherosclerotic vessels, cross sections of the innominate artery and right common carotid artery were analyzed. Photoshop CS5 extended software (Adobe) was used to measure circumferences of internal elastic lamina, external elastic lamina, and lumen, as well as medial, intimal, and luminal cross-sectional areas. Staining with Alcian blue was performed according to the manufacturer's instructions.

For immunohistochemistry of paraffin sections, sections were dewaxed, rehydrated, and subsequently boiled for 18 min in 10 mM Tris/1 mM EDTA buffer, pH 9.0, for epitope retrieval. After 10-min incubation in 3% H_2O_2, sections were blocked in PBS supplemented with 5% normal goat serum for 2 h. After overnight incubation at 4°C with rabbit monoclonal anti–phospho-ERK1/2 (1:100; Cell Signaling Technology), rabbit polyclonal anti-phospho–Elk-1 (1:100; Cell Signaling Technology), or polyclonal rabbit anti–Sm α-actin (1:200; Abcam), primary antibodies were detected with biotinylated antibody to rabbit IgG followed by incubation with Avidin–Biotin complex reagent (Vectastain ABC System; Vector Laboratories) according to the manufacturer's instructions. Staining was visualized using a diaminobenzidine (DAB) peroxidase substrate kit (Vector Laboratories) according to the manufacturer's instructions, followed by counterstaining with hematoxylin for detection of nuclei where indicated. Immunostaining of phosphorylated Erk1/2 and phosphorylated Elk-1 was performed in carotid arteries that were harvested 24 h after carotid artery ligation. The fraction of positively stained medial area (phospho-Erk1/2) or positively stained nuclei (phospho–Elk-1)

Published November 5, 2012

was quantified using Photoshop CS5 Extended software (Adobe). The threshold for positive staining was (pre)defined by an independent observer who was blinded to the treatment.

For cryoimmunohistochemistry, vessels were embedded in Tissue-Tek O.C.T. freezing medium, snap frozen in liquid nitrogen, and stored at −80°C until sectioning. Immunostaining of cryosections was performed using a rabbit anti-CD3 (clone SP7; 1:100; Abcam) or Alexa Fluor 488–conjugated rat anti-CD68 (clone FA-11; 1:100; AbD Serotec). After a 10-min fixation with 4% PFA and several washing steps with PBS, cryosections were incubated with primary antibodies at 4°C overnight followed by either CF555- or CF488-labeled anti–rabbit secondary antibody (1:300; Biotium) and counterstained with cy3- or FITC-conjugated anti–Sm α-actin antibody (1:300; Sigma-Aldrich) and DAPI. This protocol was adapted for Ki67 staining by a 20-min fixation with 4% PFA and an antigen retrieval in citrate buffer (20 min boiling). Overnight incubation of primary antibody anti–mouse Ki67 (clone TEC-3; 1:20; Dako) was followed by 1-h Cy3-conjugated anti–rat IgG (1:300; Millipore) incubation. Sections were viewed with a confocal microscope (SP5; Leica).

Primary VSMC culture and immunocytochemistry. Primary VSMCs were isolated using a modified enzymatic digestion method based on Ray et al. (2001). 2 wk after tamoxifen induction, left and right common carotid arteries were isolated, perivascular tissue was removed, and vessels were cut into square pieces of ∼1-mm edge length, which were transferred into 5-ml tubes containing 1 mg/ml collagenase type II and 0.5 mg/ml elastase (both Worthington Biochemical Corporation) diluted in 500 µl serum-free DMEM. Tubes were incubated at 37°C, 5% CO_2 for 3.5 h. To stop digestion, complete DMEM, i.e., supplemented with 10% FBS (Gibco), 2 mM L-glutamine, and 100 U/ml penicillin/streptomycin, was added. After centrifugation at 3,000 *g* for 5 min, cells were resuspended in 700 µl complete DMEM containing 2 µg/ml amphotericin B (Sigma-Aldrich) and plated on a single well of a 24-well plate. The following day, medium was changed to amphotericin-free medium. For immunocytochemistry, cells at passage 3 or 4 were plated on coverslips in 12-well plates and grown to confluency. After 48 h of starvation in serum-free medium, cells were stimulated for 1 h with complete DMEM containing 20% FBS. Cells were then rinsed with PBS, fixed with 4% PFA for 10 min, and blocked for 30 min at room temperature in 0.2% Triton/2 mg/ml bovine serum albumin. Cells were then incubated with rabbit polyclonal anti–MRTF-A antibody (1:200; Santa Cruz Biotechnology, Inc.). After extensive washing with PBS, cells were incubated with an Alexa Fluor 488–conjugated secondary antibody (1:200; anti-rabbit IgG; Invitrogen) for visualization, followed by 30-min incubation with DAPI (1:1,000; Invitrogen) for detection of nuclei.

Statistical analyses. All values are expressed as mean ± SEM. Statistical comparison of two groups was performed using the unpaired Student's *t* test with p-values < 0.05 considered statistically significant. If not stated otherwise, individual KOs (Sm-q/11-KO, LARG-KO, or Sm-12/13-KO) were only compared with WTs.

We wish to thank Svea Hümmer for excellent secretarial help.

This work was supported by the Transregional Collaborative Research Center 23 (SFB/TR23) of the German Research Foundation.

The authors declare no competing financial interests.

Submitted: 13 February 2012
Accepted: 4 October 2012

REFERENCES

Andrawis, N.S., E. Wang, and D.R. Abernethy. 1996. Endothelin-1 induces an increase in total protein synthesis and expression of the smooth muscle alpha-actin gene in vascular smooth muscle cells. *Life Sci.* 59:523–528. http://dx.doi.org/10.1016/0024-3205(96)00332-3

Cho, H., C. Park, I.Y. Hwang, S.B. Han, D. Schimel, D. Despres, and J.H. Kehrl. 2008. Rgs5 targeting leads to chronic low blood pressure and a lean body habitus. *Mol. Cell. Biol.* 28:2590–2597. http://dx.doi.org/10.1128/MCB.01889-07

Chun, J., T. Hla, K.R. Lynch, S. Spiegel, and W.H. Moolenaar. 2010. International Union of Basic and Clinical Pharmacology. LXXVIII. Lysophospholipid receptor nomenclature. *Pharmacol. Rev.* 62:579–587. http://dx.doi.org/10.1124/pr.110.003111

Copeland, J.W., and R. Treisman. 2002. The diaphanous-related formin mDia1 controls serum response factor activity through its effects on actin polymerization. *Mol. Biol. Cell.* 13:4088–4099. http://dx.doi.org/10.1091/mbc.02-06-0092

Dzau, V.J., R.C. Braun-Dullaeus, and D.G. Sedding. 2002. Vascular proliferation and atherosclerosis: new perspectives and therapeutic strategies. *Nat. Med.* 8:1249–1256. http://dx.doi.org/10.1038/nm1102-1249

Ferns, G.A., E.W. Raines, K.H. Sprugel, A.S. Motani, M.A. Reidy, and R. Ross. 1991. Inhibition of neointimal smooth muscle accumulation after angioplasty by an antibody to PDGF. *Science.* 253:1129–1132. http://dx.doi.org/10.1126/science.1653454

Gohla, A., G. Schultz, and S. Offermanns. 2000. Role for G(12)/G(13) in agonist-induced vascular smooth muscle cell contraction. *Circ. Res.* 87:221–227. http://dx.doi.org/10.1161/01.RES.87.3.221

Gorenne, I., L. Jin, T. Yoshida, J.M. Sanders, I.J. Sarembock, G.K. Owens, A.P. Somlyo, and A.V. Somlyo. 2006. LPP expression during in vitro smooth muscle differentiation and stent-induced vascular injury. *Circ. Res.* 98:378–385. http://dx.doi.org/10.1161/01.RES.0000202802.34727.fd

Guilluy, C., J. Brégeon, G. Toumaniantz, M. Rolli-Derkinderen, K. Retailleau, L. Loufrani, D. Henrion, E. Scalbert, A. Bril, R.M. Torres, et al. 2010. The Rho exchange factor Arhgef1 mediates the effects of angiotensin II on vascular tone and blood pressure. *Nat. Med.* 16:183–190. http://dx.doi.org/10.1038/nm.2079

Gunaje, J.J., A.J. Bahrami, S.M. Schwartz, G. Daum, and W.M. Mahoney Jr. 2011. PDGF-dependent regulation of regulator of G protein signaling-5 expression and vascular smooth muscle cell functionality. *Am. J. Physiol. Cell Physiol.* 301:C478–C489. http://dx.doi.org/10.1152/ajpcell.00348.2010

Herroeder, S., P. Reichardt, A. Sassmann, B. Zimmermann, D. Jaeneke, J. Hoeckner, M.W. Hollmann, K.D. Fischer, S. Vogt, R. Grosse, et al. 2009. Guanine nucleotide-binding proteins of the G12 family shape immune functions by controlling CD4+ T cell adhesiveness and motility. *Immunity.* 30:708–720. http://dx.doi.org/10.1016/j.immuni.2009.02.010

Heximer, S.P., R.H. Knutsen, X. Sun, K.M. Kaltenbronn, M.H. Rhee, N. Peng, A. Oliveira-dos-Santos, J.M. Penninger, A.J. Muslin, T.H. Steinberg, et al. 2003. Hypertension and prolonged vasoconstrictor signaling in RGS2-deficient mice. *J. Clin. Invest.* 111:1259.

Hsieh, H.L., W.H. Tung, C.Y. Wu, H.H. Wang, C.C. Lin, T.S. Wang, and C.M. Yang. 2009. Thrombin induces EGF receptor expression and cell proliferation via a PKC(delta)/c-Src-dependent pathway in vascular smooth muscle cells. *Arterioscler. Thromb. Vasc. Biol.* 29:1594–1601. http://dx.doi.org/10.1161/ATVBAHA.109.185801

Jeon, E.S., W.S. Park, M.J. Lee, Y.M. Kim, J. Han, and J.H. Kim. 2008. A Rho kinase/myocardin-related transcription factor-A-dependent mechanism underlies the sphingosylphosphorylcholine-induced differentiation of mesenchymal stem cells into contractile smooth muscle cells. *Circ. Res.* 103:635–642. http://dx.doi.org/10.1161/CIRCRESAHA.108.180885

Kim, M.R., E.S. Jeon, Y.M. Kim, J.S. Lee, and J.H. Kim. 2009. Thromboxane a(2) induces differentiation of human mesenchymal stem cells to smooth muscle-like cells. *Stem Cells.* 27:191–199. http://dx.doi.org/10.1634/stemcells.2008-0363

Li, J., X. Zhu, M. Chen, L. Cheng, D. Zhou, M.M. Lu, K. Du, J.A. Epstein, and M.S. Parmacek. 2005. Myocardin-related transcription factor B is required in cardiac neural crest for smooth muscle differentiation and cardiovascular development. *Proc. Natl. Acad. Sci. USA.* 102:8916–8921. http://dx.doi.org/10.1073/pnas.0503741102

Li, S., S. Chang, X. Qi, J.A. Richardson, and E.N. Olson. 2006. Requirement of a myocardin-related transcription factor for development of mammary myoepithelial cells. *Mol. Cell. Biol.* 26:5797–5808. http://dx.doi.org/10.1128/MCB.00211-06

Lockman, K., J.S. Hinson, M.D. Medlin, D. Morris, J.M. Taylor, and C.P. Mack. 2004. Sphingosine 1-phosphate stimulates smooth muscle cell differentiation and proliferation by activating separate serum response factor co-factors. *J. Biol. Chem.* 279:42422–42430. http://dx.doi.org/10.1074/jbc.M405432200

Lorenz, K., J.P. Schmitt, E.M. Schmitteckert, and M.J. Lohse. 2009. A new type of ERK1/2 autophosphorylation causes cardiac hypertrophy. *Nat. Med.* 15:75–83. http://dx.doi.org/10.1038/nm.1893

Lu, J., T.E. Landerholm, J.S. Wei, X.R. Dong, S.P. Wu, X. Liu, K. Nagata, M. Inagaki, and M.W. Majesky. 2001. Coronary smooth muscle differentiation from proepicardial cells requires rhoA-mediated actin reorganization and p160 rho-kinase activity. *Dev. Biol.* 240:404–418. http://dx.doi.org/10.1006/dbio.2001.0403

Mack, C.P. 2011. Signaling mechanisms that regulate smooth muscle cell differentiation. *Arterioscler. Thromb. Vasc. Biol.* 31:1495–1505. http://dx.doi.org/10.1161/ATVBAHA.110.221135

Mack, C.P., A.V. Somlyo, M. Hautmann, A.P. Somlyo, and G.K. Owens. 2001. Smooth muscle differentiation marker gene expression is regulated by RhoA-mediated actin polymerization. *J. Biol. Chem.* 276:341–347. http://dx.doi.org/10.1074/jbc.M005505200

Maguire, J.J., and A.P. Davenport. 2005. Regulation of vascular reactivity by established and emerging GPCRs. *Trends Pharmacol. Sci.* 26:448–454.

Martin, K., S. Weiss, P. Metharom, J. Schmeckpeper, B. Hynes, J. O'Sullivan, and N. Caplice. 2009. Thrombin stimulates smooth muscle cell differentiation from peripheral blood mononuclear cells via protease-activated receptor-1, RhoA, and myocardin. *Circ. Res.* 105:214–218. http://dx.doi.org/10.1161/CIRCRESAHA.109.199984

Medlin, M.D., D.P. Staus, A.D. Dubash, J.M. Taylor, and C.P. Mack. 2010. Sphingosine 1-phosphate receptor 2 signals through leukemia-associated RhoGEF (LARG), to promote smooth muscle cell differentiation. *Arterioscler. Thromb. Vasc. Biol.* 30:1779–1786. http://dx.doi.org/10.1161/ATVBAHA.110.209395

Miano, J.M., X. Long, and K. Fujiwara. 2007. Serum response factor: master regulator of the actin cytoskeleton and contractile apparatus. *Am. J. Physiol. Cell Physiol.* 292:C70–C81. http://dx.doi.org/10.1152/ajpcell.00386.2006

Miralles, F., G. Posern, A.I. Zaromytidou, and R. Treisman. 2003. Actin dynamics control SRF activity by regulation of its coactivator MAL. *Cell.* 113:329–342. http://dx.doi.org/10.1016/S0092-8674(03)00278-2

Moers, A., B. Nieswandt, S. Massberg, N. Wettschureck, S. Grüner, I. Konrad, V. Schulte, B. Aktas, M.P. Gratacap, M.I. Simon, et al. 2003. G13 is an essential mediator of platelet activation in hemostasis and thrombosis. *Nat. Med.* 9:1418–1422. http://dx.doi.org/10.1038/nm943

Momotani, K., M.V. Artamonov, D. Utepbergenov, U. Derewenda, Z.S. Derewenda, and A.V. Somlyo. 2011. p63RhoGEF couples Gα(q/11)-mediated signaling to Ca2+ sensitization of vascular smooth muscle contractility. *Circ. Res.* 109:993–1002. http://dx.doi.org/10.1161/CIRCRESAHA.111.248898

Noma, K., Y. Rikitake, N. Oyama, G. Yan, P. Alcaide, P.Y. Liu, H. Wang, D. Ahl, N. Sawada, R. Okamoto, et al. 2008. ROCK1 mediates leukocyte recruitment and neointima formation following vascular injury. *J. Clin. Invest.* 118:1632–1644. http://dx.doi.org/10.1172/JCI29226

Oh, J., J.A. Richardson, and E.N. Olson. 2005. Requirement of myocardin-related transcription factor-B for remodeling of branchial arch arteries and smooth muscle differentiation. *Proc. Natl. Acad. Sci. USA.* 102:15122–15127. http://dx.doi.org/10.1073/pnas.0507346102

Olson, E.N., and A. Nordheim. 2010. Linking actin dynamics and gene transcription to drive cellular motile functions. *Nat. Rev. Mol. Cell Biol.* 11:353–365. http://dx.doi.org/10.1038/nrm2890

Owens, G.K. 1995. Regulation of differentiation of vascular smooth muscle cells. *Physiol. Rev.* 75:487–517.

Owens, G.K. 2007. Molecular control of vascular smooth muscle cell differentiation and phenotypic plasticity. *Novartis Found. Symp.* 283:174–191, discussion :191–193: 238–241. http://dx.doi.org/10.1002/9780470319413.ch14

Owens, G.K., M.S. Kumar, and B.R. Wamhoff. 2004. Molecular regulation of vascular smooth muscle cell differentiation in development and disease. *Physiol. Rev.* 84:767–801. http://dx.doi.org/10.1152/physrev.00041.2003

Parmacek, M.S. 2007. Myocardin-related transcription factors: critical coactivators regulating cardiovascular development and adaptation. *Circ. Res.* 100:633–644. http://dx.doi.org/10.1161/01.RES.0000259563.61091.e8

Pfaffl, M.W. 2001. A new mathematical model for relative quantification in real-time RT-PCR. *Nucleic Acids Res.* 29:e45. http://dx.doi.org/10.1093/nar/29.9.e45

Pipes, G.C., S. Sinha, X. Qi, C.H. Zhu, T.D. Gallardo, J. Shelton, E.E. Creemers, L. Sutherland, J.A. Richardson, D.J. Garry, et al. 2005. Stem cells and their derivatives can bypass the requirement of myocardin for smooth muscle gene expression. *Dev. Biol.* 288:502–513. http://dx.doi.org/10.1016/j.ydbio.2005.10.014

Pipes, G.C., E.E. Creemers, and E.N. Olson. 2006. The myocardin family of transcriptional coactivators: versatile regulators of cell growth, migration, and myogenesis. *Genes Dev.* 20:1545–1556. http://dx.doi.org/10.1101/gad.1428006

Posern, G., and R. Treisman. 2006. Actin' together: serum response factor, its cofactors and the link to signal transduction. *Trends Cell Biol.* 16:588–596. http://dx.doi.org/10.1016/j.tcb.2006.09.008

Raines, E.W. 2000. The extracellular matrix can regulate vascular cell migration, proliferation, and survival: relationships to vascular disease. *Int. J. Exp. Pathol.* 81:173–182. http://dx.doi.org/10.1046/j.1365-2613.2000.00155.x

Ray, J.L., R. Leach, J.M. Herbert, and M. Benson. 2001. Isolation of vascular smooth muscle cells from a single murine aorta. *Methods Cell Sci.* 23:185–188. http://dx.doi.org/10.1023/A:1016357510143

Reiter, E., S. Ahn, A.K. Shukla, and R.J. Lefkowitz. 2012. Molecular mechanism of β-arrestin-biased agonism at seven-transmembrane receptors. *Annu. Rev. Pharmacol. Toxicol.* 52:179–197. http://dx.doi.org/10.1146/annurev.pharmtox.010909.105800

Shimizu, T., T. Nakazawa, A. Cho, F. Dastvan, D. Shilling, G. Daum, and M.A. Reidy. 2007. Sphingosine 1-phosphate receptor 2 negatively regulates neointimal formation in mouse arteries. *Circ. Res.* 101:995–1000. http://dx.doi.org/10.1161/CIRCRESAHA.107.159228

Somlyo, A.P., and A.V. Somlyo. 2003. Ca2+ sensitivity of smooth muscle and nonmuscle myosin II: modulated by G proteins, kinases, and myosin phosphatase. *Physiol. Rev.* 83:1325–1358.

Staus, D.P., A.L. Blaker, J.M. Taylor, and C.P. Mack. 2007. Diaphanous 1 and 2 regulate smooth muscle cell differentiation by activating the myocardin-related transcription factors. *Arterioscler. Thromb. Vasc. Biol.* 27:478–486. http://dx.doi.org/10.1161/01.ATV.0000255559.77687.c1

Sun, Y., K. Boyd, W. Xu, J. Ma, C.W. Jackson, A. Fu, J.M. Shillingford, G.W. Robinson, L. Hennighausen, J.K. Hitzler, et al. 2006. Acute myeloid leukemia-associated Mkl1 (Mrtf-a) is a key regulator of mammary gland function. *Mol. Cell. Biol.* 26:5809–5826. http://dx.doi.org/10.1128/MCB.00024-06

Tang, K.M., G.R. Wang, P. Lu, R.H. Karas, M. Aronovitz, S.P. Heximer, K.M. Kaltenbronn, K.J. Blumer, D.P. Siderovski, Y. Zhu, and M.E. Mendelsohn. 2003. Regulator of G-protein signaling-2 mediates vascular smooth muscle relaxation and blood pressure. *Nat. Med.* 9:1506–1512. (published erratum appears in *Nat. Med.* 2004. 10:105) http://dx.doi.org/10.1038/nm958

Treisman, R. 1994. Ternary complex factors: growth factor regulated transcriptional activators. *Curr. Opin. Genet. Dev.* 4:96–101. http://dx.doi.org/10.1016/0959-437X(94)90097-3

Valant, C., J. Robert Lane, P.M. Sexton, and A. Christopoulos. 2012. The best of both worlds? Bitopic orthosteric/allosteric ligands of g protein-coupled receptors. *Annu. Rev. Pharmacol. Toxicol.* 52:153–178. http://dx.doi.org/10.1146/annurev-pharmtox-010611-134514

Wamhoff, B.R., D.K. Bowles, O.G. McDonald, S. Sinha, A.P. Somlyo, A.V. Somlyo, and G.K. Owens. 2004. L-type voltage-gated Ca2+ channels modulate expression of smooth muscle differentiation marker genes via a rho kinase/myocardin/SRF-dependent mechanism. *Circ. Res.* 95:406–414. http://dx.doi.org/10.1161/01.RES.0000138582.36921.9e

Wamhoff, B.R., K.R. Lynch, T.L. Macdonald, and G.K. Owens. 2008. Sphingosine-1-phosphate receptor subtypes differentially regulate smooth muscle cell phenotype. *Arterioscler. Thromb. Vasc. Biol.* 28:1454–1461. http://dx.doi.org/10.1161/ATVBAHA.107.159392

Wang, Z., D.Z. Wang, D. Hockemeyer, J. McAnally, A. Nordheim, and E.N. Olson. 2004. Myocardin and ternary complex factors compete for SRF to control smooth muscle gene expression. *Nature.* 428:185–189. http://dx.doi.org/10.1038/nature02382

Wettschureck, N., H. Rütten, A. Zywietz, D. Gehring, T.M. Wilkie, J. Chen, K.R. Chien, and S. Offermanns. 2001. Absence of pressure overload induced myocardial hypertrophy after conditional inactivation of Galphaq/Galpha11 in cardiomyocytes. *Nat. Med.* 7:1236–1240. http://dx.doi.org/10.1038/nm1101-1236

Wirth, A., Z. Benyó, M. Lukasova, B. Leutgeb, N. Wettschureck, S. Gorbey, P. Orsy, B. Horváth, C. Maser-Gluth, E. Greiner, et al. 2008. G12-G13-LARG-mediated signaling in vascular smooth muscle is required for salt-induced hypertension. *Nat. Med.* 14:64–68. http://dx.doi.org/10.1038/nm1666

Wuertz, C.M., A. Lorincz, C. Vettel, M.A. Thomas, T. Wieland, and S. Lutz. 2010. p63RhoGEF—a key mediator of angiotensin II-dependent signaling and processes in vascular smooth muscle cells. *FASEB J.* 24:4865–4876.PubMed http://dx.doi.org/10.1096/fj.10-155499

Xi, X.P., K. Graf, S. Goetze, W.A. Hsueh, and R.E. Law. 1997. Inhibition of MAP kinase blocks insulin-mediated DNA synthesis and transcriptional activation of c-fos by Elk-1 in vascular smooth muscle cells. *FEBS Lett.* 417:283–286. http://dx.doi.org/10.1016/S0014-5793(97)01303-3

Yoshida, T., M.H. Hoofnagle, and G.K. Owens. 2004. Myocardin and Prx1 contribute to angiotensin II-induced expression of smooth muscle alpha-actin. *Circ. Res.* 94:1075–1082. http://dx.doi.org/10.1161/01.RES.0000125622.46280.95

2.2 Die Alters-abhängige Blutdruckerhöhung ist bedingt durch eine G-Protein-vermittelte Steigerung des Tonus glatter Gefäßmuskelzellen

Age-dependent blood pressure elevation is due to increased vascular smooth muscle tone mediated by G-protein signaling. Wirth A, Wang S, Takefuji M, Tang C, **Althoff TF**, Schweda F, Wettschureck N, Offermanns S. *Cardiovasc Res*. 2016 Jan 1;109(1):131-40.

https://doi.org/10.1093/cvr/cvv249

„Arterieller Bluthochdruck ist ein entscheidender Risikofaktor für kardiovaskuläre Erkrankungen. Dabei steht die Niere und ihre natriuretische Funktion im Zentrum gängiger Erklärungsmodelle zur Pathogenese des Bluthochdrucks; allerdings bleibt der genaue Mechanismus der zum erhöhten Blutdruck führt, bei den meisten Patienten ungeklärt (essenzieller Hypertonus). Die Entwicklung des Bluthochdrucks korreliert stark mit dem Lebensalter, wobei der Blutdruckanstieg sich typischerweise in der vierten Lebensdekade beschleunigt. Auch die Ursache der Alters-abhängigen Blutdrucksteigerung ist nur unzureichend verstanden. Diese Studie untersucht nun die Rolle prokontraktiler G-Protein-abhängiger Signalwege in glatten Gefäßmuskelzellen beim Alters-abhängigen Bluthochdruck.

Vergleichbar mit Menschen mittleren Alters, haben wir bei 1 Jahr-alten Mäusen deutlich gesteigerte Blutdruckwerte, ohne Anhalt für erhöhte Gefäßsteifigkeit, eingeschränkte Nierenfunktion oder endokrine Besonderheiten beobachtet. Allerdings zeigten die Mäuse fortgeschrittenen Alters Zeichen einer endothelialen Dysfunktion sowie eine erhöhte Generation reaktiver Sauerstoffspezies (ROS) und eine gesteigerte endotheliale Endothelin-1 (ET1)-Expression. Der Alters-abhängige Blutdruck ließ sich durch Endothelin-Rezeptor A (ETA)-Antagonisten ebenso normalisieren wie durch Glattmuskel-spezifische ETA-Inaktivierung. Auch die akute Unterbrechung der nachgeschalteten, G-Protein-abhängigen Signalwege durch Induktion einer Glattmuskel-spezifischen $G\alpha_{12}/G\alpha_{13}$-, $G\alpha_q/G\alpha_{11}$- oder LARG-Defizienz mittels Tamoxifen-induzierbarer-Mausmodelle konnte die Alters-abhängige Blutdruckerhöhung unterbinden. Interessanterweise führte die Induktion einer ETA-Rezeptor-Defizienz trotz anhaltender endothelialer Dysfunktion zu einer Blutdruck-Normalisierung.

So scheint der Alters-abhängige Bluthochdruck durch eine hoch-reversible Aktivierung prokontraktiler G-Protein-abhängiger Signalwege in glatten Muskelzellen bedingt zu sein, was auf den Gefäßtonus als primären Faktor bei der Enstehung des essenziellen Bluthochdrucks hindeutet.“ Übersetzung durch den Autor.

Cardiovascular Research (2016) **109**, 131–140
doi:10.1093/cvr/cvv249

Age-dependent blood pressure elevation is due to increased vascular smooth muscle tone mediated by G-protein signalling

Angela Wirth[1,2]*, Shengpeng Wang[1], Mikito Takefuji[1], Cong Tang[1], Till F. Althoff[1], Frank Schweda[3], Nina Wettschureck[1,4], and Stefan Offermanns[1,4]*

[1]Department of Pharmacology, Max-Planck-Institute for Heart and Lung Research, Ludwigstr. 43, 61231 Bad Nauheim, Germany; [2]Institute of Pharmacology, University of Heidelberg, ImNeuenheimer Feld 366, 69120 Heidelberg, Germany; [3]Institute of Physiology, University of Regensburg, 93053 Regensburg, Germany; and [4]Medical Faculty, Goethe University Frankfurt, 60590 Frankfurt am Main, Germany

Received 7 April 2015; revised 27 October 2015; accepted 29 October 2015; online publish-ahead-of-print 4 November 2015

Time for primary review: 28 days

Aims Arterial hypertension is a major risk factor for cardiovascular diseases. The kidney and its natriuretic function are in the centre of the prevailing models to explain the pathogenesis of hypertension; however, the mechanisms underlying blood pressure elevation remain unclear in most patients. Development of hypertension is strongly correlated with age, and this blood pressure increase typically accelerates in the fourth decade of life. The cause of age-dependent blood pressure elevation is poorly understood. This study aims to understand the role of procontractile G-protein-mediated signalling pathways in vascular smooth muscle in age-dependent hypertension.

Methods and results Similar to humans at mid-life, we observed in 1-year-old mice elevated blood pressure levels without any evidence for increased vessel stiffness, impaired renal function, or endocrine abnormalities. Hypertensive aged mice showed signs of endothelial dysfunction and had an increased vascular formation of reactive oxygen species (ROS) and elevated endothelial ET-1 expression. Age-dependent hypertension could be normalized by ET_A receptor blockade, smooth muscle-specific inactivation of the gene encoding the ET_A receptor, as well as by acute disruption of downstream signalling via induction of smooth muscle-specific $G\alpha_{12}/G\alpha_{13}$, $G\alpha_q/G\alpha_{11}$, or LARG deficiency using tamoxifen-inducible smooth muscle-specific conditional mouse knock-out models. Induction of smooth muscle-specific ET_A receptor deficiency normalized the blood pressure in aged mice despite the continuous presence of signs of endothelial dysfunction.

Conclusion Age-dependent blood pressure elevation is due to a highly reversible activation of procontractile signalling in vascular smooth muscle cells indicating that increased vascular tone can be a primary factor in the development of hypertension.

Keywords Ageing • Blood pressure • Endothelin • Hypertension • Smooth muscle

1. Introduction

Arterial hypertension is a very common chronic disorder whose prevalence steadily increases, affecting currently >1 billion people worldwide.[1–3] It is a major risk factor for various other diseases, including myocardial infarction and stroke.[4,5] While the kidney and alterations in its natriuretic function have been in the centre of most models explaining the development of hypertension,[6,7] in the vast majority of hypertensive patients, the basic mechanisms underlying the pathogenesis of blood pressure elevation remain unclear.[8,9] The development of arterial hypertension is strongly correlated with age, and age-related progression of blood pressure accelerates in particular at mid-life.[10] Several factors such as increased arterial stiffness,[11,12] endothelial dysfunction including increased production of reactive oxygen species (ROS),[13–15] or decreased renal function have been suggested to be involved in age-dependent hypertension.[16] However, their relative importance and the underlying cellular mechanisms are poorly understood.

Hypertensive patients are characterized by an elevated total peripheral resistance. Peripheral resistance is controlled by a variety of local and systemic mediators that eventually influence the phosphorylation state of myosin light chain (MLC) in vascular smooth muscle cells.[17] Most contractile stimuli act through receptors which are coupled to the G-proteins G_q/G_{11} and G_{12}/G_{13}[18] and their downstream signalling

* Corresponding author. Tel: +49 6221 54 86864, E-mail: angela.wirth@pharma.uni-heidelberg (A.W.); Tel: +49 6032 705 1201, E-mail: stefan.offermanns@mpi-bn.mpg.de (S.O.)

pathways. Baseline blood pressure has been shown to depend on an intact G_q/G_{11}-mediated signalling pathway in vascular smooth muscle cells resulting in Ca^{2+}-dependent activation of the MLC kinase (MLCK) and in some cases also Rho/Rho kinase-mediated inhibition of myosin phosphatase.[19–21] In contrast, G_{12}/G_{13}, which activate the Rho/Rho kinase pathway by direct interaction with Rho guanine nucleotide exchange factors such as leukaemia-associated RhoGEF (LARG), are not required for baseline blood pressure.[20] However, G_{12}/G_{13}-mediated signalling in vascular smooth muscle cells is critically involved in salt-induced hypertension in mice.[20] Here we used mouse models with induced smooth muscle-specific endothelin ET_A-receptor deficiency and defects in downstream procontractile signalling pathways to evaluate the role of vascular smooth muscle tone regulation in age-dependent hypertension.

2. Methods

An expanded method section is available in the Supplementary material online.

2.1 Genetic mouse model

The generation of floxed alleles of the genes encoding $G\alpha_q$ (Gnaq), $G\alpha_{13}$ (Gna13), ET_A receptor (EDNRA) and LARG (Arhgef12), as well as of the null alleles of the genes encoding $G\alpha_{11}$ (Gna11) and $G\alpha_{12}$ (Gna12) has been described previously.[22–25] The generation of the inducible, smooth muscle-specific Cre transgenic mouse line (SMMHC-CreER^{T2}) has also been described previously.[20] All animal care and use procedures in this study were approved by the local authorities (Regierungspräsidia Karlsruhe and Darmstadt).

2.2 Telemetric blood pressure measurements

A radiotelemetry system (PA-C10, Data Sciences International) was used to monitor blood pressure in conscious, unrestrained mice, as described previously.[20] Data for basal blood pressure measurements were collected with a 10-s scheduled sampling every 5 min and the 24-h mean values were used for analysis. For analysing the acute effects of agonists and antagonists, data were collected continuously in 5-s intervals for up to 60 min. For agonist experiments, blood pressure values were averaged over an interval of 1 min, for antagonist experiments over an interval of 30 min after application of the receptor blocker.

2.3 Magnetic resonance imaging

Cardiac MRI measurements were performed on a 7.0T Bruker Pharmascan, equipped with a 300 mT/m gradient system, using a custom-built circularly polarized birdcage resonator and the Early Access Package for self-gated cardiac Imaging (Bruker, Ettlingen, Germany).[26] The mice were measured under volatile isoflurane (2.0%) anaesthesia. MRI data were analysed using Qmass digital imaging software (Medis, Leiden, the Netherlands).

2.4 Vessel morphometry

Mesenterial and femoral arteries from young and aged wild-type mice were harvested after perfusing the mice with 4% paraformaldehyde. Tissue were dehydrated, embedded in paraffin, and sectioned on a microtome (thickness 5 μm). Sections were stained with haematoxylin–eosin. To calculate wall-lumen ratios, vessel and luminal area were determined.

2.5 Myography

Vessel relaxation in response to cumulative addition of acetylcholine (10^{-11} M to 10^{-4} M) was measured in aortic segments precontracted with phenylephrine (10^{-6} M). The concentration–response curves of acetylcholine-induced relaxation were evaluated in separate young ($n = 7$) or aged ($n = 6$) wild-type animals and were expressed as percentage of the maximal relaxation (100%) induced by sodium nitroprusside (SNP, 10^{-5} M).

The effect of the ETA receptor antagonist BQ-123 was analysed in pressurized (75 mmHg) mesenterial arteries from young and aged wild-type animals. After pre-incubation without or with 1 μM BQ-123, acetylcholine (ACh) was added at a concentration of 1 μM. In the end of the experiment, maximal dilatation of vessels was induced by 10 mM SNP. ACh-induced relaxation was expressed as per cent of maximal relaxation induced by SNP.

2.6 Serum chemistry

For determination of serum creatinine levels, blood urea nitrogen concentration, and aldosterone, blood was collected from the retro-orbital plexus of anaesthetized (isoflurane) young and aged wild-type mice. The concentrations of urea and creatinine were measured using commercially available enzymatic kits. Plasma aldosterone was measured by RIA.

To measure plasma renin concentration, blood samples (25 μL) were obtained from young and aged, conscious, wild-type mice by submandibular venipuncture. Plasma renin activity (PRC) was measured based on the generation of angiotensin I after addition of plasma from bilaterally nephrectomized male rats as excess renin substrate.

2.7 Determination of plasma nitrate concentration

Blood samples (50 μL) were obtained under isoflurane anaesthesia from young and aged animals. Plasma nitrate concentration was measured by using a commercially available Nitrate Fluorometric Assay Kit (Cayman).

2.8 Plasma volume determination

Plasma volume was determined with the Evan's blue dilution method.

2.9 Determination of glomerular filtration rate

Renal function in conscious mice was assessed by transcutaneous measurement of FITC-sinistrin plasma clearance as described previously.[8]

2.10 Determination of sodium uptake and excretion

Mice were housed in individual metabolic cages (Tecniplast, Germany) and fed with a normal salt diet (0.7% NaCl, LASQdiet® Rod16-A, LASvendi). Thereafter, mice were switched to high-salt diet (4% NaCl, ssniff® EF R/M High Sodium). Urine volume in a 24-h period was recorded. Furthermore, body weight, food consumption, and water intake were measured daily. Urine samples were analysed for sodium and potassium concentrations (IDEXX Laboratories, Germany).

2.11 ROS detection

The production of ROS was analysed by two different methods: with an ethidium fluorescence assay and luminol derivative (L-012)-enhanced chemiluminescence analysis.

2.12 Immunohistochemistry

Cryosections of the respective tissue from young and aged WT or KO mice were stained with primary antibodies against CD102 (ICAM-2) and ET-1. Secondary antibodies were labelled with AlexaFluor 594 or AlexaFluor 488, respectively. Pictures were taken by confocal microscopy and analysed by ImageJ.

2.13 Quantitative RT–PCR

RNA was extracted from aorta with the RNA fibrous tissue kit (Qiagen) according to the manufacturer's protocol. Reverse transcriptase (RT) reaction was performed using the QuantiTect Reverse Transcription kit (Qiagen). Quantitative RT–PCR was performed using the LightCycler 480 Probe Master (Roche). Data are in all cases presented after normalization to GAPDH, and basal values were set to 1. In some cases, the relative change compared with basal conditions was calculated in addition.

2.14 Statistics

All data are presented as the mean ± standard errors of the means (S.E.M). Normality of distribution was tested by Kolmogorov–Smirnov test with $a = 0.05$. Comparisons between two groups were performed with unpaired Student's *t*-test; data sets containing multiple groups were analysed by ANOVA followed by Student Newman Keuls *post hoc* test. A value of $P < 0.05$ was considered significant. '*n*' refers to the number of independent experiments or mice per group.

3. Results

To analyse the mechanisms underlying age-dependent elevation of blood pressure, we evaluated the development of blood pressure in ageing mice. Similar to humans, the blood pressure of laboratory mice shows an age-dependent elevation by 15–20% from young animals (5–8 weeks) to animals at the age of ~1 year.[27–29] Telemetric blood pressure measurements in young and aged C57BL/6 wild-type mice confirmed an age-dependent increase in systolic and diastolic blood pressure (*Figure 1A*). MRI and intravascular pressure measurements did not reveal any differences between young and aged mice with regard to various haemodynamic parameters including left ventricular ejection fraction, cardiac output, as well as pulse pressure as a measure of vessel stiffness (*Figure 1B* and *C*). There were also no indications for alterations in the systemic renin–angiotensin–aldosterone system or the plasma volume (*Figure 1D–F*). Aged mice did not differ from young animals with regard to blood urea nitrogen, serum creatinine levels, or glomerular filtration rate (*Figure 1G–I*), indicating intact renal function. We also could not detect any signs of changes in vascular morphometry (*Figure 1J* and *K*). A five-fold increase in sodium uptake did not alter blood pressure in young and aged animals (data not shown), and aged animals did not show any sign of impaired sodium excretion compared with young mice (*Figure 1L*).

Given the absence of any obvious renal, cardiac, or endocrine cause for the increased blood pressure in aged mice, we tested whether the elevated blood pressure of aged mice depended on an increased vascular tone. We therefore blocked the activation of procontractile signalling pathways in vascular smooth muscle cells by tamoxifen-induced smooth muscle-specific deletion of genes encoding $G\alpha_q/G\alpha_{11}$ and $G\alpha_{12}/G\alpha_{13}$ using Cre/loxP-technology.[20] In young mice with smooth muscle-specific $G\alpha_q/G\alpha_{11}$ deficiency (Sm-q/11-KO), blood pressure has been shown to be reduced.[20] Sm-q/11-KO mice that had reached an age of 1 year showed a small, non-significant increase in blood pressure, which was much less pronounced than the one seen in aged wild-type animals (*Figure 2A*). Surprisingly, mice lacking $G\alpha_{12}/G\alpha_{13}$ in smooth muscle cells (Sm-12/13-KO), which at a young age are indistinguishable from wild-type mice with regard to blood pressure, were completely resistant to the age-related elevation of blood pressure seen in wild-type animals (*Figure 2A*). These data suggest that an increased activation of G_q/G_{11}- and G_{12}/G_{13}-coupled receptors on vascular smooth muscle cells underlies the elevated vascular tone in age-related blood pressure increases.

To identify potential vascular G-protein-coupled receptors involved in age-dependent hypertension, we tested the effect of various antagonists on blood pressure in young and aged mice (*Figure 2B*). While antagonists of the vasopressin V_1, α_1-adrenergic, and angiotensin II AT_1 receptors reduced blood pressure in young and aged animals to comparable degrees, the endothelin ET_A receptor antagonist darusentan had the strongest blood pressure reducing effect in aged mice while being without significant effect in young animals (*Figure 2B*). This suggests that the contribution of endothelin to the regulation of vascular tone is increased in aged mice. Due to the experimental design, we cannot exclude partial contribution of other vascular G-protein-coupled receptors to be involved in age-related hypertension. To further analyse the vascular endothelin system in aged mice and to test whether an elevated ET_A receptor activation is critically involved in age-dependent blood pressure increases, we stained several vascular beds of young and old animals for the expression of endothelin-1. When counterstained with an endothelial marker, we consistently observed strongly increased ET-1 levels in the endothelial layer of vessels from aged mice compared with young animals (*Figure 3A–C*). The observed increase in endothelial ET-1 protein levels correlated with an increased expression of the endothelin-forming enzymes, endothelin-converting enzyme (ECE)-1 and ECE-2, and the ET-1 precursor ppET-1 in the intima of vessels from aged mice (*Figure 3D*).

The fact that age-dependent blood pressure elevation can be reduced by ET_A receptor antagonists and is accompanied by increased expression of endothelin-1 strongly suggests ET-1 as a critical mediator of elevated blood pressure in aged animals. The main natural counterpart of endothelin-1 in vascular tone regulation is nitric oxide that mediates endothelium-dependent relaxation. It has been described that increased vascular ET-1 levels can result from reduced nitric oxide bioavailability due to endothelial dysfunction, a characteristic alteration found in aged vessels.[14,15,30,31] Consistent with endothelial dysfunction, we observed decreased levels of nitrate as an indicator of endothelial NO formation in the plasma from 1-year-old mice compared with young animals, and endothelium-dependent vasodilation in vessels from aged mice compared with young animals was strongly reduced (*Figure 4A* and *B*). We could confirm an increased role of ET-1 in vascular reactivity in aged mice by analysing the effect of the ET_A receptor antagonist BQ-123 on endothelium-dependent relaxation in pressurized mesenterial arteries (*Figure 4C*). While BQ-123 did not significantly change the response of vessels from young animals, ACh-induced relaxation of vessels from aged animals was smaller compared with vessels from young animals and was significantly increased after addition of BQ-123. In addition, ROS production in the vasculature of aged mice was significantly increased in comparison to young mice as indicated by staining of different vascular beds with dihydroethidium (*Figure 4E* and *F*) and L012-enhanced luminescence measurements (*Figure 4D*).

The ET_A receptor couples to both G_q/G_{11} and G_{12}/G_{13}.[19,32] To test whether this coupling is preserved in aged mice, we analysed pressure responses to ET-1 in the absence or presence of $G\alpha_q/G\alpha_{11}$ and $G\alpha_{12}/G\alpha_{13}$. Similar to young animals, the pressure responses to endothelin-1 *in vivo* were reduced in the absence of $G\alpha_q/G\alpha_{11}$ as well as $G\alpha_{12}/G\alpha_{13}$ (*Figure 5A*). This indicates that ET-1 increases vascular tone in aged mice through its receptor coupling to G_q/G_{11} and G_{12}/G_{13}. To test whether the elevated blood pressure in aged mice was indeed due to elevated procontractile signaling in vascular smooth muscle cells, we measured the effect of an acute induction of $G\alpha_q/G\alpha_{11}$ or $G\alpha_{12}/G\alpha_{13}$ deficiency in vascular smooth muscle cells on their blood pressure. *Figure 5B* and *C* show that the elevated blood pressure of aged animals dropped significantly within 3–4 days after tamoxifen-induced smooth muscle-specific deletion of G_q/G_{11}- and G_{12}/G_{13}-mediated signalling and reached levels seen in young wild-type mice. The major effector of G_{12}/G_{13} in the regulation of vascular smooth muscle tone is the Rho-GEF protein LARG (ArhGEF12).[20] We therefore also analysed the effect of an acute induction of LARG deficiency. Very similar to tamoxifen-induced smooth muscle $G\alpha_{12}/G\alpha_{13}$ deficiency, induction of LARG deficiency reduced the blood pressure of aged mice to levels found in young animals (*Figure 5D*).

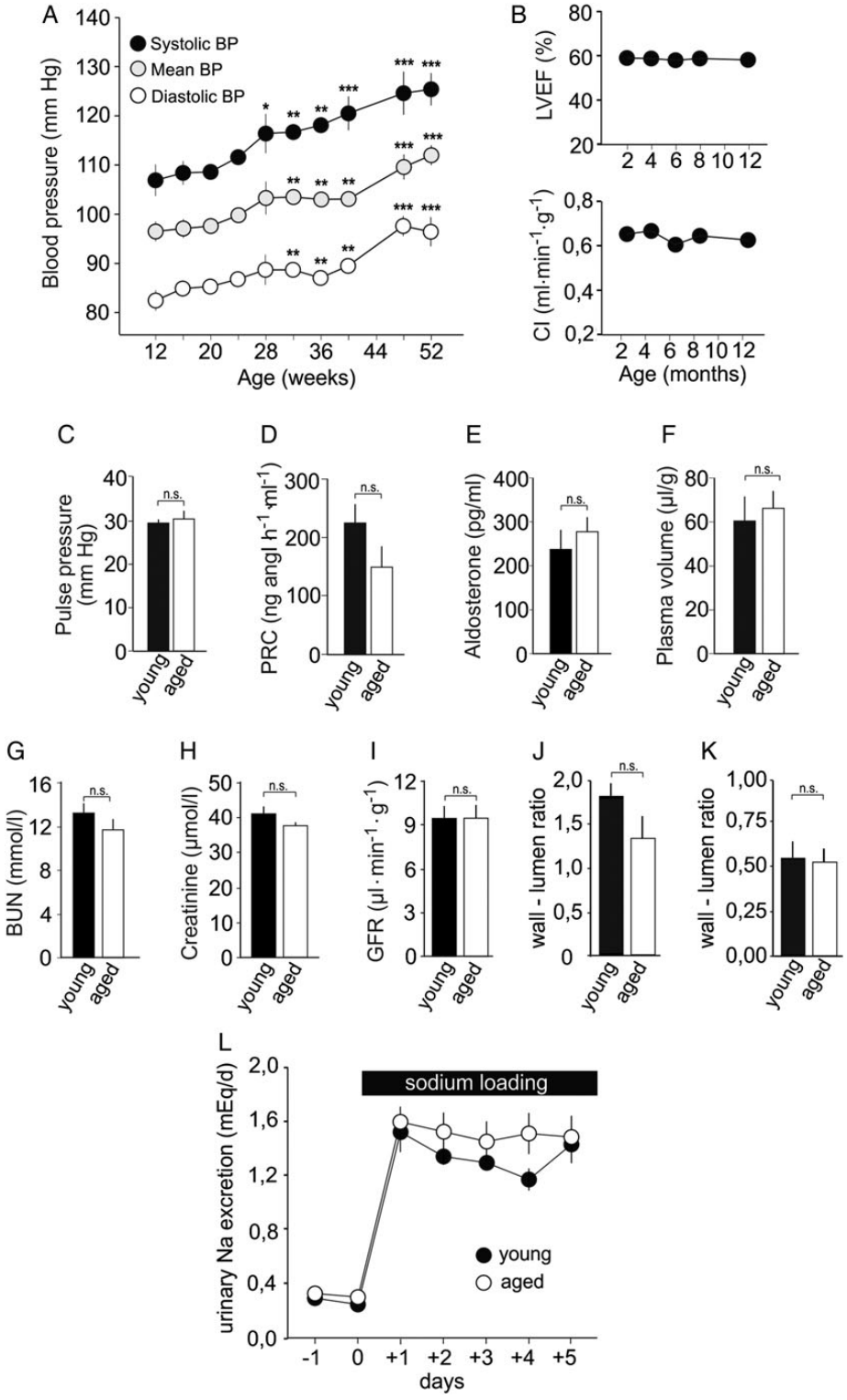

Figure 1 Age-dependent blood pressure increase in mice. (*A*) Diastolic, mean, and systolic blood pressure were monitored telemetrically in wild-type C57BL/6 mice over the indicated age period ($n = 10$). (*B*–*K*) Wild-type animals at an age of 8–12 weeks (young) and wild-type mice at an age of 1 year (aged) were analysed, and the following parameters were determined: left ventricular ejection fraction (LVEF; $n = 10$), cardiac index (CI; $n = 10$) (*B*), pulse pressure ($n = 12$–15) (*C*), plasma renin concentration (PRC; $n = 7$–10) (*D*), plasma aldosterone ($n = 11$–12) (*E*), plasma volume ($n = 5$) (*F*), as well as blood urea nitrogen ($n = 12$–15) (*G*), serum creatinine ($n = 10$–13) (*H*), glomerular filtration rate (GFR; $n = 7$) (*I*), and wall-lumen ratio of femoral ($n = 4$) (*J*) and mesenterial ($n = 4$) (*K*) arteries. (*L*) Urinary sodium excretion in young and aged mice before and after a dietary sodium load ($n = 9$–11). Shown are mean values ± S.E.M., as statistic tests repeated-measures ANOVA (*A* and *B*; *K*) or unpaired *t*-tests (*C*–*J*) were used; $^{*}P < 0.05$, $^{**}P < 0.01$, $^{***}P < 0.001$ (vs. values at 12 weeks of age).

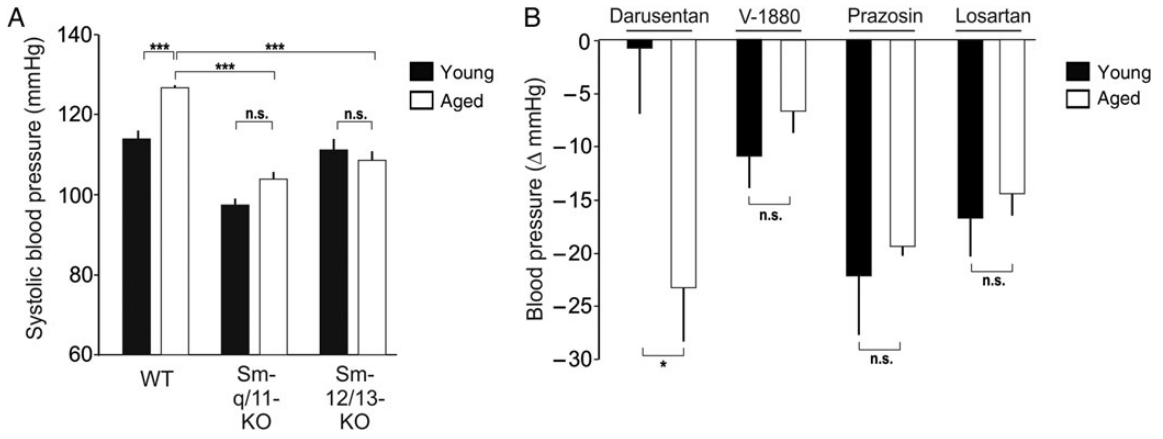

Figure 2 Age-dependent increase in blood pressure is sensitive to an ET_A blocker and requires smooth muscle G_q/G_{11} and G_{12}/G_{13}. (*A*) Systolic blood pressure in wild-type, Sm-q/11-KO, and Sm-12/13-KO mice was measured telemetrically at the age of 8–12 weeks (young) and at the age of 1 year (aged) ($n = 5–8$). All animals have been induced with tamoxifen at an age of ~7 weeks. (*B*) Effect of the ETA receptor antagonist darusentan (50 mg/kg), the V_1 antagonist V-1880 ([deamine-Pen[1]-*O*-Me-Tyr[2],Arg[8]]-vasopressin; 10 μg/kg), the α_1 antagonist prazosin (0.1 mg/kg) and the AT_1 antagonist losartan (5 mg/kg) on blood pressure in 8- to 12-week-old wild-type mice (young) and 1-year-old wild-type mice (aged). Shown is the average reduction in blood pressure during a 15-min period starting 30 min after injection of antagonists ($n = 5–8$). Shown are mean values ± S.E.M., as statistic tests two-way ANOVA (*A*) and unpaired *t*-tests (*B*) were used; $*P < 0.05$, $***P < 0.001$.

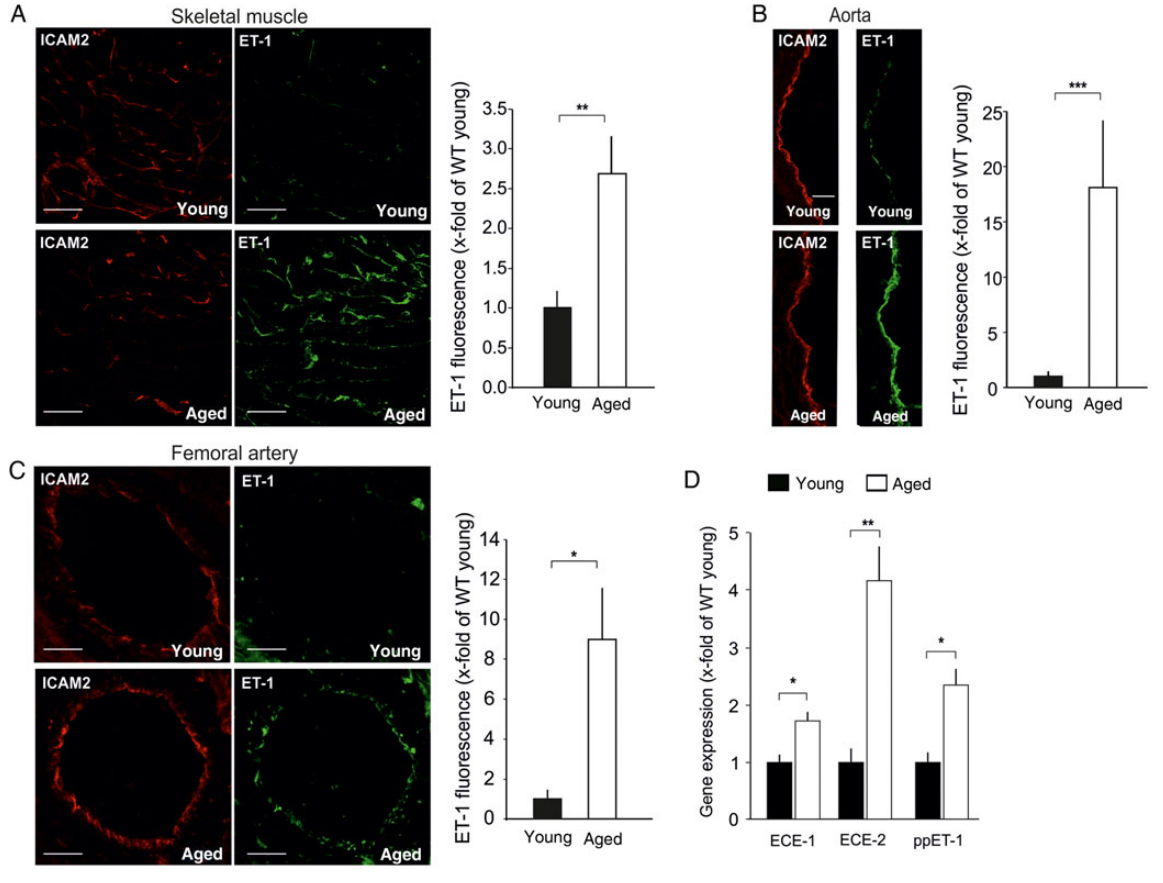

Figure 3 Increased endothelial ET-1 levels in aged mice. (*A–C*) The indicated tissues from 8- to 12-week-old wild-type mice (young) and 1-year-old wild-type mice (aged) were sectioned and stained for ICAM-2 and endothelin-1 (ET-1) ($n = 4–5$). Shown are representative images as well as the integrated density of the ET-1-positive signal. Bar lengths: 25 μm. (*D*) Quantitative RT–PCR analysis of mRNAs encoding endothelin-converting enzyme-1 (ECE-1), ECE-2, or prepro-endothelin-1 (ppET-1) in endothelial cells from aorta ($n = 3–4$). Shown are mean values ± S.E.M., as statistic tests unpaired *t*-tests were used; $*P < 0.05$; $**P < 0.01$, $***P < 0.001$.

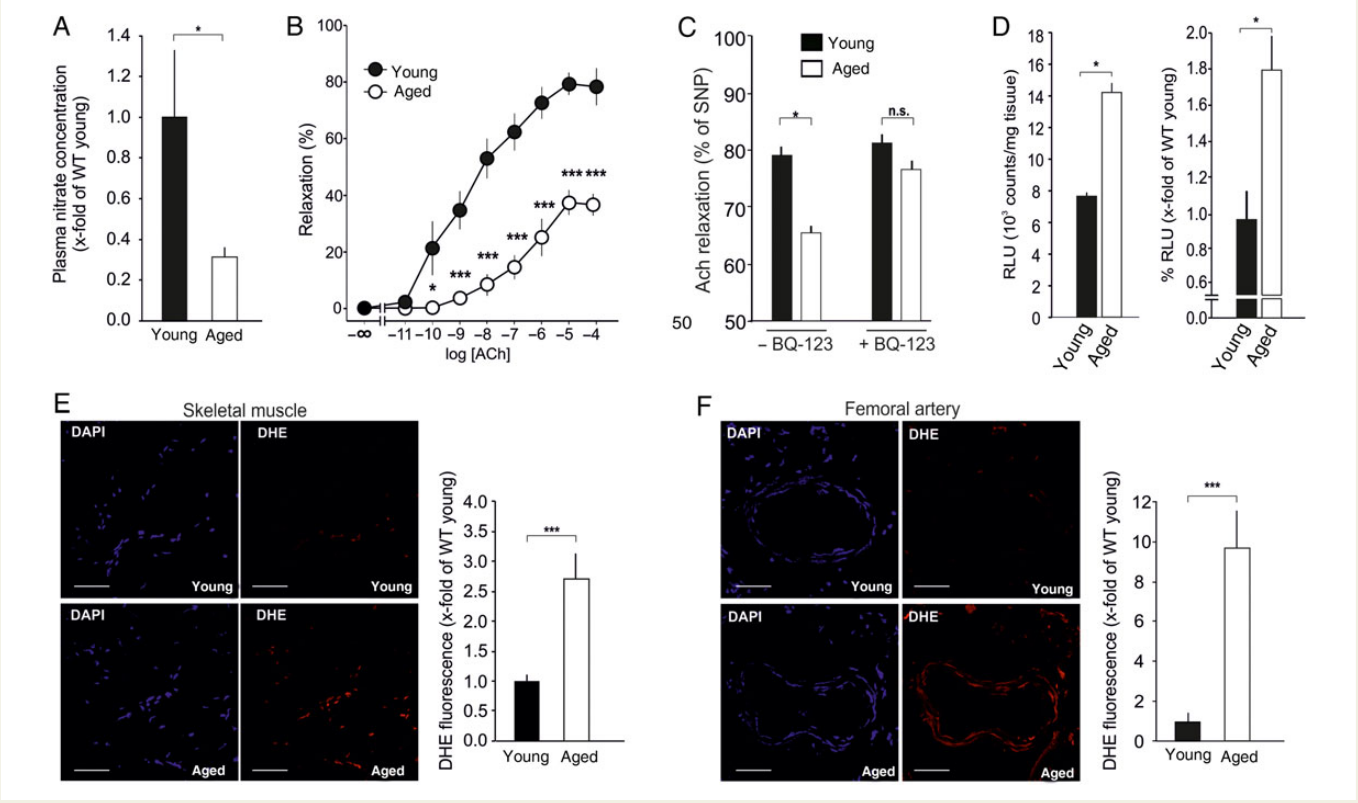

Figure 4 Endothelial dysfunction in aged mice. (*A*) Plasma samples from 8- to 12-week-old wild-type mice (young) and 1-year-old wild-type mice (aged) ($n = 8–10$) were analysed for nitrate levels as indicator for endothelial NO production. (*B*) Effect of increasing concentrations of acetylcholine (ACh) on the tone of precontracted aortic rings from 8- to 12-week-old wild-type mice (young) and 1-year-old wild-type mice (aged) ($n = 5–6$). (*C*) Effect of the ET_A-receptor antagonist BQ-123 on acetylcholine (ACh)-induced relaxation of pressurized mesenteric arteries from 8- to 12-week-old wild-type mice (young) and 1-year-old wild-type mice (aged) ($n = 5$). (*D*) ROS production in carotid arteries from 8- to 12-week-old wild-type mice (young) and 1-year-old wild-type mice (aged) ($n = 5–6$) was detected by L-012 enhanced chemiluminescence. Shown are absolute values as well as x-fold increase compared with WT young. (*E* and *F*) The indicated tissues from 8- to 12-week-old wild-type mice (young) and 1-year-old wild-type mice (aged) were sectioned and stained with DHE to analyse ROS production ($n = 8$). Shown are representative images as well as the integrated density of the DHE-positive signal. Bar length: 25 μm. Shown are mean values ± S.E.M., as statistic tests unpaired *t*-tests (*A*; *D*–*F*), repeated-measures ANOVA (*B*), or one-way ANOVA (*C*) were used; $*P < 0.05$; $**P < 0.01$, $***P < 0.001$.

To test whether the elevated vascular ET-1 levels in aged mice are responsible for their elevated blood pressure, we generated mice with inducible smooth muscle-specific deficiency of the ET_A receptor (Sm-ETA-KO). Consistent with the observations in Sm-G_{12}/G_{13}-KO mice, we found that the elevated blood pressure of aged, non-induced Sm-ETA-KO mice dropped significantly after induction of smooth muscle-specific ET_A deficiency by tamoxifen treatment (*Figure 5E*). There is also a blood pressure drop in young Sm-ETA-KO mice after tamoxifen treatment, but this effect is significantly smaller than in aged animals. Interestingly, despite the reduced blood pressure in 1-year-old, tamoxifen-induced Sm-ETA-KO mice, signs of endothelial dysfunction such as elevated ROS production, decreased plasma nitrate levels, and an increased vascular ET-1 expression were still preserved (*Figure 6*).

4. Discussion

Longitudinal and cross-sectional studies to analyse the dynamics of age-related increases in systolic blood pressure in humans identified a mid-life acceleration in blood pressure increase beginning in the fourth decade of life.[10,33,34] The cause of this early period of age-dependent elevation in blood pressure is not known. However, mid-life acceleration in blood pressure appears to be of particular importance as an early indicator of increased cardiovascular risk.[10] Similar to patients with mid-life acceleration in hypertension, we observed in 1-year-old mice elevated blood pressure levels without any evidence for structural changes or increased vessel stiffness, and hypertension in aged mice could be normalized by receptor blockade or induction of smooth muscle-specific deletion of the genes encoding ET_A, $G\alpha_{12}$/$G\alpha_{13}$, $G\alpha_q$/$G\alpha_{11}$, or the G_{12}/G_{13} effector LARG. This strongly indicates that the age-dependent hypertension at this stage is due to a fully reversible increase in procontractile signalling in vascular smooth muscle cells.

The prevailing model to explain the mechanism underlying blood pressure elevation in hypertension places the kidney in the centre and states that abnormalities of renal sodium handling increase plasma volume and systemic vascular resistance.[6,35] This concept is supported by numerous genetic studies that identified gene mutations affecting renal salt reabsorption as causes for several rare monogenic forms of hypertension.[6] However, the cause of blood pressure elevation remains unknown in the majority of hypertensive patients. Our data indicate that age-dependent elevation of blood pressure occurs at least

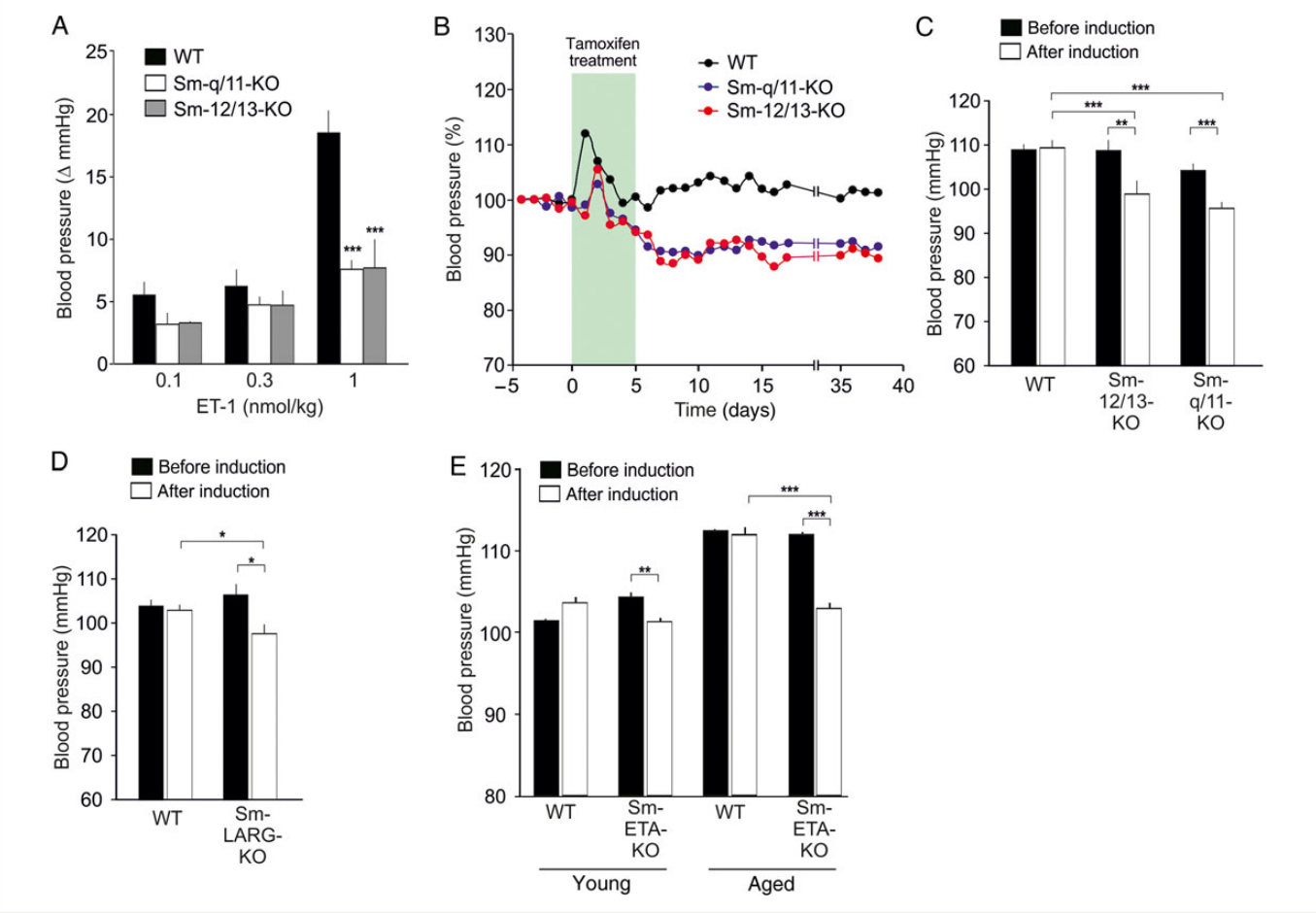

Figure 5 Elevated blood pressure in aged mice is normalized by acute induction of $G\alpha_q/G\alpha_{11}$, $G\alpha_{12}/G\alpha_{13}$, and LARG deficiency in VSMC. (*A*) Mean blood pressure was monitored telemetrically in anaesthetized aged (1 year old) mice before and after the intravenous injection of the indicated dose of endothelin-1 (ET-1). Shown is the maximal blood pressure increase in mmHg after injection of the stimulus to wild-type mice or Sm-q/11-KO or Sm-12/13-KO mice ($n = 5–8$). (*B–G*) Effect of induced smooth muscle-specific $G\alpha_q/G\alpha_{11}$ and $G\alpha_{12}/G\alpha_{13}$ deficiency (*B* and *C*), LARG deficiency (*D*), or ET_A-receptor deficiency (*E*) on blood pressure of young (8–12 weeks old) and aged (1-year-old) mice. (*B*) Representative recordings of the telemetrically measured blood pressure of wild-type, Sm-q/11-KO, Sm-12/13-KO mice. Deficiency in smooth muscle cells was induced by administration of tamoxifen on 5 consecutive days as indicated. The average blood pressure during the 5 days before injection was set to 100%. (*C–E*) Absolute values of telemetrically recorded mean arterial blood pressure in wild-type ($n = 9$), Sm-12/13-KO ($n = 8$), Sm-q/11-KO ($n = 7$) mice (*C*), Sm-LARG-KO mice ($n = 6$) (*D*), as well as wild-type ($n = 7$) and Sm-ETA-KO mice ($n = 6$) (*E*) before and after induction with tamoxifen. Blood pressure values averaged for 3 days before administration of tamoxifen (before induction) and after induction with tamoxifen (after induction) are shown. Shown are mean values ± S.E.M., as statistic tests one-way ANOVA (*A*) or two-way ANOVA (*C–E*) were used; $*P < 0.05$, $**P < 0.01$, $***P < 0.001$; n.s., not significant.

initially in the absence of any alterations in renal sodium handling. In contrast, we found that the elevated blood pressure in aged animals resulted from an increased vascular smooth muscle tone due to increased activation of G-protein-coupled receptors including the endothelin receptor ET_A. This is consistent with a critical role of endothelial endothelin-1 in ET_A-mediated blood pressure regulation[36] and supports the notion that alterations in vascular function, which cause an elevation of vascular tone, can be the primary cause for hypertension.[37,38]

The fact that age-dependent hypertension in mice was sensitive to the action of a selective endothelin ET_A receptor antagonist and could be normalized by induction of smooth muscle-specific ET_A deficiency together with the strong elevation of endothelin-1 expression in the endothelial layer of various vascular beds indicates a central role of ET-1/ET_A-signaling in age-related hypertension. Elevated ET-1 levels have previously been described in vessels of aged animals.[39,40] This is consistent with findings in aged humans showing elevated circulating ET-1 levels[41] and increased sensitivity towards the vasodilatory actions of ET_A receptor antagonists.[42,43] Ageing of blood vessels is accompanied by endothelial dysfunction with reduced nitric oxide bioavailability and increased production of reactive oxygen species,[14,15] and we could show that both phenomena can also be observed in aged mice. Given the fact that nitric oxide through various mechanisms can inhibit ET-1 expression,[30,31] the endothelial dysfunction of aged vessels with decreased nitric oxide levels and increased ROS production is a likely cause of an increased ET-1-dependent vascular tone in aged animals.

Our data show that the age-related increase in blood pressure requires intact signalling through G_q/G_{11} and G_{12}/G_{13} in vascular smooth muscle cells. Both the smooth muscle-specific deletion of $G\alpha_{12}/G\alpha_{13}$ and the loss of the predominant vascular RhoGEF LARG prevent the maintenance of age-related hypertension. In contrast, baseline blood

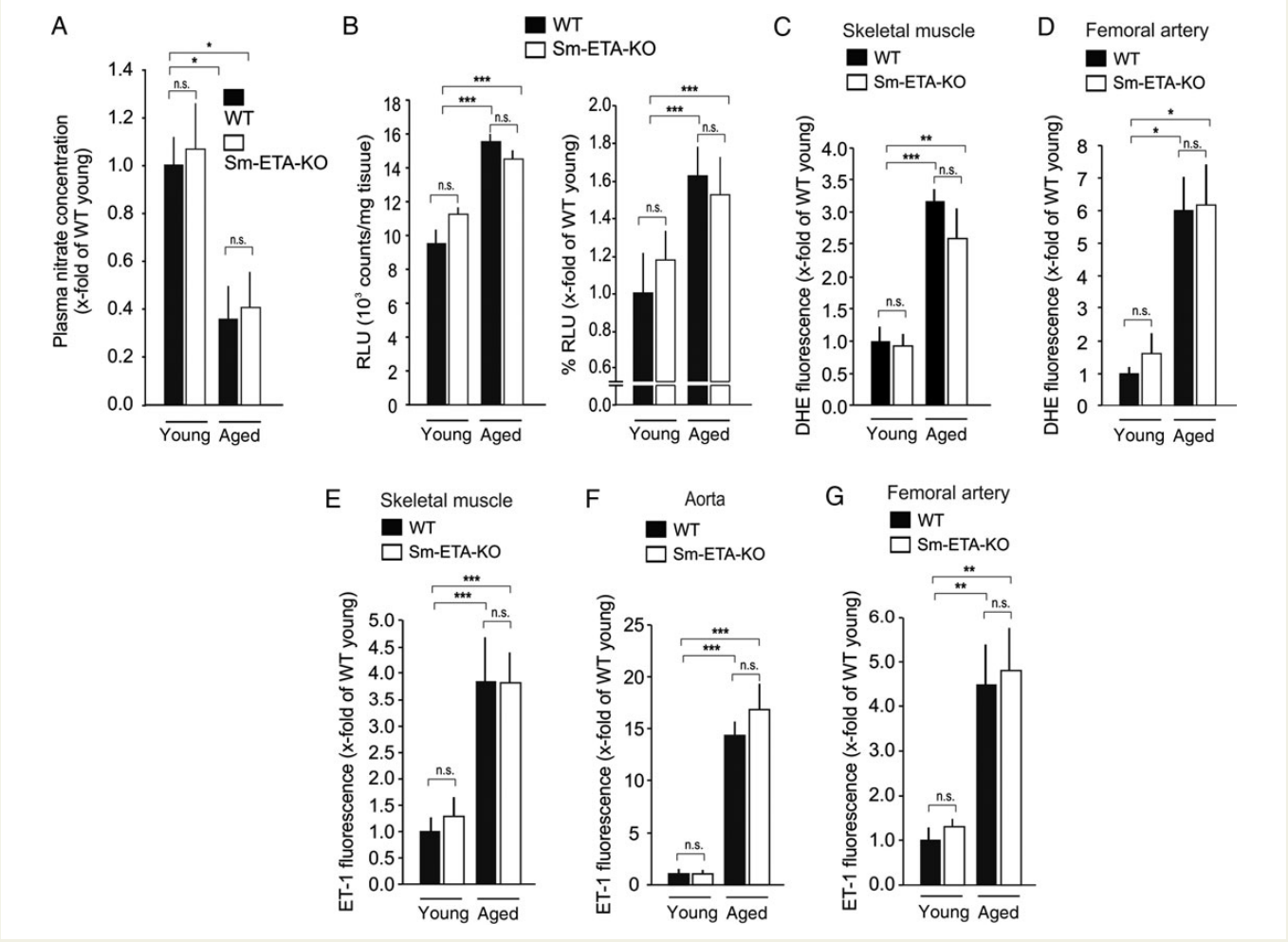

Figure 6 Endothelial dysfunction in smooth muscle-specific ET_A receptor-deficient mice. (*A*) Plasma samples from 8- to 12-week-old (young) and 1-year-old (aged) wild-type and Sm-ETA-KO mice ($n = 8–10$) were analysed for nitrate levels as indicator for endothelial NO production. (*B*) ROS production in carotid arteries from 8- to 12-week-old (young) and 1-year-old (aged) wild-type and Sm-ETA-KO mice ($n = 4–5$) was detected by L-012 enhanced chemiluminescence. Shown are absolute values as well as x-fold increase compared with WT young. (*C* and *D*) The indicated tissues from 8- to 12-week-old (young) and 1-year-old (aged) wild-type and Sm-ETA-KO mice were sectioned and stained with DHE to analyse ROS production ($n = 4–5$). Shown are the integrated density of the DHE-positive signal. Bar length: 25 μm. (*E–G*) The indicated tissues from 8- to 12-week-old (young) and 1-year-old (aged) wild-type and Sm-ETA-KO mice were sectioned and stained for ICAM-2 and endothelin-1 (ET-1) ($n = 6–8$). Shown are the integrated density of the ET-1-positive signal. All animals have been induced with tamoxifen at an age of ~8 weeks. Bar lengths: 25 μm. Shown are mean values ± S.E.M., as statistic tests two-way ANOVA was used; $^*P < 0.05$, $^{**}P < 0.01$, $^{***}P < 0.001$; n.s., not significant.

pressure depends only on G_q/G_{11}-mediated signalling.[20] This is most likely due to the fact that basal vascular tone in the young is maintained primarily by sympathetic input mediated by α_1-adrenergic receptors which are coupled to G_q/G_{11}.[18,20] The fact that smooth muscle-specific deletion of ET_A receptors is capable of preventing an age-dependent increase in blood pressure indicates that the increased expression of endothelin-1 in the aged vessel leads to the additional activation of G_{12}/G_{13}-mediated signalling through activation of the ET_A receptor on vascular smooth muscle cells which couple not only to G_q/G_{11} but also to G_{12}/G_{13}. Although inhibition of the ET_A-receptor-G_{12}/G_{13}-LARG pathway led to a reversal of age-related hypertension, signs of endothelial dysfunction were still present. This indicates that the activation of procontractile G-protein-coupled receptor-mediated signalling pathways in the vascular smooth muscle cells is ultimately the cause of elevated blood pressure in aged animals. We did not observe any defects in other smooth muscle tissues (e.g. intestinal tract) that might have been caused by the tissue-specific knock-outs and which could explain the drop in blood pressure.

Similar to age-dependent hypertension, also salt-induced hypertension depends on activation of both G_q/G_{11}- and G_{12}/G_{13}-mediated signalling.[20] Thus, a pathological elevation of blood pressure appears to be due to the recruitment of the G_{12}/G_{13}-mediated signalling pathway resulting in Rho/Rho kinase-dependent inhibition of MLC phosphorylation.[17]

ET_A receptor blockers have been successfully tested for the treatment of advanced essential hypertension; however, their use is restricted due to unwanted effects.[44,45] Given the evidence in mice and humans, increased vascular ET-1 signalling appears to be an important early step in the progression of hypertension and its consequences. Thus, ET_A receptor antagonists may also be useful for the prophylactic treatment of cardiovascular diseases. Alternatively, the blockade of

signalling pathways downstream of ET_A and related receptors can reduce elevated vascular tone also at early stages of hypertension. In particular, the inhibition of G_{12}/G_{13}-LARG-mediated signalling is an attractive approach, which is expected to normalize elevated vascular tone under hypertensive conditions while leaving normal blood pressure unaffected.

Supplementary material

Supplementary material is available at *Cardiovascular Research* online.

Acknowledgements

The authors thank Svea Hümmer and Sharon Meaney-Gardian for excellent secretarial help, Viktoria Hess for expert technical assistance, and Dr Masashi Yanagisawa (Tsukuba, Japan) for providing mice carrying a floxed allele of the gene encoding the ET_A receptor.

Conflict of interest: none declared.

Funding

This work was supported by the German Research Foundation.

References

1. Lawes CM, Vander Hoorn S, Rodgers A. Global burden of blood-pressure-related disease, 2001. *Lancet* 2008;**371**:1513–1518.
2. Franco OH, Peeters A, Bonneux L, de Laet C. Blood pressure in adulthood and life expectancy with cardiovascular disease in men and women: life course analysis. *Hypertension* 2005;**46**:280–286.
3. Kearney PM, Whelton M, Reynolds K, Muntner P, Whelton PK, He J. Global burden of hypertension: analysis of worldwide data. *Lancet* 2005;**365**:217–223.
4. Messerli FH, Williams B, Ritz E. Essential hypertension. *Lancet* 2007;**370**:591–603.
5. Lim SS, Vos T, Flaxman AD, Danaei G, Shibuya K, Adair-Rohani H, Amann M, Anderson HR, Andrews KG, Aryee M, Atkinson C, Bacchus LJ, Bahalim AN, Balakrishnan K, Balmes J, Barker-Collo S, Baxter A, Bell ML, Blore JD, Blyth F, Bonner C, Borges G, Bourne R, Boussinesq M, Brauer M, Brooks P, Bruce NG, Brunekreef B, Bryan-Hancock C, Bucello C, Buchbinder R, Bull F, Burnett RT, Byers TE, Calabria B, Carapetis J, Carnahan E, Chafe Z, Charlson F, Chen H, Chen JS, Cheng AT, Child JC, Cohen A, Colson KE, Cowie BC, Darby S, Darling S, Davis A, Degenhardt L, Dentener F, Des Jarlais DC, Devries K, Dherani M, Ding EL, Dorsey ER, Driscoll T, Edmond K, Ali SE, Engell RE, Erwin PJ, Fahimi S, Falder G, Farzadfar F, Ferrari A, Finucane MM, Flaxman S, Fowkes FG, Freedman G, Freeman MK, Gakidou E, Ghosh S, Giovannucci E, Gmel G, Graham K, Grainger R, Grant B, Gunnell D, Gutierrez HR, Hall W, Hoek HW, Hogan A, Hosgood HD III, Hoy D, Hu H, Hubbell BJ, Hutchings SJ, Ibeanusi SE, Jacklyn GL, Jasrasaria R, Jonas JB, Kan H, Kanis JA, Kassebaum N, Kawakami N, Khang YH, Khatibzadeh S, Khoo JP, Kok C, Laden F, Lalloo R, Lan Q, Lathlean T, Leasher JL, Leigh J, Li Y, Lin JK, Lipshultz SE, London S, Lozano R, Lu Y, Mak J, Malekzadeh R, Mallinger L, Marcenes W, March L, Marks R, Martin R, McGale P, McGrath J, Mehta S, Mensah GA, Merriman TR, Micha R, Michaud C, Mishra V, Hanafiah KM, Mokdad AA, Morawska L, Mozaffarian D, Murphy T, Naghavi M, Neal B, Nelson PK, Nolla JM, Norman R, Olives C, Omer SB, Orchard J, Osborne R, Ostro B, Page A, Pandey KD, Parry CD, Passmore E, Patra J, Pearce N, Pelizzari PM, Petzold M, Phillips MR, Pope D, Pope CA III, Powles J, Rao M, Razavi H, Rehfuess EA, Rehm JT, Ritz B, Rivara FP, Roberts T, Robinson C, Rodriguez-Portales JA, Romieu I, Room R, Rosenfeld LC, Roy A, Rushton L, Salomon JA, Sampson U, Sanchez-Riera L, Sanman E, Sapkota A, Seedat S, Shi P, Shield K, Shivakoti R, Singh GM, Sleet DA, Smith E, Smith KR, Stapelberg NJ, Steenland K, Stockl H, Stovner LJ, Straif K, Straney L, Thurston GD, Tran JH, Van Dingenen R, van Donkelaar A, Veerman JL, Vijayakumar L, Weintraub R, Weissman MM, White RA, Whiteford H, Wiersma ST, Wilkinson JD, Williams HC, Williams W, Wilson N, Woolf AD, Yip P, Zielinski JM, Lopez AD, Murray CJ, Ezzati M. A comparative risk assessment of burden of disease and injury attributable to 67 risk factors and risk factor clusters in 21 regions, 1990–2010: a systematic analysis for the Global Burden of Disease Study 2010. *Lancet* 2013;**380**:2224–2260.
6. Lifton RP, Gharavi AG, Geller DS. Molecular mechanisms of human hypertension. *Cell* 2001;**104**:545–556.
7. Herrera M, Coffman TM. The kidney and hypertension: novel insights from transgenic models. *Curr Opin Nephrol Hypertens* 2012;**21**:171–178.
8. Pimenta E, Calhoun DA, Oparil S. Chapter 38—etiology and pathogenesis of systemic hypertension (SECTION 3 - Hypertensive heart disease). In: Crawford MH, DiMarco JP, Paulus WJ, eds. *Cardiology*. Philadelphia: Elsevier Ltd; 2009.
9. Coffman TM. Under pressure: the search for the essential mechanisms of hypertension. *Nat Med* 2011;**17**:1402–1409.
10. Wills AK, Lawlor DA, Matthews FE, Sayer AA, Bakra E, Ben-Shlomo Y, Benzeval M, Brunner E, Cooper R, Kivimaki M, Kuh D, Muniz-Terrera G, Hardy R. Life course trajectories of systolic blood pressure using longitudinal data from eight UK cohorts. *PLoS Med* 2011;**8**:e1000440.
11. Kass DA. Ventricular arterial stiffening: integrating the pathophysiology. *Hypertension* 2005;**46**:185–193.
12. Izzo JL Jr. Arterial stiffness and the systolic hypertension syndrome. *Curr Opin Cardiol* 2004;**19**:341–352.
13. Vanhoutte PM, Shimokawa H, Tang EH, Feletou M. Endothelial dysfunction and vascular disease. *Acta Physiol (Oxf)* 2009;**196**:193–222.
14. Toda N. Age-related changes in endothelial function and blood flow regulation. *Pharmacol Ther* 2012;**133**:159–176.
15. Camici GG, Sudano I, Noll G, Tanner FC, Luscher TF. Molecular pathways of aging and hypertension. *Curr Opin Nephrol Hypertens* 2009;**18**:134–137.
16. Pimenta E, Oparil S. Management of hypertension in the elderly. *Nat Rev Cardiol* 2012;**9**:286–296.
17. Somlyo AP, Somlyo AV. Ca2+ sensitivity of smooth muscle and nonmuscle myosin II: modulated by G proteins, kinases, and myosin phosphatase. *Physiol Rev* 2003;**83**:1325–1358.
18. Maguire JJ, Davenport AP. Regulation of vascular reactivity by established and emerging GPCRs. *Trends Pharmacol Sci* 2005;**26**:448–454.
19. Gohla A, Schultz G, Offermanns S. Role for G(12)/G(13) in agonist-induced vascular smooth muscle cell contraction. *Circ Res* 2000;**87**:221–227.
20. Wirth A, Benyo Z, Lukasova M, Leutgeb B, Wettschureck N, Gorbey S, Orsy P, Horvath B, Maser-Gluth C, Greiner E, Lemmer B, Schutz G, Gutkind JS, Offermanns S. G12-G13-LARG-mediated signaling in vascular smooth muscle is required for salt-induced hypertension. *Nat Med* 2008;**14**:64–68.
21. Guilluy C, Bregeon J, Toumaniantz G, Rolli-Derkinderen M, Retailleau K, Loufrani L, Henrion D, Scalbert E, Bril A, Torres RM, Offermanns S, Pacaud P, Loirand G. The Rho exchange factor Arhgef1 mediates the effects of angiotensin II on vascular tone and blood pressure. *Nat Med* 2010;**16**:183–190.
22. Moers A, Nieswandt B, Massberg S, Wettschureck N, Gruner S, Konrad I, Schulte V, Aktas B, Gratacap MP, Simon MI, Gawaz M, Offermanns S. G13 is an essential mediator of platelet activation in hemostasis and thrombosis. *Nat Med* 2003;**9**:1418–1422.
23. Wettschureck N, Rutten H, Zywietz A, Gehring D, Wilkie TM, Chen J, Chien KR, Offermanns S. Absence of pressure overload induced myocardial hypertrophy after conditional inactivation of Galphaq/Galpha11 in cardiomyocytes. *Nat Med* 2001;**7**:1236–1240.
24. Herroeder S, Reichardt P, Sassmann A, Zimmermann B, Jaeneke D, Hoeckner J, Hollmann MW, Fischer KD, Vogt S, Grosse R, Hogg N, Gunzer M, Offermanns S, Wettschureck N. Guanine nucleotide-binding proteins of the G12 family shape immune functions by controlling CD4+ T cell adhesiveness and motility. *Immunity* 2009;**30**:708–720.
25. Kedzierski RM, Grayburn PA, Kisanuki YY, Williams CS, Hammer RE, Richardson JA, Schneider MD, Yanagisawa M. Cardiomyocyte-specific endothelin A receptor knockout mice have normal cardiac function and an unaltered hypertrophic response to angiotensin II and isoproterenol. *Mol Cell Biol* 2003;**23**:8226–8232.
26. Larson AC, White RD, Laub G, McVeigh ER, Li D, Simonetti OP. Self-gated cardiac cine MRI. *Magn Reson Med* 2004;**51**:93–102.
27. Henry JP, Meehan JP, Santisteban G, Stevens P. Age variation of the blood pressure of male CBA mice. *Fed Proc* 1963;**22**:455 (Abstr.).
28. Wu CH, Visscher MB. Measurement of blood pressure in the mouse with special reference to age. *Fed Proc* 1947;**6**:231 (Abstr.).
29. McCurley A, Pires PW, Bender SB, Aronovitz M, Zhao MJ, Metzger D, Chambon P, Hill MA, Dorrance AM, Mendelsohn ME, Jaffe IZ. Direct regulation of blood pressure by smooth muscle cell mineralocorticoid receptors. *Nat Med* 2012;**18**:1429–1433.
30. Bourque SL, Davidge ST, Adams MA. The interaction between endothelin-1 and nitric oxide in the vasculature: new perspectives. *Am J Physiol Regul Integr Comp Physiol* 2011;**300**:R1288–R1295.
31. Alonso D, Radomski MW. The nitric oxide-endothelin-1 connection. *Heart Fail Rev* 2003;**8**:107–115.
32. Arai K, Maruyama Y, Nishida M, Tanabe S, Takagahara S, Kozasa T, Mori Y, Nagao T, Kurose H. Differential requirement of G alpha12, G alpha13, G alphaq, and G beta gamma for endothelin-1-induced c-Jun NH2-terminal kinase and extracellular signal-regulated kinase activation. *Mol Pharmacol* 2003;**63**:478–488.
33. Franklin SS, Gustin W, Wong ND, Larson MG, Weber MA, Kannel WB, Levy D. Hemodynamic patterns of age-related changes in blood pressure. The Framingham Heart Study. *Circulation* 1997;**96**:308–315.
34. Whelton PK. Epidemiology of hypertension. *Lancet* 1994;**344**:101–106.
35. Guyton AC, Coleman TG, Cowley AV Jr, Scheel KW, Manning RD Jr, Norman RA Jr. Arterial pressure regulation. Overriding dominance of the kidneys in long-term regulation and in hypertension. *Am J Med* 1972;**52**:584–594.
36. Rautureau Y, Coelho SC, Fraulob-Aquino JC, Huo KG, Rehman A, Offermanns S, Paradis P, Schiffrin EL. Inducible human endothelin-1 overexpression in endothelium raises blood pressure via endothelin type A receptors. *Hypertension* 2015;**66**:347–355.

37. Mendelsohn ME. In hypertension, the kidney is not always the heart of the matter. *J Clin Invest* 2005;**115**:840–844.
38. Michael SK, Surks HK, Wang Y, Zhu Y, Blanton R, Jamnongjit M, Aronovitz M, Baur W, Ohtani K, Wilkerson MK, Bonev AD, Nelson MT, Karas RH, Mendelsohn ME. High blood pressure arising from a defect in vascular function. *Proc Natl Acad Sci USA* 2008;**105**:6702–6707.
39. Milner P, Bodin P, Loesch A, Burnstock G. Increased shear-stress leads to differential release of endothelin and ATP from isolated endothelial-cells from 4-month-old and 12-month-old male rabbit aorta. *J Vasc Res* 1992;**29**:420–425.
40. Goel A, Su B, Flavahan S, Lowenstein CJ, Berkowitz DE, Flavahan NA. Increased endothelial exocytosis and generation of endothelin-1 contributes to constriction of aged arteries. *Circ Res* 2010;**107**:242–251.
41. Donato AJ, Gano LB, Eskurza I, Silver AE, Gates PE, Jablonski K, Seals DR. Vascular endothelial dysfunction with aging: endothelin-1 and endothelial nitric oxide synthase. *Am J Physiol Heart Circ Physiol* 2009;**297**:H425–H432.
42. Thijssen DH, Rongen GA, van Dijk A, Smits P, Hopman MT. Enhanced endothelin-1-mediated leg vascular tone in healthy older subjects. *J Appl Physiol* 2007;**103**:852–857.
43. Van Guilder GP, Westby CM, Greiner JJ, Stauffer BL, DeSouza CA. Endothelin-1 vasoconstrictor tone increases with age in healthy men but can be reduced by regular aerobic exercise. *Hypertension* 2007;**50**:403–409.
44. Lazich I, Bakris GL. Endothelin antagonism in patients with resistant hypertension and hypertension nephropathy. *Contrib Nephrol* 2011;**172**:223–234.
45. Rautureau Y, Schiffrin EL. Endothelin in hypertension: an update. *Curr Opin Nephrol Hypertens* 2012;**21**:128–136.

2.3 Piezo1 und G-Proteine der Familie G_q/G_{11} induzieren endotheliale Inflammation in Abhängigkeit von Fluss-Profil und Integrin-Aktivierung.

Piezo1 and G_q/G_{11} promote endothelial inflammation depending on flow pattern and integrin activation. Albarrán-Juárez J, Iring A, Wang S, Joseph S, Grimm M, Strilic B, Wettschureck N, **Althoff TF***, Offermanns S*. *J Exp Med*. 2018 Sep 7. pii: jem.20180483.

**These senior authors contributed equally to this work*

https://doi.org/10.1084/jem.20180483

„Das Gefäß-Endothel ist kontinuierlich mechanischen Kräften, einschließlich Blutfluss-induzierten Fluid-Scherkräften ausgesetzt. Endothelzellen können unterschiedliche Fluß-Profile wahrnehmen. So wandeln sie die mechanischen Signale laminaren Flusses in atheroprotektive Signale, inklusive eNOS-Aktivierung, um, während gestörter Blutfluss in Atherosklerose-anfälligen Gefäßabschnitten eine inflammatorische Signaltransduktion inklusive NF-κB-Aktivierung induziert. Wie Endothelzellen zwischen diesen unterschiedlichen Fluß-Profilen differenzieren, ist bis dato kaum verstanden.

Hier zeigen wir, dass laminarer und gestörter Fluss den gleichen initialen Signalweg bestehend aus dem mechanosensitiven Kationen-Kanal Piezo1 und G-Proteinen der Familie G_q/G_{11} aktivieren. Allerdings führte nur gestörter, atherogener Fluß zur Piezo1- und $G\alpha_q/G\alpha_{11}$-vermittelten Integrin-Aktivierung, die wiederum in einer Focal Adhesion Kinase-abhängigen Aktivierung von NF-κB resultierte. Entsprechend zeigten Mäuse mit induzierter, Endothel-spezifischer Defizienz von Piezo1 oder $G\alpha_q/G\alpha_{11}$ eine deutlich reduzierte Integrin-Aktivierung, inflammatorische Signaltransduktion und Progression der Atherosklerose in Gefäßarealen mit atherogenem Blutfluß.

Unsere Daten identifizieren somit kritische Mechanismen der differenziellen endothelialen Mechanotransduktion, die Fluss-Profil-abhängig zwischen der Aktivierung atheroprotektiver und atherogener Signalwege unterscheiden. Zudem lassen sich aus den Ergebnissen therapeutische Strategien zur Behandlung inflammatorischer Gefäßerkrankungen wie der Atherosklerose ableiten.“ Übersetzung durch den Autor.

JEM Journal of Experimental Medicine

ARTICLE

Piezo1 and G_q/G_{11} promote endothelial inflammation depending on flow pattern and integrin activation

Julián Albarrán-Juárez[1], Andras Iring[1], ShengPeng Wang[1], Sayali Joseph[1], Myriam Grimm[1], Boris Strilic[1], Nina Wettschureck[1,3,4], Till F. Althoff[1,2,4*], and Stefan Offermanns[1,3,4*]

The vascular endothelium is constantly exposed to mechanical forces, including fluid shear stress exerted by the flowing blood. Endothelial cells can sense different flow patterns and convert the mechanical signal of laminar flow into atheroprotective signals, including eNOS activation, whereas disturbed flow in atheroprone areas induces inflammatory signaling, including NF-κB activation. How endothelial cells distinguish different flow patterns is poorly understood. Here we show that both laminar and disturbed flow activate the same initial pathway involving the mechanosensitive cation channel Piezo1, the purinergic $P2Y_2$ receptor, and G_q/G_{11}-mediated signaling. However, only disturbed flow leads to Piezo1- and G_q/G_{11}-mediated integrin activation resulting in focal adhesion kinase-dependent NF-κB activation. Mice with induced endothelium-specific deficiency of Piezo1 or $G\alpha_q/G\alpha_{11}$ show reduced integrin activation, inflammatory signaling, and progression of atherosclerosis in atheroprone areas. Our data identify critical steps in endothelial mechanotransduction, which distinguish flow pattern-dependent activation of atheroprotective and atherogenic endothelial signaling and suggest novel therapeutic strategies to treat inflammatory vascular disorders such as atherosclerosis.

Introduction

Atherosclerosis is an inflammatory disorder of large and medium-sized arteries that predisposes to myocardial infarction and stroke, which are leading causes of morbidity and mortality worldwide (GBD 2015 Mortality and Causes of Death Collaborators, 2016). It is promoted by various risk factors including high plasma levels of LDL cholesterol and triglycerides, inflammatory mediators, diabetes mellitus, obesity, arterial hypertension, and sedentary lifestyle (Herrington et al., 2016). However, in addition to these systemic factors, the local arterial microenvironment strongly influences the development of atherosclerotic lesions. Most strikingly, atherosclerosis develops selectively in curvatures, branching points, and bifurcations of the arterial system where blood flow is disturbed, while areas exposed to high laminar flow are largely resistant to atherosclerosis development (Hahn and Schwartz, 2009; Chiu and Chien, 2011; Tarbell et al., 2014).

Multiple evidence shows that high laminar flow and disturbed flow induce different signal transduction processes in endothelial cells resulting in an anti- or pro-atherogenic phenotype, respectively (Hahn and Schwartz, 2009; Chiu and Chien, 2011; Nigro et al., 2011; Tarbell et al., 2014; Zhou et al., 2014; Gimbrone and García-Cardeña, 2016; Givens and Tzima, 2016; Yurdagul et al., 2016; Nakajima and Mochizuki, 2017). Disturbed flow promotes inflammatory signaling pathways such as NF-κB activation, resulting in the expression of leukocyte adhesion molecules including VCAM-1 and ICAM-1, as well as chemokines including CCL2 (Mohan et al., 1997; Nagel et al., 1999; Feaver et al., 2010). Activation of inflammatory signaling by disturbed flow has been shown to involve a mechanosignaling complex consisting of PECAM-1, VE-cadherin, and VEGFR2 (Tzima et al., 2005), as well as activation of integrins (Finney et al., 2017). The PECAM-1/VE-cadherin/VEGFR2-mechanosignaling complex is also involved in high laminar shear stress-induced activation of anti-atherogenic signaling and, under this condition, regulates AKT to phosphorylate and activate eNOS (Fleming et al., 2005; Wang et al., 2015). Laminar flow-induced activation of this pathway has been shown to be dependent on the cation channel Piezo1, which mediates flow-induced release of ATP from endothelial cells, resulting in the activation of the G_q/G_{11}-coupled purinergic $P2Y_2$ receptor (Wang et al., 2015, 2016). How distinct flow patterns induce different endothelial phenotypes has, however, remained largely unclear.

[1]Max Planck Institute for Heart and Lung Research, Department of Pharmacology, Bad Nauheim, Germany; [2]Charité – Universitätsmedizin Berlin, Department of Cardiology and Angiology, Campus Mitte, Berlin, Germany; [3]Center for Molecular Medicine, Medical Faculty, J.W. Goethe University Frankfurt, Frankfurt, Germany; [4]German Center for Cardiovascular Research (DZHK).

*T.F. Althoff and S. Offermanns contributed equally to this paper; Correspondence to Stefan Offermanns: stefan.offermanns@mpi-bn.mpg.de; Julián Albarrán-Juárez: Julian.Albarran@mpi-bn.mpg.de.

Different flow patterns have a strong effect on the morphology of endothelial cells in that endothelial cells in areas of high laminar shear elongate and align in the direction of flow, whereas cells under disturbed flow fail to do so (Davies, 2009). In consequence, cells under sustained laminar flow receive flow only in the direction of the cell axis, whereas cells in areas of disturbed flow are randomly oriented and are exposed to flow at many different angles. Recent data suggest that the response of endothelial cells to flow is determined by the direction of flow relative to the morphological and cytoskeletal axis of the endothelial cell (Wang et al., 2013). When endothelial cells that had been preflowed to induce alignment were exposed to laminar flow in the direction of the cell axis, maximal eNOS activation was observed, while eNOS activation was undetectable when the flow direction was perpendicular to the cell axis. In contrast, activation of NF-κB was maximal at 90 degrees and undetectable when cells received flow parallel to the cell axis (Wang et al., 2013). This would explain why disturbed flow promotes inflammatory signaling, whereas sustained laminar flow promotes anti-inflammatory signaling. However, the molecular and cellular mechanisms mediating the activation of pro- and anti-atherogenic signaling depending on the flow direction are unclear.

Here we show that both laminar and disturbed flow activate the same initial mechanosignaling pathway involving Piezo1- and G_q/G_{11}-mediated signaling. However, depending on the flow pattern, endothelial cells read these signaling processes out as either atheroprotective signaling resulting in eNOS activation or as inflammatory signaling resulting in NF-κB activation. This differential cell response to the initial mechanotransduction process depends on the activation of α5 integrin, which is activated only by disturbed flow, but not by sustained laminar flow.

Results

Endothelial inflammation induced by disturbed flow requires Piezo1 and G_q/G_{11}-mediated signaling

We have previously shown that G_q/G_{11}-mediated signaling plays a critical role in mediating laminar flow-induced eNOS activation in endothelial cells by coupling Piezo1-mediated mechanotransduction via the PECAM-1/VE-cadherin/VEGFR2 complex to phosphorylation and activation of eNOS (Wang et al., 2015, 2016). To test the role of G_q/G_{11}-mediated signaling in the activation of inflammatory signaling induced by disturbed flow, we exposed human umbilical artery endothelial cells (HUA ECs) to oscillatory flow. As described before (Mohan et al., 1997), disturbed flow induced NF-κB activation as indicated by phosphorylation of p65 at serine 536 (Fig. 1 A). Surprisingly, disturbed flow-induced inflammatory signaling was blocked after knock-down of $P2Y_2$, as well as $Gα_q$ and $Gα_{11}$ (Fig. 1 A and Fig. S1 A). Very similar data were obtained after knock-down of Piezo1 (Fig. 1 A and Fig. S1 A), which has been shown to operate upstream of $P2Y_2$ and G_q/G_{11} by mediating flow-induced endothelial ATP-release (Wang et al., 2016). We also found that, similar to laminar flow (Bodin et al., 1991; John and Barakat, 2001; Yamamoto et al., 2011; Wang et al., 2016), disturbed flow also induces ATP release from endothelial cells in a Piezo1-dependent manner (Fig. 1 B).

Consistent with a role of Piezo1, $P2Y_2$, and G_q/G_{11} in the activation of endothelial NF-κB in response to disturbed flow, we found that disturbed flow applied for 48 h failed to induce nuclear translocation of p65 in endothelial cells with silenced Piezo1 or $Gα_q/Gα_{11}$ expression (Fig. 1, C and D). Since activation of NF-κB in endothelial cells has been shown to induce expression of leukocyte adhesion molecules, we tested whether knock-down of Piezo1 or $Gα_q/Gα_{11}$ affects expression of VCAM-1. When HUA ECs were exposed to disturbed flow for 48 h, a strong induction of VCAM-1 immunoreactivity and RNA expression could be observed in control cells (Fig. 1 E and Fig. S1 B). However, this effect was strongly reduced after knock-down of Piezo1 or $Gα_q/Gα_{11}$ (Fig. 1 E and Fig. S1 B). Similar results were observed for the oscillatory flow-induced up-regulation of other inflammatory genes, such as those encoding CCL2 and PDGFB (Fig. S1, C and D). Consistent with the impaired up-regulation of cell adhesion molecules and chemokines, adhesion of THP-1 monocytes to endothelial cells exposed to disturbed flow for 48 h was strongly reduced after knock-down of Piezo1 or $Gα_q/Gα_{11}$ (Fig. 1 F). These data show that Piezo1 and G_q/G_{11} do not only mediate laminar flow-induced anti-atherogenic signaling in endothelial cells, but are also required for induction of inflammatory endothelial activation in response to disturbed flow in vitro.

Endothelial Piezo1 and G_q/G_{11} deficiency results in reduced endothelial inflammation and progression of atherosclerosis

We next tested whether Piezo1, $P2Y_2$, and G_q/G_{11} mediate disturbed flow-induced endothelial inflammation also under in vivo conditions using tamoxifen-induced, endothelium-specific $Gα_q/Gα_{11}$-, $P2Y_2$-, or Piezo1-deficient mice (Korhonen et al., 2009; Wang et al., 2015, 2016). At the outer curvature of the aortic arch, which is typically exposed to continuous laminar flow, we did not see any obvious differences in the endothelial cell morphology, Vcam-1 expression, or number of Cd68-positive cells in mice with endothelium-specific Piezo1, $P2Y_2$, or $Gα_q/Gα_{11}$ deficiency (Fig. S2, A and B; and Fig. S3, A and C). However, at the inner curvature of the aortic arch, where endothelial cells are naturally exposed to disturbed, atherogenic flow, the increase in endothelial Vcam-1 expression and number of CD68-positive cells were strongly reduced after loss of endothelial Piezo1, $P2Y_2$, or $Gα_q/Gα_{11}$ expression (Fig. 2, A and B; and Fig. S3, B and C). The reduced Vcam-1 in endothelium-specific $Gα_q/Gα_{11}$- and Piezo1-deficient mice was also observed by quantitative PCR analysis (Fig. S4 A), and the reduction in the number of Cd68-positive cells was reflected by a reduced number of Cd11c-positive cells, which have been shown to be present in atheroprone areas of the aorta (Fig. S4 B; Choi et al., 2009).

To study the function of endothelial Piezo1, $P2Y_2$, and G_q/G_{11} in atherogenesis, we performed partial carotid artery ligation, a model for acutely induced disturbed flow leading together with reduced laminar flow to endothelial dysfunction and atherosclerosis (Nam et al., 2010). Induction of endothelium-specific Piezo1 or $Gα_q/Gα_{11}$ deficiency in mice lacking the LDL-receptor and fed a high-fat diet resulted in a strong reduction of endothelial inflammation indicated by reduced Vcam-1 expression 2 wk after ligation (Fig. 2 C and Fig. S4 C). 4 wk after partial carotid artery ligation, a significant reduction in neointima size was found in

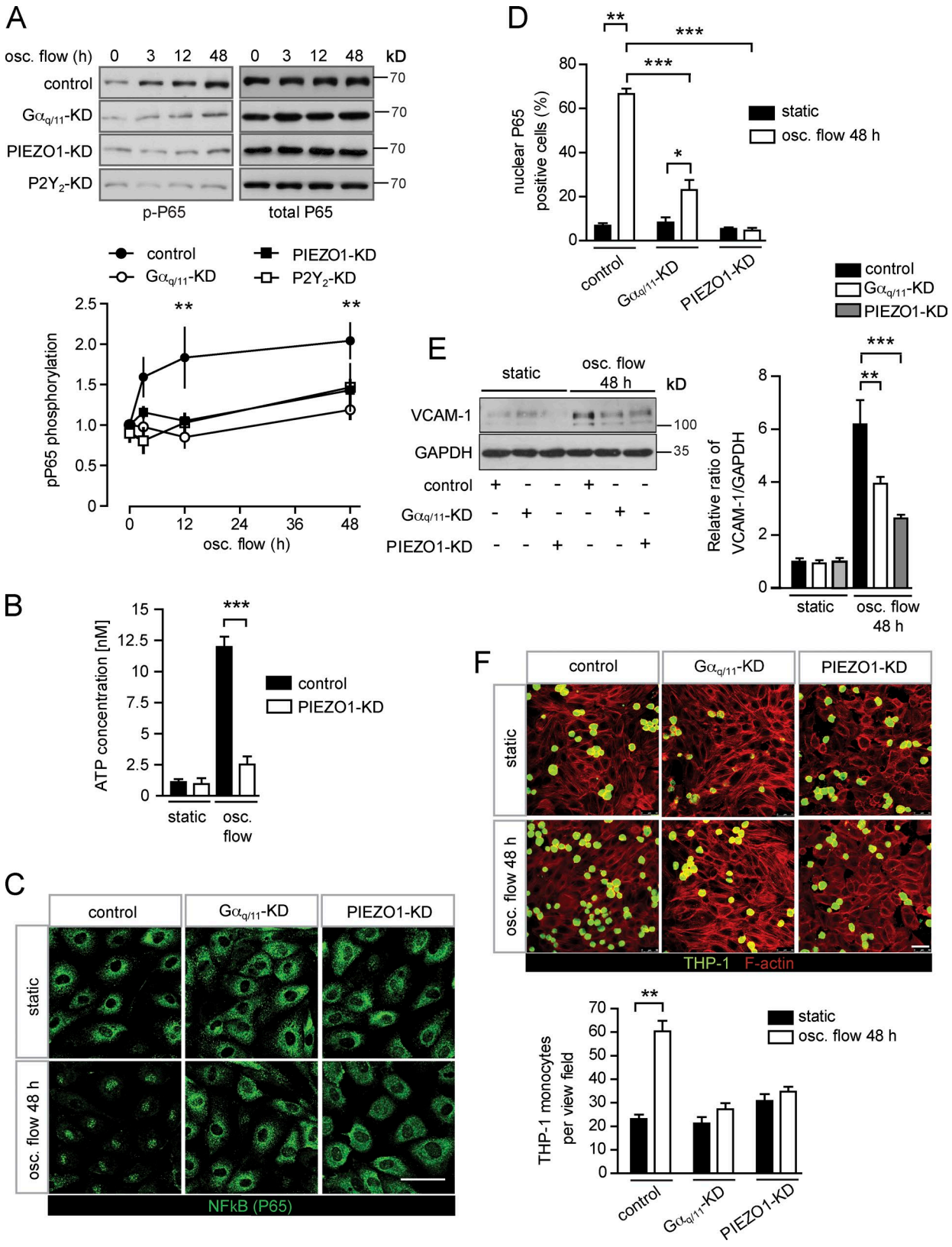

Figure 1. **Endothelial inflammation induced by disturbed flow is mediated by Piezo1 and G_q/G_{11}. (A–F)** Confluent HUAECs were transfected with scrambled (control) siRNA, siRNA directed against Piezo1, $P2Y_2$, or $G\alpha_q$ and $G\alpha_{11}$. 24 h after second transfection, cells were further grown in the absence of flow (no flow) or were exposed to low and oscillatory (osc.) flow (4 dynes/cm^2, 1 Hz) using a flow chamber (A and C–F) or a cone-plate viscometer (B), as described in Materials and methods, for the indicated time periods (A). NF-κB activation was determined by Western blotting for phosphorylated P65 (Ser536). Shown are representative blots. The linear diagram shows the densitometric evaluation of three to five independent experiments normalized to total P65. **(B)** Concentration of ATP in the supernatant of HUAECs kept under static conditions or under oscillatory flow (data are representative of a least three independent

LDL-receptor–deficient mice with endothelium-specific Piezo1, $P2Y_2$, or $G\alpha_q/G\alpha_{11}$ deficiency (Fig. 2 D and Fig. S3 D). Similar observations were made in a long-term model of atherosclerosis. After 16 wk of feeding mice a high-fat diet, development and progression of atherosclerotic plaques was significantly reduced in the aorta, the aortic root, as well as in the innominate artery of endothelium-specific Piezo1- or $G\alpha_q/G\alpha_{11}$-deficient mice lacking the LDL- receptor compared with control LDL-receptor–deficient mice (Fig. 3, A–C; and Fig. S4, C and D).

Endothelial Piezo1 and G_q/G_{11} mediate atheroprotective or atheroprone signaling depending on the flow pattern

These data indicate that endothelial Piezo1 and G_q/G_{11} mediate inflammatory endothelial signaling in response to disturbed flow resulting in endothelial dysfunction and atherosclerosis in vitro and in vivo. Interestingly, the same upstream mechanosignaling pathway also senses laminar flow and promotes eNOS activation in vitro and in vivo (Wang et al., 2015, 2016). Thus, Piezo1- and G_q/G_{11}-mediated signaling appear to be activated both by laminar and disturbed flow and mediate atheroprotective, as well as pro-atherogenic, signaling. We then wanted to understand how endothelial cells read out Piezo1- and G_q/G_{11}-mediated mechanosignaling depending on the flow pattern either as activation of anti-atherogenic signaling leading to eNOS activation or as an atherogenic stimulus resulting in inflammatory signaling and activation of NF-κB. To be able to clearly distinguish between endothelial responses to laminar and disturbed flow, we first preflowed endothelial cells by exposing them for 24 h to laminar flow, which resulted in alignment of cells in the direction of flow. Thereafter, we reexposed cells to high laminar flow parallel to the cell axis or to disturbed flow. Disturbed flow was induced by high-frequency oscillatory flow or by changing the flow direction by 90 degrees (Fig. 4 A). When preflowed control cells were reexposed to high laminar flow, we observed increased eNOS phosphorylation, whereas no activation of NF-κB indicated by phosphorylation of p65 at serine 536, and degradation of Iκ-Bα was seen (Fig. 4 B). In contrast, in preflowed cells both oscillatory flow and flow perpendicular to the morphological cell axis resulted in strong activation of NF-κB, whereas eNOS phosphorylation was unaffected (Fig. 4, C and D). Knock-down of $G\alpha_q/G\alpha_{11}$ blocked not only laminar flow-induced eNOS phosphorylation (Fig. 4 B), but also disturbed flow-induced inflammatory signaling (Fig. 4, C and D), and the same was observed after knock-down of Piezo1 (Fig. 5, A and B). This shows that in preflowed endothelial cells different downstream signaling processes are induced via Piezo1 and G_q/G_{11}, depending on the applied flow pattern.

Integrins are differentially activated by different flow patterns via Piezo1 and G_q/G_{11}

Since flow-induced endothelial NF-κB activation has been shown to be mediated by integrin α5β1 or αvβ3 and to require focal adhesion kinase (FAK) downstream of integrins (Bhullar et al., 1998; Petzold et al., 2009; Chen et al., 2015; Sun et al., 2016; Yun et al., 2016), we tested the effect of laminar and disturbed flow on FAK phosphorylation in preflowed endothelial cells. As shown in Fig. 6 (A–E), only disturbed flow was able to induce FAK activation, whereas laminar flow had no effect or rather reduced FAK activity. The FAK activation by disturbed flow was absent in cells after knock-down of $G\alpha_q$ and $G\alpha_{11}$ (Fig. 6, B and C) and Piezo1 (Fig. 6 E). Immunohistochemical analysis of the aortic arch of LDL-receptor–deficient mice showed strongly increased phosphorylation of FAK in endothelial cells of the inner curvature compared with the outer curvature (Fig. 6, F and G). Interestingly, in LDL-receptor–deficient mice lacking Piezo1 or $G\alpha_q/G\alpha_{11}$ in an endothelium-specific manner, this increased endothelial phosphorylation of FAK at the inner aortic curvature was abrogated (Fig. 6, F and G).

To discriminate between an involvement of integrin α5 and integrin αv, we knocked down expression of either integrin α-subunit. As shown in Fig. 7 A, only knock-down of integrin α5 inhibited disturbed flow-induced FAK and NF-κB activation, whereas knock-down of integrin αv was without effect. Similarly, blockade of α5β1 integrin with ATN-161, but not of αvβ3 integrin with S247, inhibited flow-induced phosphorylation of FAK and P65 (Fig. S5 A). To study flow pattern–dependent integrin activation more directly, we used antibodies recognizing the activated form of integrin α5 (Sun et al., 2016). We found that integrin α5 became activated upon disturbed flow, but not in response to laminar flow (Fig. 7, B and C), and knock-down of $G\alpha_q/G\alpha_{11}$ blocked integrin activation in response to disturbed flow (Fig. 7 C). Staining of sections from the aortic arch of LDL-receptor–deficient mice with antibody SNAKA51 directed against active integrin α5 (Clark et al., 2005), which also recognizes activated murine integrin α5 (Fig. S5, B–E), showed increased integrin activation in endothelial cells of the inner curvature compared with those of the outer curvature (Fig. 7 D). In LDL-receptor–deficient mice with induced endothelium-specific Piezo1- or $G\alpha_q/G\alpha_{11}$-deficiency, the increased endothelial integrin activation at the inner aortic curvature was strongly reduced (Fig. 7 D). These data indicate that in preflowed endothelial cells, only disturbed flow induces integrin activation and that also under in vivo conditions endothelial cells in areas of disturbed flow show Piezo1- and G_q/G_{11}-dependent increases in integrin activation and FAK phosphorylation.

experiments). **(C and D)** Cellular P65 localization was determined by staining of cells with an anti-P65 antibody. Representative micrographs are shown to quantify nuclear translocation of P65, at least 100 cells were counted per condition for each experiment (data are representative of a least three independent experiments per group). **(E)** VCAM-1 immunoreactivity was determined by Western blotting (representative blots of four independent experiments). **(F)** To study monocyte cell adhesion to HUAECs, cells were preexposed to oscillatory flow for 48 h and were incubated with fluorescently labeled THP-1 cells for 30 min at 37°C. (Shown are representative micrographs from three independent experiments). Actin fibers were stained with anti–phalloidin-Alexa Fluor 568 and visualized by confocal microscopy. Bars, 50 µm. Data represent mean values ± SEM; **, P ≤ 0.01; ***, P ≤ 0.001 (two-way ANOVA and Bonferroni's post hoc test [A, D, and E] and two-tailed Student's *t* test [B and F]).

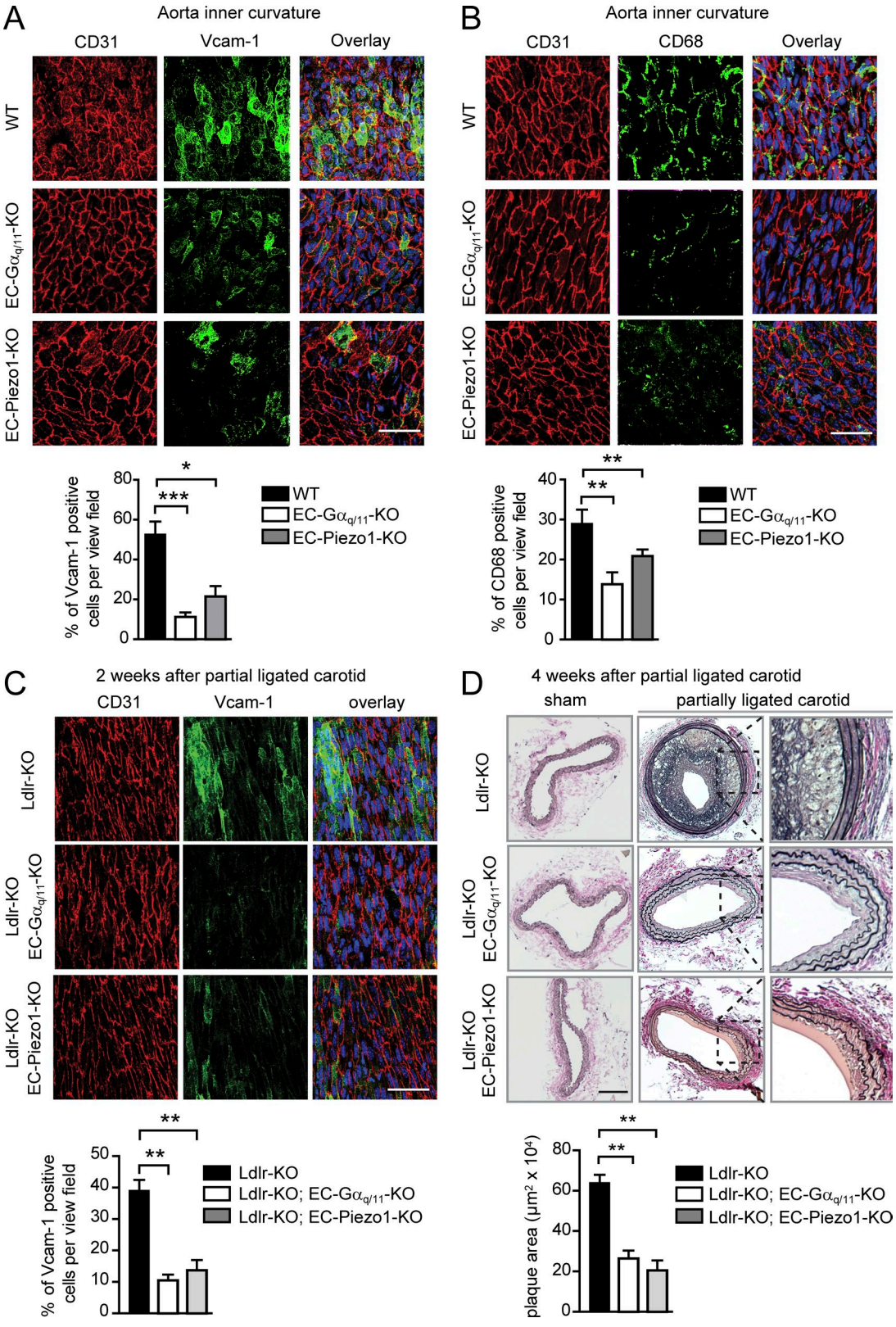

Figure 2. **Endothelial Piezo1 and G_q/G_{11} deficiency results in decreased endothelial inflammation and reduced progression of atherosclerosis. (A and B)** Shown are representative en face immuno-confocal microscopy images of the inner curvature from 12-wk-old wild-type and endothelium-specific Piezo1-KO (EC-Piezo1-KO) and $G\alpha_q/G\alpha_{11}$-KO (EC-$G\alpha_q/G\alpha_{11}$-KO) mice (n = 6 per genotype per condition). En face aortic arch preparations were triple stained with anti-CD31, anti–Vcam-1 (A) or anti-CD68 antibodies (B) and DAPI. Immunofluorescence staining was quantified as the percentage of Vcam-1–positive cells among CD31-positive cells per view field (A) and as the percentage of CD68-positive cells per view field (B). **(C and D)** Atherosclerosis-prone Ldlr-KO mice without (Ldlr-KO) or with endothelium-specific Piezo1 (Ldlr-KO; EC-Piezo1-KO) or $G\alpha_q/G\alpha_{11}$ deficiency (Ldlr-KO;EC-$G\alpha_{q/11}$-KO) were sham operated or underwent partial carotid artery ligation. **(C)** 14 d after ligation, en face preparations of the left common carotid artery (ligated artery) were stained with DAPI and

Discussion

Laminar flow and disturbed flow profoundly differ in their effects on endothelial cell morphology and function. While continuous high laminar flow induces endothelial cell elongation and alignment in the direction of flow, failure of endothelial cells to elongate and to align under disturbed flow is a hallmark of atheroprone vessel areas (Davies, 2009). It has been suggested that exposure of endothelial cells to unidirectional flow results in adaptation by altering the mechanotransduction of endothelial cells (Davies et al., 1997; Hahn and Schwartz, 2008). This is consistent with the observation that endothelial cells grown in vitro initially respond to laminar flow with both atherogenic, inflammatory, and atheroprotective, anti-inflammatory signaling. However, once cells have been exposed to laminar flow for a while, they align and show down-regulation of atherogenic, inflammatory signaling, whereas inflammatory signaling remains activated under disturbed flow (Mohan et al., 1997; Hahn and Schwartz, 2009). While the effect of fluid shear stress on endothelial cell function and signaling has been extensively studied, the majority of studies have been performed with endothelial cells, which have not been exposed to flow before the experiment. However, under in vivo conditions, endothelial cells are constantly under the influence of flow, and recent evidence indicates that the flow angle is a very critical determinant of the cellular responses to flow (Wang et al., 2013). Flow in the direction of the cell axis in prealigned cells stimulates activation of eNOS, whereas off-axis flow results in the activation of inflammatory signaling, including NF-κB activation (Wang et al., 2013). By combining in vivo experiments and in vitro studies on preflowed endothelial cell cultures, we show that atheroprotective and atherogenic signaling induced by laminar and disturbed flow, respectively, both involve Piezo1-, $P2Y_2$-, and G_q/G_{11}-mediated signaling. When this signaling cascade is activated by laminar flow, which does not induce integrin activation, it promotes atheroprotective downstream signaling such as eNOS activation. However, when activated by disturbed flow, which also induces integrin activation, pro-inflammatory signaling processes including NF-κB activation are induced (Fig. 8).

Consistent with a role of Piezo1-, $P2Y_2$-, and G_q/G_{11}-mediated mechanotransduction in inflammatory signaling via NF-κB in atheroprone vascular areas, we found that endothelium-specific loss of Piezo1, $P2Y_2$, and $G\alpha_q/G\alpha_{11}$ strongly reduced progression of atherosclerosis, and similar results were independently reported for endothelium-specific $P2Y_2$-deficient mice (Chen et al., 2017). On the other hand, we previously showed that loss of endothelial Piezo1, $P2Y_2$, and $G\alpha_q/G\alpha_{11}$ reduces flow-induced eNOS activation resulting in an increase in arterial blood pressure (Wang et al., 2015, 2016). Similar phenotypes have been observed in mice lacking PECAM-1, another component of the flow-induced signaling cascade. PECAM-1–deficient animals show reduced progression of atherosclerosis (Harry et al., 2008), while PECAM-1 has also been shown to mediate flow-induced eNOS activation (Fleming et al., 2005), and mice lacking PECAM-1 show reduced flow-induced nitric oxide (NO) formation and vasodilation (Bagi et al., 2005). While a concurrent involvement of Piezo1- and G_q/G_{11}-mediated mechanotransduction in flow-induced eNOS activation, as well as in promotion of atherosclerosis may appear counterintuitive, it is fully consistent with a role of this mechanosignaling pathway as an upstream mediator of endothelial cell responses to flow in general, irrespective of the flow pattern.

How different flow patterns direct Piezo1- and G_q/G_{11}-mediated signaling in the anti- and pro-inflammatory direction is not clear. However, we show that only disturbed flow induces integrin activation, which has been shown to mediate flow-induced NF-κB activation through FAK (Bhullar et al., 1998; Tzima et al., 2002; Orr et al., 2005, 2006). This is consistent with earlier data showing that flow induces inflammatory signaling by PECAM-1/VE-cadherin/VEGFR2- and PI-3-kinase–dependent inside-out activation of integrins, resulting in FAK-dependent NF-κB activation (Tzima et al., 2005). In contrast, under laminar flow, when integrins are not activated, the upstream signaling via G_q/G_{11} preferentially activates AKT, resulting in eNOS phosphorylation and activation (Wang et al., 2015). Activation of integrins in addition results in inhibition of cAMP signaling through activation of PDE4D (Yun et al., 2016), which would reduce eNOS activation through cAMP-dependent kinase (PKA; Boo et al., 2002; Dixit et al., 2005). However, other, so far unknown mechanisms might contribute to loss of eNOS activation in response to disturbed flow. Under in vivo conditions, activation of integrin α5β1 by disturbed flow is expected to be further promoted by the deposition of RGD-containing extracellular matrix proteins, such as fibronectin, within the endothelial cell matrix in atheroprone areas exposed to disturbed flow (Orr et al., 2005; Feaver et al., 2010).

Our observation that disturbed flow induces inflammatory signaling in prealigned endothelial cells through integrin α5 is consistent with recent reports providing evidence for a central role of integrin α5 in mediating flow-induced endothelial inflammatory signaling in vitro and in vivo (Sun et al., 2016; Yun et al., 2016; Budatha et al., 2018). However, earlier evidence suggested that also integrin αvβ3 is involved in flow-induced pro-inflammatory endothelial signaling (Bhullar et al., 1998; Chen et al., 2015). The exact mechanisms underlying the selective activation of integrins by disturbed flow, but not by laminar flow are unclear; however, similar observations have recently been made (Sun et al., 2016) and could be correlated with the ability of oscillatory shear stress to promote translocation of integrin α5 into lipid rafts, whereas pulsatile laminar shear stress caused integrin α5 to reside largely outside lipid rafts (Sun et al., 2016). How oscillatory flow, but not laminar flow, induces translocation of integrin α5 into lipid rafts is, however, unclear.

The ability of cells to sense not only the magnitude of a physical stimulus, but also its direction, has been observed in different contexts and appears to involve integrins (Swaminathan et al.,

antibodies against CD31 and Vcam-1. Vcam-1 staining was quantified as percentage of positive cells per view field. **(D)** 28 d after ligation, carotid arteries were sectioned and stained with elastic stain. Bar graphs show quantification of the intimal plaque area (n = 6 mice per genotype per condition). Bars: 50 µm (A–C) and 100 µm (D). Data represent mean ± SEM; *, $P \le 0.05$; **, $P \le 0.01$; ***, $P \le 0.001$ (one-way ANOVA and Bonferroni's post hoc test).

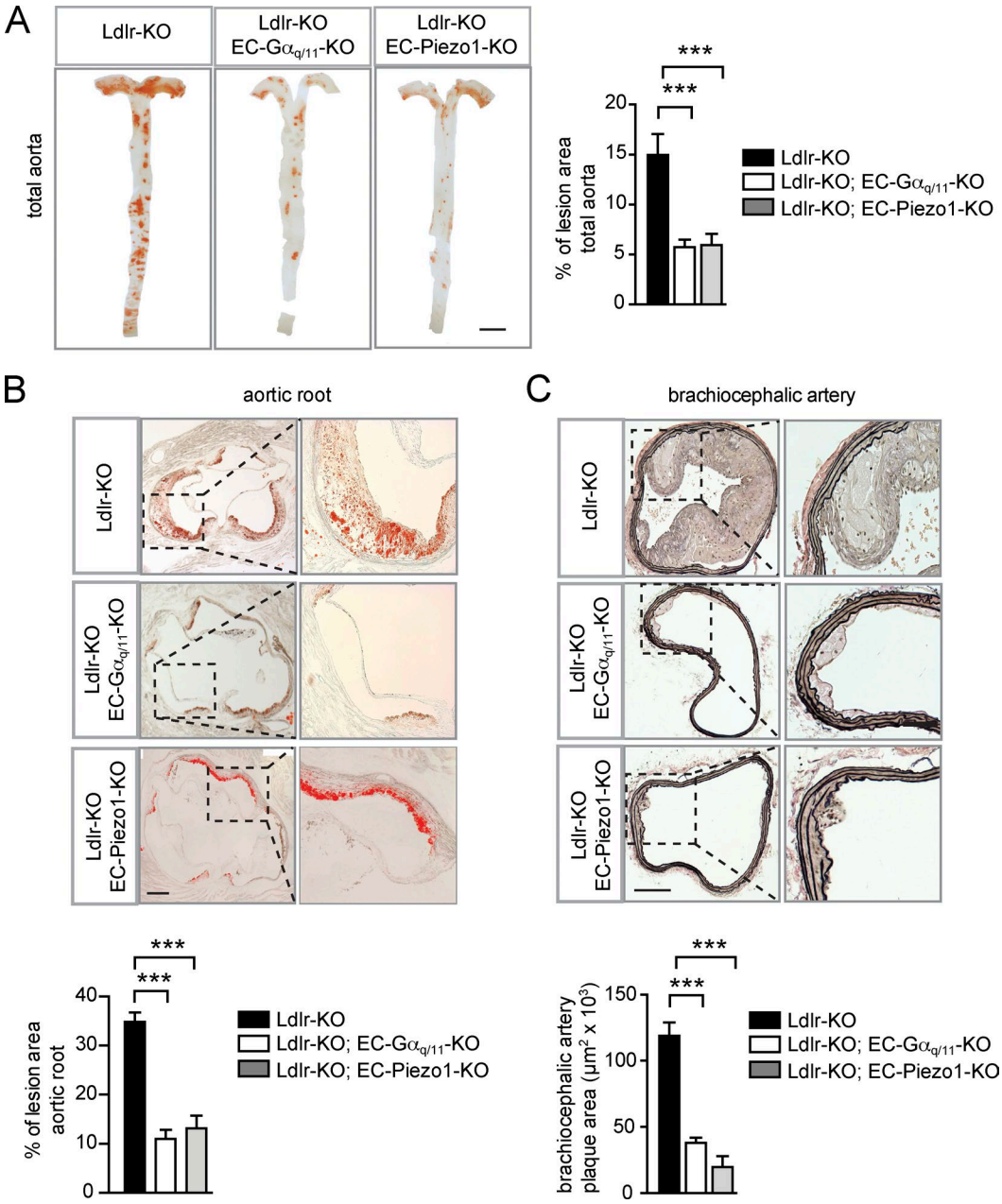

Figure 3. **Deficiency of endothelial Piezo1 and G_q/G_{11} reduces atherosclerotic plaque formation. (A–C)** Representative atherosclerotic lesions in *Ldlr*-KO mice without or with induced endothelium-specific Piezo1 deficiency (Tie2-CreER(T2);*Piezo1*$^{flox/flox}$ (Ldlr-KO;EC-Piezo1-KO)) or endothelium-specific $G\alpha_q/G\alpha_{11}$ deficiency (Cdh5-Cre;*Gnaq*$^{flox/flox}$;*Gna11*$^{-/-}$ (Ldlr-KO;EC-$G\alpha_{q/11}$-KO)) were fed a high-fat diet for 16 wk (n = 6–10 per genotype). **(A)** Representative images are shown of whole aortae that were prepared en face and stained with oil-red-O. En face atherosclerotic lesions are shown as percentage of total aorta area. **(B)** Representative oil-red-O–stained atherosclerotic lesions images in the aortic valve region (n = 6–10 per genotype). Dotted boxes are shown in higher magnifications in right panel. Plaque area was quantified as percentage of total aortic root area per genotype. **(C)** Representative images of atherosclerotic plaques observed in brachiocephalic arteries (innominate arteries). 5-µm paraffin cross sections were stained with elastic stain for assessment of morphological features. (n = 6–10 animals per genotype). Dotted boxes are shown in higher magnifications in right panel. Shown is the quantification of total plaque area in the brachiocephalic arteries. Data represent mean ± SEM; ***, P ≤ 0.001 (one-way ANOVA and Bonferroni's post hoc test). Bars: 5 mm (A); 250 µm (B); 100 µm (C).

2017a). Even though the molecular mechanism underlying the ability to sense the direction of mechanical cues remains rather obscure, recent data show that the interaction of vinculin and actin downstream of integrins occurs by forming a force-dependent catch bond that strongly depends on the direction of the applied force, and computational modeling suggests that the vinculin-actin catch bond might represent a mechanism for cellular responses to directional forces (Huang et al., 2017). Alternatively, integrins might sense force direction by molecular ordering. Recent studies indicate that integrins can be aligned and oriented by forces (Nordenfelt et al., 2017; Swaminathan et al., 2017b). Such directional orientation of integrins and associated molecules, including talin (Liu et al., 2015), might be a basis for direction-dependent mechanosensing. This would also be

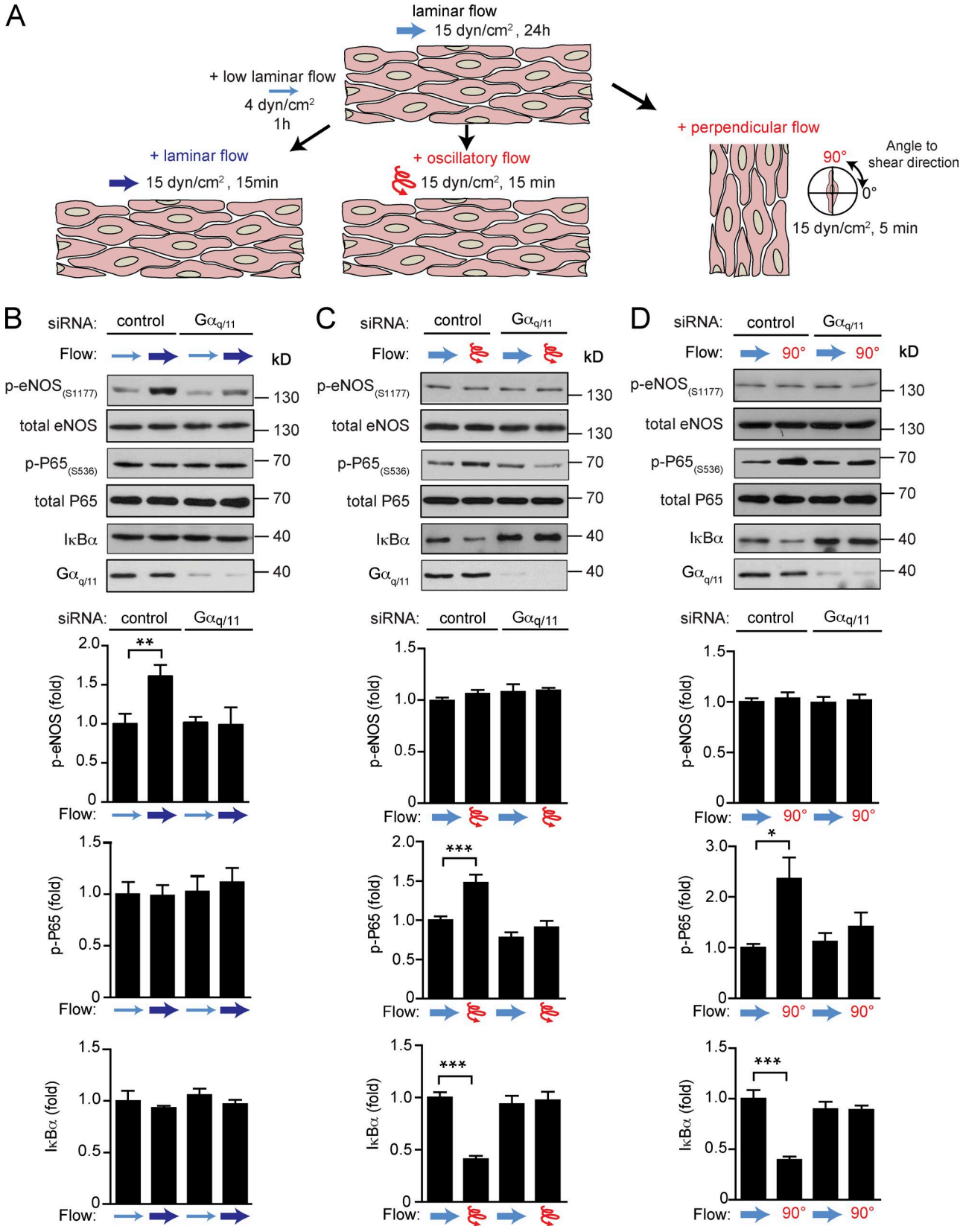

Figure 4. **Endothelial G_q/G_{11} mediates atheroprotective or atheroprone signaling upon stimulation by different flow patterns. (A)** Diagram of work flow. Endothelial cells were first exposed to laminar flow for 24 h. Thereafter, cells were reexposed to high laminar flow to induce atheroprotective signaling. Alternatively, cells were exposed to either disturbed flow (high frequency oscillatory flow) or flow direction was changed by 90 degrees to induce atherogenic signaling. **(B–D)** HUAECs were transfected with scrambled siRNA (control) or siRNA directed against $G\alpha_q$ and $G\alpha_{11}$ ($G\alpha_{q/11}$). Thereafter, cells were preflowed for 24 h (15 dynes/cm²) and then subjected to low flow for 1 h (4 dynes/cm²) and/or high flow for 15 min (15 dynes/cm²; B) or to oscillatory flow (15 dynes/cm²,

supported by earlier data showing that exposure of endothelial cells to uni-directional flow results in a remodeling of focal adhesions in the direction of flow (Davies et al., 1994, 1997). It remains to be tested whether endothelial integrins and downstream protein complexes align and orient themselves under the influence of directional flow. It is conceivable that such molecular orientation could affect integrin downstream signaling in response to particular flow patterns in a way that, e.g., laminar flow results in an adaptation, which suppresses integrin signaling in response to continuous flow in one direction, but still allows for integrin signaling in response to flow coming from different angles.

Our data indicate that Piezo1 and G_q/G_{11} play a central role in sensing disturbed flow to induce pro-inflammatory signaling. This leads to the question how Piezo1 is activated by disturbed flow, which induces endothelial fluid shear stress of different degrees and in different directions. Endothelial fluid shear stress has been proposed to result in lateral membrane tension independent of the flow direction (Fung and Liu, 1993; White and Frangos, 2007). Since Piezo1 has been described to be in particular sensitive to membrane bilayer tension (Lewis and Grandl, 2015; Cox et al., 2016), this is consistent with a role of Piezo1 in direct endothelial flow sensing independently of the flow direction.

Collectively, our data indicate that Piezo1 and G_q/G_{11}-mediated downstream signaling processes are involved in endothelial mechanosignaling by primarily sensing flow intensity independently of the flow direction. In cells exposed to disturbed flow coming from different directions, cells do not align, and integrins are activated in a G_q/G_{11}-dependent manner, resulting in FAK-mediated NF-κB activation and pro-inflammatory effects. In contrast, if cells are exposed to sustained laminar flow, integrins appear to be resistant to G_q/G_{11}-mediated activation, and Piezo1- and G_q/G_{11}-dependent signaling primarily promotes atheroprotective signaling, including activation of eNOS. This explains why constant high laminar shear stress induces activation of eNOS and production of NO in athero-resistant areas, whereas failure of parallel endothelial cell alignment due to disturbed flow promotes inflammatory signaling through, e.g., NF-κB in atheroprone areas (Baeyens et al., 2014; Baeyens and Schwartz, 2016). We also uncovered a key role of Piezo1/G_q/G_{11}-mediated mechanotransduction in the development and progression of atherosclerosis. Despite the elevation of systemic blood pressure, which we previously observed, the net effect of an endothelium-specific inactivation of Piezo1 or $G\alpha_q/G\alpha_{11}$ is clearly a strong reduction of atherosclerotic lesions, underscoring the direct atherogenic function of Piezo1/G_q/G_{11}-mediated mechanotransduction. However, inhibition of the flow-sensor pathway involving Piezo1 and G_q/G_{11} is not a good therapeutic strategy to reduce atherosclerosis progression since it may lead to increased vascular tone and blood pressure. Signaling via integrins or downstream of integrins appear to be a more promising approach to promote atheroprotection without altering vascular tone.

Materials and methods

Cell culture

HUAECs were purchased from Provitro AG and cultured in endothelial growth medium (EGM-2; Lonza), supplemented with 5% FBS; 2MV BulletKit; Lonza). Only confluent cells at passage ≤4 were used in experiments. THP-1 monocyte cells were obtained from Sigma (88081201), cultured in RPMI 1641 medium (Invitrogen), and supplemented with 2 mM glutamine and 10% FBS.

siRNA-mediated knock-down

HUAECs at 70% confluence were transfected with control siRNA (AllStars Negative siRNA, Qiagen, 1027280) and siRNAs against Piezo1, $G\alpha_q$, $G\alpha_{11}$, $P2Y_2$, ITGA5, and ITGAV (all from Qiagen) by using Opti-MEM (Thermo Fisher) and Lipofectamine RNAiMAX (Invitrogen) for 6 h on two consecutive days as described (Wang et al., 2015). The targeted sequences of human siRNAs directed against RNAs encoding Piezo1, $G\alpha_q$, $G\alpha_{11}$, P2Y2, ITGA5, and ITG AV were *Piezo1*: 5′-CCAAGTACTGGATCTATGT-3′, 5′-GCAAGTTCG TGCGCGGATT-3′, and 5′-AGAAGAAGATCGTCAAGTA-3′; *GNAQ*: 5′-CAGGACACATCGTTCGATTTA-3′ and 5′-CAGGAATGCTATGAT AGACGA-3′; *GNA11*: 5′-AGCGACAAGATCATCTACTCA-3′ and 5′-AACGTGACATCCATCATGTTT-3′; *P2RY2*: 5′-CCCTTCAGCACG GTGCTCT-3′, 5′-CTGCCTAGGGCCAAGCGCA-3′, and 5′-GCTCGT ACGCTTTGCCCGA-3′; *ITGA5*: 5′-AATCCTTAATGGCTCAGACAT-3′ and 5′-CAGGGTCTACGTCTACCTGCA-3′; and *ITGAV*: 5′-GAGTGC AATCTTGTACGTAAA-3′ and 5′-CAGGCAATAGAGATTATGCCA-3′.

Shear-stress experiments

HUAECs were seeded in μ-slide $I^{0.4}$ Luer ibiTreat chambers (Ibidi, 80176) and unidirectional laminar or oscillatory flow was applied on confluent monolayers using the Ibidi pump system (Ibidi, 10902). Unidirectional constant laminar flow was used to mimic blood flow profile in atheroprotected areas of the vasculature. Oscillatory flow or perpendicular flow (90 degrees with respect to cell axis orientation) was used to mimic disturbed blood flow in atheroprone areas of the vasculature. After cells were adapted to laminar flow (15 dynes/cm^2) for 24 h, cells were subjected to (1) low laminar flow 4 dynes/cm^2 for 1 h and then 15 dynes/cm^2 for 15 min (unidirectional flow protocol) or (2) oscillatory flow 15 dynes/cm^2 for 15 min 1 Hz (oscillatory flow protocol). For long term disturbed flow experiments, HUAECs were exposed to 0, 3, 12, and 48 h of oscillatory low flow (4 dynes/cm^2 with a frequency of 1 Hz). To modify the cell axis orientation during flow stimulation we used a custom-made parallel-flow chamber as previously described (Wang et al., 2012). In brief, cells were seeded onto round glass slides (Schott; diameter, 40 mm), which had been coated with 50 μg/ml fibronectin for 1 h. Then, slides with a confluent monolayer of HUAECs were mounted onto the bottom of the chamber (dimensions, 104 × 50 mm). Laminar flow of 15 dynes/cm^2 for 24 h was imposed on the cells by perfusing culture medium through the channel between the endothelial cell–con-

1 Hz for 15 min; C) or to perpendicular flow (90 degrees) for 5 min (D). Thereafter, cells were lysed and phosphorylated eNOS (Ser1177), phosphorylated P65 (Ser536), and total IκBα, eNOS, P65, and $G\alpha_q/G\alpha_{11}$ levels were analyzed by immunoblotting. Shown are representative blots from three to five independent experiments. Bar diagrams show the densitometric evaluation of corresponding immunoblots. Data represent mean ± SEM; *, P ≤ 0.05; **, P ≤ 0.01 ***, P ≤ 0.001 (two-tailed Student's *t* test).

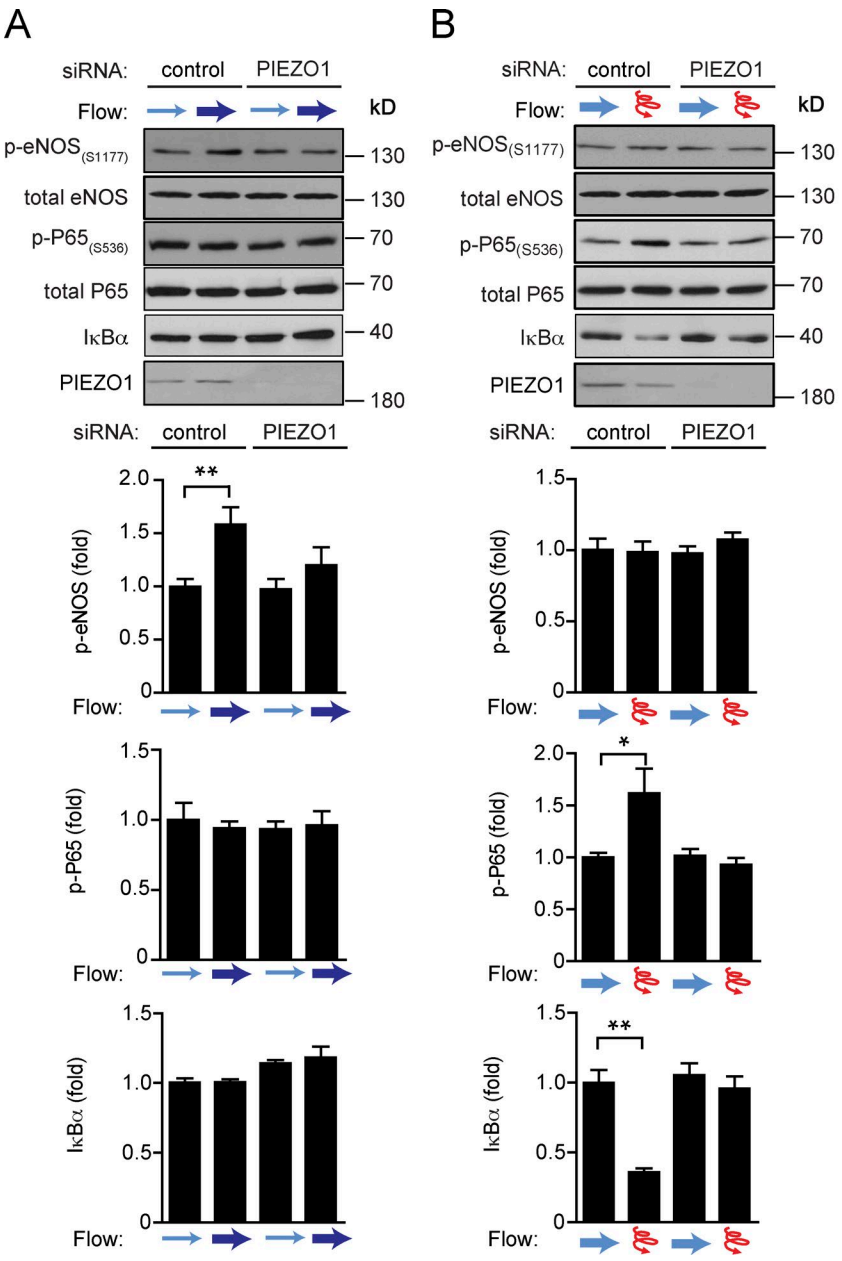

Figure 5. **Endothelial Piezo1 mediates atheroprotective or atheroprone signaling depending on the flow pattern. (A and B)** HUAECs were transfected with scrambled siRNA (control) or siRNAs directed against Piezo1 (PIEZO1). Thereafter, cells were preflowed for 24 h (15 dynes/cm^2) and then reexposed to laminar flow as in Fig. 4 B (A) or to oscillatory flow as in Fig. 4 C (B). Cells were then lysed and phosphorylated eNOS (Ser1177), phosphorylated P65 (Ser536), and total levels of IκBα, eNOS, P65, and Piezo1 were analyzed by immunoblotting. Shown are representative blots from three to five independent experiments. Bar diagrams show the densitometric evaluation of corresponding immunoblots. Data represent mean ± SEM; *, P ≤ 0.05 (two-tailed Student's *t* test).

taining glass slide and an acrylic plate in the flow chamber. Cells were then exposed to a change in the flow direction of 90 degrees for 5 min. During the experiments, flow units were maintained at 37°C in a humidified atmosphere with 5% CO_2 in a tissue culture incubator. After the experiment, cells were immediately lysed in radioimmunoprecipitation assay (RIPA) buffer supplemented with protease and phosphatase inhibitors and placed at −80°C for subsequent Western blotting analysis.

For experiments to determine ATP levels, the BioTech-Flow System cone-plate viscosimeter (MOS Technologies) was used to expose cells to fluid shear stress. The cone of this system has an angle of 2.5 degrees and rotates on top of a 33-cm^2 cell culture dish containing 3 ml of medium. Shear stress was calculated with the following formula (assuming a Reynolds number of <1): $\tau = \eta \times 2\pi \times n/0.044$ (τ: shear stress; η: viscosity; n: rotational speed; Buschmann et al., 2005).

Determination of ATP concentration

ATP concentration was determined as described (Wang et al., 2016). In brief, HUAECs were seeded in a flow chamber of the BioTech-Flow system (MOS Technologies). 24 h after the second siRNA transfection, cells were starved in serum-free medium for 4 h and were then kept under static conditions or were exposed to oscillatory flow at 4 dynes/cm^2 (at a rotation speed of 28 rpm, 40 amplitude, and 1 Hz) for 5 min. ATP concentration in the supernatant was determined using a bioluminescence assay (Molecular Probes, A22066) according to the manufacturer's instructions. For each siRNA condition, three biological replicates were performed and evaluated. To inhibit ectonucleotidases, 30 µM of ARL67156 (Tocris) was added to the extracellular solution 20 min before the experiment. Luminescence intensity was measured with a Flexstation-3 (Molecular Devices), and ATP amounts were calculated using a calibration curve with ATP standards.

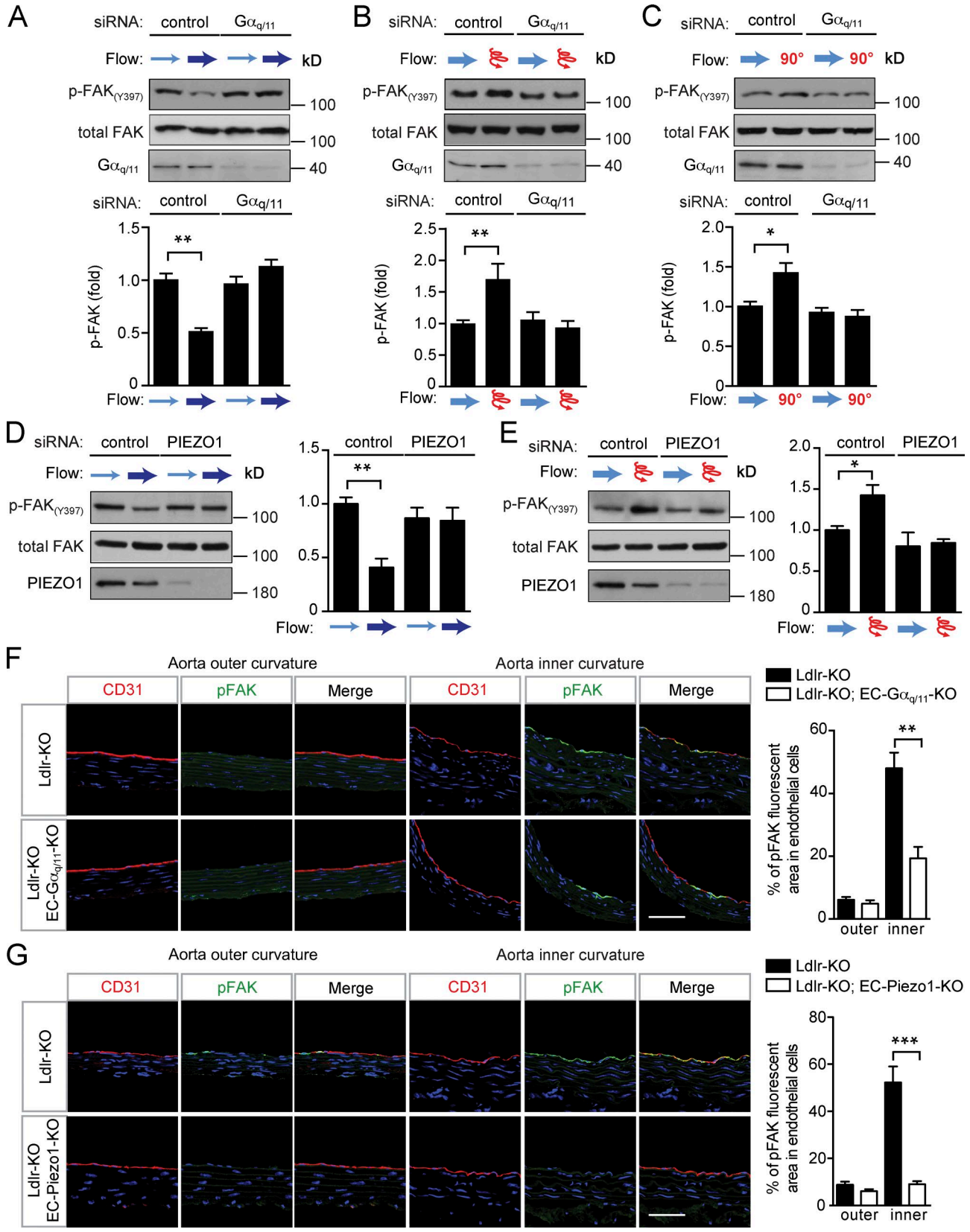

Figure 6. **FAK is differentially activated by different flow patterns via Piezo1 and G_q/G_{11}. (A–E)** HUAECs were transfected with scrambled siRNA (control) or siRNA directed against $G\alpha_q$ and $G\alpha_{11}$ ($G\alpha_{q/11}$; A–C) or against Piezo1 (D and E) and exposed to laminar or disturbed flow as described in Fig. 4 A. Activation of integrin signaling was determined by immunoblotting for phosphorylated focal adhesion kinase (pFAK, Y397). Bar diagrams show densitometric evaluation of immunoblots (quantification of three to five independent experiments). **(F and G)** Ldlr-KO mice without or with endothelium-specific $G\alpha_q/G\alpha_{11}$ deficiency (Ldlr-KO;EC-$G\alpha_{q/11}$-KO; F) or endothelium-specific Piezo1 deficiency (Ldlr-KO;EC-Piezo1-KO) were fed a high-fat diet for 4 wk (n = 4–6 mice per genotype). Cross

Western blot analysis, immunoprecipitation

Total protein was extracted from HUAECs using RIPA buffer supplemented with protease inhibitors (10 mg/ml of leupeptin, pepstatin A, 4-(2-aminoethyl)benzensulfonylfluorid and aprotinin), and phosphatase inhibitors (PhosSTOP, Roche). Total cell lysates were subjected to SDS-PAGE electrophoresis and transferred to nitrocellulose membranes. After blocking (5% BSA at room temperature for 1 h), the membranes were incubated with gentle agitation overnight at 4°C with the following primary antibodies: anti–phospho-eNOS (Ser1177, 9571), anti–phospho-P65 (Ser536 [93H1], 3033), anti–phospho-FAK (Tyr397, 3283), anti–integrin α V (4711), anti-FAK (D2R2E, 13009), anti–NF-κB P65 (C22B4, 4764), anti-GAPDH (14C10, 2118), and anti-IκBα (44D4, 4812), all from Cell Signaling. Total anti-eNOS antibody was from BD Biosciences (610296). Anti-$G\alpha_q/G\alpha_{11}$ (sc-392) was from Santa Cruz Biotechnology. Anti-Piezo1 (15939-1-AP) was from Proteintech. Anti-integrin α5 (EPR7854, ab150361) and anti–VCAM-1 (EPR5047, ab134047) were from Abcam. The membranes were then washed three times for 5 min each with TBST and incubated with HRP-conjugated secondary antibodies (Cell Signaling, dilution 1:3,000) followed by chemiluminescence detection using ECL substrate (Pierce) according to the manufacturer's protocol. Band intensities from immunoblotting were quantified by densitometry using ImageJ software (Abramoff et al., 2004).

For immunoprecipitation, protein lysates were centrifuged at 10,000 *g* at 4°C for 10 min, and supernatants were incubated with antibodies recognizing activated integrin α5 (GeneTex, GTX86905) overnight at 4°C with rocking. Supernatants were subsequently incubated with protein A/G PLUS-agarose (Santa Cru; 1 µg of antibody per 100 µg protein and 20 µl beads in 50 µl lysis buffer) for 4 h at 4°C. Then, the beads were collected by centrifugation (10,000 *g* at 4°C for 1 min) and washed three times with RIPA lysis buffer with protease inhibitors. Immunoprecipitates were subjected to SDS-PAGE and transferred to nitrocellulose membranes, and immunoblotting was performed with anti-integrin α5 antibodies.

Monocyte adhesion assay

HUAECs transfected with siRNAs were grown in the absence of flow (static) or were exposed to oscillatory flow (4 dynes/cm^2, with changes in flow direction every 2 s for 48 h) in µ-slides I$^{0.4}$ Luer (Ibidi). Monocytic THP-1 cells (Sigma) were labeled with 0.5 µM Calcein AM (Thermo Fisher) for 30 min at 37°C, washed with PBS, and resuspended at a concentration of 10^6 cells in endothelial cell medium. Labeled THP-1 cells were then perfused over the HUAECs with a flow rate of 1 ml/min and incubated for 30 min at 37°C. Non-adherent cells were removed by perfusing cells with endothelial cell medium for 3 min with a flow rate of 1 ml/min. Cells were fixed in flow chambers for 10 min in 4% paraformaldehyde (PFA), washed three times with PBS, and incubated with Alexa Fluor 568 phalloidin (1 U/ml; Thermo Fisher, A12380) to visualize actin fibers. Endothelial cells and adherent THP-1 cells were then analyzed by confocal microscopy. Two to four objective fields were randomly selected to count adherent THP-1 cells in each slide, and three independent experiments were performed.

Quantitative real-time PCR analysis

HUAECs transfected with siRNAs were exposed to 0, 3, 24, and 48 h of oscillatory low flow (4 dynes/cm^2, 1 Hz) in µ-slides I$^{0.4}$ Luer (Ibidi). Total RNA was isolated from endothelial cell monolayers using the RNeasy Micro kit (Qiagen) according to the manufacturer's protocol. Complementary DNA synthesis was performed using the ProtoScript II Reverse Transcription kit (New England BioLabs, M0368S). Quantitative real-time PCR was performed using primers designed with the online tool provided by Roche and the Light-Cycler 480 Probe Master System (Roche). Each reaction was run in triplicates, and relative gene expression levels were normalized to human β-actin (ACTB). Relative expression was calculated using the ΔΔCt method. Primer sequences used were *GNAQ*: forward 5′-GACTACTTCCCAGAATATGATGGAC-3′, reverse 5′-GGTTCAGGTCCACGAACATC-3′; *GNA11*: forward 5′-GATCCTCTACAAGTACGAGCAGAAC-3′, reverse 5′- ACTGATGCTCGAAGGTGGTC-3′; *ACTB*: forward 5′-GCTACGAGCTGCCTGACG-3′, reverse 5′-GGCTGGAAGAGTGCCTCA-3′; *Piezo1*: forward 5′-TCGCTGGTCTACCTGCTCTT-3′, reverse 5′-GGCCTGTGTGACCTTGGA-3′; *VCAM-1*: forward 5′-GAAGTTTAACACTTGATGTTCAAGGA-3′, reverse 5′-AGGATGCAAAATAGAGCACGA-3′; *CCL2* (*MCP-1*): forward 5′-AGTCTCTGCCGCCCTTCT-3′, reverse 5′-GTGACTGGGGCATTGATTG-3′; *PDGFb*: forward 5′-TGATCTCCAACGCCTGCT-3′, reverse 5′-CCTTCCATCGGATCTCGTAA-3′; and *P2YR2*: forward 5′-TAACCTGCCACGACACCTC-3, reverse 5′-CTGAGCTGTAGGCCACGAA-3.

Genetic mouse models

All mice were backcrossed onto the C57BL/6 background for a minimum of eight generations. Experiments were performed with littermates as controls. Male and female animals at an age of 8–12 wk were used if not stated otherwise. Mice were housed under a 12-h light–dark cycle with free access to food and water and under specific pathogen–free conditions. The generation of inducible endothelium-specific $G\alpha_q/G\alpha_{11}$-deficient mice (Tie2-CreER^{T2};*Gnaq*$^{f/f}$;*Gna11*$^{-/-}$ [EC-q/11-KO]), inducible endothelium-specific $P2Y_2$-deficient mice (Tie2-CreER^{T2};*P2ry2*$^{f/f}$ [EC-$P2Y_2$-KO]), and inducible endothelium-specific Piezo1-deficient mice (Tie2-CreER^{T2};*Piezo1*$^{f/f}$ [EC-Piezo1-KO]) was described previously (Korhonen et al., 2009; Wang et al., 2015, 2016). For atherosclerosis studies, $G\alpha_q/G\alpha_{11}$-deficient mice were bred also on the constitutive Cadherin-5-Cre (Alva et al., 2006) together with the low-density lipoprotein receptor knockout (*Ldlr*-KO; Ishibashi et al., 1993) background. All animal experiments were performed according to the animal ethics committees of the Regierungspräsidia Karlsruhe and Darmstadt.

sections of the inner and outer curvatures of aortic arches were stained with antibodies against phosphorylated FAK (Y397, green) and against the endothelial marker CD31 (red) and with DAPI (blue). Data are representative of six to eight microscope field areas per animal. Bar diagrams show percentage of area stained by anti-pFAK antibody of total endothelial cell area defined by staining by anti-CD31 antibody (based on analysis of at least five sections each from at least four different animals). Bars, 50 µm. Data represent mean ± SEM; *, P ≤ 0.05; **, P ≤ 0.01; ***, P ≤ 0.001 (two-tailed Student's *t* test).

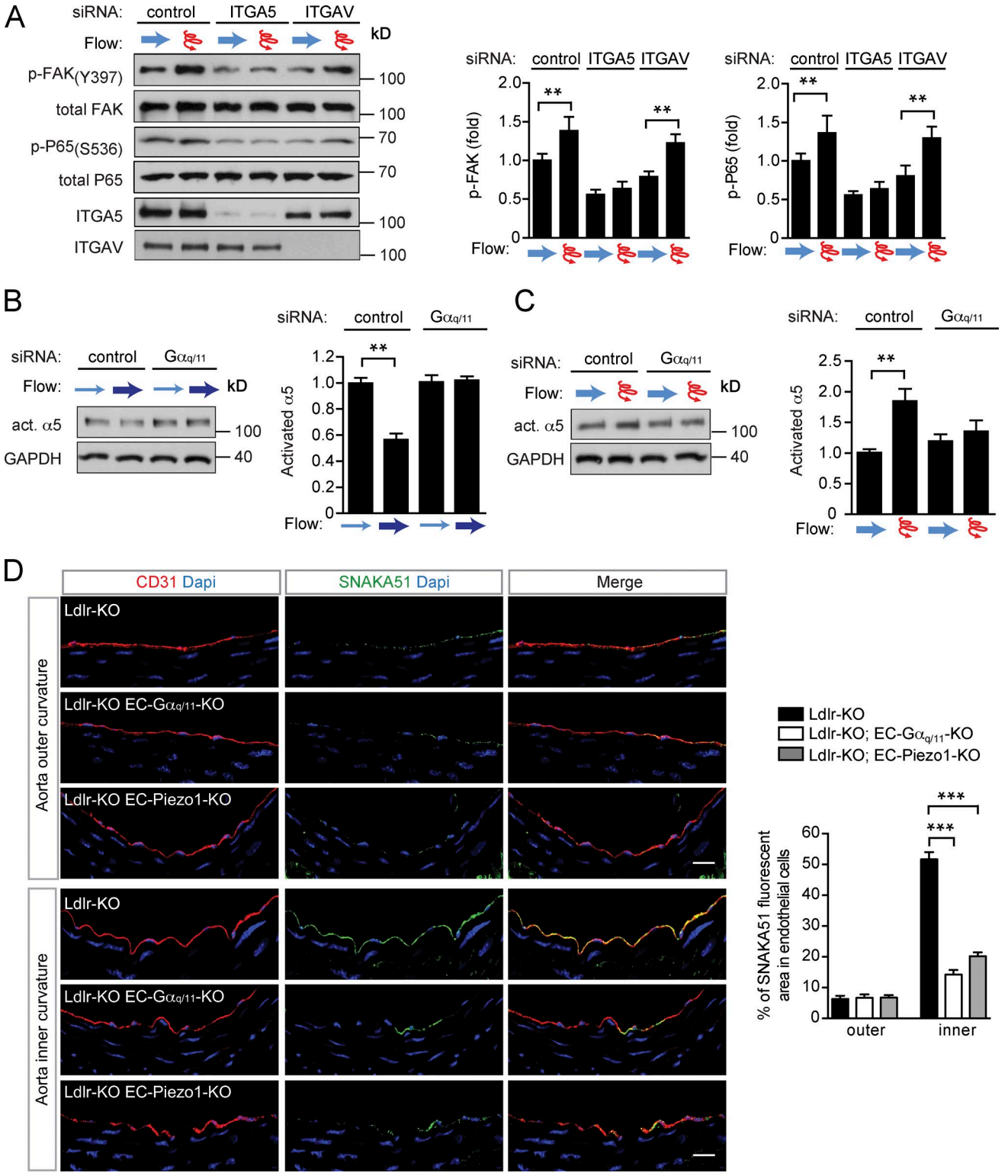

Figure 7. **Integrins are differentially activated by different flow patterns via Piezo1 and G_q/G_{11}. (A–C)** HUAECs were transfected with scrambled siRNA (control) or siRNA directed against ITGA5 and ITGAV (A) or against $G\alpha_q$ and $G\alpha_{11}$ ($G\alpha_{q/11}$; B and C) and were exposed to laminar or disturbed flow as described in Fig. 4 A. Activation of integrin signaling was determined by immunoblotting for phosphorylated focal adhesion kinase (pFAK, Y397; A) or by immunoprecipitation of activated α5 integrin (B and C). P65 activation was determined by anti–phospho-P65 (S536) antibodies (A). Bar diagrams show densitometric evaluation of immunoblots (quantification of three to five independent experiments). **(D)** Ldlr-KO mice without or with endothelium-specific $G\alpha_q/G\alpha_{11}$ deficiency (Ldlr-KO;EC-$G\alpha_{q/11}$-KO) endothelium-specific Piezo1-deficiency (Ldlr-KO;EC-Piezo1-KO) were fed a high-fat diet for 4 wk (n = 4–6 mice per genotype). Cross sections of the inner and outer curvatures of aortic arches were immunostained with antibodies against activated α5 integrin (SNAKA51; green), against the endothelial marker CD31 (red) or with DAPI (blue). Bar diagrams show percentage of area stained by anti-activated α5 integrin antibody of total endothelial cell area defined by staining by anti-CD31 antibody (based on analysis of at least five sections each from at least four different animals). Bars, 25 µm. Data represent mean ± SEM; *, P ≤ 0.05; **, P ≤ 0.01; ***, P ≤ 0.001 (two-tailed Student's t test).

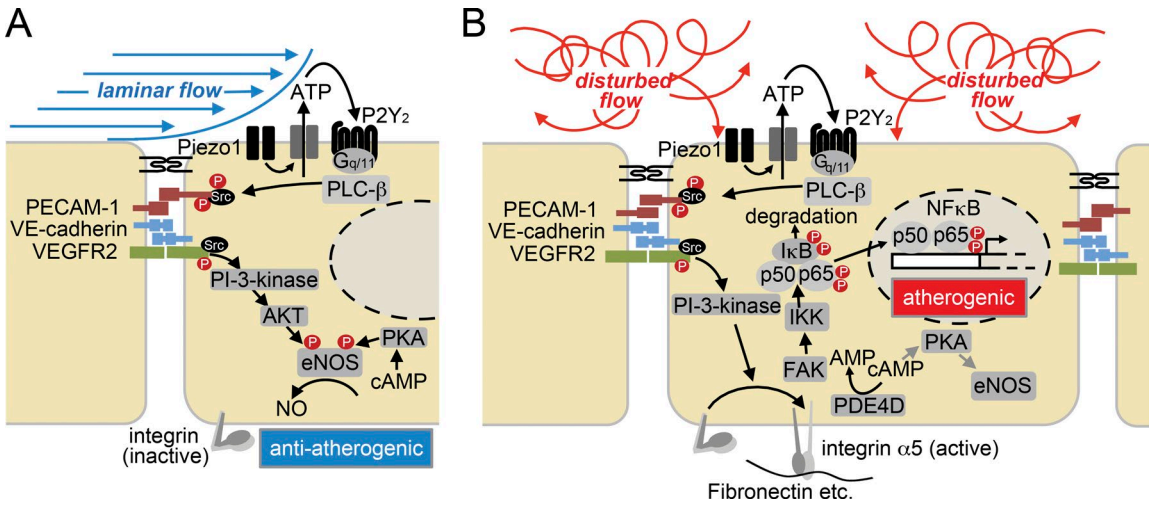

Figure 8. **Model of the role of Piezo1 and G_q/G_{11} proteins in endothelial response to different flow patterns. (A and B)** Laminar flow (A) and disturbed flow (B) activate the same initial signaling processes involving the mechanosensitive cation channel Piezo1 and the purinergic receptor $P2Y_2$, as well as G_q/G_{11}-mediated signaling and activation of the mechanosignaling complex consisting of PECAM-1, VE-cadherin, and VEGFR2. In cells exposed to laminar flow, integrins are not activated and this initial signal transduction pathway promotes atheroprotective signaling including activation of eNOS through PI-3-kinase and AKT. Through incompletely understood pathways, eNOS is also activated by cAMP acting through protein kinase A (PKA). In cells exposed to disturbed flow, activation of the initial signaling pathway results in integrin activation, which promotes via focal adhesion kinase (FAK) NF-κB activation and atherogenic signaling, as well as reduced eNOS activation by promoting cAMP degradation via activation of phosphodiesterase 4D (PDE4D).

For atherosclerosis analysis, Cre recombinase was activated in male *Ldlr*-KO mice at 6–8 wk of age by intraperitoneal injections of tamoxifen (Sigma, T5648; 1 mg per animal/day on five consecutive days). 5 d after the last tamoxifen injection, mice were fed a high-fat diet for 16 wk to induce development of atherosclerotic lesions. Diet contained 21% butterfat and 1.5% cholesterol (Ssniff, TD88137). Thereafter, animals were sacrificed, and atherosclerotic lesions were analyzed as described below.

Partial carotid ligation

Partial carotid ligation was performed as described before (Nam et al., 2009). In brief, mice at 12 wk of age were anaesthetized by intraperitoneal injection of ketamine (120 mg/kg, Pfizer) and xylazine (16 mg/kg, Bayer) and placed on a heated surgical pad. After hair removal, a midline cervical incision was made, and the left internal and external carotid arteries were exposed and partially ligated with 6.0 silk sutures (Serag-Wiessner), leaving the superior thyroid artery intact. Skin was sutured with absorbable 6.0 silk suture (CatGut) and animals were monitored until recovery in a chamber on a heating pad after the surgery. Animals were fed a high-fat diet for 2 or 4 wk (Ssniff, TD88137), at which time their carotid arteries were harvested. To determine atherosclerotic lesions, left (partially ligated) and right (sham) carotid arteries were removed and fixed in 4% PFA overnight. Fixed vessels were embedded in paraffin. Serial sections (5 µm) were made through the entire carotid arteries and stained with accustain elastic stain (Sigma) according to manufacturer's instructions. Plaque area was calculated by subtracting the lumen area from the area circumscribed by the internal elastic lamina.

Determination of P65 nuclear translocation

HUAECs were transfected with scrambled (control) siRNA or siRNA directed against Piezo1 or $G\alpha_q$ and $G\alpha_{11}$ in µ-slide $I^{0.4}$ Luer slides (Ibidi). 24 h after the second siRNA transfection, cells were grown in the absence of flow (static) or were exposed to oscillatory flow for 48 h. Cells were fixed in flow chambers for 10 min in 4% PFA followed by permeabilization and blocking (0.2% Triton X-100 and 2 mg/ml BSA in 1× PBS at room temperature for 1 h). Cells were then incubated in flow chambers with primary antibody directed against P65 (C22B4, 4764; Cell Signaling), overnight at 4°C (dilution 1:100). After gentle washing with PBS (three times), cells were incubated with corresponding Alexa Fluor 488–conjugated secondary antibody (1:200; Invitrogen) together with DAPI for detection of nuclei (1 ng/ml) for 1 h at room temperature in the dark. Stained monolayers were analyzed by using a confocal microscope (SP5 Leica).

Histology and immunostaining

For en face immunofluorescence staining, animals were perfused via the left ventricle with 15 ml saline containing heparin (40 units/ml), followed by 15 ml of 4% PFA in PBS. The aorta was removed and opened along the ventral midline. Mouse aortae were fixed with 4% PFA for 45 min at room temperature. Tissue permeabilization and blocking was performed by incubation with 0.2% TritonX-100 (in PBS) and 1% BSA for 1 h in PBS at room temperature under rocking. Atheroprotected and atheroprone areas from the outer and inner curvature of the aorta were dissected. Vessels were incubated at 4°C overnight in PBS containing primary antibodies (dilution 1:100) directed against CD31 (Abcam, ab24590), Vcam-1 (BD Pharmingen, Clone 429, 550547), and CD68 (Serotec, MCA1957). After washing three times in PBS, aortae were incubated with Alexa Fluor 488– and Alexa Fluor 594–conjugated secondary antibodies (1:200; Invitrogen) together with DAPI (1 ng/ml; Invitrogen) for 1 h at room temperature in the dark. After washing three times with PBS, tissues were mounted en face with FluoroMount (Sigma, F4680) for confocal imaging. For

en face oil-red-O staining of atherosclerotic plaques, aortae were fixed in 4% PFA overnight at 4°C after perfusion (4% PFA, 20 mM EDTA, 5% sucrose in 15 ml PBS). Thereafter, connective tissue and the adventitia were removed, and vessels were cut, opened and pinned en face onto a glass plate coated with silicon. After rinsing with distillated water for 10 min and subsequently with 60% isopropanol, vessels were stained en face with oil-red-O for 30 min with gentle shaking, and were rinsed again in 60% isopropanol and then in tap water for 10 min. Samples were mounted on the coverslips with the endothelial surface facing upwards with glycerol gelatin aqueous mounting media (Sigma).

For morphological analysis of atherosclerotic plaques, the innominate artery and the aortic sinus area attached to the heart were dissected and embedded in optimal cutting temperature medium (Tissue-Tek^{R}). Frozen innominate arteries were mounted in a cryotome, and a defined segment 500 to 1,000 µm distal from the origin of the innominate artery was sectioned (10 µm). Sections were then stained with accustain elastic stain kit (Sigma) according to the manufacturer's protocol. Frozen aortic outflow tracts were sectioned (10 µm) and stained with oil-red-O for 30 min and mounted with glycerol gelatin. Photoshop CS5 extended software (Adobe), was used to measure atherosclerotic plaque sizes and luminal cross-sectional areas.

To analyze the endothelial layer of the inner and outer aortic curvature, control LDL-receptor–deficient mice or animals with endothelium-specific $G\alpha_q/G\alpha_{11}$ deficiency (Ldlr-KO;EC-$G\alpha_{q/11}$-KO) were fed a high-fat diet for 4 wk. Aortic arches were cryosectioned (10 µm) and fixed with ice-cold acetone for 10 min. Optimal cutting temperature tissue-freezing medium (Sakura) was removed by washing with PBS three times for 5 min each, and sections were immunostained with antibodies against phosphorylated FAK (Y397, 1:100 dilution; Cell Signaling, 3283), CD31 (1:100 dilution; BD Biosciences, 550274), or against activated integrin α5 (SNAKA51; Novus Biologicals, NBP2-50146) overnight at 4°C. After washing three times with PBS, bound primary antibodies were detected using Alexa Fluor 488– or 594–conjugated secondary antibodies (Thermo Fisher, 1:200). DAPI (1 ng/ml; Invitrogen) was used to label cell nuclei. Sections were viewed with a confocal microscope (Leica, SP5). For quantification of pFAK and activated integrin α5 staining at the inner and outer curvature, the endothelial cell area was defined by CD31 staining using ImageJ software, and the fluorescent signal indicating pFAK and integrin α5 was then calculated as percentage of total endothelial cell area.

Peripheral blood mononuclear cell (PBMC) isolation

Mouse blood was collected by retro-orbital bleeding into EDTA treated tubes (Microvette, NC0973120). The whole blood volume (~1 ml per mouse) was then diluted with 1× Dulbecco's PBS without calcium and magnesium (ratio, 1:1). The diluted samples were subjected to density gradient separation on Ficoll Paque PREMIUM 1.084 (GE Healthcare, GE17-5446-02). After centrifugation, the PBMC layer was collected and washed with red blood cell lysis buffer (Sigma, R7757) to remove remaining red blood cells. PBMC were then washed in 1× PBS and stained for flow cytometric analysis with fluorescently labeled anti–CD45-FITC (eBioscience, clone 30-F11), anti-CD11b-eFluor450 (eBioscience, clone M1/70), anti–Ly6c-PE-Cy7 (Biolegend, clone HK1.4), and anti-Ter119-APC (eBioscience, Ter119) antibodies (at a concentration of 0.2–0.4 µg per 10^6 cells). Samples were analyzed using a FACSCanto II (BD Biosciences).

Aortic single cell preparation and flow cytometric analysis

For FACS analysis, animals were anesthetized and their vasculature was perfused by cardiac puncture with 1× PBS containing 20 U/ml of heparin to remove blood from all vessels. Under a dissection microscope, whole aortae were excised and carefully cleaned of all perivascular fat and the adventitia layer was removed in a Petri dish containing 1× PBS. Using micro-scissors, aortic arch segments were opened and inner curvature area was identified. The inner curvature areas from four mice were pooled and analyzed. Inner curvature segments were cut into very small pieces and digested by incubation with an enzyme mixture containing 450 U/ml collagenase I (Sigma, SCR103), 60 U/ml DNase1 (New England Biolabs, M0303), and 312.5 U/ml collagenase II (Worthington, LS004177) in DMEM without serum (Gibco) at 37°C for 30 min with shaking. Single cell suspensions were prepared by passing the digested aorta segments through a 70-µm cell strainer followed by a 40-µm cell strainer (Falcon). Cells were incubated with 7AAD dye (BD Biosciences, 559925) and fluorescently labeled antibodies against CD11c-FITC (BD Biosciences, clone HL3) for 20 min at room temperature in the dark. Samples were analyzed using a FACSCanto II (BD Biosciences).

Intimal RNA isolation from murine aortic curvature

Aortic inner and outer curvature intimal mRNA isolation was performed as previously described (Jongstra-Bilen et al., 2006; Nam et al., 2009) with some minor modifications. In brief, mice were anesthetized and their vasculature was perfused by cardiac puncture with 1× PBS containing 20 U/ml of heparin to remove blood from all vessels. Under a dissection microscope, ascending aorta, aortic arch, and a portion of descending aorta were excised from each mouse. Then aortae were carefully cleaned of all perivascular fat, and the adventitia layer was removed in a Petri dish containing RNA-later reagent (RNA-later, Qiagen). Using micro-scissors, aortic arch segments were opened and inner and outer curvature areas were isolated. Intimal cells from these regions were gently scraped with a 26-G needle, flushed with 150 µl QIAzol lysis reagent (Qiagen), and the eluate was collected in a microfuge tube. RNA isolation was performed using an miRNeasy mini kit (Qiagen) according to manufacturer's instructions. For each experiment, intimal cells were pooled from two aortae. Data were normalized to the housekeeping gene *Hprt*. Murine primer sequences are as follows: *Hprt*: forward 5′-GTCAACGGGGGACATAAAAG-3′, reverse 5′-CAACAATCAAGACATTCTTTCCA-3′; and *Vcam-1*: forward 5′-CCGGTCACGGTCAAGTGT-3′, reverse 5′-CAGATCAATCTCCAGCCTGTAA-3′.

SNAKA51 staining in murine lung endothelial cells (MLECs)

C57BL/6 mouse primary lung endothelial cells (Pelobiotech, C57-6011) were plated in µ-slide $I^{0.4}$ Luer ibiTreat chambers (Ibidi, 80176) and transfected with scrambled (control) siRNA or siRNA directed against *Itga5*. The targeted sequences of mouse siRNAs directed against RNAs encoding *Itga5* were 5′-ACCATTCAATTT

GACAGCAAA-3′, 5′-CAGATCCATGGAAGTCAGAAA-3′, and 5′-AGCGGGAATACCAGCCATTTA-3′. 24 h after the second siRNA transfection, cells were grown in the absence of flow (static) or were exposed to oscillatory flow for 24 h. Cells were fixed in flow chambers for 10 min in 4% PFA followed by permeabilization and blocking (0.2% Triton X-100 and 2 mg/ml BSA in 1× PBS at room temperature for 1 h). Cells were then incubated in flow chambers with primary antibody directed against activated integrin α5, SNAKA51 (Novus Biologicals, NBP2-50146), overnight at 4°C (1:100 dilution). After gentle washing with PBS (three times), cells were incubated with corresponding Alexa Fluor 488–conjugated secondary antibody (1:200, Invitrogen) together with DAPI for detection of nuclei (1 ng/ml) for 1 h at room temperature in the dark. Stained monolayers were analyzed by using a confocal microscope (SP5 Leica).

Pharmacological inhibition of integrin signaling

HUAECs were seeded in µ-slide $I^{0.4}$ Luer ibiTreat chambers (80176, Ibidi) and unidirectional laminar or oscillatory flow was applied as described above. After cells were adapted to laminar flow for 24 h, confluent monolayers were treated with 50 µmol/L of the α5β1 integrin inhibitor ATN-161 (Tocris, 6058) or with 1 µmol/L of the αv integrin inhibitor S247 (Tocris, 5870), for 10 min and shear stress-induced signaling was assessed.

Total cholesterol assay

Following a 4-h fast, mice were anesthetized with isoflurane and retro-orbital blood was obtained via EDTA-coated microcapillary tubes (Microvette, NC0973120). Cholesterol levels from mouse plasma (dilution 1:400) were quantified using a cholesterol fluorometric assay kit (Cayman, 10007640) according to manufacturer's instructions.

Statistical analysis

Statistical data analysis is included in every figure and described in detail on the respective figure legends. The exact P values and number of cells analyzed per condition (*n*) are stated in the figures and figure legends. All experiments were repeated three times (independent replicates); *n* represents a pool across these experimental replicates. Trial experiments or experiments done previously were used to determine sample size with adequate statistical power. Samples were excluded in cases where RNA/cDNA quality or tissue quality after processing was poor (below commonly accepted standards). Data are presented as means ± SEM. All statistical analyses were performed using Prism 5 software (GraphPad). A level of $P < 0.05$ was considered significant and reported to the graphs. Comparisons between two groups were performed using unpaired two-tailed Student's *t* test and multiple group comparisons at different time points were performed by ANOVA followed by Bonferroni's post hoc test.

Online supplemental material

Fig. S1 shows the knock-down efficiency of Piezo1, P2RY2, $G\alpha_q$, and $G\alpha_{11}$ in HUAECs, as well as the effect of $G\alpha_q/G\alpha_{11}$- and Piezo1 knock-down on oscillatory flow-induced expression of VCAM-1, CCL2, and PDGFB in HUAECs. Fig. S2 shows Vcam-1 expression and presence of CD68-positive cells in the endothelium and subendothelium of the aortic outer curvature of wild-type and EC- $G\alpha_{q/11}$-KO and EC-Piezo1-KO animals. Fig. S3 shows Vcam-1 expression in the endothelium of the inner and outer curvature of the aorta from EC-$P2Y_2$-KO mice, as well as the plaque/neointima area of Ldlr-KO;EC-$P2Y_2$-KO mice after partial carotid artery ligation. Fig. S4 shows Vcam-1 mRNA levels in the inner and outer aortic curvature of wild-type, EC-$G\alpha_{q/11}$-KO, and EC-Piezo1-KO mice, presence of $CD11c^+$-cells in the inner curvature of wild-type, EC-$G\alpha_{q/11}$-KO, and EC-Piezo1-KO mice, and the total cholesterol plasma levels and levels of Ly6c-positive cells in the blood of Ldlr-KO, Ldlr-KO;EC-$G\alpha_{q/11}$-KO, and Ldlr-KO;EC-Piezo1-KO mice. Fig. S5 shows the effect of the integrin α5 and αv blockers ATN-161 and S247 on disturbed flow-induced phosphorylation of FAK and P65 in HUAECs, as well as data indicating that the monoclonal anti-integrin α5 antibody SNAKA51 can recognize activated mouse integrin α5.

Acknowledgments

The authors wish to thank Karin Jäcklein, Ulrike Krüger, and Claudia Ullmann for their expert technical assistance and Svea Hümmer for excellent secretarial help. The authors wish to thank Reinhard Fässler for helpful discussions.

Part of the work was supported by the German Research Foundation's Transregional Collaborative Research Center 23 (SFB/TR23) and the Collaborative Research Center 834 (SFB834).

The authors declare no competing financial interests.

Author contributions: J. Albarrán-Juárez performed most of the in vitro and in vivo experiments, analyzed and discussed data, and contributed to writing of the manuscript; T.F. Althoff performed initial in vitro and in vivo experiments, initiated the study, analyzed and discussed data, and contributed to writing of the manuscript; A. Iring, S. Wang, S. Joseph, M. Grimm, and B. Strilic helped with ATP measurements, generation and analysis of Piezo1-deficent mice, analysis of atherosclerosis, and immunofluorescence imaging; N. Wettschureck initiated and supervised study, discussed data, and commented on the manuscript; S. Offermanns initiated and supervised study, discussed data, and wrote the manuscript.

Submitted: 12 March 2018
Revised: 22 June 2018
Accepted: 1 August 2018

References

Abramoff, M.D., P.J. Magalhaes, and S.J. Ram. 2004. Image Processing with ImageJ. *Biophoton. Int.* 11:36–42.

Alva, J.A., A.C. Zovein, A. Monvoisin, T. Murphy, A. Salazar, N.L. Harvey, P. Carmeliet, and M.L. Iruela-Arispe. 2006. VE-Cadherin-Cre-recombinase transgenic mouse: a tool for lineage analysis and gene deletion in endothelial cells. *Dev. Dyn.* 235:759–767. https://doi.org/10.1002/dvdy.20643

Baeyens, N., and M.A. Schwartz. 2016. Biomechanics of vascular mechanosensation and remodeling. *Mol. Biol. Cell.* 27:7–11. https://doi.org/10.1091/mbc.e14-11-1522

Baeyens, N., M.J. Mulligan-Kehoe, F. Corti, D.D. Simon, T.D. Ross, J.M. Rhodes, T.Z. Wang, C.O. Mejean, M. Simons, J. Humphrey, and M.A. Schwartz.

2014. Syndecan 4 is required for endothelial alignment in flow and atheroprotective signaling. *Proc. Natl. Acad. Sci. USA.* 111:17308–17313. https://doi.org/10.1073/pnas.1413725111

Bagi, Z., J.A. Frangos, J.C. Yeh, C.R. White, G. Kaley, and A. Koller. 2005. PECAM-1 mediates NO-dependent dilation of arterioles to high temporal gradients of shear stress. *Arterioscler. Thromb. Vasc. Biol.* 25:1590–1595. https://doi.org/10.1161/01.ATV.0000170136.71970.5f

Bhullar, I.S., Y.S. Li, H. Miao, E. Zandi, M. Kim, J.Y. Shyy, and S. Chien. 1998. Fluid shear stress activation of IkappaB kinase is integrin-dependent. *J. Biol. Chem.* 273:30544–30549. https://doi.org/10.1074/jbc.273.46.30544

Bodin, P., D. Bailey, and G. Burnstock. 1991. Increased flow-induced ATP release from isolated vascular endothelial cells but not smooth muscle cells. *Br. J. Pharmacol.* 103:1203–1205. https://doi.org/10.1111/j.1476-5381.1991.tb12324.x

Boo, Y.C., J. Hwang, M. Sykes, B.J. Michell, B.E. Kemp, H. Lum, and H. Jo. 2002. Shear stress stimulates phosphorylation of eNOS at Ser(635) by a protein kinase A-dependent mechanism. *Am. J. Physiol. Heart Circ. Physiol.* 283:H1819–H1828. https://doi.org/10.1152/ajpheart.00214.2002

Budatha, M., J. Zhang, Z.W. Zhuang, S. Yun, J.E. Dahlman, D.G. Anderson, and M.A. Schwartz. 2018. Inhibiting Integrin α5 Cytoplasmic Domain Signaling Reduces Atherosclerosis and Promotes Arteriogenesis. *J. Am. Heart Assoc.* 7:e007501. https://doi.org/10.1161/JAHA.117.007501

Buschmann, M.H., P. Dieterich, N.A. Adams, and H.J. Schnittler. 2005. Analysis of flow in a cone-and-plate apparatus with respect to spatial and temporal effects on endothelial cells. *Biotechnol. Bioeng.* 89:493–502. https://doi.org/10.1002/bit.20165

Chen, J., J. Green, A. Yurdagul Jr., P. Albert, M.C. McInnis, and A.W. Orr. 2015. αvβ3 Integrins Mediate Flow-Induced NF-κB Activation, Proinflammatory Gene Expression, and Early Atherogenic Inflammation. *Am. J. Pathol.* 185:2575–2589. https://doi.org/10.1016/j.ajpath.2015.05.013

Chen, X., S. Qian, A. Hoggatt, H. Tang, T.A. Hacker, A.G. Obukhov, P.B. Herring, and C.I. Seye. 2017. Endothelial Cell-Specific Deletion of P2Y2 Receptor Promotes Plaque Stability in Atherosclerosis-Susceptible ApoE-Null Mice. *Arterioscler. Thromb. Vasc. Biol.* 37:75–83. https://doi.org/10.1161/ATVBAHA.116.308561

Chiu, J.J., and S. Chien. 2011. Effects of disturbed flow on vascular endothelium: pathophysiological basis and clinical perspectives. *Physiol. Rev.* 91:327–387. https://doi.org/10.1152/physrev.00047.2009

Choi, J.H., Y. Do, C. Cheong, H. Koh, S.B. Boscardin, Y.S. Oh, L. Bozzacco, C. Trumpfheller, C.G. Park, and R.M. Steinman. 2009. Identification of antigen-presenting dendritic cells in mouse aorta and cardiac valves. *J. Exp. Med.* 206:497–505. https://doi.org/10.1084/jem.20082129

Clark, K., R. Pankov, M.A. Travis, J.A. Askari, A.P. Mould, S.E. Craig, P. Newham, K.M. Yamada, and M.J. Humphries. 2005. A specific alpha5beta1-integrin conformation promotes directional integrin translocation and fibronectin matrix formation. *J. Cell Sci.* 118:291–300. https://doi.org/10.1242/jcs.01623

Cox, C.D., C. Bae, L. Ziegler, S. Hartley, V. Nikolova-Krstevski, P.R. Rohde, C.A. Ng, F. Sachs, P.A. Gottlieb, and B. Martinac. 2016. Removal of the mechanoprotective influence of the cytoskeleton reveals PIEZO1 is gated by bilayer tension. *Nat. Commun.* 7:10366. https://doi.org/10.1038/ncomms10366

Davies, P.F. 2009. Hemodynamic shear stress and the endothelium in cardiovascular pathophysiology. *Nat. Clin. Pract. Cardiovasc. Med.* 6:16–26. https://doi.org/10.1038/ncpcardio1397

Davies, P.F., A. Robotewskyj, and M.L. Griem. 1994. Quantitative studies of endothelial cell adhesion. Directional remodeling of focal adhesion sites in response to flow forces. *J. Clin. Invest.* 93:2031–2038. https://doi.org/10.1172/JCI117197

Davies, P.F., K.A. Barbee, M.V. Volin, A. Robotewskyj, J. Chen, L. Joseph, M.L. Griem, M.N. Wernick, E. Jacobs, D.C. Polacek, et al. 1997. Spatial relationships in early signaling events of flow-mediated endothelial mechanotransduction. *Annu. Rev. Physiol.* 59:527–549. https://doi.org/10.1146/annurev.physiol.59.1.527

Dixit, M., A.E. Loot, A. Mohamed, B. Fisslthaler, C.M. Boulanger, B. Ceacareanu, A. Hassid, R. Busse, and I. Fleming. 2005. Gab1, SHP2, and protein kinase A are crucial for the activation of the endothelial NO synthase by fluid shear stress. *Circ. Res.* 97:1236–1244. https://doi.org/10.1161/01.RES.0000195611.59811.ab

Feaver, R.E., B.D. Gelfand, C. Wang, M.A. Schwartz, and B.R. Blackman. 2010. Atheroprone hemodynamics regulate fibronectin deposition to create positive feedback that sustains endothelial inflammation. *Circ. Res.* 106:1703–1711. https://doi.org/10.1161/CIRCRESAHA.109.216283

Finney, A.C., K.Y. Stokes, C.B. Pattillo, and A.W. Orr. 2017. Integrin signaling in atherosclerosis. *Cell. Mol. Life Sci.* 74:2263–2282. https://doi.org/10.1007/s00018-017-2490-4

Fleming, I., B. Fisslthaler, M. Dixit, and R. Busse. 2005. Role of PECAM-1 in the shear-stress-induced activation of Akt and the endothelial nitric oxide synthase (eNOS) in endothelial cells. *J. Cell Sci.* 118:4103–4111. https://doi.org/10.1242/jcs.02541

Fung, Y.C., and S.Q. Liu. 1993. Elementary mechanics of the endothelium of blood vessels. *J. Biomech. Eng.* 115:1–12. https://doi.org/10.1115/1.2895465

GBD 2015 Mortality and Causes of Death Collaborators. 2016. Global, regional, and national life expectancy, all-cause mortality, and cause-specific mortality for 249 causes of death, 1980-2015: a systematic analysis for the Global Burden of Disease Study 2015. *Lancet.* 388:1459–1544. https://doi.org/10.1016/S0140-6736(16)31012-1

Gimbrone, M.A. Jr., and G. García-Cardeña. 2016. Endothelial Cell Dysfunction and the Pathobiology of Atherosclerosis. *Circ. Res.* 118:620–636. https://doi.org/10.1161/CIRCRESAHA.115.306301

Givens, C., and E. Tzima. 2016. Endothelial Mechanosignaling: Does One Sensor Fit All? *Antioxid. Redox Signal.* 25:373–388. https://doi.org/10.1089/ars.2015.6493

Hahn, C., and M.A. Schwartz. 2008. The role of cellular adaptation to mechanical forces in atherosclerosis. *Arterioscler. Thromb. Vasc. Biol.* 28:2101–2107. https://doi.org/10.1161/ATVBAHA.108.165951

Hahn, C., and M.A. Schwartz. 2009. Mechanotransduction in vascular physiology and atherogenesis. *Nat. Rev. Mol. Cell Biol.* 10:53–62. https://doi.org/10.1038/nrm2596

Harry, B.L., J.M. Sanders, R.E. Feaver, M. Lansey, T.L. Deem, A. Zarbock, A.C. Bruce, A.W. Pryor, B.D. Gelfand, B.R. Blackman, et al. 2008. Endothelial cell PECAM-1 promotes atherosclerotic lesions in areas of disturbed flow in ApoE-deficient mice. *Arterioscler. Thromb. Vasc. Biol.* 28:2003–2008. https://doi.org/10.1161/ATVBAHA.108.164707

Herrington, W., B. Lacey, P. Sherliker, J. Armitage, and S. Lewington. 2016. Epidemiology of Atherosclerosis and the Potential to Reduce the Global Burden of Atherothrombotic Disease. *Circ. Res.* 118:535–546. https://doi.org/10.1161/CIRCRESAHA.115.307611

Huang, D.L., N.A. Bax, C.D. Buckley, W.I. Weis, and A.R. Dunn. 2017. Vinculin forms a directionally asymmetric catch bond with F-actin. *Science.* 357:703–706. https://doi.org/10.1126/science.aan2556

Ishibashi, S., M.S. Brown, J.L. Goldstein, R.D. Gerard, R.E. Hammer, and J. Herz. 1993. Hypercholesterolemia in low density lipoprotein receptor knockout mice and its reversal by adenovirus-mediated gene delivery. *J. Clin. Invest.* 92:883–893. https://doi.org/10.1172/JCI116663

John, K., and A.I. Barakat. 2001. Modulation of ATP/ADP concentration at the endothelial surface by shear stress: effect of flow-induced ATP release. *Ann. Biomed. Eng.* 29:740–751. https://doi.org/10.1114/1.1397792

Jongstra-Bilen, J., M. Haidari, S.N. Zhu, M. Chen, D. Guha, and M.I. Cybulsky. 2006. Low-grade chronic inflammation in regions of the normal mouse arterial intima predisposed to atherosclerosis. *J. Exp. Med.* 203:2073–2083. https://doi.org/10.1084/jem.20060245

Korhonen, H., B. Fisslthaler, A. Moers, A. Wirth, D. Habermehl, T. Wieland, G. Schütz, N. Wettschureck, I. Fleming, and S. Offermanns. 2009. Anaphylactic shock depends on endothelial Gq/G11. *J. Exp. Med.* 206:411–420. https://doi.org/10.1084/jem.20082150

Lewis, A.H., and J. Grandl. 2015. Mechanical sensitivity of Piezo1 ion channels can be tuned by cellular membrane tension. *eLife.* 4:e12088. https://doi.org/10.7554/eLife.12088

Liu, J., Y. Wang, W.I. Goh, H. Goh, M.A. Baird, S. Ruehland, S. Teo, N. Bate, D.R. Critchley, M.W. Davidson, and P. Kanchanawong. 2015. Talin determines the nanoscale architecture of focal adhesions. *Proc. Natl. Acad. Sci. USA.* 112:E4864–E4873. https://doi.org/10.1073/pnas.1512025112

Mohan, S., N. Mohan, and E.A. Sprague. 1997. Differential activation of NF-kappa B in human aortic endothelial cells conditioned to specific flow environments. *Am. J. Physiol.* 273:C572–C578. https://doi.org/10.1152/ajpcell.1997.273.2.C572

Nagel, T., N. Resnick, C.F. Dewey Jr., and M.A. Gimbrone Jr. 1999. Vascular endothelial cells respond to spatial gradients in fluid shear stress by enhanced activation of transcription factors. *Arterioscler. Thromb. Vasc. Biol.* 19:1825–1834. https://doi.org/10.1161/01.ATV.19.8.1825

Nakajima, H., and N. Mochizuki. 2017. Flow pattern-dependent endothelial cell responses through transcriptional regulation. *Cell Cycle.* 16:1893–1901. https://doi.org/10.1080/15384101.2017.1364324

Nam, D., C.W. Ni, A. Rezvan, J. Suo, K. Budzyn, A. Llanos, D. Harrison, D. Giddens, and H. Jo. 2009. Partial carotid ligation is a model of acutely induced disturbed flow, leading to rapid endothelial dysfunction and

atherosclerosis. *Am. J. Physiol. Heart Circ. Physiol.* 297:H1535–H1543. https://doi.org/10.1152/ajpheart.00510.2009

Nam, D., C.W. Ni, A. Rezvan, J. Suo, K. Budzyn, A. Llanos, D.G. Harrison, D.P. Giddens, and H. Jo. 2010. A model of disturbed flow-induced atherosclerosis in mouse carotid artery by partial ligation and a simple method of RNA isolation from carotid endothelium. *J. Vis. Exp.* (40):1861.

Nigro, P., J. Abe, and B.C. Berk. 2011. Flow shear stress and atherosclerosis: a matter of site specificity. *Antioxid. Redox Signal.* 15:1405–1414. https://doi.org/10.1089/ars.2010.3679

Nordenfelt, P., T.I. Moore, S.B. Mehta, J.M. Kalappurakkal, V. Swaminathan, N. Koga, T.J. Lambert, D. Baker, J.C. Waters, R. Oldenbourg, et al. 2017. Direction of actin flow dictates integrin LFA-1 orientation during leukocyte migration. *Nat. Commun.* 8:2047. https://doi.org/10.1038/s41467-017-01848-y

Orr, A.W., J.M. Sanders, M. Bevard, E. Coleman, I.J. Sarembock, and M.A. Schwartz. 2005. The subendothelial extracellular matrix modulates NF-kappaB activation by flow: a potential role in atherosclerosis. *J. Cell Biol.* 169:191–202. https://doi.org/10.1083/jcb.200410073

Orr, A.W., M.H. Ginsberg, S.J. Shattil, H. Deckmyn, and M.A. Schwartz. 2006. Matrix-specific suppression of integrin activation in shear stress signaling. *Mol. Biol. Cell.* 17:4686–4697. https://doi.org/10.1091/mbc.e06-04-0289

Petzold, T., A.W. Orr, C. Hahn, K.A. Jhaveri, J.T. Parsons, and M.A. Schwartz. 2009. Focal adhesion kinase modulates activation of NF-kappaB by flow in endothelial cells. *Am. J. Physiol. Cell Physiol.* 297:C814–C822. https://doi.org/10.1152/ajpcell.00226.2009

Sun, X., Y. Fu, M. Gu, L. Zhang, D. Li, H. Li, S. Chien, J.Y. Shyy, and Y. Zhu. 2016. Activation of integrin α5 mediated by flow requires its translocation to membrane lipid rafts in vascular endothelial cells. *Proc. Natl. Acad. Sci. USA.* 113:769–774. https://doi.org/10.1073/pnas.1524523113

Swaminathan, V., G.M. Alushin, and C.M. Waterman. 2017a. Mechanosensation: A Catch Bond That Only Hooks One Way. *Curr. Biol.* 27:R1158–R1160. https://doi.org/10.1016/j.cub.2017.09.023

Swaminathan, V., J.M. Kalappurakkal, S.B. Mehta, P. Nordenfelt, T.I. Moore, N. Koga, D.A. Baker, R. Oldenbourg, T. Tani, S. Mayor, et al. 2017b. Actin retrograde flow actively aligns and orients ligand-engaged integrins in focal adhesions. *Proc. Natl. Acad. Sci. USA.* 114:10648–10653. https://doi.org/10.1073/pnas.1701136114

Tarbell, J.M., Z.D. Shi, J. Dunn, and H. Jo. 2014. Fluid Mechanics, Arterial Disease, and Gene Expression. *Annu. Rev. Fluid Mech.* 46:591–614. https://doi.org/10.1146/annurev-fluid-010313-141309

Tzima, E., M.A. Del Pozo, W.B. Kiosses, S.A. Mohamed, S. Li, S. Chien, and M.A. Schwartz. 2002. Activation of Rac1 by shear stress in endothelial cells mediates both cytoskeletal reorganization and effects on gene expression. *EMBO J.* 21:6791–6800. https://doi.org/10.1093/emboj/cdf688

Tzima, E., M. Irani-Tehrani, W.B. Kiosses, E. Dejana, D.A. Schultz, B. Engelhardt, G. Cao, H. DeLisser, and M.A. Schwartz. 2005. A mechanosensory complex that mediates the endothelial cell response to fluid shear stress. *Nature.* 437:426–431. https://doi.org/10.1038/nature03952

Wang, C., H. Lu, and M.A. Schwartz. 2012. A novel in vitro flow system for changing flow direction on endothelial cells. *J. Biomech.* 45:1212–1218. https://doi.org/10.1016/j.jbiomech.2012.01.045

Wang, C., B.M. Baker, C.S. Chen, and M.A. Schwartz. 2013. Endothelial cell sensing of flow direction. *Arterioscler. Thromb. Vasc. Biol.* 33:2130–2136. https://doi.org/10.1161/ATVBAHA.113.301826

Wang, S., A. Iring, B. Strilic, J. Albarrán Juárez, H. Kaur, K. Troidl, S. Tonack, J.C. Burbiel, C.E. Müller, I. Fleming, et al. 2015. $P2Y_2$ and Gq/G_{11} control blood pressure by mediating endothelial mechanotransduction. *J. Clin. Invest.* 125:3077–3086. https://doi.org/10.1172/JCI81067

Wang, S., R. Chennupati, H. Kaur, A. Iring, N. Wettschureck, and S. Offermanns. 2016. Endothelial cation channel PIEZO1 controls blood pressure by mediating flow-induced ATP release. *J. Clin. Invest.* 126:4527–4536. https://doi.org/10.1172/JCI87343

White, C.R., and J.A. Frangos. 2007. The shear stress of it all: the cell membrane and mechanochemical transduction. *Philos. Trans. R. Soc. Lond. B Biol. Sci.* 362:1459–1467. https://doi.org/10.1098/rstb.2007.2128

Yamamoto, K., K. Furuya, M. Nakamura, E. Kobatake, M. Sokabe, and J. Ando. 2011. Visualization of flow-induced ATP release and triggering of Ca2+ waves at caveolae in vascular endothelial cells. *J. Cell Sci.* 124:3477–3483. https://doi.org/10.1242/jcs.087221

Yun, S., M. Budatha, J.E. Dahlman, B.G. Coon, R.T. Cameron, R. Langer, D.G. Anderson, G. Baillie, and M.A. Schwartz. 2016. Interaction between integrin α5 and PDE4D regulates endothelial inflammatory signalling. *Nat. Cell Biol.* 18:1043–1053. https://doi.org/10.1038/ncb3405

Yurdagul, A. Jr., A.C. Finney, M.D. Woolard, and A.W. Orr. 2016. The arterial microenvironment: the where and why of atherosclerosis. *Biochem. J.* 473:1281–1295. https://doi.org/10.1042/BJ20150844

Zhou, J., Y.S. Li, and S. Chien. 2014. Shear stress-initiated signaling and its regulation of endothelial function. *Arterioscler. Thromb. Vasc. Biol.* 34:2191–2198. https://doi.org/10.1161/ATVBAHA.114.303422

Supplemental material

Albarran-Juarez et al., https://doi.org/10.1084/jem.20180483

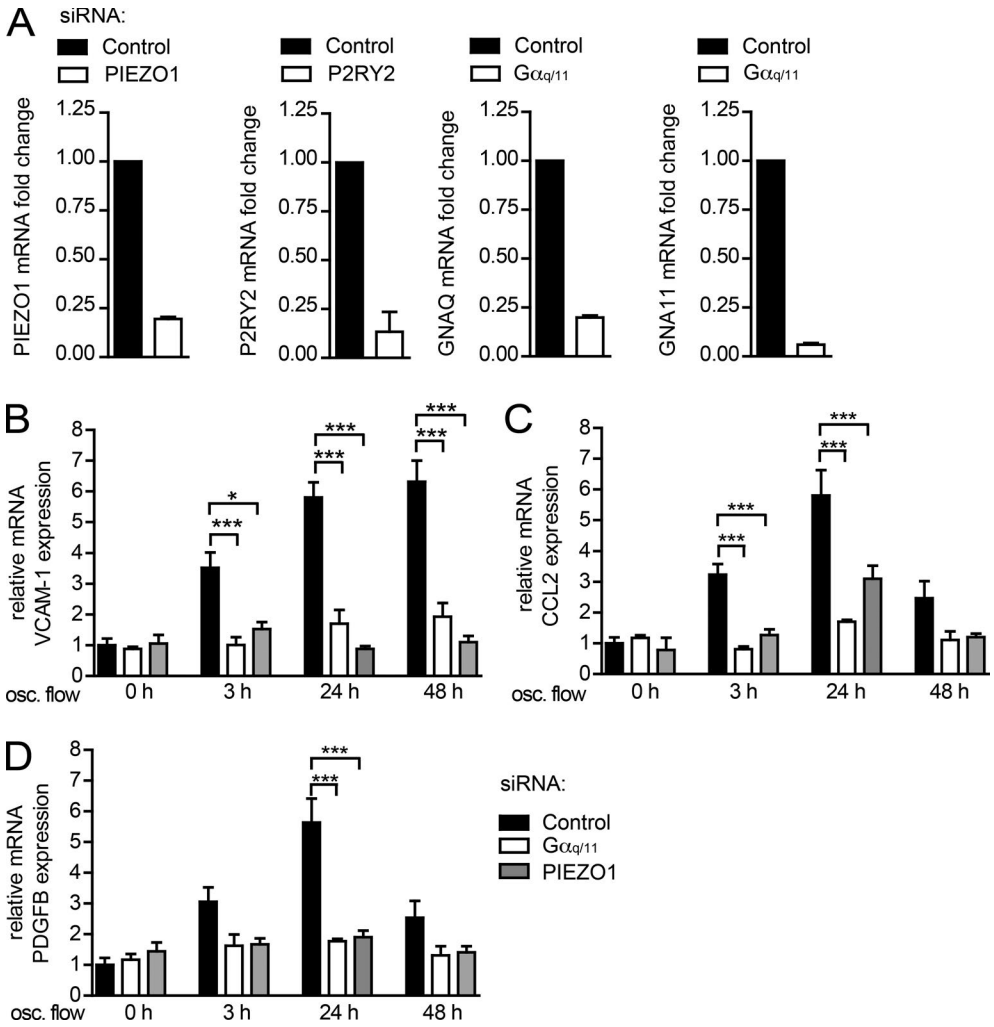

Figure S1. **Knock-down efficiency of $G\alpha_q$, $G\alpha_{11}$, $P2Y_2$, and Piezo1 in HUAECs and expression of inflammatory markers upon disturbed flow. (A)** Quantitative RT-PCR was performed 48 h after the second siRNA transfection (data from triplicates of three independent experiments). **(B–D)** HUAECs were transfected with scrambled siRNA (control) or siRNA directed against $G\alpha_q$ and $G\alpha_{11}$ ($G\alpha_{q/11}$) or Piezo1 and were cultured under static conditions or exposed to disturbed flow in a flow chamber (oscillatory [osc.] flow, 4 dynes/cm^2 at 1 Hz) for the indicated time points. Shown is the mRNA expression of VCAM-1 (B), CCL2 (C), and PDGFB (D) analyzed by quantitative real-time PCR and normalized to human ACTB expression (data from triplicates of three independent experiments). Data represent mean ± SEM; *, P ≤ 0.05; ***, P ≤ 0.001 (one-way ANOVA and Bonferroni's post hoc test).

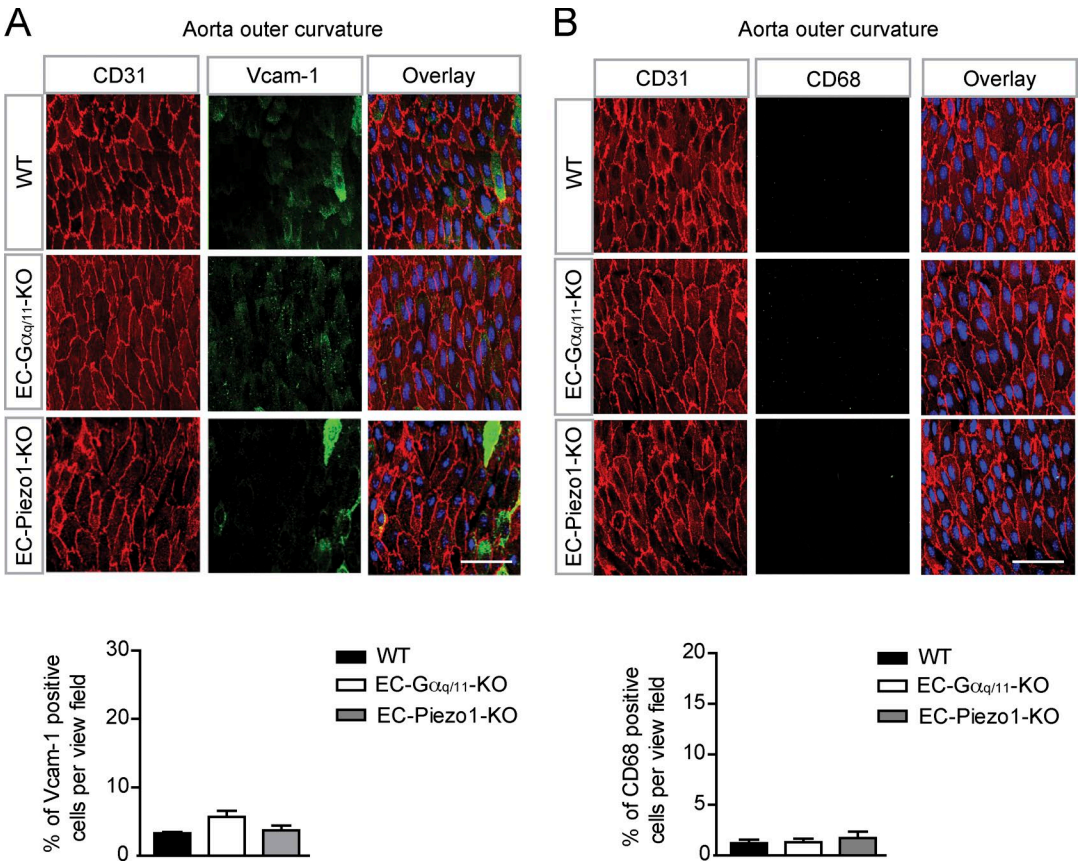

Figure S2. **En face analysis of the aortic outer curvature. (A and B)** Shown are representative en face immuno-confocal microscopy images of the outer curvature. En face aortic arch preparations from 12-wk-old wild-type, endothelium-specific $G\alpha_q/G\alpha_{11}$-KO (EC-$G\alpha_{q/11}$-KO) and Piezo1-KO (EC-Piezo1-KO) mice (n = 6 animal per genotype per condition) were stained with antibodies against CD31, Vcam-1 (A) or CD68 (B) and with DAPI. Immunofluorescence staining was quantified as the percentage of Vcam-1–positive cells among CD31-positive cells per view field (A) or as the percentage of CD68-positive cells per view field (B). Bars, 50 µm. Data represent mean ± SEM (one-way ANOVA and Bonferroni's post hoc test).

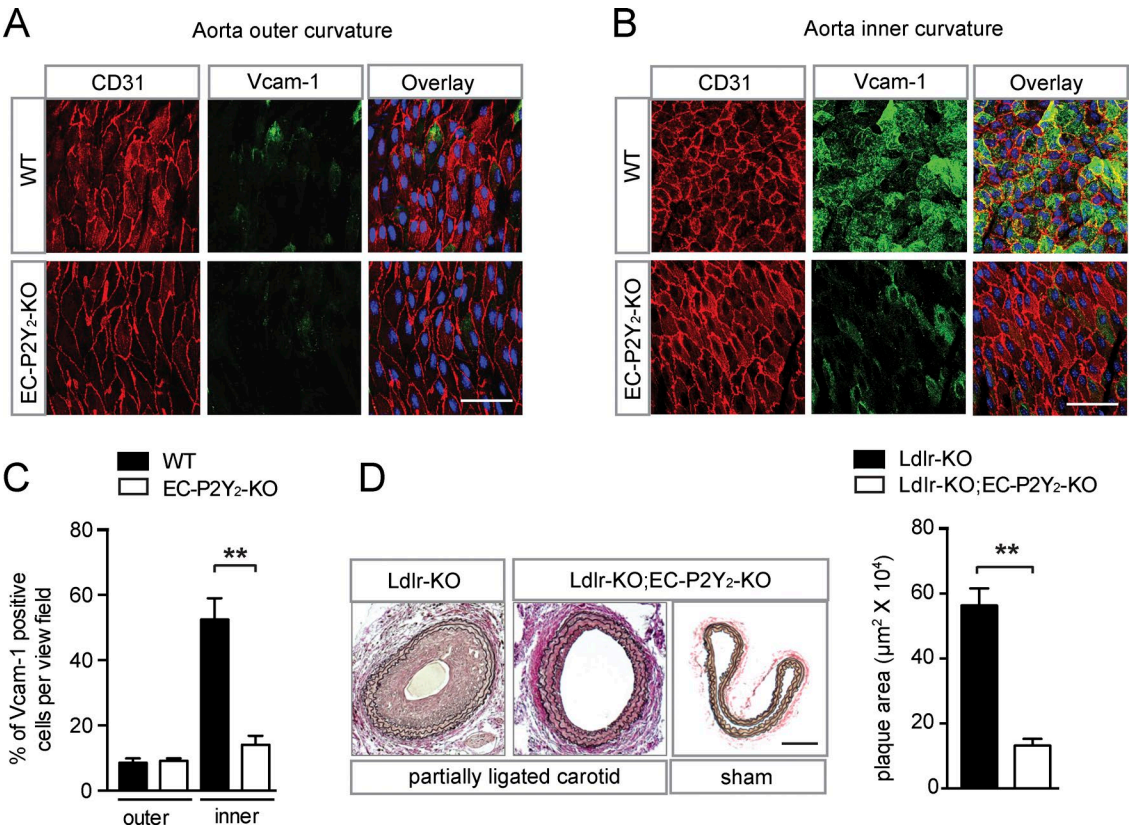

Figure S3. **Analysis of endothelium-specific P2Y2-deficient mice. (A and B)** Representative en face immuno-confocal microscopy image of the outer (A) and inner curvature (B) from 12-wk-old wild-type (control) and endothelium-specific $P2Y_2$-KO mice (EC-P2Y2-KO; n = 5 per genotype). Tissues were stained with anti-CD31 and anti–Vcam-1 antibodies, as well as with DAPI. **(C)** Immunofluorescence staining was quantified as the percentage of Vcam-1–positive cells among CD31-positive cells per view field. **(D)** Ldlr-deficient mice without or with endothelium-specific $P2Y_2$ deficiency (Ldlr-KO;EC-P2Y2-KO) underwent partial ligation of the left carotid artery. 28 d after ligation, carotid arteries were sectioned and stained with elastic stain. Bar diagram shows quantification of the intimal plaque area (n = 6 mice per genotype). Bars, 50 µm. Data represent mean ± SEM; **, P ≤ 0.01 (Student's t test).

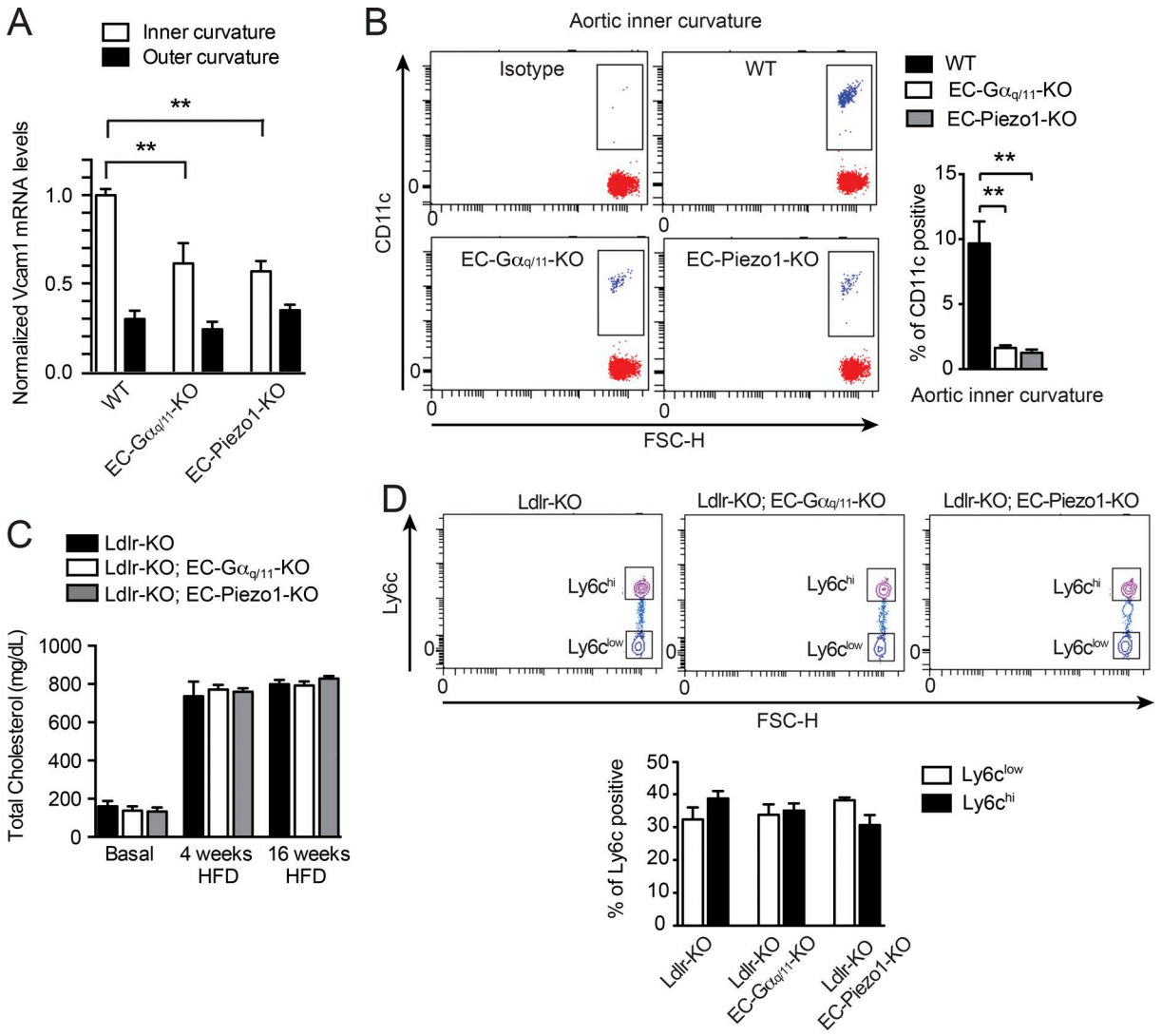

Figure S4. **Endothelial inflammation and atherosclerosis model. (A)** Expression of Vcam-1 mRNA in the intima/subintima of the inner curvature of the aorta from wild-type, EC-Gα_q/Gα_{11}-KO, and EC-Piezo1-KO animals (data from triplicates of three independent experiments; for each experiment two animal samples were pooled; total of six mice per genotype). **(B)** Flow cytometric analysis of live Cd11c-positive cells in the intima/subintima of the inner curvature of the aorta from wild-type, EC-Gα_q/Gα_{11}-KO, and EC-Piezo1-KO animals (total of six mice per genotype). **(C)** Cholesterol levels in the plasma of Ldl-receptor–deficient mice (Ldlr-KO) and Ldlr-KO mice with endothelial cell-specific Gα_q/Gα_{11} deficiency (EC-Gα_q/Gα_{11}-KO) or endothelium-specific Piezo1 deficiency (EC-Piezo1-KO). Six to eight mice per genotype were used. HFD: high-fat diet. **(D)** Levels of Cd45$^+$/Cd11b$^+$/Ly6c^{low} and Cd45$^+$/Cd11b$^+$/Ly6c^{high} cells in the blood of Ldl-receptor–deficient mice (Ldlr-KO), Ldlr-KO; EC-Gαq/Gα11-KO, and Ldlr-KO;EC-Piezo1-KO (total of three to four mice per genotype). Data represent mean ± SEM; **, P ≤ 0.01 (Student's *t* test [A]; one-way ANOVA and Bonferroni's post hoc test [B]).

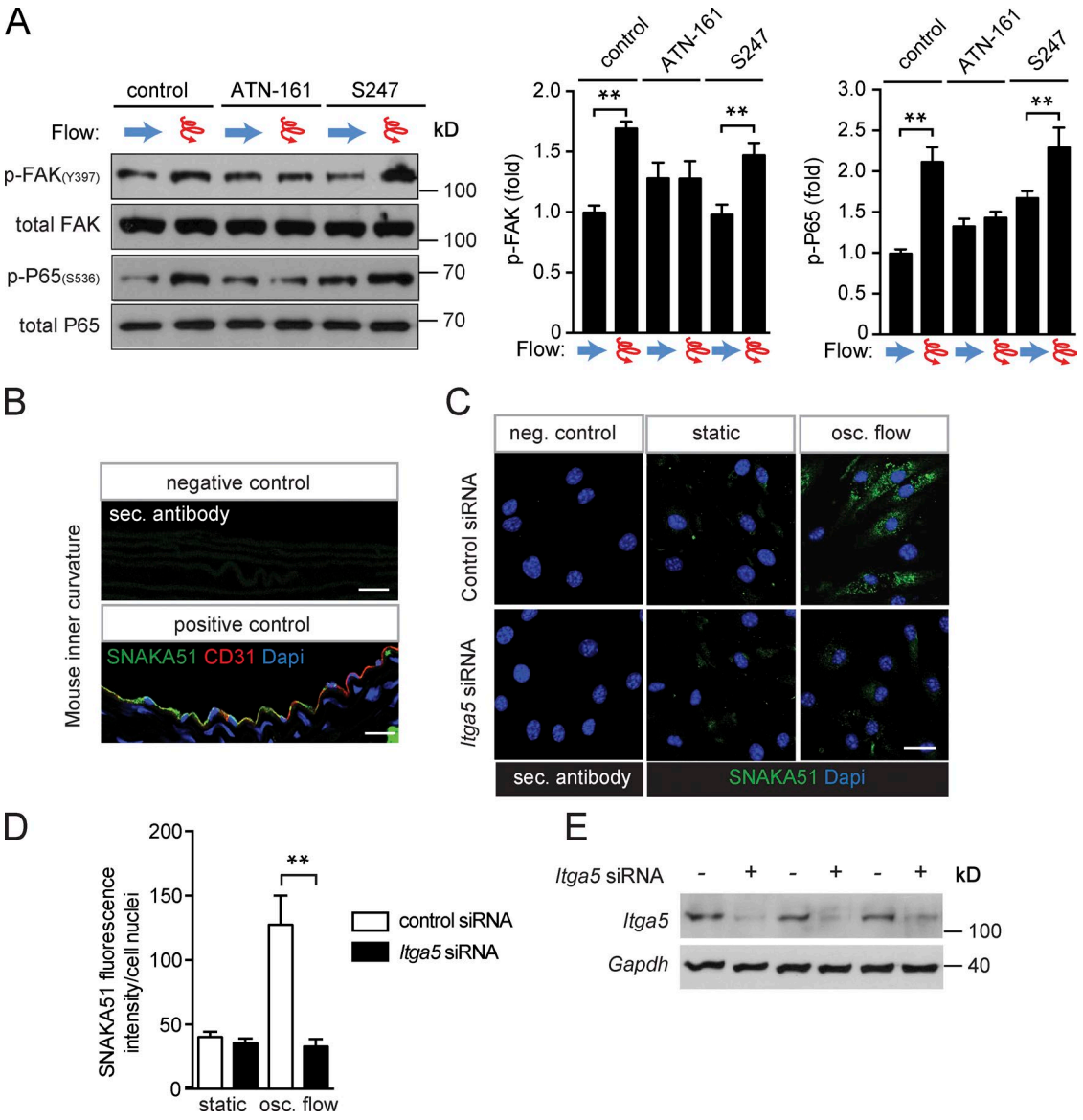

Figure S5. **Integrin α5 is involved in endothelial response to disturbed flow. (A)** HUAECs were incubated with the α5β1 and αvβ3 integrin blocker ATN-161 and S247, respectively, and were exposed to laminar or disturbed flow as described in Fig. 4 A. Activation of integrin signaling was determined by immunoblotting for phosphorylated focal adhesion kinase (pFAK, Y397), and P65 activation was determined by anti–phospho-P65 (S536) antibodies. Bar diagrams show densitometric evaluation of immunoblots (quantification of three to five independent experiments). **(B)** Cross sections of the inner curvature of aortic arches from LDL-receptor–deficient mice fed a high-fat diet for 4 wk were immunostained with SNAKA51, CD31, and DAPI, followed by corresponding labeled secondary antibodies (positive control) or only stained with Alexa Fluor 488– and 594–labeled secondary antibodies (negative control). Shown are representative images of a total of four animals. **(C)** Mouse lung endothelial cells (MLECs) were transfected with control siRNA or with siRNA directed against murine integrin α5 (Itga5) and were kept either under static conditions or were exposed to oscillatory flow for 24 h by the Ibidi flow chamber system. Thereafter cells were immunostained with an antibody against activated α5 integrin (SNAKA51; green) and were stained with DAPI (blue). Negative controls were only incubated with the secondary antibody and DAPI (data of three independent experiments). **(D and E)** Bar diagram (D) shows the quantification of immunocytochemical images and the knock-down efficiency of the siRNA directed against integrin α5, which was analyzed by immunoblotting (E). Data represent mean ± SEM; **, $P \leq 0.01$ (Student's *t* test [A and D]). Bars: 25 µm (B); 50 µm (C).

2.4 G_{13}-Protein-vermittelte Signaltransduktion ist für die Entwicklung von Nachlast-bedingtem Herzmuskel-Umbau und Herzinsuffizienz essenziell

G13-Mediated Signaling Pathway Is Required for Pressure Overload-Induced Cardiac Remodeling and Heart Failure. Takefuji M, Wirth A, Lukasova M, Takefuji S, Boettger T, Braun T, **Althoff T**, Offermanns S, Wettschureck N. *Circulation*. 2012 Oct 16;126(16):1972-82.

https://doi.org/10.1161/CIRCULATIONAHA.112.109256

„Kardiale Umbauprozesse infolge Druck- oder Volumen-Belastung spielen eine entscheidende Rolle bei der Pathogenese der Herzinsuffizienz. Bezüglich der Umwandlung dieser mechanischen Belastungen in strukturelle Anpassungsvorgänge wurden unterschiedliche Mechanismen postuliert, einer davon ist die Freisetzung humoraler Faktoren wie Angiotensin II und Endothelin-1, die wiederum myokardiale Hypertrophie und Fibrosierung begünstigen. Dabei spricht eine Fülle an Daten dafür, dass die prohypertrophen Effekte dieser Faktoren von Rezeptoren vermittelt werden, die an heterotrimere G-Proteine der Familie G_q/G_{11} koppeln. Die Mehrzahl dieser G_q/G_{11}-gekoppelten Rezeptoren, vermögen auch G-Proteine der Familie G_{12}/G_{13} zu aktivieren, aber die Rolle von G_{12}/G_{13} im Rahmen kardialer Umbauprozesse ist nicht bekannt.

Wir haben nun mittels siRNA-vermittelter Inhibition in vitro und konditionaler Kardiomyozyten-spezifischer Gen-Inaktivierung in vivo die Rolle G_{12}/G_{13}-abhängiger Signalwege in Modellen für Druckbelastungs-induzierten kardialen Umbau untersucht. So zeigen wir im Detail, dass die induzierbare Kardiomyozyten-spezifische Inaktivierung der α-Untereinheiten von G_{13} ($G\alpha_{13}$) keinen Einfluss auf die basale Herzfunktion hat, aber Mäuse ebenso effektiv vor Druckbelastungs-induzierter Hypertrophie und Fibrosierung schützt wie eine Inaktivierung von $G\alpha_q/G\alpha_{11}$. Darüber hinaus beugte die Inaktivierung von $G\alpha_{13}$ im Verlauf von einem Jahr nach Beginn der Druckbelastung der Entwicklung einer Herzinsuffizienz vor. Auf der molekularen Ebene zeigen wir, dass G_{13}, aber nicht G_q/G_{11}, die Agonisten-induzierte Expression Hypertrophie-spezifischer Gene über die Aktivierung der kleinen GTPase RhoA und die konsekutive Aktivierung transkriptioneller Kofaktoren der Myokardin-Familie kontrolliert.

Unsere Daten zeigen, dass die G_{12}/G_{13}-Familie heterotrimerer G-Proteine zentral am Druckbelastungs-induzierten kardialen Umbau beteiligt ist und eine zentrale Rolle bei der Transition zur Herzinsuffizienz spielt.“ Übersetzung durch den Autor.

G_{13}-Mediated Signaling Pathway Is Required for Pressure Overload–Induced Cardiac Remodeling and Heart Failure

Mikito Takefuji, Angela Wirth, Martina Lukasova, Seiko Takefuji, Thomas Boettger, Thomas Braun, Till Althoff, Stefan Offermanns and Nina Wettschureck

Circulation. 2012;126:1972-1982; originally published online September 12, 2012;
doi: 10.1161/CIRCULATIONAHA.112.109256
Circulation is published by the American Heart Association, 7272 Greenville Avenue, Dallas, TX 75231

Print ISSN: 0009-7322. Online ISSN: 1524-4539

G_{13}-Mediated Signaling Pathway Is Required for Pressure Overload–Induced Cardiac Remodeling and Heart Failure

Mikito Takefuji, MD; Angela Wirth, PhD; Martina Lukasova, PhD; Seiko Takefuji, MD; Thomas Boettger, PhD; Thomas Braun, MD, PhD; Till Althoff, MD; Stefan Offermanns, MD; Nina Wettschureck, MD

Background—Cardiac remodeling in response to pressure or volume overload plays an important role in the pathogenesis of heart failure. Various mechanisms have been suggested to translate mechanical stress into structural changes, one of them being the release of humoral factors such as angiotensin II and endothelin-1, which in turn promote cardiac hypertrophy and fibrosis. A large body of evidence suggests that the prohypertrophic effects of these factors are mediated by receptors coupled to the $G_{q/11}$ family of heterotrimeric G proteins. Most $G_{q/11}$-coupled receptors, however, can also activate G proteins of the $G_{12/13}$ family, but the role of $G_{12/13}$ in cardiac remodeling is not understood.

Methods and Results—We use siRNA-mediated knockdown in vitro and conditional gene inactivation in vivo to study the role of the $G_{12/13}$ family in pressure overload–induced cardiac remodeling. We show in detail that inducible cardiomyocyte-specific inactivation of the α subunit of G_{13}, $G\alpha_{13}$, does not affect basal heart function but protects mice from pressure overload–induced hypertrophy and fibrosis as efficiently as inactivation of $G\alpha_{q/11}$. Furthermore, inactivation of $G\alpha_{13}$ prevents the development of heart failure up to 1 year after overloading. On the molecular level, we show that $G\alpha_{13}$, but not $G\alpha_{q/11}$, controls agonist-induced expression of hypertrophy-specific genes through activation of the small GTPase RhoA and consecutive activation of myocardin-related transcription factors.

Conclusion—Our data show that the $G_{12/13}$ family of heterotrimeric G proteins is centrally involved in pressure overload–induced cardiac remodeling and plays a central role in the transition to heart failure. **(*Circulation*. 2012;126: 1972-1982.)**

Key Words: heart failure ■ hypertrophy, left ventricular ■ mice ■ signal transduction ■ ventricular remodeling

Myocardial hypertrophy is the adaptive response of the heart to pressure or volume overload, eg, in valve disease, in arterial hypertension, or after myocardial infarction. Hallmarks of cardiomyocyte hypertrophy are increases in cell size and protein content, the re-expression of a fetal gene program including β myosin heavy chain (βMHC) or atrial natriuretic peptide, and the expression of immediate early genes.[1,2] Under conditions of prolonged overload, the initially compensatory hypertrophic response may become maladaptive, resulting in chronic heart failure.[3–5] The mechanisms underlying overload-induced cardiac remodeling have been studied intensively, and in addition to direct mechanical stress as the primary stimulus, a variety of humoral or locally acting factors have been implicated, including cytokines, growth factors, and various agonists at G protein–coupled receptors.[1–3,5] As an example, stretch was shown to cause local release of endothelin-1 (ET-1) or angiotensin II (AngII) from cardiomyocytes, and impaired end-organ perfusion results in sympathetic activation and catecholamine release.[1,2,6,7] In addition, extracellular nucleotides such as UDP and ATP are released from stretched cardiomyocytes and contribute to cardiac fibrosis in an autocrine/paracrine manner.[8] All these mediators can activate receptors that are coupled to the $G_{q/11}$ family of heterotrimeric G proteins, and genetic inactivation or inhibition of this G-protein family was shown to protect mice from pressure overload–induced hypertrophy and consecutive cardiac dysfunction in vivo.[9–11] Intracellular signaling pathways that have been suggested to mediate $G_{q/11}$-dependent cardiomyocyte hypertrophy are mitogen-activated protein kinase signaling, the PI3K/Akt/GSK-3 pathway, or calcium-calmodulin–dependent calcineurin phosphorylation.[1,2,5,12] Interestingly, many $G_{q/11}$-coupled receptors can also signal through $G_{12/13}$, a ubiquitously

Clinical Perspective on p 1982

Received April 2, 2012; accepted September 6, 2012.

From the Departments of Pharmacology (M.T., M.L., S.T., T.A., S.O., M.W.) and Cardiac Development and Remodeling (T.B., T.B.), Max-Planck-Institute for Heart and Lung Research, Bad Nauheim, Germany; and Institute of Pharmacology, University of Heidelberg, Heidelberg, Germany (A.W.).

The online-only Data Supplement is available with this article at http://circ.ahajournals.org/lookup/suppl/doi:10.1161/CIRCULATIONAHA.112.109256/-/DC1.

Correspondence to Nina Wettschureck, MD, Department of Pharmacology, Max-Planck-Institute for Heart and Lung Research, Ludwigstrasse 43, 61231 Bad Nauheim, Germany. E-mail Nina.Wettschureck@mpi-bn.mpg.de

Circulation **is available at http://circ.ahajournals.org** **DOI: 10.1161/CIRCULATIONAHA.112.109256**

expressed G-protein family that consists of 2 members, G_{12} and G_{13}, the α subunits of which, $G\alpha_{12}$ and $G\alpha_{13}$, share 67% amino acid sequence identity.[13] $G\alpha_{12}$ and $G\alpha_{13}$ have been shown to interact with a number of intracellular signaling molecules, including type I and type II classic cadherins, radixin, A-kinase anchoring proteins, nonreceptor tyrosine kinases, and protein phosphatases, but the best-characterized effector pathway is stimulation of the small GTPase RhoA, a well-known regulator of the actin cytoskeleton.[13,14] In neonatal rat ventricular myocytes (NRVMs), overexpression of constitutively active $G\alpha_{13}$ has been shown to increase cell size and hypertrophic gene expression,[15] and interference with $G\alpha_{12/13}$ signaling by overexpression of inhibitory peptides reduced AngII- and ET-1–induced activation of Jun N-terminal kinase.[16] A direct assessment of the cardiac function of $G\alpha_{12/13}$, however, has been impossible because $G\alpha_{13}$-deficient mice die as a result of defective angiogenesis at day 9.5 of embryonic development.[17] We describe here the generation and analysis of mice with inducible, cardiomyocyte-specific deletion of $G\alpha_{12}$ and $G\alpha_{13}$ and show that $G\alpha_{13}$ is critically involved in pressure overload–induced cardiac remodeling and the consecutive development of heart failure by exerting RhoA/myocardin-related transcription factor (MRTF)–dependent transcriptional regulation.

Methods

Materials and Chemicals

AngII, ET-1, and tamoxifen were purchased from Sigma-Aldrich (St. Louis, MO). C3-exoenzyme (cell-permeable Rho inhibitor [CT03]) came from Cytoskeleton (Denver, CO). Antibodies to $G\alpha_{13}$ (sc-26788), $G\alpha_{q/11}$ (sc-392), MRTF-A (sc-21558), MRTF-B (sc-47282), p-ERK (sc-7383), c-Myc (sc-40), and β-actin (sc-47778) were from Santa Cruz Biotechnology (Santa Cruz, CA). Antibodies to total ERK (137F5) were from Cell Signaling (Beverly, MA). The plasmid of MRTF-A was a kind gift from Dr H. Nakano (Juntendo University, Japan). The plasmids of RhoA mutants were a kind gift from Dr K. Kaibuchi (Nagoya University, Japan).

Experimental Animals

Gna13$^{fl/fl}$*;12*$^{-/-}$ mice and *Gnaq*$^{fl/fl}$*;11*$^{-/-}$-deficient mice have been reported previously.[11,18] Cre-mediated recombination of floxed alleles was induced by intraperitoneal injection of 1 mg tamoxifen dissolved in 50 μL Miglyol oil on 5 consecutive days. Vehicle-treated mice received Miglyol only. For in vivo experiments, tamoxifen-treated αMHC-CreERT2$^{\pm}$;*Gna13*$^{wt/wt}$ mice were used as controls. Experiments were performed 2 weeks after the end of induction.

Surgical Interventions: Transverse Aortic Constriction, Osmotic Minipumps

Transverse aortic constriction (TAC) was performed in male mice 8 to 10 weeks old. TAC was created by ligating the transverse aorta between the right innominate and left common carotid arteries against a blunted 24-gauge needle with a 7–0 suture. The needle was then gently retracted. The sham procedure was identical except that the aorta was not ligated. For the implantation of osmotic minipumps, male mice 12 to 14 weeks of age were anesthetized with isoflurane, and osmotic minipumps releasing AngII (150 ng·g^{-1}·h^{-1}; Alzet, Cupertino, CA) were implanted subcutaneously in the back region where they remained for 4 weeks.

Determination of Activated RhoA

NRVMs or adult mouse cardiomyocytes were incubated in serum-free medium for 18 hours and then treated with 1 μmol/L ET-1 or AngII for 3 minutes. Activated RhoA was measured by the G-LISA RhoA activation assay kit (Cytoskeleton) using 0.5 mg/mL protein per sample.

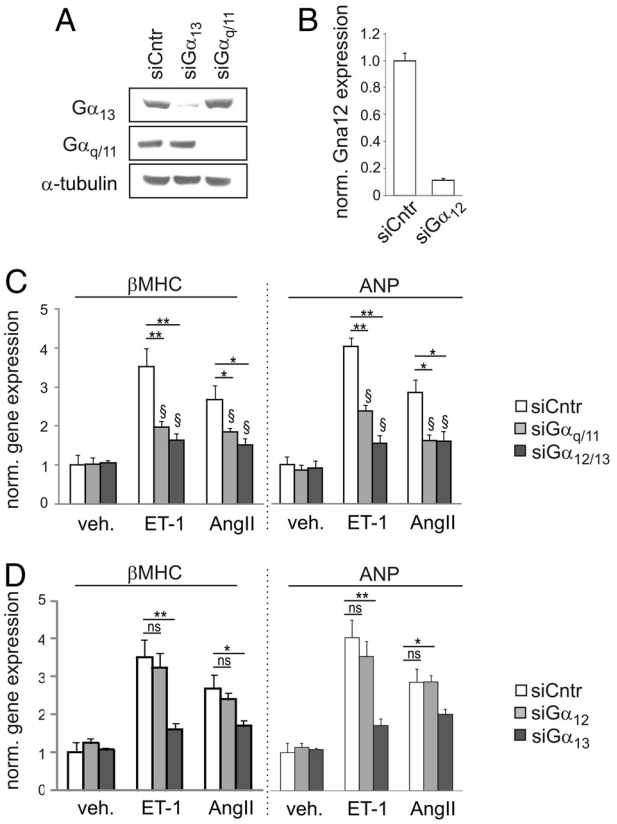

Figure 1. G proteins of the $G_{12/13}$ family contribute to agonist-induced expression of hypertrophy genes in neonatal rat ventricular myocytes (NRVMs). **A**, To estimate knockdown efficiency, protein extracts from siRNA-transfected NRVMs were immunoblotted with antibodies directed against $G\alpha_{13}$, $G\alpha_{q/11}$, and α-tubulin as loading control. **B**, Efficiency of siRNA-mediated knockdown of Gna12 (gene-encoding $G\alpha_{12}$) was determined by quantitative reverse transcriptase–polymerase chain reaction (RT-PCR). **C** and **D**, Upregulation of β-myosin heavy chain (βMHC) or atrial natriuretic peptide (ANP) expression 24 hours after stimulation with endothelin-1 (ET-1), angiotensin II (AngII), or vehicle (veh.) was determined by quantitative RT-PCR after siRNA-mediated knockdown of $G\alpha_{q/11}$ (si$G\alpha_{q/11}$), $G\alpha_{12/13}$ (si$G\alpha_{12/13}$), $G\alpha_{12}$ (si$G\alpha_{12}$), or $G\alpha_{13}$ (si$G\alpha_{13}$) or treatment with scrambled control siRNA (siCntr) (n=4). n Indicates number of independent experiments. *P<0.05; **P<0.01; §P<0.05 vs vehicle-treated sample of the same genotype.

Supplemental Methods

For the generation and characterization of αMHC-CreERT2 mice, isolation of adult mouse left ventricular cardiomyocyte, cell culture techniques, mRNA expression analysis, microarray analysis, Western blotting, histological analyses, and magnetic resonance imaging (MRI), please see Methods in the online-only Data Supplement.

Statistical Analyses

Data are presented as mean±SEM. Normality of distribution was tested by the Kolmogorov-Smirnov test with α=0.05. Comparisons between 2 groups were performed with an unpaired Student t test; comparisons between >2 groups, by ANOVA followed by the Bonferroni post hoc test. Comparisons between >2 groups at different time points were done by repeated-measures ANOVA/Bonferroni post hoc test. Survival curves were analyzed by use of Kaplan-Meier estimators and log-rank (Mantel-Cox) test. Through-

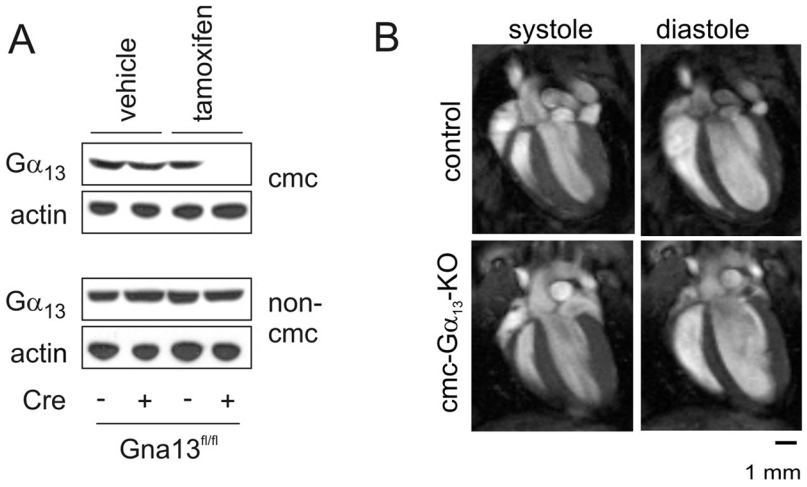

Figure 2. Basal characterization of cardiomyocyte-specific $G\alpha_{13}$-deficient mice (cmc-$G\alpha_{13}$-KO). **A**, Protein extracts from isolated adult cardiomyocytes (cmc) and noncardiomyocytes (noncmc) of vehicle- or tamoxifen-treated α-myosin heavy chain (αMHC)–CreERT2 (Cre)–negative and –positive $Gna13^{fl/fl}$ mice were blotted and probed with antibodies directed against $G\alpha_{13}$ and α-actin (as loading control). **B** and **C**, Representative images (**B**) and statistical evaluation (**C**) of cardiac magnetic resonance imaging analysis 6 months after tamoxifen induction in control mice and cmc-$G\alpha_{13}$-KOs (n=5). BW indicates body weight; CI, cardiac index; HR, heart rate; LVEDV, left ventricular end-diastolic volume; LVEDWT, left ventricular end-diastolic wall thickness; LVEF, left ventricular ejection fraction; LVESV, left ventricular end-systolic volume; and n, number of mice per experimental group.

C

	tamoxifen (6 months)	
	control	cmc-$G\alpha_{13}$-KO
BW (g)	30,14 ± 0,48	28,62 ± 0,66
HR (beats / min)	488,2 ± 16,77	488,0 ± 10,20
LVEDV (µl)	62,34 ± 3,32	59,55 ± 2,67
LVESV (µl)	25,56 ± 1,13	23,91 ± 0,85
LVEF (%)	58,88 ± 0,83	59,74 ± 1,10
CI (ml/min/g)	0,5920 ± 0,03	0,6059 ± 0,02
LVEDWT (µm)	839,0 ± 13,67	811,6 ± 7,56

out this article, n refers to the number of independent experiments or mice per group.

Results

G Proteins of the $G_{12/13}$ Family Mediate Agonist-Induced Expression of Hypertrophy Genes In Vitro

To investigate the relative contribution of $G_{12/13}$ and $G_{q/11}$ to cardiomyocyte hypertrophy in vitro, we performed siRNA-mediated knockdown of $G\alpha_q$ and $G\alpha_{11}$ (the 2 major α subunits of the $G_{q/11}$ family), $G\alpha_{12}$, and $G\alpha_{13}$ in NRVMs (Figure 1A and 1B). When stimulated with ET-1 or AngII, control NRVMs upregulated the expression of hypertrophy-specific genes such as βMHC or atrial natriuretic peptide, and this response was significantly reduced but not abrogated after knockdown of $G\alpha_{q/11}$ (Figure 1C), pointing to an involvement of other G-protein families. Indeed, knockdown of $G\alpha_{12/13}$ also significantly reduced AngII- or ET-1–mediated re-expression of hypertrophy-specific genes, and the degree of reduction was comparable to the effect of $G\alpha_{q/11}$ knockdown (Figure 1C). This effect was due mainly to the loss of $G\alpha_{13}$, whereas knockdown of $G\alpha_{12}$ had only minor consequences (Figure 1D). G protein–coupled receptor–independent signaling pathways that have been implicated in cardiac hypertrophy such as insulin-like growth factor-1–induced phosphorylation of Akt[2,5] were not altered (Figure I in the online-only Data Supplement). These findings suggest that agonist-induced hypertrophy requires activation of both $G\alpha_{q/11}$- and $G\alpha_{12/13}$-dependent signaling pathways in cultured NRVMs.

Generation and Basal Characterization of Cardiomyocyte-Specific $G\alpha_{13}$-Deficient Mice

To test whether $G\alpha_{12/13}$ also contributed to myocardial hypertrophy in vivo, we generated mice with cardiomyocyte-specific deficiency for $G\alpha_{13}$ and $G\alpha_{12/13}$. To do so, we used a newly generated Cre-transgenic mouse line in which a fusion protein of the codon-improved recombinase Cre and a tamoxifen-inducible estrogen receptor mutant (CreERT2) is expressed under control of the cardiomyocyte-specific α-myosin heavy chain (αMHC) promoter present on a bacterial artificial chromosome (Figure IIA in the online-only Data Supplement). β-Galactosidase staining of tissue sections from αMHC-CreERT2/Rosa26LacZ double-transgenic mice showed Cre-mediated recombination in the heart after tamoxifen treatment, whereas no recombination was observed in other organs (Figure IIB and IIC in the online-only Data Supplement). MRI analysis of cardiac function did not reveal any differences between αMHC-CreERT2–negative and –positive mice before and 3 months after tamoxifen treatment (Table I in the online-only Data Supplement).

αMHC-CreERT2 mice were crossed to animals carrying a floxed version of *Gna13*,[18] the gene coding for $G\alpha_{13}$, and in

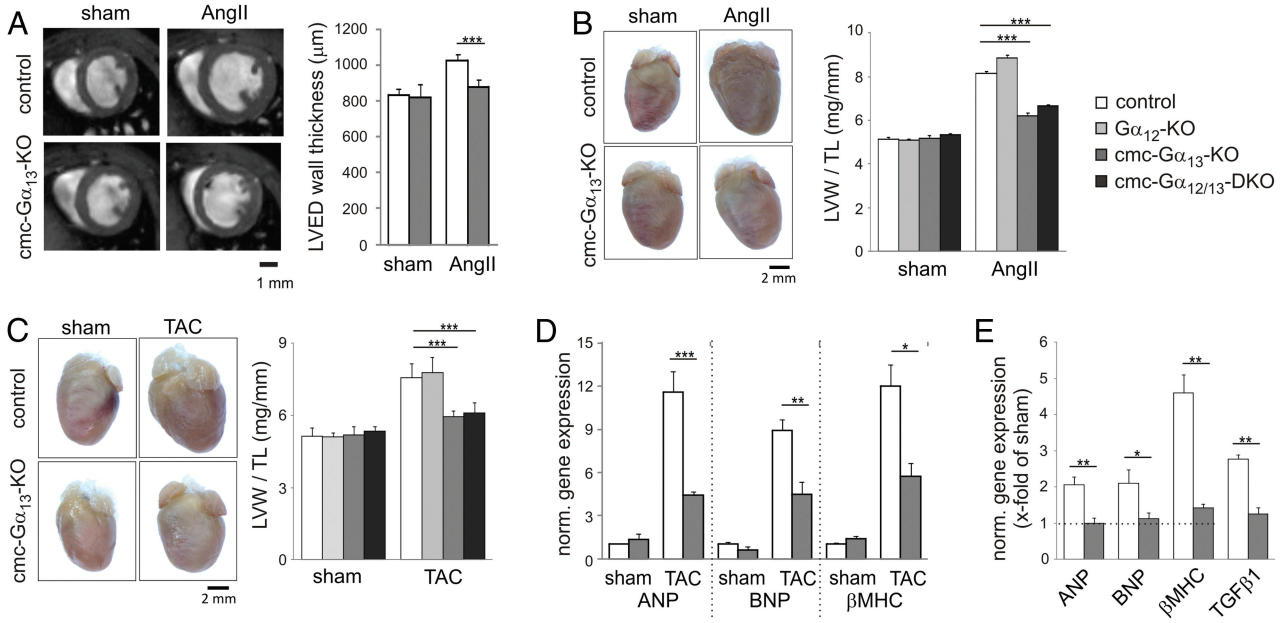

Figure 3. Cardiomyocyte-specific $G\alpha_{13}$-deficient mice (cmc-$G\alpha_{13}$-KOs) show reduced pressure overload–induced hypertrophy in vivo. **A** and **B**, Changes in left ventricular end-diastolic (LVED) wall thickness as determined by magnetic resonance imaging (**A**) or postmortem analysis of cardiac morphology and left ventricular weight to tibia length (LVW/TL) ratio (**B**) 4 weeks after continuous infusion of angiotensin II (AngII) or vehicle (sham) through a osmotic minipump (n=5–8). **C**, Cardiac morphology and LVW/TL ratio 4 weeks after transverse aortic constriction (TAC) or sham surgery (n=8–12). **D**, Gene expression in whole hearts 28 days after surgery (n=5). **E**, Gene expression in isolated cardiomyocytes 5 days after surgery (n=3; data presented as relative increase compared with sham-treated group). n Indicates number of mice per experimental group.*$P<0.05$; **$P<0.01$; ***$P<0.001$.

some cases also to constitutively $G\alpha_{12}$-deficient mice[19] to produce cardiomyocyte-specific $G\alpha_{13}$- and $G\alpha_{12/13}$ double-deficient animals (cmc-$G\alpha_{13}$-KO and cmc-$G\alpha_{12/13}$-DKO, respectively). To induce Cre-mediated recombination of floxed *Gna13* alleles, animals were treated at 6 to 8 weeks of age with intraperitoneal injections of 1 mg tamoxifen on 5 consecutive days, and the efficiency of cardiomyocyte-specific recombination was determined 2 weeks later by Western blot analysis. Whereas $G\alpha_{13}$ was undetectable in purified cardiomyocytes from tamoxifen-treated αMHC-CreERT2$^{\pm}$;*Gna13*$^{fl/fl}$ mice, no changes were observed in the noncardiomyocyte population (Figure 2A). We performed MRI and histological analyses to assess the morphological and functional consequences of induced inactivation of $G\alpha_{13}$ in cardiomyocytes but did not find differences with respect to the ratio of heart weight to body weight (control, 5.59±0.26 mg/g; cmc-$G\alpha_{13}$-DKO, 5.62±0.27 mg/g), macroscopic and microscopic morphology (data not shown), or cardiac function at 6 months after tamoxifen treatment (Figure 2B and 2C).

Cmc-$G\alpha_{13}$-KO Mice Are Protected From Pressure Overload–Induced Hypertrophy, Fibrosis, and Heart Failure Development

To study the role of $G\alpha_{13}$ in cardiomyocyte hypertrophy in vivo, we used a model of continuous AngII infusion that promotes cardiac remodeling both through myocyte-autonomous mechanisms and induction of arterial hypertension.[20] In control mice, continuous AngII infusion resulted in a significant increase in wall thickness as determined by MRI (Figure 3A) or postmortem analysis of the ratio of left ventricular weight to tibia length (Figure 3B), and this response was strongly reduced in cmc-$G\alpha_{13}$-KOs (Figure 3A and 3B). $G\alpha_{12}$ seemed dispensable for the hypertrophic response because $G\alpha_{12}$-deficient mice showed normal hypertrophy and concomitant inactivation of $G\alpha_{12}$ and because $G\alpha_{13}$ did not alter the phenotype of cmc-$G\alpha_{13}$-KOs (Figure 3B). To investigate whether $G\alpha_{13}$ was also required in other models of pressure overload, we performed TAC. Also in this model, 4 weeks after surgery, cmc-$G\alpha_{13}$-KOs showed a significantly lower ratio of left ventricular weight to tibia length, whereas $G\alpha_{12}$-deficient mice again responded normally (Figure 3C). We next assessed transcriptional changes 4 weeks after TAC and found that upregulation of hypertrophy-specific genes such as atrial natriuretic peptide, brain natriuretic peptide, or βMHC was significantly reduced in hearts of cmc-$G\alpha_{13}$-KOs (Figure 3D), and similar changes were observed in isolated cardiomyocytes as early as 5 days after TAC (Figure 3E). Interestingly, we found that proinflammatory growth factors such as transforming growth factor-β1 also were upregulated in cardiomyocytes from control hearts but not in cardiomyocytes of cmc-$G\alpha_{13}$-KOs (Figure 3E).

We next determined fibrotic changes in picrosirius red–stained cardiac sections. We found that 4 weeks after AngII infusion (Figure 4A) or TAC (Figure 4B), cmc-$G\alpha_{13}$-KOs showed significantly less fibrosis than control mice and that the expression of collagen isoforms was reduced (Figure 4C). Importantly, in control mice in both models, cardiac remodeling was accompanied by a decrease in ejection fraction, and this deterioration of cardiac output function was significantly attenuated in cmc-$G\alpha_{13}$-KOs (Figure 4D and 4E).

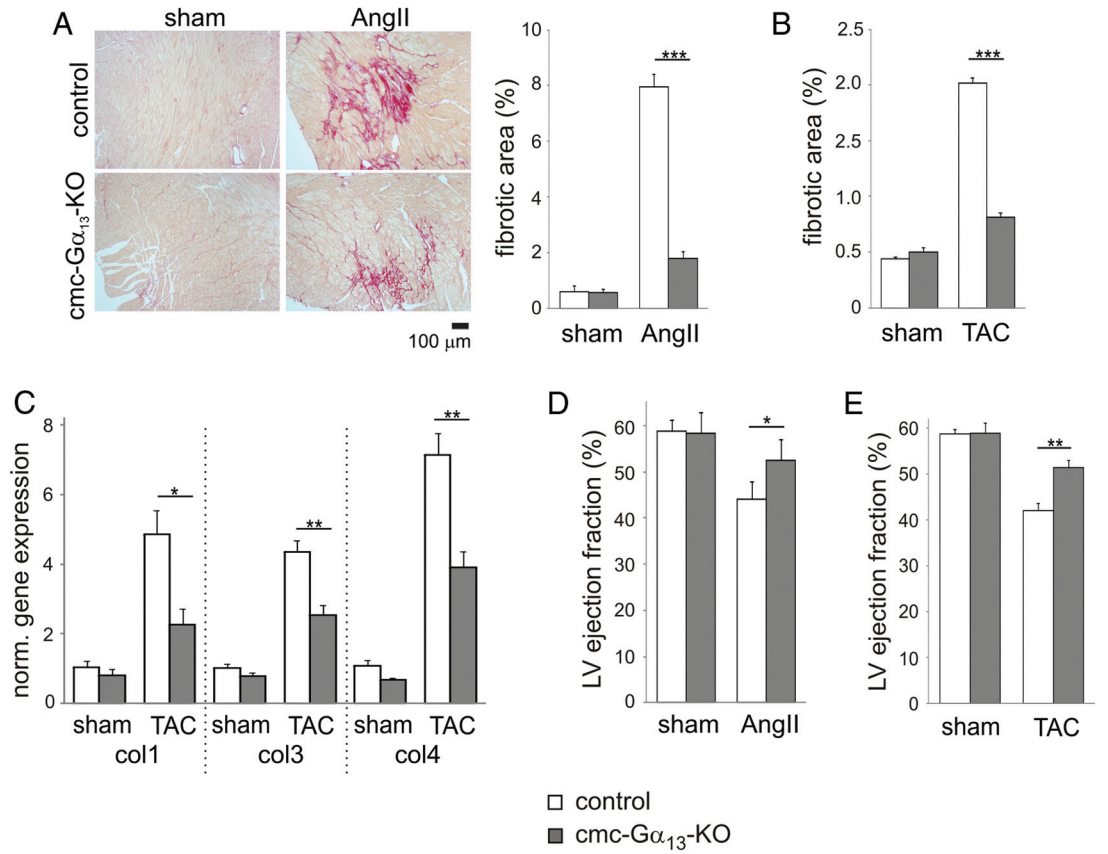

Figure 4. Reduced fibrosis and preserved ejection fraction in cardiomyocyte-specific $G\alpha_{13}$-deficient mice (cmc-$G\alpha_{13}$-KOs) after pressure overloading. **A** and **B**, Fibrotic changes in left ventricles 4 weeks after continuous angiotensin II (AngII) infusion (**A**) or transverse aortic constriction (TAC; **B**) were determined by picrosirius red staining (n=6–8). **C**, Expression of collagen isoforms 1, 3, and 4 (col1, col3, and col4) 4 weeks after TAC was determined by quantitative reverse transcriptase–polymerase chain reaction in cDNAs from whole hearts of control and mutant mice (n=5). **D** and **E**, Left ventricular (LV) ejection fraction (determined by magnetic resonance imaging) 4 weeks after induction of pressure overload by continuous AngII infusion (**D**) or TAC (**E**; n=6). n Indicates number of mice per experimental group.*$P<0.05$; **$P<0.01$; ***$P<0.001$.

Signaling Pathways Mediating the Effects of $G\alpha_{13}$ and $G\alpha_{q/11}$ During Cardiac Remodeling

Cardiomyocyte-specific inactivation of the G-protein family $G_{q/11}$ has previously been shown to result in strongly reduced hypertrophic responses in vivo,[11] but a quantitative comparison with our present findings is difficult because different Cre lines and experimental models were used. To allow a direct comparison between $G_{12/13}$ and $G_{q/11}$ with respect to cardiac function, we generated tamoxifen-inducible, cardiomyocyte-specific $G\alpha_{q/11}$ double-deficient mice (cmc-$G\alpha_{q/11}$-KO) by mating the αMHC-CreERT2 line to mice carrying floxed Gnaq alleles and constitutively Gna11-deficient mice.[11] Western blotting experiments confirmed the cardiomyocyte-specific loss of $G\alpha_{q/11}$, and MRI analyses did not reveal any abnormalities in basal cardiac function after tamoxifen treatment (data not shown). Cmc-$G\alpha_{q/11}$-KOs were as protected from AngII- or TAC-induced hypertrophy (Figure 5A and 5D) and fibrosis (Figure 5B and 5E) as cmc-$G\alpha_{13}$-KOs, and the preservation of ejection fraction was comparable (Figure 5C and 5F). We conclude from these findings that both $G\alpha_{13}$ and $G\alpha_{q/11}$ critically contribute to overload-induced cardiac hypertrophy, fibrosis, and deterioration of ejection fraction in vivo.

We next addressed the question of whether $G\alpha_q$ and $G\alpha_{13}$ converge on the same downstream signaling pathways or signal independently of each other. Several mechanisms have been suggested as to how the $G_{q/11}$ family controls hypertrophic gene expression, one of them being protein kinase C–dependent activation of mitogen-activated protein kinase signaling.[12,21] We found that although ET-1– and AngII-induced phosphorylation of the mitogen-activated protein kinase ERK1/2 was abrogated in $G\alpha_{q/11}$ knockdown cells, it was unchanged in the absence of $G\alpha_{13}$ (Figure 6A), suggesting that $G\alpha_{13}$ signaling does not feed into the mitogen-activated protein kinase pathway. G proteins of the $G_{12/13}$ family have been shown to interact with a number of intracellular signaling molecules, but the best-characterized effector is the small GTPase RhoA,[13,14] which in some cases may also be activated by $G_{q/11}$.[22] We found that inactivation of $G\alpha_{13}$, but not of $G\alpha_{q/11}$, abrogated agonist-induced RhoA activation in NRVMs and isolated adult murine cardiomyocytes (Figure 6B and 6C), indicating that $G\alpha_{13}$ is the main mediator of agonist-dependent RhoA activation in cardiomyocytes. To investigate whether loss of $G\alpha_{13}$-dependent RhoA activation was sufficient to explain reduced gene expression in response to prohypertrophic agonists, we pretreated NRVMs with the RhoA inhibitor C3 exoenzyme. C3 exoenzyme fully mimicked the effect of $G\alpha_{13}$ knockdown (Figure 6D), suggesting that $G\alpha_{13}$ controls hypertrophic gene expression through

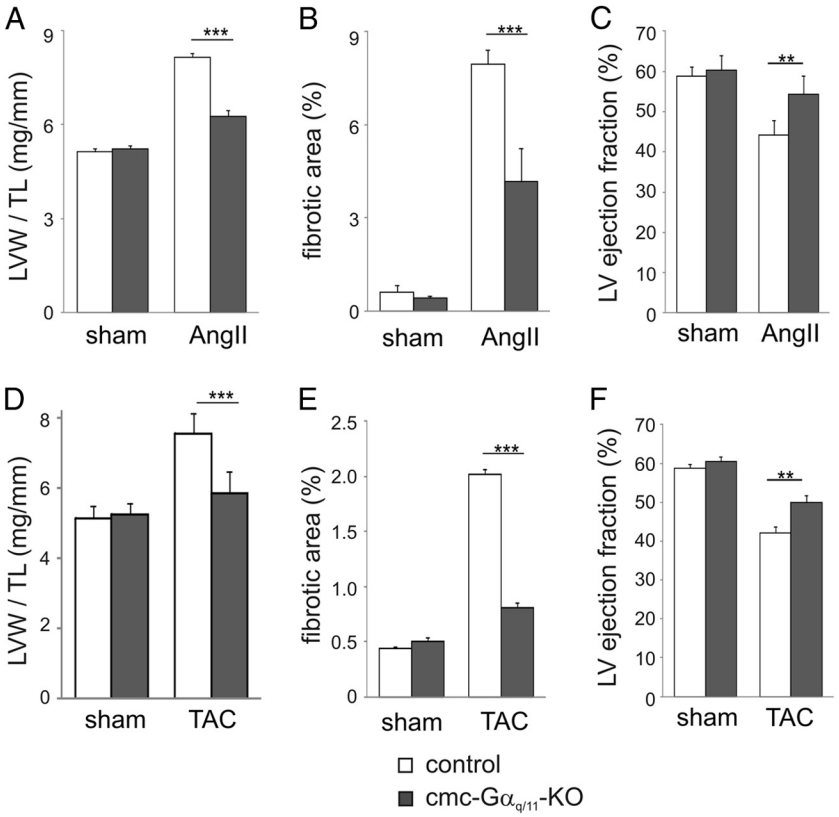

Figure 5. Cardiac remodeling in tamoxifen-inducible, cardiomyocyte-specific $G\alpha_{q/11}$ double-deficient mice (cmc-$G\alpha_{q/11}$-KOs). **A** through **C**, Cardiac remodeling induced by continuous angiotensin II (AngII) infusion: left ventricular (LV) weight/tibia length ratio (LVW/TL) (**A**), fibrotic changes in LVs in picrosirius red–stained sections (**B**), and LV ejection fraction in magnetic resonance imaging (**C**) 4 weeks after the onset of treatment. **D** through **F**, Cardiac remodeling induced by transverse aortic constriction (TAC; as described for **A**–**C**; n=5–8). n indicates number of mice per experimental group. $^{**}P<0.01$; $^{***}P<0.001$.

RhoA. Importantly, TAC-induced RhoA activation also depended on $G\alpha_{13}$ but not on $G\alpha_{q/11}$ (Figure 6E), whereas $G_{q/11}$-mediated effects such as induction of immediate early genes[1] were not affected by loss of $G\alpha_{13}$ (Figure 6F). Taken together, these findings suggest that $G\alpha_{q/11}$ and $G\alpha_{13}$ signal through independent pathways and are not arranged sequentially, a notion that is supported by the finding that knockdown of $G\alpha_{12/13}$ did not affect the ability of constitutively active $G\alpha_q$ to induce hypertrophic gene expression (Figure IIIA in the online-only Data Supplement), nor did knockdown of $G\alpha_{q/11}$ affect constitutively active $G\alpha_{13}$–induced effects (Figure IIIB in the online-only Data Supplement).

To delineate potential differences between $G\alpha_{13}$- and $G\alpha_{q/11}$-mediated hypertrophic responses on the transcriptional level, we performed whole-genome expression profiling 14 days after TAC. We found 235 genes that were at least 2-fold regulated in wild-type hearts in response to TAC, and most of these genes showed reduced regulation in both knockout models (Table II in the online-only Data Supplement), whereas 8 genes showed a >2-fold difference in regulation between cmc-$G\alpha_{13}$ and cmc-$G\alpha_{q/11}$-KOs (Figure IVA in the online-only Data Supplement). Because five of the these genes—tissue inhibitor of metalloproteinase-1 (*Timp1*), serine (or cysteine) peptidase inhibitor 3N (*Serpina3n*), tenascin (*Tnc*), fibromodulin (*Fmod*), and cartilage oligmeric matrix protein (*Comp*)—have been implicated in fibrosis,[23–27] we compared the transcriptional regulation of a batch of fibrosis-related genes 14 days after TAC by reverse transcriptase–polymerase chain reaction (Figure IVB in the online-only Data Supplement). These analyses confirmed that upregulation of *Timp1*, *Serpina3n*, and *Tnc* relied mainly on $G\alpha_{13}$, whereas upregulation of *Fmod* and *Comp* depended more strongly on $G\alpha_{q/11}$. However, upregulation of genes classically implicated in cardiac fibrosis such as collagen isoforms, connective tissue growth factor, periostin (*Postn*), or lysyl oxidase (*Lox*) required both $G\alpha_{q/11}$ and $G\alpha_{13}$. Interestingly, 2 of the 8 differentially regulated genes were myosin light chain isoforms, and reverse transcriptase–polymerase chain reaction showed that also expression of the Myl9 isoform was selectively regulated by $G\alpha_{13}$ (Figure IVC in the online-only Data Supplement). In our search for additional differences between $G\alpha_{q/11}$ and $G\alpha_{13}$, we focused on cellular functions that have been implicated in $G\alpha_q$-dependent heart failure development, eg, altered production of reactive oxygen species, apoptosis, calcium handling, and β-adrenergic desensitization.[28–31] Although TAC-induced increases in reactive oxygen species production depended predominantly on $G\alpha_{q/11}$ (Figure VA in the online-only Data Supplement), downregulation of calcium handling genes or components of the β-adrenergic signaling pathway was more strongly affected by loss of $G\alpha_{13}$ (Figure VB and VC in the online-only Data Supplement). Neither transcriptional nor histological analysis revealed differences in apoptosis at 14 days after TAC (data not shown), but 1 year after TAC, both knockout lines showed significantly reduced cardiac apoptosis (Figure VD in the online-only Data Supplement).

MRTFs Mediate the Effect of $G\alpha_{13}$/RhoA on Gene Expression

To understand how $G\alpha_{13}$-mediated RhoA activation was linked to induction of the hypertrophic gene program, we studied the potential involvement of MRTFs, which have

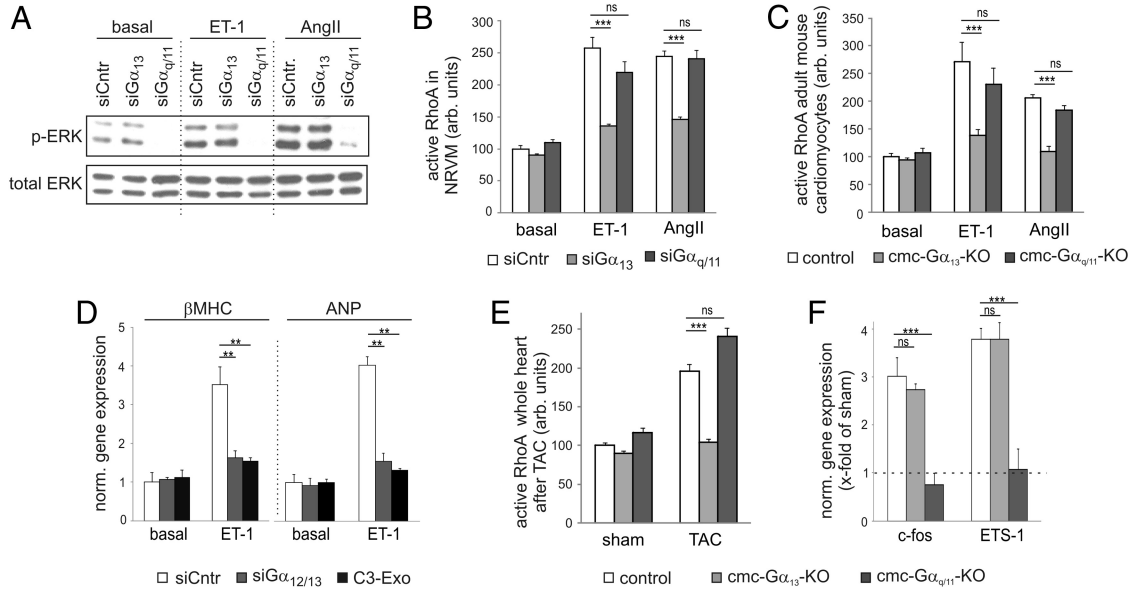

Figure 6. Gα_{13} and G$\alpha_{q/11}$ control cardiac remodeling through independent signaling pathways. **A**, After 3 minutes of agonist stimulation, protein extracts from siRNA-transfected neonatal rat ventricular myocytes (NRVMs) were immunoblotted with antibodies directed against p42/44 ERK or total ERK (data representative of 3 independent experiments). **B**, RhoA activation 3 minutes after application of G protein–coupled receptor (GPCR) agonists in siRNA-treated NRVMs (n=4). **C**, Quantitative reverse transcriptase–polymerase chain reaction (RT-PCR) analysis of β-myosin heavy chain (βMHC) and atrial natriuretic peptide (ANP) expression 24 hours after endothelin-1 (ET-1) stimulation in NRVMs treated with siRNAs or RhoA inhibitor C3 exoenzyme (C3-Exo; n=4). **D**, RhoA activation 3 minutes after application of GPCR agonists in isolated adult murine cardiomyocytes (n=4). **E**, RhoA activation in left ventricles 3 days after transverse aortic constriction (TAC; n=3). **F**, Quantitative RT-PCR analysis of immediate early gene expression in isolated cardiomyocytes 3 days after TAC (n=3; data presented as relative increase compared with sham-treated group). n Indicates number of independent experiments. $^{**}P<0.01$; $^{***}P<0.001$.

been shown to translocate on RhoA-mediated actin polymerization to the nucleus where they act as coactivators of serum response factor (SRF)–dependent gene transcription.[32] We found that various hypertrophic stimuli caused translocation of myc-tagged MRTF-A in cardiac H9c2 cells and that this response was significantly impaired after knockdown of Gα_{13} but not after knockdown of G$\alpha_{q/11}$ (Figure 7A). In line with this, overexpression of wild-type RhoA or constitutively active RhoA^{V14} enhanced nuclear MRTF-A shuttling (Figure 7B). To investigate whether RhoA-dependent MRTF translocation contributed to transcriptional regulation, we studied RhoA-induced expression of SRF-dependent genes after knockdown of MRTFs (Figure 7C). These experiments showed that overexpression of RhoA^{V14} induced transcriptional activity of cotransfected SRF luciferase reporter constructs and that this response was significantly impaired after knockdown of MRTF-A, the closely related MRTF-B, or both (Figure 7D). In addition, knockdown of MRTFs also strongly reduced ET-1–induced upregulation of βMHC expression in NRVMs (Figure 7E), indicating that MRTFs are crucial for the re-expression of hypertrophy genes in response to hypertrophic agonists.

Cmc-Gα_{13}-KOs Are Protected From Heart Failure Development for Up to 1 Year After TAC

Finally, we investigated whether reduced hypertrophy and fibrosis in cmc-Gα_{13}-KOs resulted in long-term beneficial effects with respect to cardiac function. Interestingly, starting at ≈7 months after TAC, control mice showed increased mortality compared with cmc-Gα_{13}-KOs (Figure 8A), and MRI analysis of surviving control mice at 1 year after TAC showed significantly increased left ventricular end-diastolic volumes (Figure 8B) and massively reduced ejection fraction (Figure 8C), suggestive of chronic heart failure. Postmortem analysis showed that 1 year after TAC cmc-Gα_{13}-KOs displayed reduced cardiac fibrosis (Figure 8D), lower expression of heart failure markers such as atrial natriuretic peptide and brain natriuretic peptide, and reduced expression of proapoptotic genes (Figure 8E).

Discussion

We show in this study that the G-protein α subunit Gα_{13} is not required for maintaining basal heart function but critically contributes to pressure overload–induced hypertrophy and fibrosis and the transition to heart failure. In vitro overexpression studies support a role of $G_{12/13}$ in NRVMs,[15,16,33] but cardiomyocyte-specific knockout models were so far not available. Interestingly, a study using cardiac-restricted overexpression of the RGS domain of p115RhoGEF, a peptide known to inhibit $G_{12/13}$ signaling, reported impaired fibrosis but no reduction of hypertrophy,[8] which is in obvious contrast to our own findings. This discrepancy might be explained by incomplete inhibition of Gα_{13}-mediated signaling in p115-RGS transgenic mice, for example, resulting from the fact that the αMHC promoter driving expression of the inhibitory peptide is downregulated as early as 6 hours after the onset of pressure overload.[34] In addition, the αMHC promoter is active already during embryogenesis, potentially causing developmental defects and/or complex compensatory responses. In our model of tamoxifen-inducible Cre-mediated

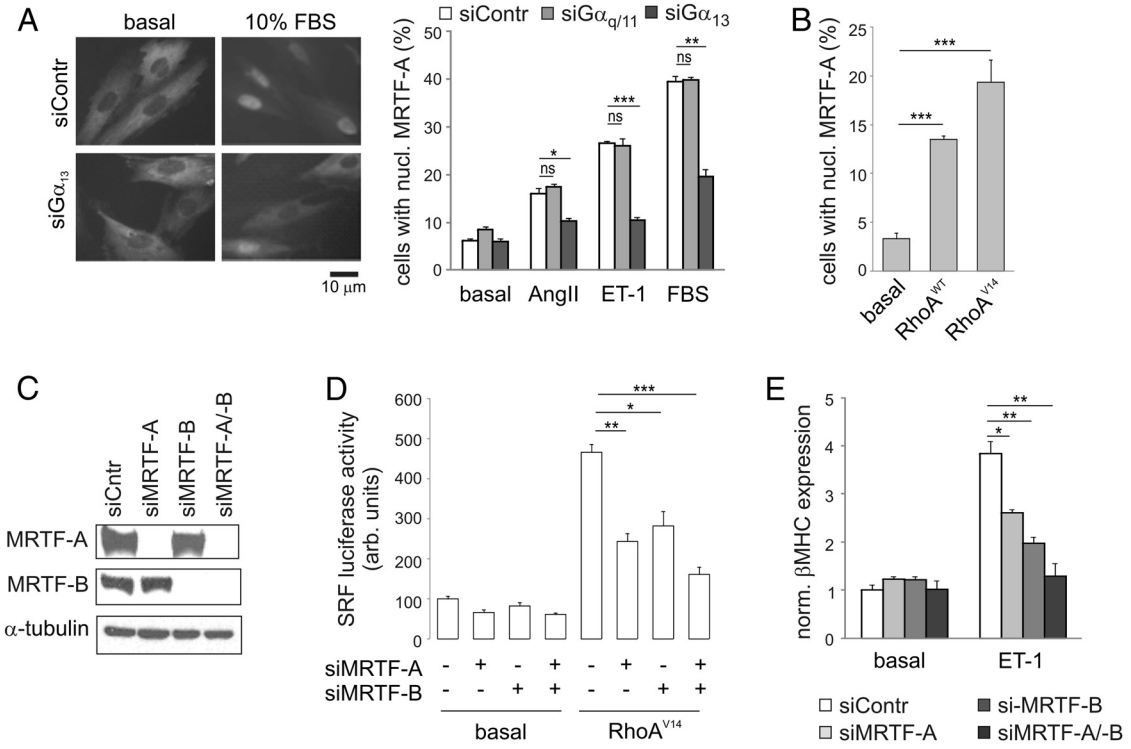

Figure 7. $G\alpha_{13}$ regulates hypertrophic gene expression through myocardin-related transcription factors (MRTFs). **A**, Translocation of myc-tagged MRTF-A in response to hypertrophic stimuli in siRNA-treated in H9c2 cells (n=3). **B**, Effect of wild-type ($RhoA^{WT}$) and constitutively active ($RhoA^{V14}$) RhoA on localization of myc-tagged MRTF-A in H9c2 cells (n=3). **C**, Efficiency of MRTF-A/-B knockdown in H9c2 cells as shown by immunoblotting with anti–MRTF-A/-B antibodies (α-tubulin as loading control). **D**, Effect of $RhoA^{V14}$ on serum response factor (SRF)–luciferase activity in H9c2 cells after siRNA-mediated knockdown of MRTF-A and/or MRTF-B (n=3). **E**, Effect of siRNA-mediated knockdown of MRTF-A/-B on endothelin-1 (ET-1)–induced upregulation of β-myosin heavy chain (βMHC) expression in neonatal rat ventricular myocytes (n=3). n, number of independent experiments. $^*P<0.05$; $^{**}P<0.01$; $^{***}P<0.001$.

inactivation, developmental defects can be excluded, and the degree of recombination is nearly complete, as judged by Western blotting. The αMHC-CreERT2 mouse line used in this study differs from the previously described αMHC-MerCreMer transgenic line[35] in 3 ways. First, a bacterial artificial chromosome–transgenic approach was chosen to increase the specificity and stability of transgene expression.[36] Second, the mutant estrogen receptor ligand binding domain ERT2 was used that confers higher affinity for the ligand tamoxifen.[37] Third, the prokaryotic Cre was replaced by a codon-improved Cre sequence adapted to mammalian codon usage.[37] Importantly, αMHC-CreERT2–positive mice did not differ from control littermates with respect to cardiac MRI parameters before or 1 and 6 months after tamoxifen treatment, showing that expression of CreERT2 itself does not affect heart function.

Our data show that $G\alpha_{13}$ is required not only for G protein–coupled receptor–induced hypertrophic effects in vitro but also for pressure overload–induced effects in vivo. Mechanical stretch has been shown to cause release of ET-1, AngII, or extracellular nucleotides from the myocardium,[6–8] and it is possible that as-yet unknown local mediators or even ligand-independent mechanisms of G protein–coupled receptor activation[38] contribute to $G\alpha_{13}$-mediated hypertrophic effects in vivo. Although inactivation of $G\alpha_{13}$ led to a strong reduction of cardiac remodeling, deletion of $G\alpha_{12}$ was without obvious effects, an observation that has also been made in other cell systems, eg, in platelets[18] or during embryonic development.[19] Possible explanations are differences between $G\alpha_{12}$ and $G\alpha_{13}$ with respect to receptor coupling[39] or effector preference,[40] but whether these differences are relevant under conditions of pressure overload in cardiomyocytes is currently unknown.

Interestingly, cardiomyocyte-specific inactivation of $G\alpha_{13}$ is as efficient in the prevention of cardiomyocyte hypertrophy as inactivation of $G\alpha_{q/11}$, leading to the question of whether these G proteins signal independently of each other or share downstream effectors. The fact that ERK1/2 phosphorylation depended on $G\alpha_{q/11}$ but not on $G\alpha_{13}$ and RhoA activation depended on $G\alpha_{13}$ but not $G\alpha_{q/11}$ indicated that the G-protein families use separate intracellular signaling pathways. Because the $G_{q/11}$ family has been implicated in the release of local mediators or hormones from various cell types,[13] it might be hypothesized that the 2 G-protein families act in a sequential manner, with $G\alpha_{13}$ being activated by a mediator released after activation of $G\alpha_{q/11}$. Nonetheless, the fact that TAC-induced RhoA activation is normal in the absence of $G\alpha_{q/11}$ but abrogated in cmc-$G\alpha_{13}$-KOs speaks against a sequential activation. This notion is further supported by the finding that overexpression of neither constitutively active $G\alpha_q$ nor constitutively active $G\alpha_{13}$ requires the presence of the respective other G-protein family to induce hypertrophy in vitro. However, overexpression of G proteins may lead to nonphysiological effects; therefore, we cannot completely

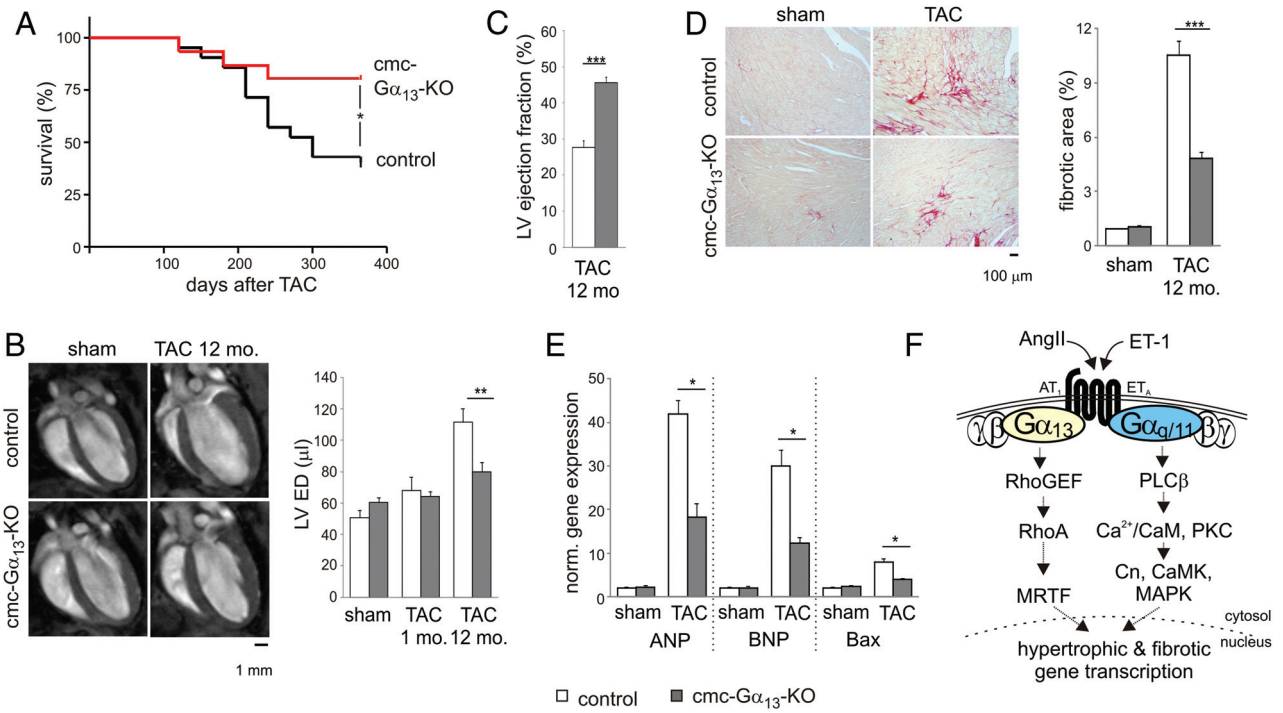

Figure 8. Cardiomyocyte-specific $G\alpha_{13}$-deficient mice (cmc-$G\alpha_{13}$-KOs) are protected from heart failure development for up to 1 year after transverse aortic constriction (TAC). **A**, Survival plot for control mice and cmc-$G\alpha_{13}$-KOs up to 1 year after TAC (n=14–18). **B**, Changes in left ventricular (LV) end-diastolic (LVED) volume as determined by magnetic resonance imaging (MRI) 1 and 12 months after TAC (n=5–6). **C**, LV ejection fraction (determined by MRI) 12 months after TAC (n=5–6). **D**, Cardiac fibrosis (as determined by picrosirius red staining) 1 year after sham surgery or TAC (n=6). **E**, Gene expression 1 year after TAC as determined by quantitative reverse transcriptase–polymerase chain reaction in whole hearts (n=6). **F**, Schematic diagram showing G_{13}- and $G_{q/11}$-dependent signaling cascades activated in response to hypertrophic stimuli like endothelin (ET-1) and angiotensin II (AngII). G protein–coupled receptors such as the endothelin ET_A receptor or the angiotensin II AT_1 receptor can couple to G proteins of both the $G_{q/11}$ family and the $G_{12/13}$ family. ANP indicates atrial natriuretic peptide; BNP, brain natriuretic peptide; Cn calcineurin; CaM, calmodulin; CaMK, Ca^{2+}/calmodulin-dependent protein kinase; Gα, Gβ, and Gγ, G protein subunits α, β, γ; MAPK, mitogen-activated protein kinases; MRTF, myocardin-related transcription factor; NFAT, nuclear factor of activated T cells; PKC, protein kinase C; PLCβ, phospholipase Cβ; and RhoGEF, Rho-specific guanine nucleotide exchange factor. n Indicates number of mice per experimental group. *$P<0.05$; **$P<0.01$; ***$P<0.001$.

exclude sequentiality. Taken together, these findings suggest that 2 different G protein–mediated signaling pathways are required to mount the full hypertrophic response: $G\alpha_{q/11}$-dependent stimulation of PLCβ with consecutive calcium mobilization and protein kinase C activation on one hand and $G\alpha_{13}$-dependent RhoA activation on the other (Figure 8F). The involvement of RhoA is in line with a number of in vitro studies showing that overexpression of activated RhoA caused upregulation of hypertrophy-specific genes and myofibrillogenesis, whereas inhibition of RhoA prevented increases in cell size or protein synthesis in response to G protein–coupled receptor agonists or stretch.[41,42]

Although the functional consequences of $G\alpha_{13}$ deficiency and $G\alpha_{q/11}$ deficiency seem very similar, we identified some cellular effects that depended preferentially on $G\alpha_{q/11}$ like reactive oxygen species production or upregulation of fibrosis-associated genes such as *Fmod* and *Comp*. Other genes potentially involved in cardiac fibrosis (*Timp1*, *Serpina3n*, *Tnc*) were predominantly regulated by $G\alpha_{13}$, as was downregulation of the components of the calcium handling machinery or β-adrenergic signaling. These findings are only partly in accordance with findings in $G\alpha_q$-overexpressing mice,[28–31,43] which is most likely due to the differences between hypertrophic decompensation in response to forced $G\alpha_q$ overexpression and cardiac remodeling induced by pressure overloading. Interestingly, our data suggest that deficiency for $G\alpha_{13}$ prevents downregulation of myosin light chain expression, which might have consequences for contractility and contribute to preserved ejection fraction in cmc-$G\alpha_{13}$-KOs.[44]

The hypertrophic responses of the heart, although initially thought to be beneficial, may become maladaptive if the initial stimulus persists and is then associated with an increased risk of arrhythmia, coronary heart disease, and heart failure.[3,4] The mechanisms underlying the transition from compensatory to maladaptive hypertrophy and remodeling are not well defined, but alterations in contractile proteins, β-adrenergic desensitization, abnormalities in calcium handling, and cardiomyocyte apoptosis with consequent fibrotic replacement are most likely contributing factors.[3,29,41] Although its role in cardiomyocyte survival and apoptosis seems to depend on the pathophysiological context,[45] RhoA-mediated induction of apoptosis might contribute to the development of dilated cardiomyopathy and heart failure in mice with cardiac overexpression of RhoA.[41,46,47] In line with a putative role of prolonged RhoA activation in the transition to heart failure, we found that cardiomyocyte apoptosis and fibrosis were reduced in cmc-$G\alpha_{13}$-KOs. A second possible explanation for the reduced fibrosis and improved survival of cmc-$G\alpha_{13}$-KOs lies in the ability of cardiomyocytes to

produce growth factors such as transforming growth factor-β1, which is known to enhance the inflammatory and fibrotic response to pressure overload.[48] We found that TAC-induced upregulation of transforming growth factor-β1 was significantly reduced in Gα_{13}-deficient cardiomyocytes as early as 5 days after TAC, indicating that the Gα_{13} signaling pathway controls fibrosis through secretion of transforming growth factor-β1. Both factors together, reduced cardiomyocyte growth factor production and decreased apoptosis, might explain why mutant mice are protected from left ventricular decompensation and premature death.

The exact mechanism by which RhoA contributes to hypertrophy and fibrosis is unclear. Because RhoA was implicated in the regulation of the actin-myosin cytoskeleton, previous studies have focused on its role in sarcomere organization and myofibrillogenesis.[42] From our findings in H9c2 cells and NRVMs, we hypothesize that Gα_{13} mediates its hypertrophic effects through MRTF-A and MRTF-B, both coactivators of SRF.[32] This assumption is supported not only by recent studies showing a role of MRTF-A in cardiac hypertrophy[49] and fibrosis[50] but also by the facts that SRF is a significant regulator of most hypertrophy-specific genes and that overexpression of SRF results in cardiac hypertrophy in vivo.[5]

Taken together, our results show that the signaling cascade Gα_{13}-RhoA-MRTF is not required for basal heart function but regulates the expression of hypertrophic and fibrotic genes in cardiomyocytes. The finding that inactivation of Gα_{13} prevents cardiac decompensation for up to 1 year after the onset of pressure overload makes this signaling pathway a promising target for therapeutic intervention in chronic heart failure.

Sources of Funding

Dr Takefuji was supported by a fellowship program of Japan Research Foundation for Clinical Pharmacology.

Disclosures

None.

References

1. Ruwhof C, van der Laarse A. Mechanical stress-induced cardiac hypertrophy: mechanisms and signal transduction pathways. *Cardiovasc Res*. 2000;47:23–37.
2. Heineke J, Molkentin JD. Regulation of cardiac hypertrophy by intracellular signalling pathways. *Nat Rev Mol Cell Biol*. 2006;7:589–600.
3. Hill JA, Olson EN. Cardiac plasticity. *N Engl J Med*. 2008;358:1370–1380.
4. Drazner MH. The progression of hypertensive heart disease. *Circulation*. 2011;123:327–334.
5. Frey N, Olson EN. Cardiac hypertrophy: the good, the bad, and the ugly. *Annu Rev Physiol*. 2003;65:45–79.
6. Sadoshima J, Xu Y, Slayter HS, Izumo S. Autocrine release of angiotensin II mediates stretch-induced hypertrophy of cardiac myocytes in vitro. *Cell*. 1993;75:977–984.
7. Ito H, Hirata Y, Adachi S, Tanaka M, Tsujino M, Koike A, Nogami A, Murumo F, Hiroe M. Endothelin-1 is an autocrine/paracrine factor in the mechanism of angiotensin II-induced hypertrophy in cultured rat cardiomyocytes. *J Clin Invest*. 1993;92:398–403.
8. Nishida M, Sato Y, Uemura A, Narita Y, Tozaki-Saitoh H, Nakaya M, Ide T, Suzuki K, Inoue K, Nagao T, Kurose H. P2Y6 receptor-Galpha12/13 signalling in cardiomyocytes triggers pressure overload-induced cardiac fibrosis. *EMBO J*. 2008;27:3104–3115.
9. Esposito G, Rapacciuolo A, Naga Prasad SV, Takaoka H, Thomas SA, Koch WJ, Rockman HA. Genetic alterations that inhibit in vivo pressure-overload hypertrophy prevent cardiac dysfunction despite increased wall stress. *Circulation*. 2002;105:85–92.
10. Akhter SA, Luttrell LM, Rockman HA, Iaccarino G, Lefkowitz RJ, Koch WJ. Targeting the receptor-Gq interface to inhibit in vivo pressure overload myocardial hypertrophy. *Science*. 1998;280:574–577.
11. Wettschureck N, Rutten H, Zywietz A, Gehring D, Wilkie TM, Chen J, Chien KR, Offermanns S. Absence of pressure overload induced myocardial hypertrophy after conditional inactivation of Galphaq/Galpha11 in cardiomyocytes. *Nat Med*. 2001;7:1236–1240.
12. Clerk A, Sugden PH. Signaling through the extracellular signal-regulated kinase 1/2 cascade in cardiac myocytes. *Biochem Cell Biol*. 2004;82:603–609.
13. Wettschureck N, Offermanns S. Mammalian G proteins and their cell type specific functions. *Physiol Rev*. 2005;85:1159–1204.
14. Kaibuchi K, Kuroda S, Amano M. Regulation of the cytoskeleton and cell adhesion by the Rho family GTPases in mammalian cells. *Annu Rev Biochem*. 1999;68:459–486.
15. Finn SG, Plonk SG, Fuller SJ. G alpha 13 stimulates gene expression and increases cell size in cultured neonatal rat ventricular myocytes. *Cardiovasc Res*. 1999;42:140–148.
16. Arai K, Maruyama Y, Nishida M, Tanabe S, Takagahara S, Kozasa T, Mori Y, Nagao T, Kurose H. Differential requirement of G alpha12, G alpha13, G alphaq, and G beta gamma for endothelin-1-induced c-Jun NH2-terminal kinase and extracellular signal-regulated kinase activation. *Mol Pharmacol*. 2003;63:478–488.
17. Offermanns S, Mancino V, Revel JP, Simon MI. Vascular system defects and impaired cell chemokinesis as a result of Galpha13 deficiency. *Science*. 1997;275:533–536.
18. Moers A, Nieswandt B, Massberg S, Wettschureck N, Gruner S, Konrad I, Schulte V, Aktas B, Gratacap MP, Simon MI, Gawaz M, Offermanns S. G13 is an essential mediator of platelet activation in hemostasis and thrombosis. *Nat Med*. 2003;9:1418–1422.
19. Gu JL, Muller S, Mancino V, Offermanns S, Simon MI. Interaction of G alpha(12) with G alpha(13) and G alpha(q) signaling pathways. *Proc Natl Acad Sci U S A*. 2002;99:9352–9357.
20. Schluter KD, Wenzel S. Angiotensin II: a hormone involved in and contributing to pro-hypertrophic cardiac networks and target of anti-hypertrophic cross-talks. *Pharmacol Ther*. 2008;119:311–325.
21. Wang Y. Mitogen-activated protein kinases in heart development and diseases. *Circulation*. 2007;116:1413–1423.
22. Chikumi H, Vazquez-Prado J, Servitja JM, Miyazaki H, Gutkind JS. Potent activation of RhoA by Galpha q and Gq-coupled receptors. *J Biol Chem*. 2002;277:27130–27134.
23. Mormone E, Lu Y, Ge X, Fiel MI, Nieto N. Fibromodulin, an oxidative stress-sensitive proteoglycan, regulates the fibrogenic response to liver injury in mice. *Gastroenterology*. 2012;142:612–621 e615.
24. Coronado MJ, Brandt JE, Kim E, Bucek A, Bedja D, Abston ED, Shin J, Gabrielson KL, Mitzner W, Fairweather D. Testosterone and interleukin-1beta increase cardiac remodeling during coxsackievirus B3 myocarditis via serpin A 3n. *Am J Physiol Heart Circ Physiol*. 2012;302:H1726–H1736.
25. Frangogiannis NG. Matricellular proteins in cardiac adaptation and disease. *Physiol Rev*. 2012;92:635–688.
26. Nishioka T, Suzuki M, Onishi K, Takakura N, Inada H, Yoshida T, Hiroe M, Imanaka-Yoshida K. Eplerenone attenuates myocardial fibrosis in the angiotensin II-induced hypertensive mouse: involvement of tenascin-C induced by aldosterone-mediated inflammation. *J Cardiovasc Pharmacol*. 2007;49:261–268.
27. Inui S, Shono F, Nakajima T, Hosokawa K, Itami S. Identification and characterization of cartilage oligomeric matrix protein as a novel pathogenic factor in keloids. *Am J Pathol*. 2011;179:1951–1960.
28. Adams JW, Sakata Y, Davis MG, Sah VP, Wang Y, Liggett SB, Chien KR, Brown JH, Dorn GW 2nd. Enhanced Galphaq signaling: a common pathway mediates cardiac hypertrophy and apoptotic heart failure. *Proc Natl Acad Sci U S A*. 1998;95:10140–10145.
29. Dorn GW 2nd, Hahn HS. Genetic factors in cardiac hypertrophy. *Ann N Y Acad Sci*. 2004;1015:225–237.
30. Satoh M, Matter CM, Ogita H, Takeshita K, Wang CY, Dorn GW 2nd, Liao JK. Inhibition of apoptosis-regulated signaling kinase-1 and prevention of congestive heart failure by estrogen. *Circulation*. 2007;115:3197–3204.
31. Shi J, Zhang YW, Summers LJ, Dorn GW 2nd, Wei L. Disruption of ROCK1 gene attenuates cardiac dilation and improves contractile

function in pathological cardiac hypertrophy. *J Mol Cell Cardiol*. 2008; 44:551–560.
32. Olson EN, Nordheim A. Linking actin dynamics and gene transcription to drive cellular motile functions. *Nat Rev Mol Cell Biol*. 2010;11:353–365.
33. Nishida M, Tanabe S, Maruyama Y, Mangmool S, Urayama K, Nagamatsu Y, Takagahara S, Turner JH, Kozasa T, Kobayashi H, Sato Y, Kawanishi T, Inoue R, Nagao T, Kurose H. G alpha 12/13- and reactive oxygen species-dependent activation of c-Jun NH2-terminal kinase and p38 mitogen-activated protein kinase by angiotensin receptor stimulation in rat neonatal cardiomyocytes. *J Biol Chem*. 2005;280:18434–18441.
34. Deckmann AC, Theizen TH, Medrano FJ, Franchini KG, Pereira GA. Immediate response of myocardium to pressure overload includes transient regulation of genes associated with mitochondrial bioenergetics and calcium availability. *Genet Mol Biol*. 2010;33:12–16.
35. Sohal DS, Nghiem M, Crackower MA, Witt SA, Kimball TR, Tymitz KM, Penninger JM, Molkentin JD. Temporally regulated and tissue-specific gene manipulations in the adult and embryonic heart using a tamoxifen-inducible Cre protein. *Circ Res*. 2001;89:20–25.
36. Gong S, Zheng C, Doughty ML, Losos K, Didkovsky N, Schambra UB, Nowak NJ, Joyner A, Leblanc G, Hatten ME, Heintz N. A gene expression atlas of the central nervous system based on bacterial artificial chromosomes. *Nature*. 2003;425:917–925.
37. Feil R, Wagner J, Metzger D, Chambon P. Regulation of Cre recombinase activity by mutated estrogen receptor ligand-binding domains. *Biochem Biophys Res Commun*. 1997;237:752–757.
38. Zou Y, Akazawa H, Qin Y, Sano M, Takano H, Minamino T, Makita N, Iwanaga K, Zhu W, Kudoh S, Toko H, Tamura K, Kihara M, Nagai T, Fukamizu A, Umemura S, Iiri T, Fujita T, Komuro I. Mechanical stress activates angiotensin II type 1 receptor without the involvement of angiotensin II. *Nat Cell Biol*. 2004;6:499–506.
39. Gohla A, Offermanns S, Wilkie TM, Schultz G. Differential involvement of Galpha12 and Galpha13 in receptor-mediated stress fiber formation. *J Biol Chem*. 1999;274:17901–17907.
40. Fukuhara S, Chikumi H, Gutkind JS. RGS-containing RhoGEFs: the missing link between transforming G proteins and Rho? *Oncogene*. 2001; 20:1661–1668.
41. Miyamoto S, Del Re DP, Xiang SY, Zhao X, Florholmen G, Brown JH. Revisited and revised: is RhoA always a villain in cardiac pathophysiology? *J Cardiovasc Transl Res*. 2010;3:330–343.
42. Clerk A, Sugden PH. Small guanine nucleotide-binding proteins and myocardial hypertrophy. *Circ Res*. 2000;86:1019–1023.
43. D'Angelo DD, Sakata Y, Lorenz JN, Boivin GP, Walsh RA, Liggett SB, Dorn GW 2nd. Transgenic Galphaq overexpression induces cardiac contractile failure in mice. *Proc Natl Acad Sci U S A*. 1997;94:8121–8126.
44. Kamm KE, Stull JT. Signaling to myosin regulatory light chain in sarcomeres. *J Biol Chem*. 2011;286:9941–9947.
45. Xiang SY, Vanhoutte D, Del Re DP, Purcell NH, Ling H, Banerjee I, Bossuyt J, Lang RA, Zheng Y, Matkovich SJ, Miyamoto S, Molkentin JD, Dorn GW 2nd, Brown JH. RhoA protects the mouse heart against ischemia/reperfusion injury. *J Clin Invest*. 2011;121:3269–3276.
46. Del Re DP, Miyamoto S, Brown JH. RhoA/Rho kinase up-regulate Bax to activate a mitochondrial death pathway and induce cardiomyocyte apoptosis. *J Biol Chem*. 2007;282:8069–8078.
47. Sah VP, Minamisawa S, Tam SP, Wu TH, Dorn GW 2nd, Ross J Jr, Chien KR, Brown JH. Cardiac-specific overexpression of RhoA results in sinus and atrioventricular nodal dysfunction and contractile failure. *J Clin Invest*. 1999;103:1627–1634.
48. Koitabashi N, Danner T, Zaiman AL, Pinto YM, Rowell J, Mankowski J, Zhang D, Nakamura T, Takimoto E, Kass DA. Pivotal role of cardiomyocyte TGF-beta signaling in the murine pathological response to sustained pressure overload. *J Clin Invest*. 2011;121:2301–2312.
49. Kuwahara K, Kinoshita H, Kuwabara Y, Nakagawa Y, Usami S, Minami T, Yamada Y, Fujiwara M, Nakao K. Myocardin-related transcription factor A is a common mediator of mechanical stress- and neurohumoral stimulation-induced cardiac hypertrophic signaling leading to activation of brain natriuretic peptide gene expression. *Mol Cell Biol*. 2010;30: 4134–4148.
50. Small EM, Thatcher JE, Sutherland LB, Kinoshita H, Gerard RD, Richardson JA, Dimaio JM, Sadek H, Kuwahara K, Olson EN. Myocardin-related transcription factor-a controls myofibroblast activation and fibrosis in response to myocardial infarction. *Circ Res*. 2010;107:294–304.

CLINICAL PERSPECTIVE

Cardiac remodeling in response to pressure or volume overload plays an important role in the pathogenesis of heart failure. Various mechanisms have been suggested to translate mechanical stress into structural changes, eg, the release of humoral factors such as angiotensin II and endothelin-1, which are believed to induce cardiac hypertrophy through activation of receptors coupled to the $G_{q/11}$ family of heterotrimeric G proteins. Most $G_{q/11}$-coupled receptors, however, can also activate G proteins of the $G_{12/13}$ family, but the role of $G_{12/13}$ in cardiac remodeling is not understood. We show in this study that inducible, cardiomyocyte-specific inactivation of the α subunit of G_{13}, $G\alpha_{13}$, does not affect basal heart function but protects mice from pressure overload–induced hypertrophy and fibrosis as efficiently as inactivation of $G\alpha_{q/11}$. Furthermore, inactivation of $G\alpha_{13}$ prevents the development of heart failure up to 1 year after overloading. On the molecular level, we show that $G\alpha_{13}$, but not $G\alpha_{q/11}$, controls agonist-induced expression of hypertrophy-specific genes through activation of the small GTPase RhoA and consecutive activation of myocardin-related transcription factors. Taken together, our results show that the signaling cascade $G\alpha_{13}$-RhoA–myocardin-related transcription factor regulates the expression of hypertrophic and fibrotic genes in cardiomyocytes. The finding that inactivation of $G\alpha_{13}$ prevents cardiac decompensation for up to 1 year after the onset of pressure overload makes this signaling pathway a promising target for therapeutic intervention in chronic heart failure.

SUPPLEMENTAL MATERIAL

Supplemental Methods

Generation and characterization of αMHC-CreERT2 mice

To generate tamoxifen-inducible cardiomyocyte-specific Cre-transgenic mice, a cassette consisting of the CreERT2 cDNA followed by a polyadenylation signal from bovine growth hormone and a module containing the β-lactamase gene flanked by frt sites [1] was introduced into the start codon of the mouse αMHC (MYH6) gene (Accession No: NM_001164171.1) carried by BAC RP23-93K3 (from Chori BACPAC Resources Center) using RedE/T-mediated recombination [2]. Correctly targeted recombinants were verified by Southern blotting and PCR. After FLPe-mediated recombination, the recombined BAC was injected into male pronuclei derived from fertilized FvB/N oocytes. Transgenic offspring was analyzed for BAC insertion by PCR. To verify the inducibility and specificity of the Cre fusion protein, we mated αMHC-CreERT2 mice with mice of the Cre-reporter transgenic line Gt(ROSA)26Sortm1sor (ROSA26-LacZ) (obtained from the Jackson Laboratories, Bar Harbor, ME, USA). We treated double transgenic progeny from αMHC-CreERT2 and ROSA26-LacZ crosses with tamoxifen (intraperitoneal injections of 1 mg per day for five consecutive days) or vehicle alone and sacrificed them one week after the end of induction. Histological analysis of β-galactosidase activity was performed on 12 µm cryosections according to standard protocols. Genotyping of transgenic animals was done using primers P1 (5´-CTTACCCCACATAGACCTCTGACA-3´) and P2 (5´-TGCTGTTGGATGGTCTTCACAG-3´).

Isolation of adult mouse left ventricular cardiomyocyte

Adult mouse cardiomyocyte were isolated as previously described [3]. Briefly, the heart was removed quickly and cannulated from the aorta with a blunted 27G needle to allow retrograde perfusion of the coronary arteries. The heart was first washed with 50 ml of perfusion buffer (113 mM NaCl, 4.7 mM KCl, 0.6 mM KH_2PO_4, 1.2 mM $MgSO_4$, 12mM $NaHCO_3$, 10 mM $KHCO_3$, 10 mM HEPES, 30 mM Taurine, 10 mM 2,3-Butanedione monoxime, 5.5 mM Glucose, pH 7.46), then digested with 75 ml of digesting buffer (perfusion buffer with 0.05 mg/ml Liberase DH (Roche, Mannheim, Germany) and 12.5 µM $CaCl_2$). The heart was removed from the perfusion apparatus and the left ventricle was minced with a forceps in digesting buffer. The calcium concentration was slowly increased from 12.5 µM to 1 mM. Undissociated clumps were removed by filtration through 100 µm nylon mesh. Centrifugation (50 x g, 1 min) was performed 3 times to enrich cardiomyocytes. The cardiomyocytes were seeded on laminin-coated dishes (2 µg laminin/cm^2) after the last centrifugation. To collect non-cardiomyocyte cells, the supernatant after the first centrifugation was seeded on uncoated dishes. Two hours after seeding, attached cells were collected as non-cardiomyocyte cells.

Isolation of neonatal rat ventricular cardiomyocytes

Neonatal rat ventricular myocytes (NRVM) were isolated from 1-2 days old rat neonates using a kit from Worthington Biochemical Corporation (Lakewood, NJ, USA). After digestion, cells were pre-plated for 1 h to remove nonmyocytes, plated on cell culture dishes pre-coated with 1% gelatin (Sigma-Aldrich) and then cultured in Dulbecco´s modified Eagle´s medium (DMEM) with 10% fetal bovine serum. The following day, cells were cultured in serum-free DMEM medium containing 100 µM 5-bromo 2´-deoxy-uridine (BrdU; Sigma-Aldrich). NRVM were transfected with siRNAs (Qiagen, Chatsworth, CA, USA or Sigma-Aldrich) using Lipofectamine RNAiMAX (Invitrogen, San Diego, CA, USA) 3 h and 20 h after plating according to the manufacturer´s instructions. The following siRNA target sequences were used: $G\alpha_{13}$: 5´-CAGCAACGTGATCAAAGGTAT-3´; $G\alpha_{12}$: 5´-CCGCGACACCATCTTCGACAA-3´; $G\alpha_{q}$: 5´-AAGCACTCTTTAGAACCATTA-3´; $G\alpha_{11}$: 5´-CACAACTGGCATCATCGAGTA-3´; Mkl1 (MRTF-A): 5´-CAATTTGCCTCCACTTAGT-3´; Mkl2 (MRTF-B): 5´-CTTAGAACCTGTGAACAGT-3´.

Cell culture

For luciferase assays, H9c2 cells cultured in 10-cm dishes were transfected with siRNA using Lipofectamine RNAiMAX 24 h and 48 h after plating. Four hours after the second siRNA transfection, cells were transfected with pGL4.34-luc2P/SRF-RE (5 µg, Promega, Madison, WI, USA) and HA-RhoA plasmids (15 µg) using Lipofectamine 2000 (Invitrogen). Four hours after plasmid transfection, the growth medium was replaced with serum-free medium. After a 40-h serum-free incubation, cells were washed with phosphate-buffered saline (PBS) twice and collected in PBS using a cell scraper. The samples were centrifuged and the supernatants were discarded. Luciferase activities were measured using a luciferase assay system (Promega). To determine MRTF-A translocation, H9c2 cells were transfected with pcDNA3-myc MRTF-A using Lipofectamine 2000. The cells were incubated in serum-free medium for 24 h before being treated with 1 µM ET-1 or AngII for 1 h and fixed with 4% formaldehyde in PBS. The subcellular distribution of myc-tagged MRTF-A was determined by immunostaining with an anti-myc antibody. At least 200 transfected cells were counted in each group.

mRNA expression analysis

RNA was extracted from left ventricles with the RNA fibrosis tissue kit (Qiagen) and from NRVM or adult mouse cardiomyocytes with the RNeasy Mini kit (Qiagen) according to the manufacture´s protocol. In some cases, NRVM were pretreated with C3-Exoenzyme for 4 h at a concentration of 1µg/ml. Reverse transcriptase (RT) reaction was performed using the QuantiTect Reverse Transcription kit (Qiagen).

Quantitative RT-PCR for rat genes was done using the LightCycler 480 SYBR Green Master (Roche) and the following primers:

Rat $G\alpha_{12}$ 5´-CGGCAAGTCCACCTTCCTCAAGC-3´/5´-TGGTGTCGCGGAACTCCAGCA-3´;

rat βMHC 5´-GAGGGCGGACATTGCCGAGT-3´/5´-AAGGCTCCAGGTCTCAGGGCTTC-3´;

rat αskA 5´- ACCGCAAATGCTTCTAGGCGCA -3´/5´- GGGGCCACCCTGCAACCATAG-3´;
rat ANP 5´-CAGACCGATGAAGCGGGGGC-3´/5´-TCTTCGCAGGCTCCGAGGGC-3´;
rat BNP 5´- AGCGCCTTCCGGATCCAGGA -3´/5´- CAAGCGACTGACTGCGCCGA-3´;
rat GAPDH 5´-GGGCTCTCTGCTCCTCCCTGTT-3´/5´-CGTCCGATACGGCCAAATCCGT-3´;

Quantification of mouse genes was done using the LightCycler 480 Probe Master System (Roche) and the following primers and probes:
mouse ANP: 5´-CACAGATCTGATGGATTTCAAGA-3´/5´-CCTCATCTTCTACCGGCATC-3´/probe 25;
mouse BNP: 5´-GTCAGTCGTTTGGGCTGTAAC-3´/5´-AGACCCAGGCAGAGTCAGAA-3´/probe 71;
mouse βMHC: 5´-CGCATCAAGGAGCTCACC-3´/5´-CTGCAGCCGCAGTAGGTT-3/probe 6´;
mouse TGF β1: 5´-TGGAGCAACATGTGGAACTC-3´/5´-CAGCAGCCGGTTACCAAGaccaag-3´/probe 72;
mouse Col1a1: 5´-CATGTTCAGCTTTGTGGACCT-3´/5´-GCAGCTGACTTCAGGGATGT-3´/probe 15;
mouse Col3a1: 5´-TCCCCTGGAATCTGTGAATC-3´/5´-TGAGTCGAATTGGGGAGAAT-3´/probe 49;
mouse Col4a1: 5´-TTAAAGGACTCCAGGGACCAC-3´/5´- CCCACTGAGCCTGTCACAC-3´/probe 56;
mouse BAX: 5´-GTGAGCGGCTGCTTGTCT-3´/5´-GGTCCCGAAGTAGGAGAGGA-3´/probe 83;
mouse GAPDH: 5´-AGCTTGTCATCAACGGGAAG-3´/5´-TTTGATGTTAGTGGGGTCTCG-3´/probe 9;
mouse Adcy5: 5´- CCAGAAGCATGACAATGTGAG-3´/5´- TGACCAGTTCTTGGGCAGTA-3´/probe 64;
mouse Adcy6: 5´- CTGGCAGCTCAACAGCAG-3´/5´- AGGAAGAGCACCACGTTAGC-3´/probe 38;
mouse Adrb1: 5´- CATCATGGGTGTGTTCACG -3´/5´- GGAAAGCCTTCACCACGTT -3´/probe 71;
mouse Adrb2:5´- TGCTATCACATCGCCCTTC-3´/5´- ACCACTCGGGCCTTATTCTT -3´/probe 40;
mouse Atp2a1: 5´- ACGGAGACTGCTCTCACCAC-3´/5´- ATGAGTTGGCGGATCACC-3´/probe 22;
mouse Atp2a2:5´-TGGTGATATAGTGGAAATTGCTG-3/5-GAGTTGTAGACTTGATGGATGTCAA-3/probe18;
mouse Col8a1: 5´-GCCAGCCAAGCCTAAATGT-3´/5´-CAGAGTTCAGGGAAATGATGAA-3´/probe 3;
mouse Comp: 5´- CCAAGAAGAATGACGATCAGAA-3´/5´- CGGGGACAGTTGTCAGCTA-3´/probe 85;
mouse CTGF: 5´- TGACCTGGAGGAAAACATTAAGA-3´/5´- AGCCCTGTATGTCTTCACACTG -3´/probe 71;
mouse Fmod: 5´- CAGGGCAACAGGATCAATG-3´/5´- CTGCAGCTTGGAGAAGTTCAT-3´/probe 77;
mouse Lox: 5´-ATGCCAACACACAGAGGAGA-3´/5´-AGGTGTCATAACATCCAGGACTC-3´/probe 41;
mouse Myl4: 5´-CAAGCACATCATGTCTGGGTA-3´/5´-TGGATCTCTTGCTTTCTCACG-3´/probe 80;
mouse Myl7: 5´-CACCGTCTTCCTCACACTCTT-3´/5´-AGGCACTCAGGATGGCTTC-3´/probe 7;
mouse Myl9: 5´-GATAAGGAGGACCTGCACGA-3´/5´-GCCCTCCAGATACTCGTCTG-3´/probe 60;
mouse Pln: 5´- CACGTCAGAATCTCCAGAACC-3´/5´- GCTCTTCACAGAAGCATCACA-3´/probe 84;
mouse Car3: 5´- GCCCTGGTCAGCATCTTATG-3´/5´- GGACCACCCCTCAGCATAG-3´/probe 21;
mouse Postn: 5´- CGGGAAGAACGAATCATTACA-3´/5´- ACCTTGGAGACCTCTTTTTGC -3´/probe 10;
mouse Ryr2: 5´- GGCCCTAATTAGAGGAAATCG-3´/5´- GGGCTCTCCACTAACACACAG-3´/probe 99;
mouse Serpina3n: 5´-GGGATGATCAAGGAACTGGTC-3´/5´-GCACCTTCCATTTGGCTTT-3´/probe 85;
mouse Timp1: 5´-GCAAAGAGCTTTCTCAAAGACC-3/5-AGGGATAGATAAACAGGGAAACACT-3/probe 76;

mouse Tnc: 5´- CCACCTCCCATGTCCTGA-3´/5´- CCAGGGAAGGCACTTCTTC-3´/probe 1;

Data are in all cases presented after normalization to GAPDH, and basal values were set to 1. In some cases in addition the relative change compared to basal conditions was calculated.

Microarray analysis

Left cardiac ventricles were dissected from PBS-perfused animals 14 days after TAC or sham surgery (data from 2 independent samples per group), and total RNA was isolated using the TRIzol method (Invitrogen). RNA quality was checked on the Agilent 2100 Bioanalyzer using the RNA 6000 Nano Kit. For mRNA expression analysis, the Affymetrix GeneChip Mouse Gene 1.0 St array was employed with the Affymetrix WT terminal labeling and hybridization protocol strictly according to the manufacturer's instructions. Data were analyzed by the RMA algorithm using the Affymetrix Expression Console and DNAStar ArrayStar 5 Software.

Western blotting

Samples were subjected to sodium dodecyl sulfate polyacrylamide gel electrophoresis (SDS-PAGE), transferred to nitrocellulose transfer membranes (Whatman, Dassel, Germany), and then incubated with primary antibodies as indicated. Equal loading was checked by antibody to α-tublin or actin. To determine the effect of IGF-1 on Akt phosphorylation, NRVM were isolated from 1-2 days old rat neonates and cultured in DMEM with 10% fetal bovine serum. The following day, cells were cultured in serum-free DMEM medium. NRVM were transfected with siRNA for $G\alpha_{13}$. Forty eight hours after siRNA transfection, NRVM were incubated in DMEM containing 100 nM insulin-like growth factor I (Sigma-Aldrich) for 10 minutes. Antibodies to p-Akt (Ser473, Cell Signaling) and total-Akt (sc-7126, Santa Cruz) were used for western blotting.

Histological analyses

Freshly dissected heart tissue was fixed in 4% paraformaldehyde, dehydrated and embedded in paraffin. Embedded hearts were stained with picrosirius red according to standard protocol. Twenty randomly chosen frames from the sections were quantified to assess the degree of heart fibrosis using NIH ImageJ software. Dihydroethidium (DHE) staining was performed as described previously [4]. In brief, freshly frozen left ventricular myocardium (10 µm-slices) was incubated at 37 ^{o}C for 1 hour with dihydroethidium (Life Techonologies; 2 µmol/L) as described previously. Ethidium fluorescence was examined by fluorescent microscopy. TUNEL staining of nuclei positive for DNA strand breaks was performed using the "Cell Death Detection kit" (Roche, Indianapolis, IN) according to the manufacturer´s instructions. Briefly, paraffin-embedded sections were deparaffinized and rehydrated. The sections were then incubated with Proteinase K at room temperature for 30 min. The sections were incubated with TUNEL reaction mixture at 37 ^{o}C for 1 hour. Nuclear density was determined by manual counting of DAPI-stained nuclei. At least 10000 DAPI-positive cells were counted in each animal.

Magnetic Resonance Imaging

Cardiac MRI measurements were performed on a 7.0 T Bruker Pharmascan, equipped with a 300 mT/m gradient system, using a custom-built circularly polarized birdcage resonator and the Early Access Package for self-gated cardiac Imaging (Bruker, Ettlingen, Germany) [5]. The mice were measured under volatile isoflurane (2.0 %) anesthesia. The measurement is based on the gradient echo method (repetition time = 6.2 ms; echo time = 1.6 ms; field of view = 2.20 x 2.20 cm; slice thickness = 1.0 mm; matrix = 128 x 128; repetitions = 100). The imaging plane was localized using scout images showing the 2- and 4- chamber view of the heart, followed by acquisition in short axis view, orthogonal on the septum in both scouts. Multiple contiguous short-axis slices consisting of 9 or 10 slices were acquired for complete coverage of the left ventricle. MRI data were analyzed using Qmass digital imaging software (Medis, Leiden, Netherlands).

Supplemental Figures

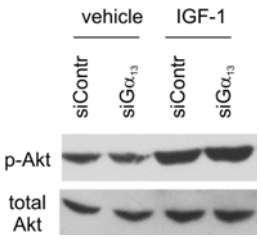

Suppl. Fig. 1: **IGF-1-induced Akt phosphorylation is not affected by knockdown of $G\alpha_{13}$.** Exemplary immunoblot showing phosphorylation of Akt at serine 473 in response to 100 nM IGF-1 in NRVM transfected with scrambled siRNA (siContr) or after knockdown of $G\alpha_{13}$.

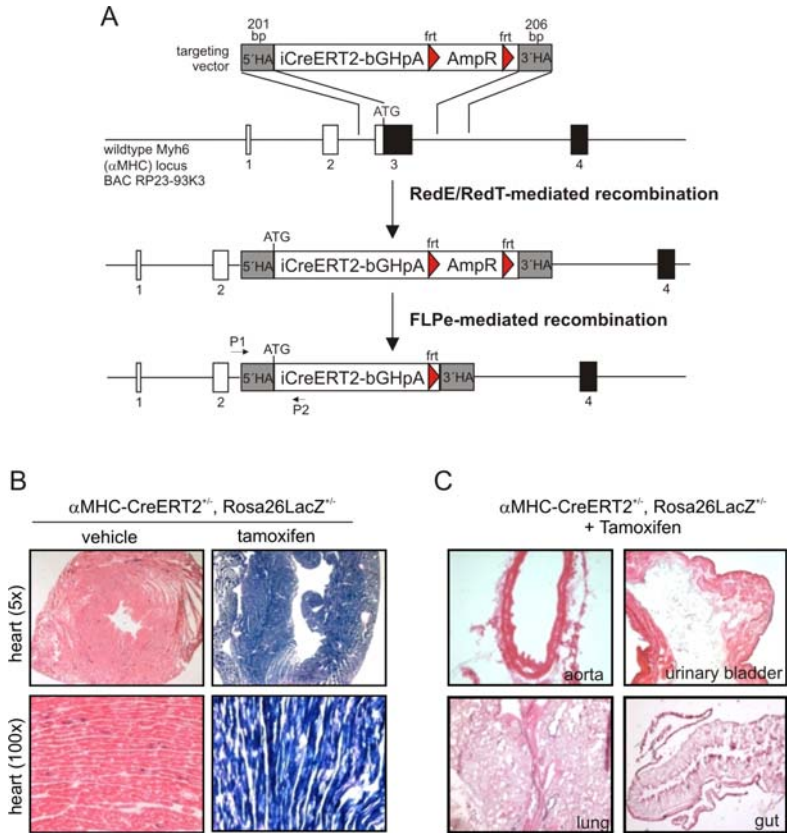

Suppl. Fig. 2: Generation and characterization of tamoxifen-inducible, cardiomyocyte-specific Cre expressing mice (αMHCCreERT2). **A, T**argeting scheme for the generation of αMHCCreERT2 mice. A BAC transgenic approach[2] was used to generate a tamoxifen-inducible, cardiomyocyte-specific Cre mouse line in which a fusion protein of iCre, a Cre version optimized for mammalian codon usage, and the tamoxifen-inducible estrogen receptor mutant ERT2 (ERT2)[6] is expressed under control of the cardiomyocyte-specific α-myosin heavy chain (α-MHC) promoter. **B, C,** Cardiomyocyte-specific Cre/LoxP-mediated recombination was evaluated by crossing the α MHC-CreERT2 line with the Rosa26Lacz reporter line, which expresses the lacZ gene upon Cre-induced recombination[7]. Beta galactosidase staining of tissue sections from α MHC-CreERT2/Rosa26LacZ double transgenic mice shows Cre-mediated recombination as blue staining. No recombination was observed in hearts of vehicle-treated mice or in other organs.

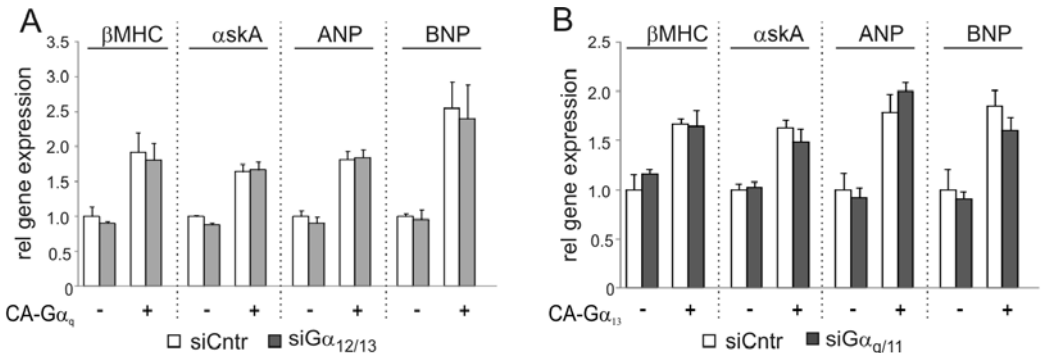

Suppl. Fig. 3: Upregulation of hypertrophy-specific genes in response to overexpression of constitutively active (CA) $G\alpha_q$ after knockdown of $G\alpha_{12/13}$ (A) or in response to overexpression of CA-$G\alpha_{13}$ after knockdown of $G\alpha_{q/11}$ (B) was determined by qRT-PCR in cardiac H9c2 cells (n = 3). βMHC, β-myosin heavy chain; αskA, α-skeletal actin; ANP, atrial natriuretic peptide; BNP, brain natriuretic peptide.

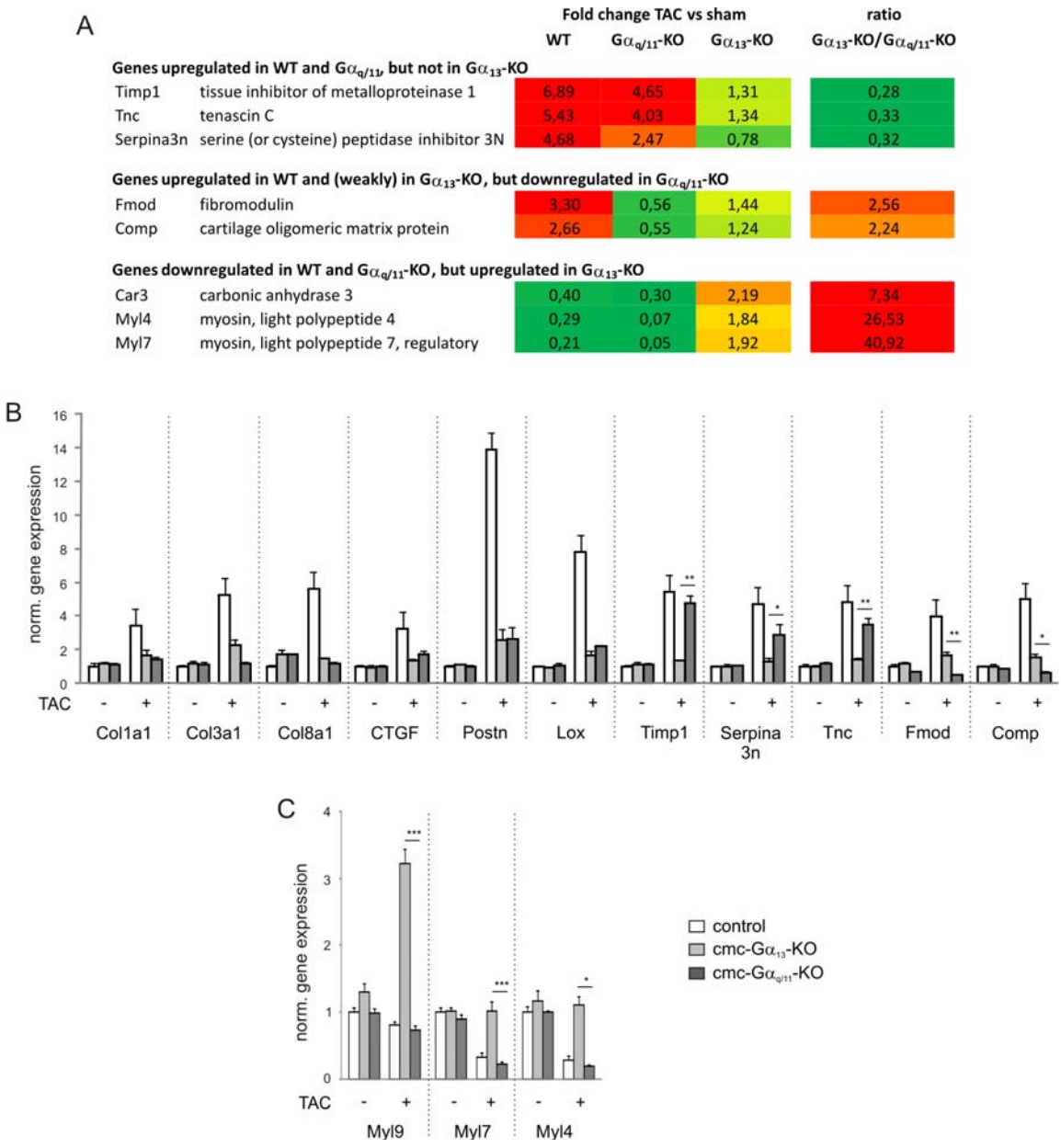

Suppl. Fig. 4: Transcriptional differences between control mice, cmc-Gα$_{13}$-KOs and cmc-Gα$_{q/11}$-KOs 14 days after TAC. A, Genes that show an at least twofold difference in expression between cmc-Gα$_{13}$-KO and cmc-Gα$_{q/11}$-KO at day 14 after TAC (n = 2). **B, C,** Changes in expression of fibrosis-related genes (B) and myosin light chain isoforms (C) as determined by quantitative RT-PCR analysis in left ventricles 14 days after TAC (n = 3). Abbreviations: Col1a1: Collagen isoform 1a1; Col3a1: Collagen isoform 3a1; Col8a1: Collagen isoform 8a1; Comp: Cartilage oligomeric matrix protein; CTGF: connective tissue growth factor; Fmod: Fibromodulin; Lox: Lysyl oxidase; Myl4: Myosin light chain isoform 4; Myl7: Myosin light chain isoform 7; Myl9: Myosin light chain isoform 9; Postn: Periostin; Serpina3n: Serine (or cysteine) peptidase inhibitor 3N; Timp1: Tissue inhibitor of metalloproteinase-1; Tnc: Tenascin. *, $p < 0.05$, **, $p < 0.01$, ***, $p < 0.001$; ns, not signficant.

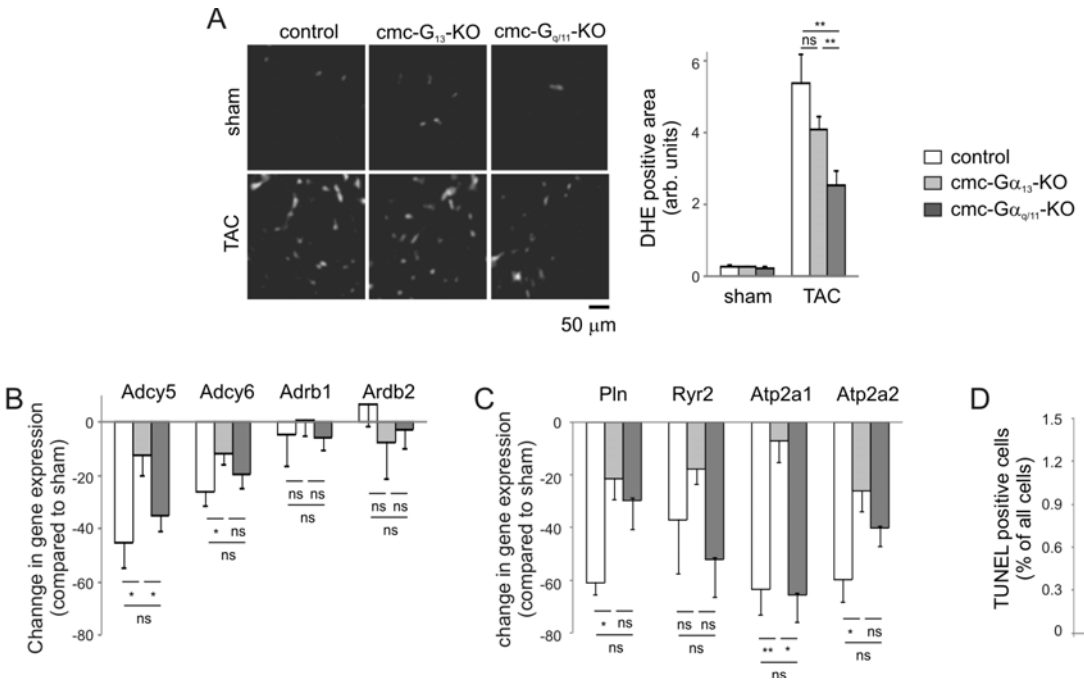

Suppl. Fig. 5: Differences between control mice, cmc-Gα_{13}-KOs and cmc-G$\alpha_{q/11}$-KOs after TAC. A, ROS production was determined 14 days after TAC by dihydroethidium staining of left ventricular sections (n = 4-6). **B, C,** Changes in expression of genes involved in β-adrenergic signaling (B) and calcium handling (C) as determined by quantitative RT-PCR analysis in left ventricles 14 days after TAC (n = 4-6). **D,** Apoptosis was determined by TUNEL staining in left ventricles 1 year after TAC (n = 3). Adcy5, Adcy6, Adenylate cyclase isoforms 5 and 6; Adrb1, Adrb2, β-adrenergic receptors 1 and 2; Pln, Phospholamban; Ryr2, Ryanodine receptor 2; Atp2a1, Atp2a2; Sarcoplasmic/endoplasmic reticulum calcium ATPases 1 and 2. *, $p<0.05$, **, $p<0.01$; ns, not significant.

Supplemental Tables

Suppl. Table 1	before tamoxifen		3 months after tamoxifen	
	Cre negative WT	Cre positive WT	Cre negative WT	Cre positive WT
BW (g)	27,03 ± 0,3966	27,75 ± 0,2500	29,40 ± 1,107	29,55 ± 0,4699
HR (beats / min)	468,8 ± 9,096	459,5 ± 9,717	471,5 ± 12,58	467,5 ± 14,36
LVEDV (µl)	58,99 ± 2,009	61,24 ± 2,655	64,46 ± 3,295	66,33 ± 2,505
LVESV (µl)	23,49 ± 0,9384	24,05 ± 1,211	26,42 ± 0,9388	27,34 ± 0,6095
LVEF (%)	60,20 ± 0,3229	60,64 ± 1,141	58,88 ± 1,068	58,70 ± 0,7396
CI (ml/min/g)	0,6151 ± 0,01411	0,6130 ± 0,01815	0,6072 ± 0,01819	0,6141 ± 0,01054
LVEDWT (µm)	850,3 ± 1,073	849,7 ± 2,913	856,9 ± 20,64	859,7 ± 17,37

Suppl. Table 1: Body weight and heart parameters as determined by MRI in αMHC-CreERT2-negative and –positive littermates before and 3 months after tamoxifen treatment (n = 4 per group). BW, body weight; HR, heart rate; LVEDV, left ventricular end-diastolic volume; LVESV: left ventricular end-systolic volume; LVEF: left ventricular ejection fraction; CI: cardiac index; LVEDWT: left ventricular end-diastolic wall thickness.

Supplemental Table 2: Transcriptional changes 14 days after TAC in left ventricles from wildtypes (WT), cmc-$G\alpha_{q/11}$-KOs ($G\alpha_{q/11}$-KO) and cmc-$G\alpha_{13}$-KOs ($G\alpha_{13}$-KO) as determined by whole gene transcriptional profiling. Displayed are genes which showed more than 2-fold up- or downregulation in wildtype hearts after TAC compared to sham.

Supplemental Table 2		Fold change WT-TAC vs. sham	Fold change $G\alpha_{q/11}$-KO-TAC vs. sham	Fold change $G\alpha_{13}$-KO-TAC vs. sham
Postn	periostin, osteoblast specific factor	8,75	1,65	1,58
Lox	lysyl oxidase	8,47	1,80	1,08
Thbs4	thrombospondin 4	7,56	1,15	1,12
Cilp	cartilage intermediate layer protein, nucleotide pyrophosphohydrol.	7,41	1,12	1,07
Timp1	tissue inhibitor of metalloproteinase 1	6,89	4,65	1,31
Cthrc1	collagen triple helix repeat containing 1	6,87	1,18	1,01
Myh7	myosin, heavy polypeptide 7, cardiac muscle, beta	6,78	2,88	5,49
Ccna2	cyclin A2	6,54	2,43	2,17
Col8a1	collagen, type VIII, alpha 1	6,35	1,99	1,59
Sfrp2	secreted frizzled-related protein 2	6,16	0,94	1,58
Gm129	predicted gene 129	5,80	3,50	2,17
Mki67	antigen identified by monoclonal antibody Ki 67	5,66	2,21	2,08
Tnc	tenascin C	5,43	4,03	1,34
Cks2	CDC28 protein kinase regulatory subunit 2	5,30	2,03	1,93
Serpine1	serine (or cysteine) peptidase inhibitor, clade E, member 1	5,17	2,47	1,42
Top2a	topoisomerase (DNA) II alpha	4,99	1,82	1,86
Mfap5	microfibrillar associated protein 5	4,88	1,65	1,45
Hist1h2ab	histone cluster 1, H2ab	4,86	1,29	1,47
D17H6S56E-5	DNA segment, Chr 17, human D6S56E 5	4,80	1,99	1,87
Hist2h3b	histone cluster 2, H3b	4,78	1,83	1,98
Fn1	fibronectin 1	4,73	1,52	1,33
Serpina3n	serine (or cysteine) peptidase inhibitor, clade A, member 3N	4,68	2,47	0,78
Cdk1	cyclin-dependent kinase 1	4,64	1,67	1,87
Hist1h3b	histone cluster 1, H3b	4,62	1,76	1,97
Hist1h3c	histone cluster 1, H3c	4,60	1,75	1,97
Cks2	CDC28 protein kinase regulatory subunit 2	4,55	1,81	1,76
Hist1h3d	histone cluster 1, H3d	4,53	1,74	1,92
Gm129	predicted gene 129	4,49	2,55	2,02
Prc1	protein regulator of cytokinesis 1	4,48	1,62	1,56
Col12a1	collagen, type XII, alpha 1	4,45	1,16	1,29
Hist1h3i	histone cluster 1, H3i	4,38	1,67	1,86
Hist2h3c1	histone cluster 2, H3c1	4,36	1,80	1,89
Ltbp2	latent transforming growth factor beta binding protein 2	4,35	1,13	1,05
Hist1h3a	histone cluster 1, H3a	4,31	1,67	1,87
Hist1h3g	histone cluster 1, H3g	4,29	1,64	1,82
Hist1h3h	histone cluster 1, H3h	4,28	1,66	1,83
Cks2	CDC28 protein kinase regulatory subunit 2	4,24	1,80	1,62
Anln	anillin, actin binding protein	4,20	1,54	1,50
Pamr1	peptidase domain containing ass. with muscle regen. 1	4,18	1,08	0,88
Ccnb2	cyclin B2	4,18	1,91	1,78
Fibin	fin bud initiation factor homolog (zebrafish)	4,17	1,21	1,38
C1qtnf3	C1q and tumor necrosis factor related protein 3	4,17	1,11	1,05
Hist1h3e	histone cluster 1, H3e	4,15	1,64	1,83
Hist1h2ak	histone cluster 1, H2ak	4,03	1,63	1,91
Mfap4	microfibrillar-associated protein 4	4,01	0,99	1,41
Fstl1	follistatin-like 1	3,80	1,58	1,56
Sprr1a	small proline-rich protein 1A	3,72	1,62	0,96
Ctgf	connective tissue growth factor	3,63	1,91	1,30
Mest	mesoderm specific transcript	3,62	2,47	2,52

Supplemental Table 2 cont'd (page 2)		Fold change WT-TAC vs. sham	Fold change $G\alpha_{q/11}$-KO-TAC vs. sham	Fold change $G\alpha_{13}$-KO-TAC vs. sham
Frzb	frizzled-related protein	3,52	1,40	1,48
Sfrp1	secreted frizzled-related protein 1	3,51	1,50	1,15
Aspn	asporin	3,41	1,04	1,20
2810417H13Rik	RIKEN cDNA 2810417H13 gene	3,38	1,49	1,45
Kif11	kinesin family member 11	3,37	1,70	1,58
Fmod	fibromodulin	3,30	0,56	1,44
Col1a1	collagen, type I, alpha 1	3,26	1,21	1,32
Col3a1	collagen, type III, alpha 1	3,23	1,34	1,48
Star	steroidogenic acute regulatory protein	3,22	1,58	1,04
Bub1	budding uninhibited by benzimidazoles 1 homolog (S. cerevisiae)	3,22	1,51	1,28
Acta1	actin, alpha 1, skeletal muscle	3,20	2,90	2,60
Thbs1	thrombospondin 1	3,20	1,59	1,15
Nusap1	nucleolar and spindle associated protein 1	3,18	1,48	1,26
Hist1h2an	histone cluster 1, H2an	3,15	1,65	1,80
Col1a2	collagen, type I, alpha 2	3,14	1,20	1,34
Hist1h2ao	histone cluster 1, H2ao	3,10	1,64	1,79
Hist1h2af	histone cluster 1, H2af	3,10	1,63	1,79
Hist1h2ah	histone cluster 1, H2ah	3,09	1,64	1,79
Hist1h2ad	histone cluster 1, H2ad	3,08	1,62	1,79
Hist1h2ai	histone cluster 1, H2ai	3,06	1,62	1,79
Hist1h2ao	histone cluster 1, H2ao	3,04	1,61	1,78
Ms4a7	membrane-spanning 4-domains, subfamily A, member 7	3,02	0,86	1,06
Hist1h2ag	histone cluster 1, H2ag	3,01	1,61	1,76
Gxylt2	glucoside xylosyltransferase 2	3,01	0,89	1,09
Col14a1	collagen, type XIV, alpha 1	3,00	1,10	1,38
Emp1	epithelial membrane protein 1	2,97	1,64	1,54
Fndc1	fibronectin type III domain containing 1	2,96	1,13	1,28
Serpinb1a	serine (or cysteine) peptidase inhibitor, clade B, member 1a	2,95	1,46	1,32
Kif23	kinesin family member 23	2,94	1,59	1,51
Itgbl1	integrin, beta-like 1	2,94	1,01	1,10
Nox4	NADPH oxidase 4	2,94	0,84	0,96
Ddah1	dimethylarginine dimethylaminohydrolase 1	2,94	1,53	1,03
Prnd	prion protein dublet	2,92	1,59	2,51
Hist1h2ai	histone cluster 1, H2ai	2,92	1,58	1,74
Svep1	sushi, von Willebrand factor type A, EGF and pentraxin domain containing 1	2,89	1,17	0,95
G530011O06Rik	RIKEN cDNA G530011O06 gene	2,88	2,40	1,51
Casc5	cancer susceptibility candidate 5	2,85	1,55	1,47
Ccnb1	cyclin B1	2,84	1,43	1,55
Tgfb2	transforming growth factor, beta 2	2,83	1,52	1,54
Adamts2	a disintegrin-like and metallopeptidase (reprolysin type) with thrombospondin type 1 motif, 2	2,83	1,35	1,28
Dbp	D site albumin promoter binding protein	2,79	2,76	2,42
Srpx2	sushi-repeat-containing protein, X-linked 2	2,77	1,17	1,13
Enpp1	ectonucleotide pyrophosphatase	2,76	1,47	1,17
Ect2	ect2 oncogene	2,76	1,58	1,36
Kif18b	kinesin family member 18B	2,72	1,29	1,31
Arhgap11a	Rho GTPase activating protein 11A	2,71	1,43	1,19
Ckap2	cytoskeleton associated protein 2	2,68	1,23	1,32
Comp	cartilage oligomeric matrix protein	2,66	0,55	1,24
Fbn1	fibrillin 1	2,66	1,53	1,30
Hist1h2bb	histone cluster 1, H2bb	2,64	2,10	1,42
Cd109	CD109 antigen	2,63	1,61	1,91

Supplemental Table 2 cont'd (page 3)		Fold change WT-TAC vs. sham	Fold change $G\alpha_{q/11}$-KO-TAC vs. sham	Fold change $G\alpha_{13}$-KO-TAC vs. sham
Plk1	polo-like kinase 1 (Drosophila)	2,63	1,62	1,44
Nppa	natriuretic peptide type A	2,62	1,81	2,15
Mastl	microtubule associated serine	2,62	1,15	1,18
Tpx2	TPX2, microtubule-associated protein homolog (Xenopus laevis)	2,62	1,48	1,31
Loxl2	lysyl oxidase-like 2	2,62	1,22	1,21
Hist2h2ac	histone cluster 2, H2ac	2,62	1,64	1,72
Prr11	proline rich 11	2,61	1,46	1,38
Racgap1	Rac GTPase-activating protein 1	2,61	1,33	1,34
Lxn	latexin	2,58	1,90	1,62
Col5a2	collagen, type V, alpha 2	2,57	1,13	1,24
Per3	period homolog 3 (Drosophila)	2,56	2,03	2,23
Hist2h2aa1	histone cluster 2, H2aa1	2,56	1,72	1,76
Wisp2	WNT1 inducible signaling pathway protein 2	2,55	1,03	1,14
Tcf19	transcription factor 19	2,54	1,42	1,35
Per2	period homolog 2 (Drosophila)	2,51	1,77	1,56
Cd72	CD72 antigen	2,50	1,19	0,82
Hist2h2aa1	histone cluster 2, H2aa1	2,49	1,70	1,78
Ccnb1	cyclin B1	2,48	1,24	1,34
Cenpn	centromere protein N	2,48	1,60	1,46
Foxm1	forkhead box M1	2,45	1,47	1,41
Pqlc3	PQ loop repeat containing	2,45	1,14	1,04
Cxcl10	chemokine (C-X-C motif) ligand 10	2,44	1,33	1,08
Aurkb	aurora kinase B	2,43	1,25	1,27
Mmp2	matrix metallopeptidase 2	2,43	0,86	1,14
Neil3	nei like 3 (E. coli)	2,43	1,24	1,32
Hist1h1b	histone cluster 1, H1b	2,42	1,44	1,54
Gria3	glutamate receptor, ionotropic, AMPA3 (alpha 3)	2,42	0,95	1,15
Anxa1	annexin A1	2,41	1,24	1,35
Loxl3	lysyl oxidase-like 3	2,41	1,09	1,16
Stil	Scl	2,41	1,45	1,24
Ctsk	cathepsin K	2,39	1,26	1,40
Hist2h2ab	histone cluster 2, H2ab	2,36	1,57	1,63
Xirp2	xin actin-binding repeat containing 2	2,35	1,30	1,21
Adamtsl2	ADAMTS-like 2	2,35	1,04	1,20
Vcan	versican	2,33	1,85	1,28
Ncaph	non-SMC condensin I complex, subunit H	2,33	1,21	1,38
Smc2	structural maintenance of chromosomes 2	2,32	1,44	1,10
Tspan4	tetraspanin 4	2,31	1,65	1,41
Kif4	kinesin family member 4	2,30	1,26	1,34
Mtap1b	microtubule-associated protein 1B	2,30	1,66	1,48
C330027C09Rik	RIKEN cDNA C330027C09 gene	2,30	1,31	0,99
Loxl1	lysyl oxidase-like 1	2,30	1,24	1,18
Mybpc2	myosin binding protein C, fast-type	2,28	2,41	1,64
Serpinf1	serine (or cysteine) peptidase inhibitor, clade F, member 1	2,28	1,08	1,11
Ccl8	chemokine (C-C motif) ligand 8	2,27	1,02	0,92
Meox1	mesenchyme homeobox 1	2,27	1,77	0,99
Hist2h2aa1	histone cluster 2, H2aa1	2,27	1,70	1,75
Fhl1	four and a half LIM domains 1	2,26	2,20	1,25
Nlrc3	NLR family, CARD domain containing 3	2,26	1,48	1,40
Uck2	uridine-cytidine kinase 2	2,26	1,70	0,94

Supplemental Table 2 cont'd (page 4)		Fold change WT-TAC vs. sham	Fold change $G\alpha_{q/11}$-KO-TAC vs. sham	Fold change $G\alpha_{13}$-KO-TAC vs. sham
Ncapg2	non-SMC condensin II complex, subunit G2	2,25	1,34	1,05
Cercam	cerebral endothelial cell adhesion molecule	2,25	1,15	1,13
Mpeg1	macrophage expressed gene 1	2,25	1,01	0,92
Aldh1a2	aldehyde dehydrogenase family 1, subfamily A2	2,23	2,00	1,02
Ckap2l	cytoskeleton associated protein 2-like	2,23	1,33	1,21
Hist1h2bk	histone cluster 1, H2bk	2,21	1,65	1,33
Ifit3	interferon-induced protein with tetratricopeptide repeats 3	2,20	1,35	1,58
Bub1b	budding uninhibited by benzimidazoles 1 homolog, beta (S. cerevisiae)	2,20	1,27	1,25
Capg	capping protein (actin filament), gelsolin-like	2,20	1,63	1,13
Itih5	inter-alpha (globulin) inhibitor H5	2,19	1,31	1,57
Fam198b	family with sequence similarity 198, member B	2,19	1,50	1,57
Pdgfrl	platelet-derived growth factor receptor-like	2,19	0,80	1,14
Tgfb3	transforming growth factor, beta 3	2,18	1,04	1,23
Ccnb1	cyclin B1	2,18	1,20	1,32
Abi3bp	ABI gene family, member 3 (NESH) binding protein	2,17	1,00	1,43
Ube2c	ubiquitin-conjugating enzyme E2C	2,16	1,59	1,32
Hist1h2bl	histone cluster 1, H2bl	2,15	1,64	1,31
Hist2h2aa1	histone cluster 2, H2aa1	2,15	1,67	1,72
D2Ertd750e	DNA segment, Chr 2, ERATO Doi 750, expressed	2,15	1,45	1,39
Uchl1	ubiquitin carboxy-terminal hydrolase L1	2,15	1,02	0,87
Bhlhe40	basic helix-loop-helix family, member e40	2,14	2,40	1,74
Hist1h2bj	histone cluster 1, H2bj	2,14	1,58	1,31
Hist1h2bn	histone cluster 1, H2bn	2,13	1,60	1,30
Bgn	biglycan	2,13	1,23	1,23
Kif22	kinesin family member 22	2,13	1,49	1,43
Cnksr1	connector enhancer of kinase suppressor of Ras 1	2,13	1,73	0,92
Csrp2	cysteine and glycine-rich protein 2	2,12	1,19	1,51
Fcrls	Fc receptor-like S, scavenger receptor	2,12	0,90	0,94
Dpysl3	dihydropyrimidinase-like 3	2,11	1,64	1,42
Stmn1	stathmin 1	2,11	1,35	1,43
Ace	angiotensin I converting enzyme (peptidyl-dipeptidase A) 1	2,11	1,18	1,09
Esco2	establishment of cohesion 1 homolog 2 (S. cerevisiae)	2,10	1,11	1,32
Mrc2	mannose receptor, C type 2	2,09	1,14	1,10
Runx1	runt related transcription factor 1	2,09	1,01	0,86
Clec4n	C-type lectin domain family 4, member n	2,09	1,19	1,03
Fam38b	family with sequence similarity 38, member B	2,08	1,27	1,32
Serpine2	serine (or cysteine) peptidase inhibitor, clade E, member 2	2,08	1,52	1,05
Lum	lumican	2,08	0,98	1,35
Hist1h2bf	histone cluster 1, H2bf	2,07	1,52	1,32
Phlda3	pleckstrin homology-like domain, family A, member 3	2,07	1,08	1,31
Ly86	lymphocyte antigen 86	2,07	0,92	0,97
Sparc	secreted acidic cysteine rich glycoprotein	2,06	1,38	1,45
Ms4a14	membrane-spanning 4-domains, subfamily A, member 14	2,05	0,75	0,91
Dtl	denticleless homolog (Drosophila)	2,05	1,34	1,22
Stmn1	stathmin 1	2,05	1,31	1,37
Sulf1	sulfatase 1	2,05	1,38	1,23
Ccl3	chemokine (C-C motif) ligand 3	2,04	2,13	1,43
Dbf4	DBF4 homolog (S. cerevisiae)	2,04	1,17	1,22
Depdc1a	DEP domain containing 1a	2,04	1,23	1,37
Fat1	FAT tumor suppressor homolog 1 (Drosophila)	2,03	1,30	1,17

Supplemental Table 2 cont'd (page 5)		Fold change WT-TAC vs. sham	Fold change $G\alpha_{q/11}$-KO-TAC vs. sham	Fold change $G\alpha_{13}$-KO-TAC vs. sham
Anxa2	annexin A2	2,03	1,69	1,44
Kif26b	kinesin family member 26B	2,03	1,02	1,27
Wee1	WEE 1 homolog 1 (S. pombe)	2,03	1,37	1,34
Kdelr3	KDEL (Lys-Asp-Glu-Leu) endoplasmic reticulum protein retention receptor 3	2,03	1,32	1,20
Ppic	peptidylprolyl isomerase C	2,03	1,08	1,35
Ncapg	non-SMC condensin I complex, subunit G	2,03	1,17	1,19
Tyms	thymidylate synthase	2,02	1,36	1,19
C79407	expressed sequence C79407	2,02	1,10	1,16
Mad2l1	MAD2 mitotic arrest deficient-like 1 (yeast)	2,02	1,16	1,15
Kif20a	kinesin family member 20A	2,01	1,57	1,43
Hhipl1	hedgehog interacting protein-like 1	2,01	1,33	1,07
Aebp1	AE binding protein 1	2,01	1,18	1,02
Fam38b	family with sequence similarity 38, member B	2,00	1,15	1,02
Igf1	insulin-like growth factor 1	2,00	1,17	1,06
Atad2	ATPase family, AAA domain containing 2	2,00	1,19	1,03
Rgs2	regulator of G-protein signaling 2	0,50	0,91	0,85
Kcnv2	potassium channel, subfamily V, member 2	0,50	0,80	0,52
A530016L24Rik	RIKEN cDNA A530016L24 gene	0,50	0,74	0,90
Scd4	stearoyl-coenzyme A desaturase 4	0,48	0,64	1,05
Pla2g5	phospholipase A2, group V	0,46	0,88	0,93
Hmgcs2	3-hydroxy-3-methylglutaryl-Coenzyme A synthase 2	0,46	0,52	0,58
Ucp3	uncoupling protein 3 (mitochondrial, proton carrier)	0,46	0,66	0,55
Tmem171	transmembrane protein 171	0,45	0,48	0,49
Phkg1	phosphorylase kinase gamma 1	0,43	0,96	0,78
Mrgprh	MAS-related GPR, member H	0,43	0,83	0,98
Car3	carbonic anhydrase 3	0,40	0,30	2,19
Ces1d	carboxylesterase 1D	0,40	0,70	0,89
Ces1d	carboxylesterase 1D	0,40	0,70	0,89
Penk	preproenkephalin	0,39	0,94	0,87
Retnla	resistin like alpha	0,39	1,36	0,72
Npas2	neuronal PAS domain protein 2	0,37	0,57	0,51
Aldob	aldolase B, fructose-bisphosphate	0,31	0,36	0,34
Myl4	myosin, light polypeptide 4	0,29	0,07	1,84
Arntl	aryl hydrocarbon receptor nuclear translocator-like	0,29	0,52	0,43
Myl7	myosin, light polypeptide 7, regulatory	0,21	0,05	1,92

Supplemental Table 2: Transcriptional changes 14 days after TAC in left ventricles from wildtypes (WT), cmc-$G\alpha_{q/11}$-KOs ($G\alpha_{q/11}$-KO) and cmc-$G\alpha_{13}$-KOs ($G\alpha_{13}$-KO) as determined by whole gene transcriptional profiling. Displayed are genes which showed more than 2-fold up- or downregulation in wildtype hearts after TAC compared to sham.

Supplemental references

1. Casanova E, Fehsenfeld S, Mantamadiotis T, Lemberger T, Greiner E, Stewart AF, Schutz G. A CamKIIalpha iCre BAC allows brain-specific gene inactivation. *Genesis.* 2001;31:37-42.

2. Muyrers JP, Zhang Y, Testa G, Stewart AF. Rapid modification of bacterial artificial chromosomes by ET-recombination. *Nucleic Acids Res.* 1999;27:1555-1557.

3. Zhou YY, Wang SQ, Zhu WZ, Chruscinski A, Kobilka BK, Ziman B, Wang S, Lakatta EG, Cheng H, Xiao RP. Culture and adenoviral infection of adult mouse cardiac myocytes: methods for cellular genetic physiology. *Am J Physiol Heart Circ Physiol.* 2000;279:H429-436.

4. Satoh M, Matter CM, Ogita H, Takeshita K, Wang CY, Dorn GW, 2nd, Liao JK. Inhibition of apoptosis-regulated signaling kinase-1 and prevention of congestive heart failure by estrogen. *Circulation.* 2007;115:3197-3204.

5. Larson AC, White RD, Laub G, McVeigh ER, Li D, Simonetti OP. Self-gated cardiac cine MRI. Magn Reson Med. 2004;51:93-102.

6. Feil R, Brocard J, Mascrez B, LeMeur M, Metzger D, Chambon P. Ligand-activated site-specific recombination in mice. Proc Natl Acad Sci U S A. 1996;93:10887-10890.

7. Soriano P. Generalized lacZ expression with the ROSA26 Cre reporter strain. *Nat Genet.* 1999;21:70-71.

Correction

In the article by Takefuji et al, "A G_{13}-Mediated Signaling Pathway is Required for Pressure Overload-Induced Cardiac Remodeling and Heart Failure," which was published ahead of print on September 12, 2012, an error occurred.

The article was initially published with an incomplete set of figures; specifically, Figure 8 was missing.

The error has been corrected in the current online version of the article. The Editorial Office regrets the error.

2.5 Anhaltend erhöhte residuale Thrombozytenaktivität nach koronarer Stentimplantation bei Patienten mit Myokardinfarkt verglichen mit elektiven Patienten.

Sustained enhancement of residual platelet reactivity after coronary stenting in patients with myocardial infarction compared to elective patients. **Althoff TF**, Fischer M, Langer E, Ziemer S, Baumann G. *Thromb Res* (2010), 125(5), e190-6.

https://doi.org/10.1016/j.thromres.2010.01.003

„Einleitung: Eine erhöhte Thrombozyten-Reaktivität trotz dualer anti-thrombozytären Therapie ist mit einem erhöhten kardiovaskulären Risiko assoziiert. Aktuelle Leitlinien empfehlen für Patienten mit Myokardinfarkt und elektive Patienten einheitliche antithrombozytäre Regimen der Erhaltungstherapie nach perkutaner Koronarintervention. Vor diesem Hintergrund wollten wir demonstrieren, dass die residuale Thrombozyten-Reaktivität nach Myokardinfarkt anhaltend erhöht ist, was eine intensivierte antithrombozytäre Therapie erforderlich machen würde.

Material und Methoden: In dieser prospektiven, kontrollierten Studie wurden insgesamt 66 Patienten nach koronarer Stentimplantation im Rahmen eines Myokardinfarktes (n=36) oder nach elektiver koronarer Stentimplantation (n=30) eingeschlossen. Die Thrombozyten-Reaktivität auf Adenosin-5-Diphosphat und Arachidon-Säure unter Behandlung mit Clopidogrel (75 mg/d) und Acetylsalicylsäure (100 mg/d) wurde 48 Stunden und 30 Tage nach Stentimplantation simultan mittels Licht-Transmissions-Aggregometrie und Multi-Elektroden-Impedanz-Aggregometrie (Multiplate analyzer) bestimmt.

Ergebnisse: 48 Stunden nach koronarer Stentimplantation zeigten sich sämtliche Maße der residualen Thrombozyten-Reaktivität in der Gruppe der Infarktpatienten signifikant erhöht. Nach einem mittleren Nachverfolgungszeitraum von 37 Tagen, zeigte sich die residuale Thrombozytenreaktivität auf Adenosin-5-Disphosphat weiterhin durchweg erhöht, wenn auch statistisch nicht signifikant. Im Gegensatz dazu, nahm die residuale Thrombozytenaktivität in Reaktion auf Arachidonsäure in diesem Zeitraum signifikant ab und erreichte nach 37 Tagen wieder Normwerte. In Regressionsanalysen haben wir zudem den stattgehabten Myokardinfarkt, erhöhtes C-reaktives Protein und erhöhtes Fibrinogen als unabhängige Prädiktoren einer erhöhten Thrombozyten-Reaktivität 48 Stunden nach Stentimplantation identifiziert.

Patienten, die sich einer koronaren Stentimplantation im Rahmen eines akuten Myokardinfarkts unterziehen, zeigen also eine erhöhte residuale Thrombozyten-Reaktivität, die über mindestens 48 Stunden anhält. Diese Daten bieten eine Rationale

für eine kontinuierliche intensivierte antithrombozytäre Therapie nach Myokardinfarkt.“ Übersetzung durch den Autor.

3 Diskussion

3.1 Residuale Thrombozytenreaktivität nach Myokardinfarkt

G_q/G_{11}- und G_{12}/G_{13}-gekoppelte Rezeptoren und die entsprechenden intrazellulären Signalwege spielen als pharmakologische Zielstrukturen schon jetzt eine zentrale Rolle bei der Behandlung kardiovaskulärer Erkrankungen, auch wenn insbesondere die Funktion der G_{12}/G_{13}-vermittelten Signaltransduktion bis dato kaum untersucht war. Die initialen Studien zu den beiden G-Protein-Familien wurden in Thrombozyten durchgeführt; entsprechend ist die Rolle der G_q/G_{11}- bzw. G_{12}/G_{13}-vermittelten Signaltransduktion in keinem Bereich so gut definiert wie bei der Thrombozyten-Aktivierung und –Aggregation(Klages, Brandt, Simon, Schultz, & Offermanns, 1999; Moers et al., 2003; Offermanns, 2006; Offermanns, Hu, & Simon, 1996; Offermanns, Laugwitz, Spicher, & Schultz, 1994; Offermanns, Toombs, Hu, & Simon, 1997). So basieren sämtliche Standard-Ansätze der therapeutischen Thrombozyten-Aggregationshemmung (Acetylsalicylsäure und P2Y12-Inhibitoren) letztlich auf der Inhibition G-Protein-vermittelter Signalwege. Allerdings kamen in den letzten Jahren erhebliche Zweifel an der zuverlässigen Wirksamkeit dieser Medikamente auf. So hat unsere hier vorgestellte Patientenstudie gezeigt, dass die duale Thrombozyteninhibition durch den P2Y12-Inhibitor Clopidogrel und Acetylsalicylsäure im Kontext eines akuten Myokardinfarkts unzureichend ist, und die residuale Thrombozytenreaktivität nach Myokardinfarkt trotz dieser dualen antithrombozytären Therapie über mehrere Wochen erhöht bleibt(Althoff, Fischer, Langer, Ziemer, & Baumann, 2010). In der Zwischenzeit wurden mit Prasugrel und Ticagrelor zwei potentere P2Y12-Inhibitoren eingeführt. Dabei haben die großen randomisierten Zulassungsstudien dieser Substanzen unsere Beoboachtungen indirekt bestätigt, indem eine Überlegenheit der intensivierten antithrombozytären Therapie nach Myokardinfarkt mit Prasugrel oder Ticagrelor gegenüber dem weniger potenten Clopidogrel nachgewiesen wurde(Wallentin et al., 2009; Wiviott et al., 2007). So war die residuale Thrombozytenreaktivität mit diesen potenteren Substanzen gegenüber Clopidogrel deutlich verringert, was – wie von uns vermutet – in einem klinischen Nutzen im Verlauf nach Myokardinfarkt resultierte.

3.2 Myokardiale Hypertrophie und Herzinsuffizienz

Wie oben erläutert, war insbesondere die Funktion der G_{12}/G_{13}-vermittelten Signaltransduktion in Zelltypen und Geweben jenseits von Thrombozyten bis dato kaum untersucht. So war zwar bereits über eine wesentliche Rolle G_q/G_{11}-abhängiger Signalwege bei der kardiomyozytären Hypertrophie infolge einer kardialen Druckbelastung (erhöhte Nachlast) berichtet worden(Takefuji et al., 2012). Wir konnten nun aber erstmals zeigen, dass auch die G_{12}/G_{13}-vermittelte Signaltransduktion bei maladaptiven Prozessen dieser Art eine entscheidende

Rolle spielt. So waren G_{12}/G_{13} nicht nur an Nachlast-induzierten kardialen Umbauprozessen beteiligt, sondern auch entscheidend für die Transition von Myokardhypertrophie hin zur manifesten Herzinsuffizienz. Diese Erkenntnisse vermögen den klinischen Erfolg einer Inhibierung der G_{12}/G_{13}- und G_q/G_{11}-vermittelten Signaltransduktion des Angiotensin II-Rezeptors Typ 1 mit Hilfe von ACE-Hemmern oder entsprechender Rezeptor-Antagonisten (AT1-Antagonisten) gut zu erklären(Ponikowski et al., 2016). Zudem imponieren vor dem Hintergrund unserer Arbeit auch nachgeschaltete Effektoren von G_{12}/G_{13}, wie beispielsweise die kleine GTPase RhoA als erfolgversprechende pharmakologische Zielmoleküle im Kontext der Herzinsuffizienz.

3.3 Kardiale Elektrophysiologie und Herzrhythmusstörungen

Während der Einfluss G_{12}/G_{13}- und G_q/G_{11}--vermittelter Signalwege auf myokardiale Kontraktilität und kardiale Umbauprozesse durch die hier beschriebenen und weitere Studien gut untersucht ist, ist die Rolle dieser Signalwege im Kontext der kardialen Elektrophysiologie gänzlich unbekannt. Beispielsweise deutet die Tatsache, dass die G_{12}/G_{13}- und G_q/G_{11}-gekoppelten Rezeptoren AT1, ET sowie adrenerge und muscarinerge (M3) Rezeptoren die Entstehung von Vorhofflimmern wesentlich begünstigen, auf eine Beteiligung an der Pathogenese dieser Herzrhythmusstörung hin(Berridge, 2009; Boldt et al., 2003; Burrell, Molenaar, Dawson, & Kaumann, 2000; Ducharme et al., 2006; Disertori et al., 2009; Kitazawa et al., 2009; Madrid et al., 2002; Maggioni et al., 2005; Ono et al., 1994; Schneider et al., 2010; Tinker, Finlay, Nobles, & Opel, 2016; Tuomi, Chidiac, & Jones, 2010; Wachtell et al., 2005; Yorikane & Koike, 1990; Yorikane, Koike, & Miyake, 1991; Yorikane, Shiga, Miyake, & Koike, 1990). Darüber hinaus spielen G_q/G_{11}-abhängige Inositol-3-Phosphat Rezeptoren am sarkoplasmatischen Reticulum eine wesentliche Rolle bei der Generation verzögerter Nachdepolarisationen, die wiederum einer der Hauptauslöser für Vorhofflimmer-Episoden beim Menschen sind(Li, Zima, Sheikh, Blatter, & Chen, 2005; Yamada et al., 2002; Zhao et al., 2007; Zima & Blatter, 2004). So konnte gezeigt werden, dass die Aktivierung von Inositol-3-Phosphat Rezeptoren durch Endothelin-1 zur diastolischen Calcium-Freisetzung (Calcium-Leck) führt und späte Nachdepolarisationen sowie Arrhythmien induziert(Li et al., 2005; Zima & Blatter, 2004). Zudem ist eine kardiomyozytäre Defizienz der Regulatoren G-Protein-vermittelter Signaltransduktion, RGS2(Tuomi et al., 2010) oder RGS4(Guasch et al., 2013; Opel et al., 2015), die beide G_q/G_{11} inhibieren, mit einer gestörten Calcium-Homöostase assoziiert und prädisponiert entsprechende transgene Mäuse für Vorhofflimmern. Diese und andere Daten legen nahe, das insbesondere die G_q/G_{11}-vermittelte Signaltransduktion eine wesentliche Rolle bei der Entstehung von Vorhofflimmern spielt. Die Tatsache, dass neben humoralen Faktoren auch akute oder chronische mechanische Reize Vorhofflimmern auslösen bzw. begünstigen können, deutet ebenfalls auf eine Beteiligung von G_q/G_{11} hin(Franz

& Bode, 2003; Peyronnet, Nerbonne, & Kohl, 2016). So beschreibt ja unsere oben aufgeführte Studie die zentrale Funktion dieser G-Protein-Isoformen bei der Wahrnehmung und intrazellulären Weiterleitung mechanischer Signale (Mechanotransduktion)(Albarran-Juarez et al., 2018). Vor diesem Hintergrund haben wir transgene Mäuse mit einer induzierbaren, Kardiomyozyten-spezifischen G_q/G_{11}-Defizienz in einem Modell zur Induktion von Vorhofflimmern, begünstigt durch vagale Aktivierung, untersucht. Dabei wurde bei narkotisierten Mäusen ein Elektroden-Katheter über die rechte V. jugularis interna in rechtem Vorhof und rechter Kammer positioniert und eine elektrophysiologische Untersuchung durchgeführt. Hierbei war die Induzierbarkeit von Vorhofflimmern durch programmierte elektrische Stimulation in G_q/G_{11}-defizienten Tieren deutlich herabgesetzt, und zwar sowohl vor als auch nach vagaler Aktivierung mittels Carbachol (Abb. 1, Althoff et al. unveröffentliche Daten). Diese in vivo-Experimente zeigen, legen eine wesentliche Funktion G_q/G_{11}-vermittelter Signalwege bei der Entstehung von Vorhofflimmern nahe. Der genaue Mechanismus und die Frage ob auch hier die G_q/G_{11}-abhängige Mechanotransduktion eine Rolle spielt, werden in einem aktuellen Projekt unserer Arbeitsgruppe adressiert.

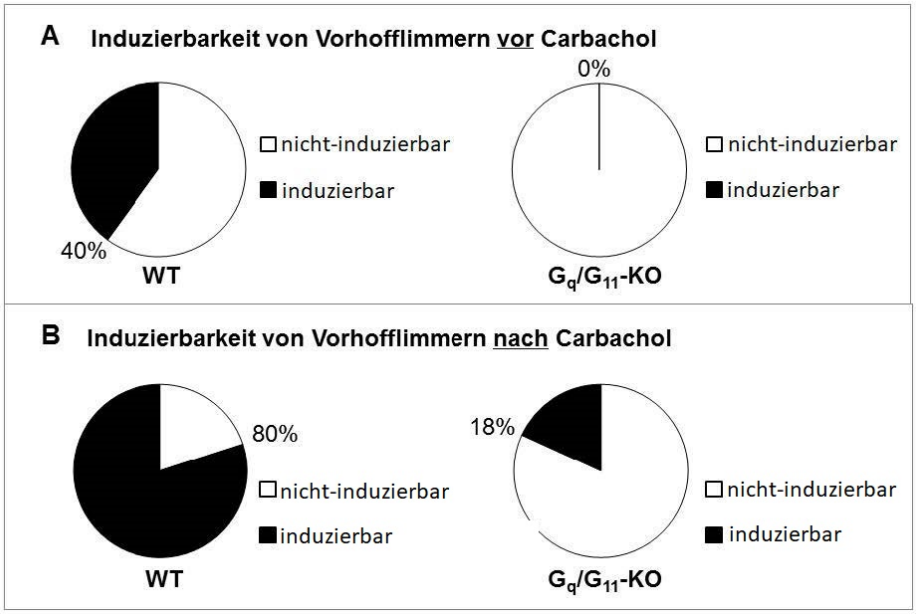

Abbildung 1. Induzierbarkeit von Vorhofflimmern *(Althoff, unveröffentlichte Daten)*

3.4 Regulation von Gefäßtonus und essentiellem Hypertonus

Die zentrale Rolle G_q/G_{11}- und G_{12}/G_{13}-abhängiger Signalwege bei der Gefäßtonus-Regulation und deren synergistische Wirkung bezüglich der Myosin-Leichtketten-Phosphorylierung in glatten Muskelzellen ist mittlerweile gut etabliert; allerdings war der Mechanismus pathologischer Veränderungen des Gefäßtonus wie beim essentiellen Hypertonus oder Altershypertonus bis dato weitgehend ungeklärt (Althoff & Offermanns, 2015b). Wir konnten

nun aufklären, dass es sich beim Alters-abhängigen Bluthochdruck tatsächlich um eine Dysregulation des Gefäßtonus handelt. Dabei zeigen unsere Studien, dass der erhöhte Gefäßtonus über das prokontraktile Peptid Endothelin-1 und den entsprechenden G_q/G_{11}- und G_{12}/G_{13}-gekoppelten Endothelin-1-Rezeptor A vermittelt wird. Interessanterweise waren beide G-Protein-abhängigen Signalwege, G_q/G_{11} und G_{12}/G_{13}, für die Entwicklung des Altershypertonus essentiell. Vor diesem Hintergrund erscheint die medikamentöse Antagonisierung des Endothelin-1-Rezeptors A als vielversprechender Ansatz zur Prävention bzw. Behandlung des Alters-abhängigen Hypertonus. Die Anwendung derzeit zugelassener Endothelin-Rezeptor-Antagonisten ist zwar aufgrund des Nebenwirkungsprofils limitiert. Allerdings befinden sich derzeit neue Wirkstoffe mit günstigerem Nebenwirkungsprofil in klinischer Erprobung. So wurde noch im Jahr unserer Veröffentlichung eine klinische Phase II-Studie mit einem von der Firma Actelion neu-entwickelten Endothelin-Rezeptor-Antagonisten zur Dosisfindung hinsichtlich der Behandlung des essentiellen Hypertonus initiiert.

3.5 Gefäßerkrankungen und Atherosklerose

Eine Fülle experimenteller und präklinischer Daten suggeriert, dass die im Kontext der Herzinsuffizienz oder der pulmonalen Hypertonie so erfolgreiche Inhibierung G_{12}/G_{13}- und G_q/G_{11}-abhängiger Signalwege durch AT1- bzw. Endothelin-Rezeptor-Antagonisten auch im Kontext systemischer Gefäßumbauprozesse oder der Atherosklerose von Nutzen sind(Schiffrin, 2002; Schmieder, 2005). Konventionelle AT1- bzw. Endothelin-Rezeptor Antagonisten inhibieren mit dem jeweiligen Rezeptor G_{12}/G_{13}- und G_q/G_{11}-abhängige Signalwege gleichermaßen, wobei die positiven Effekte ganz überwiegend der G_q/G_{11}-Inhibition zugeschrieben werden(Schiffrin, 2002; Schmieder, 2005). So wirkte sich auch in unseren hier vorgestellten Studien die genetische Inaktivierung von G_q/G_{11} in Endothelzellen oder in glatten Muskelzellen durchweg protektiv gegenüber Gefäßerkrankungen aus (Albarran-Juarez et al., 2018; Althoff et al., 2012). Eine Inhibierung der vaskulären G_{12}/G_{13}-vermittelten Signaltransduktion hingegen, hatte eine exzessive Beschleunigung pathologischer Gefäßumbauprozesse und eine dramatische Atherosklerose-Exazerbation zur Folge(Althoff et al., 2012). Während die G_{12}/G_{13}- und G_q/G_{11}-abhängigen Signalwege also im Kontext der myokardialen Hypertrophie und Herzinsuffizienz sowie der Blutdruckregulation synergistisch wirken(Althoff et al., 2012; Wirth et al., 2008; Wirth et al., 2016), scheinen sie die Entwicklung von Gefäßerkrankungen gegensätzlich zu beeinflussen (Abb. 2).

Im Rahmen dieser Studien konnten wir zudem die zentrale Rolle von G_q/G_{11} bei der Wahrnehmung Fluss-induzierter Scherkräfte und Umwandlung der mechanischen Signale in proinflammatorische intrazelluläre Signale (atherogene Mechanotransduktion) aufdecken. Darüber hinaus konnten wir zeigen, dass G_q/G_{11} und G_{12}/G_{13} die Differenzierung glatter Gefäßmuskelzellen antagonistisch regulieren, indem sie die Rekrutierung transkriptioneller Ko-Faktoren der Ternary-Complex-Factor-Familie bzw. der Myokardin-Familie durch Serum Response Faktor kontrollieren.

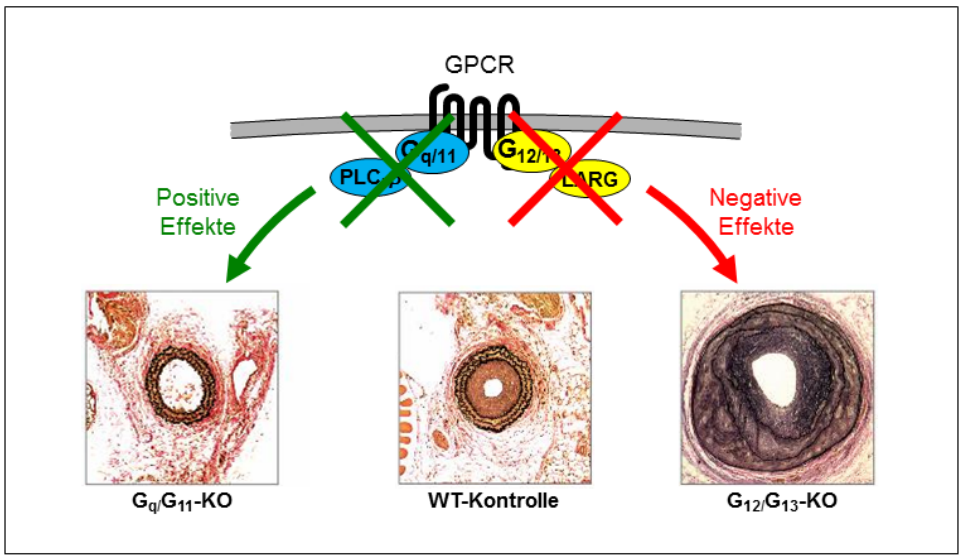

Abbildung 2. Antagonistische Regulation pathologischer Gefäßumbauprozesse
Gefäßquerschnitte 4 Wochen nach Carotis-Ligatur in transgenen Mäusen mit konditionaler glattmuskel-spezifischer G_q/G_{11}- bzw. G_{12}/G_{13}-Defizienz sowie Kontrolltieren mit entsprechenden Wildtyp-Allelen. (*Althoff, unveröffentlicht; auf Basis von Althoff et al. J Exp Med 2012*)

3.6 Funktionell-selektive GPCR-Liganden (biased GPCR ligands)

Vor dem Hintergrund unserer Beobachtungen ist es folglich wenig verwunderlich, dass sich der postulierte Nutzen konventioneller Angiotensin- oder Endothelin-Rezeptor Antagonisten, die G_{12}/G_{13}- und G_q/G_{11}-abhängige Signalwege gleichermaßen inhibieren, in klinischen Studien bezüglich Atherosklerose oder koronarer Restenose (Neointima-Hyperplasie) nicht bestätigte. Vielmehr erscheint eine selektive Inhibition des G_q/G_{11}-Signalwegs aus pharmakologischer Sicht erstrebenswert. Während man hierzu G_q/G_{11} oder seine intrazellulären Effektoren direkt inhibieren könnte, bietet eine entsprechende Modulation auf Rezeptorebene wesentliche Vorteile. So gewährleistet der Rezeptor als Angriffspunkt eine gewisse Gewebe- und Kontext-Spezifität, was die Effektivität der Behandlung erhöht und Nebenwirkungen minimiert. Diese pharmakologischen Vorteile von GPCRs-Liganden werden nicht zuletzt durch die Tatsache reflektiert, dass diese Wirkstoffgruppe nach wie vor über ein

Drittel aller zugelassen Medikamente sowie einen relevanten Anteil der Neuentwicklungen ausmacht(Garland, 2013). In diesem Zusammenhang haben Arbeiten von Brian Kobilka und Robert Lefkowitz, für die diese 2012 mit dem Nobel-Preis ausgezeichnet wurden, zum Konzept der funktionellen Selektivität von GPCR-Liganden geführt („ligand-biased signaling“). Dieses beschreibt die Selektivität von Liganden bzw. Rezeptor-Konformationen bezüglich unterschiedlicher intrazellulärer Signalwege und eröffnet eine neue Dimension für die Entwicklung Rezeptor-basierter Medikamente (Reiter et al., 2012; Wisler, Xiao, Thomsen, & Lefkowitz, 2014). Vor diesem Hintergrund versuchen wir derzeit, selektive AT1R-Antagonisten zu identifizieren bzw. zu entwickeln, die spezifisch den G_q/G_{11}-Signalweg inhibieren ohne die Signaltransduktion via G_{12}/G_{13} zu beeinträchtigen (G_q/G_{11}-selektive Antagonisten) bzw., die diese sogar induzieren G_{12}/G_{13}-biased ligands).

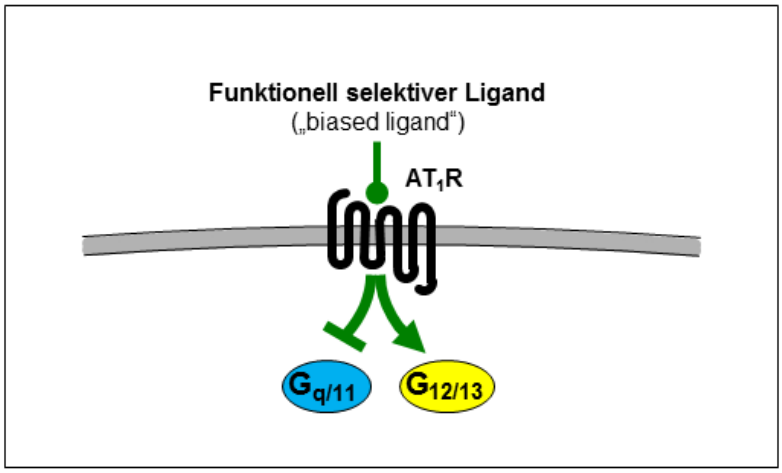

Abbildung 3. Prinzip einer G_q/G_{11}-selektiven AT1-Antagonisierung *(Althoff, unveröffentlicht)*

3.7 TRV023 als selektiver AT1R-Antagonist

So haben wir systematisch bekannte AT1R-Liganden untersucht und mit dem Angiotensin-Analogon Sar-Arg-Val-Tyr-Lys-His-Pro-Ala-OH (TRV023) einen Kandidaten mit vielversprechendem Signal-Profil im Sinne eines $G_{q/11}$-selektiven Antagonismus am AT1-Rezeptor identifiziert. Dieses Peptid wurde in der Vergangenheit bereits als β-Arrestin-selektiver Rezeptor-Agonist beschrieben, der sämtliche G-Protein-abhängigen Signalwege inhibiert. Allerdings wurde TRV023 bis dato nur auf die G_q/G_{11}-vermittelte Signaltransduktion hin untersucht, während der Einfluss auf andere G-Protein-Isoformen nie definiert wurde (Felker et al., 2015; Monasky et al., 2013; Violin et al., 2010).

In der Tat konnten wir mit Hilfe eines Galaktosidase/Biolumineszenz-Assays bestätigen, dass TRV023, im Gegensatz zu den konventionellen Antagonisten Losartan und Telmisartan, die β-Arrestin-vermittelte Signaltransduktion nicht beeinträchtigt. Umgekehrt zeigten Fluoreszenz-basierte Calcium-Assays, dass die antagonistische Aktivität von TRV023 bzgl. G_q/G_{11} sogar

potenter ausgeprägt ist als die der konventionellen Antagonisten. Der entscheidende Befund ist jedoch, dass TRV023 die G_{12}/G_{13}-vermittelte Signaltransduktion via RhoA (Luciferase-Reporter-Assay) nicht beeinträchtigte, während die konventionellen Antagonisten diesen Signalweg effektiv inhibierten (Abb.4A, Althoff et al., unveröffentlichte Daten). Die o.g. Signaling-Assays haben den Nachteil, dass sie die Aktivierung nachgeschalteter („Downstream"-)Effektoren des jeweiligen Signalwegs als Surrogat-Parameter, nicht aber die Aktivierung der G-Proteine selbst messen. Diesbezüglich haben unsere Kooperationspartner Céline Gales (INSERM Toulouse, Frankreich) und Stéphane Laporte (McGill University, Montreal, Kanada) Biolumineszenz-Resonz-Energie-Transfer (BRET)-basierte Biosensoren entwickelt, die Aktivierung des jeweiligen Signalwegs präzise und direkt auf Ebene der G-Proteine detektieren. Diese uns zur Verfügung gestellten Sensoren haben wir im engen Austausch mit unseren Kooperationspartnern und im Rahmen einer Hospitation in Toulouse etabliert. Die mit Hilfe dieser innovativen BRET-Assays generierten Daten bestätigen unsere Hypothese und die oben beschriebenen Daten in vollem Umfang (Abb.4B, Althoff et al., unveröffentlichte Daten). Auf Basis der Gesamtheit unserer erhobenen Daten gehen wir also davon aus, dass wir mit TRV023 tatsächlich einen Gq-selektiven ATR1-Antagonisten identifiziert haben.

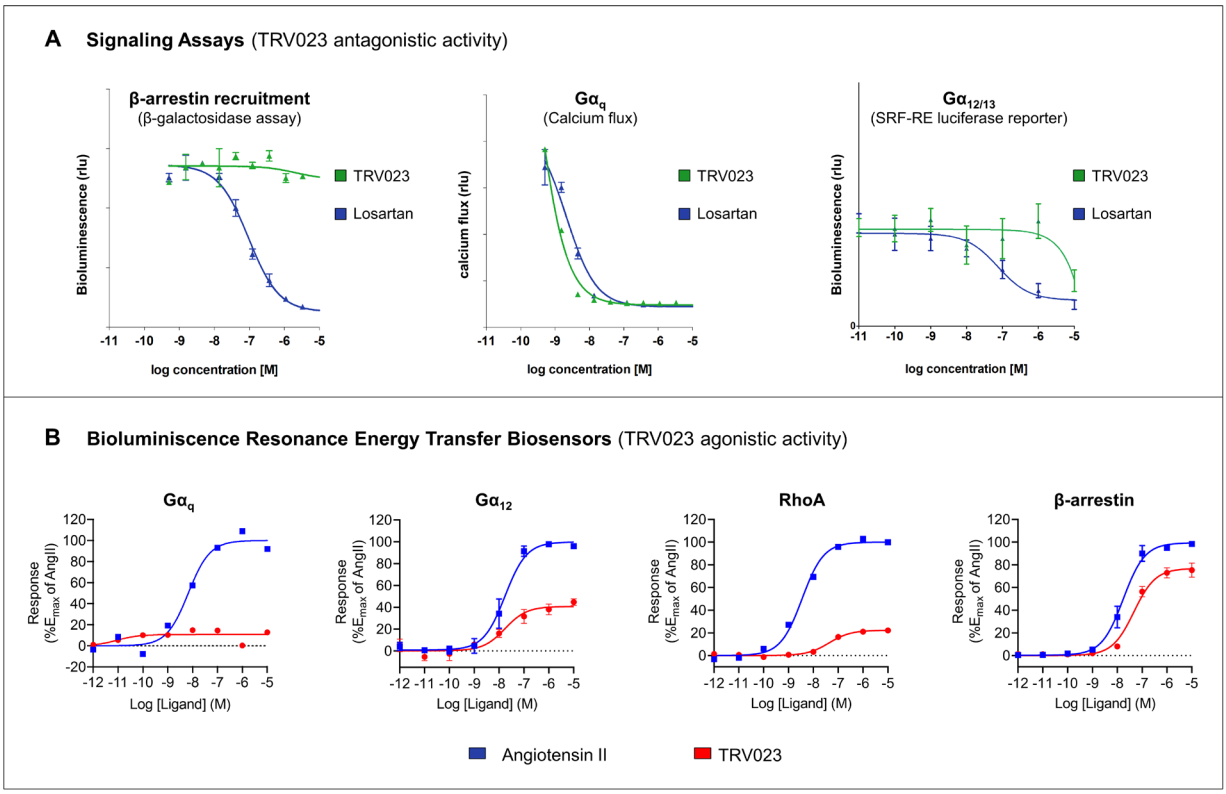

Abbildung 4. G-Protein-vermittelte Signaltransduktion. A Surrogat-Assays für $G\alpha_q$- (Kalzium-Flux), $G\alpha_{12/13}$- (SRF-RE Luciferase Gen-Reporter-Assay) und β-Arrestin-Aktivierung (β-Galactosidase Assay). **B** Biolumineszenz-Resonanz-Energie-Transfer-basierte direkte Messungen der Aktivierung von $G\alpha_q$, $G\alpha_{12}$, RhoA und β-Arrestin *(Althoff, unveröffentlichte Daten)*

3.8 TRV023 und Atherosklerose

Inwieweit diese funktionelle Selektivität von TRV023 tatsächlich von therapeutischem Vorteil sein könnte, haben wir mit Hilfe zweier unterschiedlicher muriner Atherosklerose-Modelle untersucht – einem Modell der beschleunigten Atherosklerose (partielle Carotis-Ligatur) sowie einem Langzeit Atherosklerose-Modell. So wurden die Wirkstoffe bzw. die Vehikel-Kontrolle ApoE-defizienten Mäusen unter hochkalorischer Diät über osmotische Minimpumpen kontinuierlich subkutan appliziert. Dabei reduzierte TRV023, nicht aber der konventionelle AT1-Antagonist Losartan, die Plaque-Entwicklung gegenüber der Vehikel-Kontrolle in beiden Modellen signifikant (Abb. 5, Althoff et al., unveröffentlichte Daten). So deuten unsere Ergebnisse darauf hin, dass die selektive Inhibition der AT1-abhängigen G_q/G_{11}-vermittelten Signaltransduktion mittels funktionell-selektiver Liganden ein vielversprechender Ansatz zur Behandlung der Atherosklerose sein könnte.

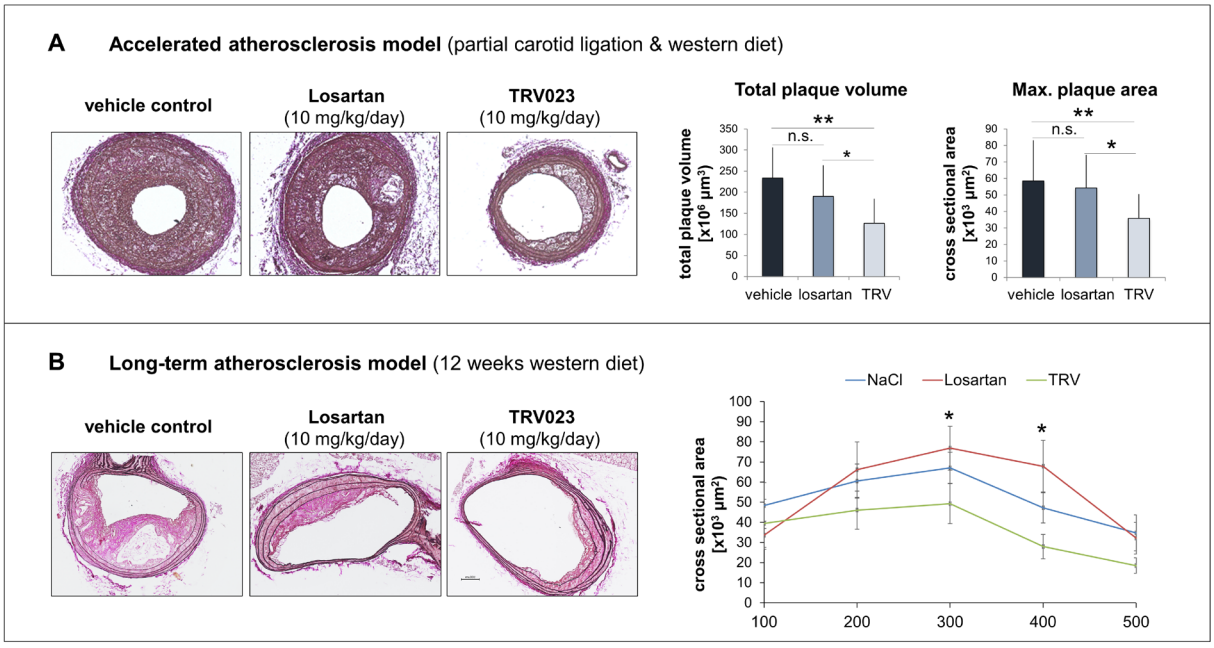

Abbildung 5. TRV023 anti-atherosklerotische Effekte. Mäuse wurden mit TRV023, Losartan oder Vehikel-Kontrolle behandelt, die jeweils über subkutane osmotische Pumpen kontinuierlich appliziert wurden. **A** Modell der beschleunigten Atherosklerose: Bei ApoE-defizienten Mäusen unter hoch-kalorischer Diät wurde eine partielle Ligatur der linken Arteria carotis communis durchgeführt. Drei Wochen nach partieller Ligatur bzw. 12 Wochen nach Einleitung einer Western-Diät wurden die Karotiden für histologische Analysen isoliert. B Langzeit-Atherosklerose-Versuch: ApoE-defiziente Mäuse wurden über 12 Wochen einer hoch-kalorischen Diät ausgesetzt.
(Althoff, unveröffentlichte Daten)

3.9 Conclusio

In Anbetracht der vielfältigen, Zelltyp-abhängigen Funktionen G_{12}/G_{13}- und G_q/G_{11}-abhängiger Signalwege, die wir in den hier vorgestellten Studien herausarbeiten konnten, erscheint eine Zelltyp-spezifische und funktionell selektive Modulierung G-Protein-gekoppelter Rezeptoren vielversprechender als derzeit etablierte Therapie-Ansätze mit konventionellen Rezeptor-Antagonisten.

Vor diesem Hintergrund eröffnet das Konzept funktionell-selektiver GPCR Liganden (biased ligands) eine neue Dimension in der Pharmakotherapie kardiovaskulärer Erkrankungen. Basierend auf einer unmittelbar aus unseren Arbeiten abgeleiteten Hypothese, konnten wir dieses Potenzial am konkreten Beispiel des Angiotensin-Analogons TRV023, welches wir als G_q/G_{11}-selektiven AT1-Antagonisten identifiziert haben, bestätigen. Darüber hinaus kooperieren wir derzeit mit Strukturbiologen, um die strukturelle Basis G_q/G_{11}- versus G_{12}/G_{13}-selektiver Signaltransduktion mittels molekularer Modellierung und Proteinkristallographie zu untersuchen und so den Weg hin zu einer Struktur-basierten Medikamenten-Entwicklung zu ebnen.

4 Zusammenfassung

Einige der erfolgreichsten kardiovaskulären Therapien greifen an G-Protein-gekoppelten Rezeptoren (GPCRs) wie dem Angiotensin II-Rezeptor Typ 1 (AT1-Antagonisten und ACE-Hemmer), dem Endothelin-1-Rezeptor (Endothelin-Rezeptor-Antagonisten) oder dem Thromboxan-Rezeptor (Acetylsalicylsäure) an. Diese und andere kardiovaskuläre Rezeptoren haben gemein, dass sie dual an G-Proteine der Familien G_q/G_{11} und G_{12}/G_{13} koppeln, wobei insbesondere die Funktion der G_{12}/G_{13}-vermittelten Signaltransduktion mangels adäquater Methoden lange Zeit unerforscht blieb.

Im Rahmen der hier vorgestellten Arbeiten haben wir nun Rolle dieser beiden G-Protein-Familien und ihre klinische Relevanz systematisch im Kontext der verschiedenen kardiovaskulären Erkrankungen Zelltyp-spezifisch herausgearbeitet. So konnten wir zeigen, dass die etablierte duale antithrombozytäre Therapie mit Clopidogrel und Acetylsaliylsäure, die letztlich eine Inhibition der G_q/G_{11}- und G_{12}/G_{13}-vermittelten Signaltransduktion des P2Y12-Rezeptors bzw. des Thromboxan A2-Rezeptors bewirken, im Verlauf nach Myokardinfarkt unzureichend ist. Mittlerweile wird Clopidogrel in diesem Kontext durch die neu entwickelten potenteren P2Y12-Antagonisten Ticagrelor und Prasugrel ersetzt. Dabei haben die entsprechenden Zulassungsstudien unsere Beobachtung einer erhöhten residualen Thrombozytenreaktivität nach Myokardinfarkt unter dualer antithrombozytärer Therapie mit Clopidogrel und Acetylsalicylsäure bestätigt.

Auch die direkte oder indirekte Inhibition der Angiotensin-Rezeptor-abhängigen G_q/G_{11}- und G_{12}/G_{13}-vermittelten Signaltransduktion, durch Angiotensin-Rezeptor- (AT1-)Antagonisten bzw. ACE-Hemmer ist mittlerweile gut etabliert und stellt eine Standardtherapie bei chronischer Herzinsuffizienz oder Myokard-Hypertrophie dar. Bis dato wurde die positive Wirkung dieser Medikamente der G_q/G_{11}-Inhibition zugeschrieben, wobei die Funktion G_{12}/G_{13}-abhängiger Signalwege in diesem Kontext nicht untersucht war. In unseren in vitro- und in vivo-Studien konnten wir nun zeigen, dass die kardiomyozytäre G_{12}/G_{13}-vermittelte Signaltransduktion in diesem Zusammenhang eine ebensowichtige Rolle spielt. Dabei haben wir neben G_{12}/G_{13} weitere Komponenten des entsprechenden Signalwegs, wie beispielsweise RhoA oder LARG, als potenzielle pharmakologische Angriffspunkte identifiziert.

G_q/G_{11}- und G_{12}/G_{13}-abhängige Signalwege spielen auch eine zentrale Rolle bei der Gefäßtonus- und damit der Blutdruck-Regulation. Dabei wirken sie synergistisch im Sinne eine Steigerung der Myosin-Leichtketten-Phosphorylierung glatter Muskelzellen. Im Gegensatz zur physiologischen Blutdruckregulation, waren die Pathomechanismen des essentiellen Hypertonus oder Altershypertonus jedoch bis dato weitgehend ungeklärt. Wir konnten nun aufklären, dass der Alters-abhängige Bluthochdruck über den prokontraktilen Endothelin-1-

Rezeptor A und die nachgeschalteten G_q/G_{11}- und G_{12}/G_{13}-abhängigen Signalwege vermittelt wird. Vor diesem Hintergrund erscheint die medikamentöse Antagonisierung des Endothelin-1-Rezeptors A als vielversprechender Ansatz zur Prävention bzw. Behandlung des Alters-abhängigen Hypertonus. Zwar ist die Anwendung derzeit zugelassener Endothelin-Rezeptor-Antagonisten durch Nebenwirkungen limitiert, es wurden aber zwischenzeitlich entsprechende klinische Studien zu neu-entwickelten Endothelin-Rezeptor-Antagonisten mit günstigerem Nebenwirkungsprofil initiiert.

Während die G_{12}/G_{13}- und G_q/G_{11}-abhängigen Signalwege im Kontext der myokardialen Hypertrophie und Herzinsuffizienz sowie der Gefäßtonus-Regulation synergistisch wirken, scheinen sie die Entwicklung von Gefäßerkrankungen gegensätzlich zu beeinflussen (Abb. 5).

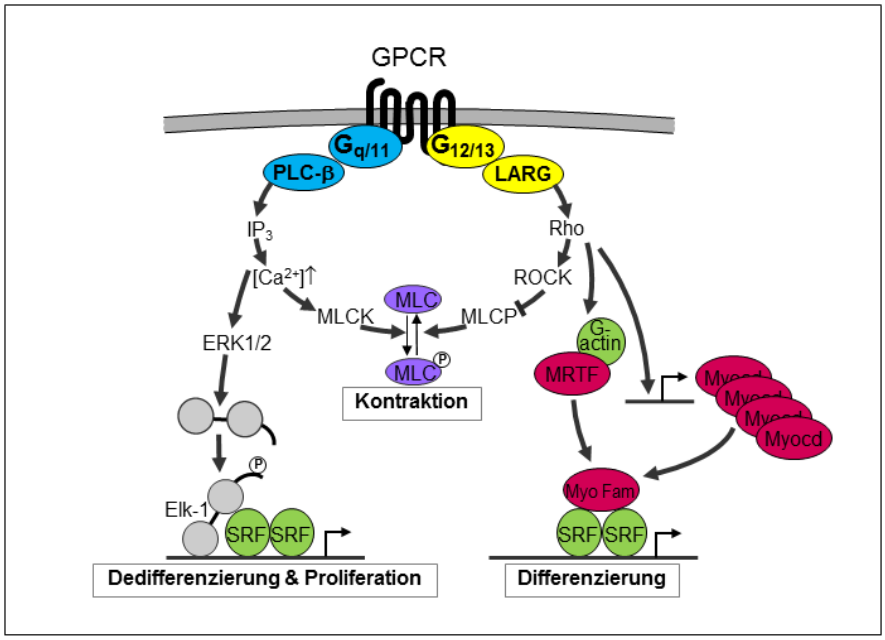

Abbildung 5. G_{12}/G_{13}- und G_q/G_{11}-vermittelte Signaltransduktion in glatten Muskelzellen
Agonistische Regulation der Myosin-Leichtketten-Phosphorylierung und Kontraktion sowie Antagonistische Regulation der glattmuskulären Differenzierung und Proliferation. (PLC Pospholipase C, ROCK Rho-Kinase, IP_3 Inositol-1,4,5-Trisphosphat, MLCK Myosin-Leichtketten-Kinase, MLCP Myosin Leichtketten-Phosphatase, MRTF Myocardin-related Transcription Factor A, Myocd Myocardin, Myo Myokardin-Familie transkriptioneller Co-Faktoren (inkl. MRTF und Myocd).

(Althoff, auf Basis von Althoff & Offermanns J Mol Med 2015)

So hatte eine Inaktivierung der G_{12}/G_{13}-vermittelten Signaltransduktion in Endothelzellen oder glatten Muskelzellen dramatische Folgen im Sinne einer Beschleunigung pathologischer Umbauprozesse sowie einer Atherosklerose-Exazerbation. Jegliche G_q/G_{11}-Inhibierung hingegen wirkte sich protektiv aus. Während konventionelle Rezeptor-Antagonisten G_q/G_{11} und G_{12}/G_{13} gleichermaßen inhibieren, erscheint eine selektive Inhibition des G_q/G_{11}-

abhängigen Signalwegs in diesem Kontext vielversprechender. In diesem Zusammenhang haben Arbeiten von Brian Kobilka und Robert Lefkowitz, für die diese 2012 mit dem Nobel-Preis ausgezeichnet wurden, zum Konzept der funktionellen Selektivität von GPCR-Liganden geführt (ligand-biased signaling). Dieses beschreibt die Selektivität von Liganden bzw. Rezeptor-Konformationen bezüglich unterschiedlicher intrazellulärer Signalwege und eröffnet eine neue Dimension für die Entwicklung Rezeptor-basierter Medikamente. So versuchen wir, funktionell-selektive Rezeptor-Liganden zu entwickeln, die spezifisch den G_q/G_{11}-Signalweg inhibieren ohne die Signaltransduktion via G_{12}/G_{13} zu beeinträchtigen. Dabei haben wir mit dem Angiotensin-Analogon TRV023 bereits einen G_q/G_{11}–selektiven AT1-Antagonisten identifiziert. Interessanterweise beeinflusste dieser Ligand die Atherosklerose-Entwicklung in zwei unterschiedlichen Tiermodellen im Gegensatz zu konventionellen Angiotensin-Antagonisten positiv, was unsere Hypothese bestätigte.

Darüber hinaus kooperieren wir derzeit mit Strukturbiologen, um die strukturelle Basis G_q/G_{11}- versus G_{12}/G_{13}-selektiver Signaltransduktion mittels molekularer Modellierung und Proteinkristallographie zu untersuchen und so den Weg hin zu einer Struktur-basierten Medikamenten-Entwicklung zu ebnen.

5 Literaturverzeichnis

Albarran-Juarez, J., Iring, A., Wang, S., Joseph, S., Grimm, M., Strilic, B., . . . Offermanns, S. (2018). Piezo1 and Gq/G11 promote endothelial inflammation depending on flow pattern and integrin activation. *J Exp Med*. doi:10.1084/jem.20180483

Althoff, T. F., Albarran Juarez, J., Troidl, K., Tang, C., Wang, S., Wirth, A., . . . Offermanns, S. (2012). Procontractile G protein-mediated signaling pathways antagonistically regulate smooth muscle differentiation in vascular remodeling. *J Exp Med, 209*(12), 2277-2290. doi:10.1084/jem.20120350

Althoff, T. F., Fischer, M., Langer, E., Ziemer, S., & Baumann, G. (2010). Sustained enhancement of residual platelet reactivity after coronary stenting in patients with myocardial infarction compared to elective patients. *Thromb Res, 125*(5), e190-196. doi:10.1016/j.thromres.2010.01.003

Althoff, T. F., & Offermanns, S. (2015a). G-protein-mediated signaling in vascular smooth muscle cells - implications for vascular disease. *J Mol Med (Berl)*. doi:10.1007/s00109-015-1305-z

Althoff, T. F., & Offermanns, S. (2015b). G-protein-mediated signaling in vascular smooth muscle cells - implications for vascular disease. *J Mol Med (Berl), 93*(9), 973-981. doi:10.1007/s00109-015-1305-z

Berridge, M. J. (2009). Inositol trisphosphate and calcium signalling mechanisms. *Biochim Biophys Acta, 1793*(6), 933-940. doi:10.1016/j.bbamcr.2008.10.005

Boldt, A., Wetzel, U., Weigl, J., Garbade, J., Lauschke, J., Hindricks, G., . . . Dhein, S. (2003). Expression of angiotensin II receptors in human left and right atrial tissue in atrial fibrillation with and without underlying mitral valve disease. *J Am Coll Cardiol, 42*(10), 1785-1792. Retrieved from https://www.ncbi.nlm.nih.gov/pubmed/14642689

Burrell, K. M., Molenaar, P., Dawson, P. J., & Kaumann, A. J. (2000). Contractile and arrhythmic effects of endothelin receptor agonists in human heart in vitro: blockade with SB 209670. *J Pharmacol Exp Ther, 292*(1), 449-459. Retrieved from http://www.ncbi.nlm.nih.gov/pubmed/10604982

Ducharme, A., Swedberg, K., Pfeffer, M. A., Cohen-Solal, A., Granger, C. B., Maggioni, A. P., . . . Investigators, C. (2006). Prevention of atrial fibrillation in patients with symptomatic chronic heart failure by candesartan in the Candesartan in Heart failure: Assessment of Reduction in Mortality and morbidity (CHARM) program. *Am Heart J, 152*(1), 86-92. Retrieved from http://www.ncbi.nlm.nih.gov/pubmed/16838426

Felker, G. M., Butler, J., Collins, S. P., Cotter, G., Davison, B. A., Ezekowitz, J. A., . . . Pang, P. S. (2015). Heart failure therapeutics on the basis of a biased ligand of the angiotensin-2 type 1 receptor. Rationale and design of the BLAST-AHF study (Biased Ligand of the Angiotensin Receptor Study in Acute Heart Failure). *JACC Heart Fail, 3*(3), 193-201. doi:10.1016/j.jchf.2014.09.008

Franz, M. R., & Bode, F. (2003). Mechano-electrical feedback underlying arrhythmias: the atrial fibrillation case. *Prog Biophys Mol Biol, 82*(1-3), 163-174.

Galie, N., Hoeper, M. M., Humbert, M., Torbicki, A., Vachiery, J. L., Barbera, J. A., . . . Guidelines, E. S. C. C. f. P. (2009). Guidelines for the diagnosis and treatment of pulmonary hypertension: the Task Force for the Diagnosis and Treatment of Pulmonary Hypertension of the European Society of Cardiology (ESC) and the European Respiratory Society (ERS), endorsed by the International Society of Heart and Lung Transplantation (ISHLT). *Eur Heart J, 30*(20), 2493-2537. doi:10.1093/eurheartj/ehp297

Garland, S. L. (2013). Are GPCRs still a source of new targets? *J Biomol Screen, 18*(9), 947-966. doi:10.1177/1087057113498418

Guasch, E., Benito, B., Qi, X., Cifelli, C., Naud, P., Shi, Y., . . . Nattel, S. (2013). Atrial fibrillation promotion by endurance exercise: demonstration and mechanistic exploration in an animal model. *J Am Coll Cardiol, 62*(1), 68-77. doi:10.1016/j.jacc.2013.01.091

Harris, I. S., Treskov, I., Rowley, M. W., Heximer, S., Kaltenbronn, K., Finck, B. N., . . . Muslin, A. J. (2004). G-protein signaling participates in the development of diabetic cardiomyopathy. *Diabetes, 53*(12), 3082-3090. Retrieved from https://www.ncbi.nlm.nih.gov/pubmed/15561937

Disertori, M., Latini, R., Barlera, S., Franzosi, M. G., Staszewsky, L., . . . Tognoni, G. (2009). Valsartan for prevention of recurrent atrial fibrillation. *N Engl J Med, 360*(16), 1606-1617. doi:10.1056/NEJMoa0805710

Kitazawa, T., Asakawa, K., Nakamura, T., Teraoka, H., Unno, T., Komori, S., . . . Wess, J. (2009). M3 muscarinic receptors mediate positive inotropic responses in mouse atria: a study with muscarinic receptor knockout mice. *J Pharmacol Exp Ther, 330*(2), 487-493. doi:10.1124/jpet.109.153304

Klages, B., Brandt, U., Simon, M. I., Schultz, G., & Offermanns, S. (1999). Activation of G12/G13 results in shape change and Rho/Rho-kinase-mediated myosin light chain phosphorylation in mouse platelets. *J Cell Biol, 144*(4), 745-754.

Korhonen, H., Fisslthaler, B., Moers, A., Wirth, A., Habermehl, D., Wieland, T., . . . Offermanns, S. (2009). Anaphylactic shock depends on endothelial Gq/G11. *J Exp Med, 206*(2), 411-420. doi:10.1084/jem.20082150

Li, X., Zima, A. V., Sheikh, F., Blatter, L. A., & Chen, J. (2005). Endothelin-1-induced arrhythmogenic Ca2+ signaling is abolished in atrial myocytes of inositol-1,4,5-trisphosphate(IP3)-receptor type 2-deficient mice. *Circ Res, 96*(12), 1274-1281. doi:10.1161/01.RES.0000172556.05576.4c

Luscher, T. F., Enseleit, F., Pacher, R., Mitrovic, V., Schulze, M. R., Willenbrock, R., . . . Heart Failure, E. T. R. B. T. (2002). Hemodynamic and neurohumoral effects of selective endothelin A (ET(A)) receptor blockade in chronic heart failure: the Heart Failure ET(A) Receptor Blockade Trial (HEAT). *Circulation, 106*(21), 2666-2672. Retrieved from http://www.ncbi.nlm.nih.gov/pubmed/12438291

Madrid, A. H., Bueno, M. G., Rebollo, J. M., Marin, I., Pena, G., Bernal, E., . . . Moro, C. (2002). Use of irbesartan to maintain sinus rhythm in patients with long-lasting persistent atrial fibrillation: a prospective and randomized study. *Circulation, 106*(3), 331-336. Retrieved from http://www.ncbi.nlm.nih.gov/pubmed/12119249

Maggioni, A. P., Latini, R., Carson, P. E., Singh, S. N., Barlera, S., Glazer, R., . . . Val-He, F. T. I. (2005). Valsartan reduces the incidence of atrial fibrillation in patients with heart failure: results from the Valsartan Heart Failure Trial (Val-HeFT). *Am Heart J, 149*(3), 548-557. doi:10.1016/j.ahj.2004.09.033

Moers, A., Nieswandt, B., Massberg, S., Wettschureck, N., Gruner, S., Konrad, I., . . . Offermanns, S. (2003). G13 is an essential mediator of platelet activation in hemostasis and thrombosis. *Nat Med, 9*(11), 1418-1422. doi:10.1038/nm943

Monasky, M. M., Taglieri, D. M., Henze, M., Warren, C. M., Utter, M. S., Soergel, D. G., . . . Solaro, R. J. (2013). The beta-arrestin-biased ligand TRV120023 inhibits angiotensin II-induced cardiac hypertrophy while preserving enhanced myofilament response to calcium. *Am J Physiol Heart Circ Physiol, 305*(6), H856-866. doi:10.1152/ajpheart.00327.2013

Nichols, M., Townsend, N., Scarborough, P., & Rayner, M. (2014). Cardiovascular disease in Europe 2014: epidemiological update. *Eur Heart J, 35*(42), 2929. doi:10.1093/eurheartj/ehu378

Offermanns, S. (2006). Activation of platelet function through G protein-coupled receptors. *Circ Res, 99*(12), 1293-1304. doi:10.1161/01.RES.0000251742.71301.16

Offermanns, S., Hu, Y. H., & Simon, M. I. (1996). Galpha12 and galpha13 are phosphorylated during platelet activation. *J Biol Chem, 271*(42), 26044-26048.

Offermanns, S., Laugwitz, K. L., Spicher, K., & Schultz, G. (1994). G proteins of the G12 family are activated via thromboxane A2 and thrombin receptors in human platelets. *Proc Natl Acad Sci U S A, 91*(2), 504-508.

Offermanns, S., Toombs, C. F., Hu, Y. H., & Simon, M. I. (1997). Defective platelet activation in G alpha(q)-deficient mice. *Nature, 389*(6647), 183-186. doi:10.1038/38284

Ono, K., Tsujimoto, G., Sakamoto, A., Eto, K., Masaki, T., Ozaki, Y., & Satake, M. (1994). Endothelin-A receptor mediates cardiac inhibition by regulating calcium and potassium currents. *Nature, 370*(6487), 301-304. doi:10.1038/370301a0

Opel, A., Nobles, M., Montaigne, D., Finlay, M., Anderson, N., Breckenridge, R., & Tinker, A. (2015). Absence of the Regulator of G-protein Signaling, RGS4, Predisposes to Atrial Fibrillation and Is Associated with Abnormal Calcium Handling. *J Biol Chem, 290*(31), 19233-19244. doi:10.1074/jbc.M115.666719

Peyronnet, R., Nerbonne, J. M., & Kohl, P. (2016). Cardiac Mechano-Gated Ion Channels and Arrhythmias. *Circ Res, 118*(2), 311-329. doi:10.1161/CIRCRESAHA.115.305043

Ponikowski, P., Voors, A. A., Anker, S. D., Bueno, H., Cleland, J. G. F., Coats, A. J. S., . . . Group, E. S. C. S. D. (2016). 2016 ESC Guidelines for the diagnosis and treatment of acute and chronic heart failure: The Task Force for the diagnosis and treatment of

acute and chronic heart failure of the European Society of Cardiology (ESC)Developed with the special contribution of the Heart Failure Association (HFA) of the ESC. *Eur Heart J, 37*(27), 2129-2200. doi:10.1093/eurheartj/ehw128

Reiter, E., Ahn, S., Shukla, A. K., & Lefkowitz, R. J. (2012). Molecular mechanism of beta-arrestin-biased agonism at seven-transmembrane receptors. *Annu Rev Pharmacol Toxicol, 52*, 179-197. doi:10.1146/annurev.pharmtox.010909.105800

Schiffrin, E. L. (2002). Vascular and cardiac benefits of angiotensin receptor blockers. *Am J Med, 113*(5), 409-418. Retrieved from http://www.ncbi.nlm.nih.gov/pubmed/12401536

Schmieder, R. E. (2005). Mechanisms for the clinical benefits of angiotensin II receptor blockers. *Am J Hypertens, 18*(5 Pt 1), 720-730. doi:10.1016/j.amjhyper.2004.11.032

Schneider, M. P., Hua, T. A., Bohm, M., Wachtell, K., Kjeldsen, S. E., & Schmieder, R. E. (2010). Prevention of atrial fibrillation by Renin-Angiotensin system inhibition a meta-analysis. *J Am Coll Cardiol, 55*(21), 2299-2307. doi:10.1016/j.jacc.2010.01.043

Sivaraj, K. K., Li, R., Albarran-Juarez, J., Wang, S., Tischner, D., Grimm, M., . . . Wettschureck, N. (2015). Endothelial Galphaq/11 is required for VEGF-induced vascular permeability and angiogenesis. *Cardiovasc Res, 108*(1), 171-180. doi:10.1093/cvr/cvv216

Sivaraj, K. K., Takefuji, M., Schmidt, I., Adams, R. H., Offermanns, S., & Wettschureck, N. (2013). G13 controls angiogenesis through regulation of VEGFR-2 expression. *Dev Cell, 25*(4), 427-434. doi:10.1016/j.devcel.2013.04.008

Strathmann, M., & Simon, M. I. (1990). G protein diversity: a distinct class of alpha subunits is present in vertebrates and invertebrates. *Proc Natl Acad Sci U S A, 87*(23), 9113-9117. Retrieved from https://www.ncbi.nlm.nih.gov/pubmed/2123549

Takefuji, M., Wirth, A., Lukasova, M., Takefuji, S., Boettger, T., Braun, T., . . . Wettschureck, N. (2012). G(13)-mediated signaling pathway is required for pressure overload-induced cardiac remodeling and heart failure. *Circulation, 126*(16), 1972-1982. doi:10.1161/CIRCULATIONAHA.112.109256

Tinker, A., Finlay, M., Nobles, M., & Opel, A. (2016). The contribution of pathways initiated via the G G-protein family to atrial fibrillation. *Pharmacol Res, 105*, 54-61. doi:10.1016/j.phrs.2015.11.008

Tuomi, J. M., Chidiac, P., & Jones, D. L. (2010). Evidence for enhanced M3 muscarinic receptor function and sensitivity to atrial arrhythmia in the RGS2-deficient mouse. *Am J Physiol Heart Circ Physiol, 298*(2), H554-561. doi:10.1152/ajpheart.00779.2009

Violin, J. D., DeWire, S. M., Yamashita, D., Rominger, D. H., Nguyen, L., Schiller, K., . . . Lark, M. W. (2010). Selectively engaging beta-arrestins at the angiotensin II type 1 receptor reduces blood pressure and increases cardiac performance. *J Pharmacol Exp Ther, 335*(3), 572-579. doi:10.1124/jpet.110.173005

Wachtell, K., Lehto, M., Gerdts, E., Olsen, M. H., Hornestam, B., Dahlof, B., . . . Devereux, R. B. (2005). Angiotensin II receptor blockade reduces new-onset atrial fibrillation and subsequent stroke compared to atenolol: the Losartan Intervention For End Point

Reduction in Hypertension (LIFE) study. *J Am Coll Cardiol, 45*(5), 712-719. doi:10.1016/j.jacc.2004.10.068

Wallentin, L., Becker, R. C., Budaj, A., Cannon, C. P., Emanuelsson, H., Held, C., . . . Investigators, P. (2009). Ticagrelor versus Clopidogrel in Patients with Acute Coronary Syndromes. *New England Journal of Medicine, 361*(11), 1045-1057. doi:10.1056/NEJMoa0904327

Wang, S., Iring, A., Strilic, B., Albarran Juarez, J., Kaur, H., Troidl, K., . . . Offermanns, S. (2015). P2Y(2) and Gq/G(1)(1) control blood pressure by mediating endothelial mechanotransduction. *J Clin Invest, 125*(8), 3077-3086. doi:10.1172/JCI81067

Wettschureck, N., & Offermanns, S. (2005). Mammalian G proteins and their cell type specific functions. *Physiol Rev, 85*(4), 1159-1204. doi:10.1152/physrev.00003.2005

Wettschureck, N., Rutten, H., Zywietz, A., Gehring, D., Wilkie, T. M., Chen, J., . . . Offermanns, S. (2001). Absence of pressure overload induced myocardial hypertrophy after conditional inactivation of Galphaq/Galpha11 in cardiomyocytes. *Nat Med, 7*(11), 1236-1240. doi:10.1038/nm1101-1236

Wirth, A., Benyo, Z., Lukasova, M., Leutgeb, B., Wettschureck, N., Gorbey, S., . . . Offermanns, S. (2008). G12-G13-LARG-mediated signaling in vascular smooth muscle is required for salt-induced hypertension. *Nat Med, 14*(1), 64-68. doi:10.1038/nm1666

Wirth, A., Wang, S., Takefuji, M., Tang, C., Althoff, T. F., Schweda, F., . . . Offermanns, S. (2016). Age-dependent blood pressure elevation is due to increased vascular smooth muscle tone mediated by G-protein signalling. *Cardiovasc Res, 109*(1), 131-140. doi:10.1093/cvr/cvv249

Wisler, J. W., Xiao, K., Thomsen, A. R., & Lefkowitz, R. J. (2014). Recent developments in biased agonism. *Curr Opin Cell Biol, 27*, 18-24. doi:10.1016/j.ceb.2013.10.008

Wiviott, S. D., Braunwald, E., McCabe, C. H., Montalescot, G., Ruzyllo, W., Gottlieb, S., . . . Investigators, T.-T. (2007). Prasugrel versus clopidogrel in patients with acute coronary syndromes. *N Engl J Med, 357*(20), 2001-2015. doi:10.1056/NEJMoa0706482

Worzfeld, T., Wettschureck, N., & Offermanns, S. (2008). G(12)/G(13)-mediated signalling in mammalian physiology and disease. *Trends Pharmacol Sci, 29*(11), 582-589. doi:10.1016/j.tips.2008.08.002

Yamada, J., Ohkusa, T., Nao, T., Ueyama, T., Yano, M., Kobayashi, S., . . . Matsuzaki, M. (2002). [Up-regulation of inositol 1, 4, 5-trisphosphate receptor expression in atrial tissue in patients with chronic atrial fibrillation]. *J Cardiol, 39*(1), 57-58. Retrieved from http://www.ncbi.nlm.nih.gov/pubmed/11828801

Yorikane, R., & Koike, H. (1990). The arrhythmogenic action of endothelin in rats. *Jpn J Pharmacol, 53*(2), 259-263. Retrieved from http://www.ncbi.nlm.nih.gov/pubmed/2200920

Yorikane, R., Koike, H., & Miyake, S. (1991). Electrophysiological effects of endothelin-1 on canine myocardial cells. *J Cardiovasc Pharmacol, 17 Suppl 7*, S159-162. Retrieved from http://www.ncbi.nlm.nih.gov/pubmed/1725317

Yorikane, R., Shiga, H., Miyake, S., & Koike, H. (1990). Evidence for direct arrhythmogenic action of endothelin. *Biochem Biophys Res Commun, 173*(1), 457-462. Retrieved from http://www.ncbi.nlm.nih.gov/pubmed/1701637

Zhao, Z. H., Zhang, H. C., Xu, Y., Zhang, P., Li, X. B., Liu, Y. S., & Guo, J. H. (2007). Inositol-1,4,5-trisphosphate and ryanodine-dependent Ca2+ signaling in a chronic dog model of atrial fibrillation. *Cardiology, 107*(4), 269-276. doi:10.1159/000095517

Zima, A. V., & Blatter, L. A. (2004). Inositol-1,4,5-trisphosphate-dependent Ca(2+) signalling in cat atrial excitation-contraction coupling and arrhythmias. *J Physiol, 555*(Pt 3), 607-615. doi:10.1113/jphysiol.2003.058529

6 Danksagung

Herrn Prof. Dr. med. Karl Stangl, Klinikdirektor der Medizinischen Klinik m.S. Kardiologie und Angiologie am Campus Mitte der Charité-Universitätsmedizin Berlin, möchte ich für seine großzügige Förderung meiner klinischen und wissenschaftlichen Ausbildung danken.

Zudem möchte ich mich bei meinem wissenschaftlichen Mentor Herrn Prof. Stefan Offermanns für die fortwährende und wertvolle Zusammenarbeit sowie die herausragende Unterstützung bedanken.

Für die gemeinsame Verwirklichung von Projekten und die vielen interessanten Diskussionen danke ich Dr. med. Mirko Völkers und Dr. rer. nat. Julian Albarran-Juarez, sowie den Mitarbeitern des kardiologischen Forschungslabors im Center for Cardiovascular Research (CCR) der Charité-Universitätsmedizin Berlin – allen voran Kerstin Wöltje, Johannes Schecker und Andrea Weller.

Für die großzügige Förderung bedanke ich mich bei der Deutschen Forschungsgemeinschaft (DFG), dem BIH Charité Clinician Scientist Programm (insbesondere Frau Prof. Dr. med. Duska Dragun), der Else Kröner-Fresenius-Stiftung, der Deutschen Herzstiftung sowie dem Deutschen Zentrum für Herz-Kreislaufforschung (DZHK, Standort Berlin).

Nicht zuletzt möchte ich meiner Familie, insbesondere meiner Frau Navina, für ihre fortwährende und liebevolle Unterstützung danken.

7 Erklärung

§ 4 Abs. 3 (k) der HabOMed der Charité

Hiermit erkläre ich, dass

- weder früher noch gleichzeitig ein Habilitationsverfahren durchgeführt oder angemeldet wurde,
- die vorgelegte Habilitationsschrift ohne fremde Hilfe verfasst, die beschriebenen Ergebnisse selbst gewonnen sowie die verwendeten Hilfsmittel, die Zusammenarbeit mit anderen Wissenschaftlern/Wissenschaftlerinnen und mit technischen Hilfskräften sowie die verwendete Literatur vollständig in der Habilitationsschrift angegeben wurden,
- mir die geltende Habilitationsordnung bekannt ist.

Ich erkläre ferner, dass mir die Satzung der Charité – Universitätsmedizin Berlin zur Sicherung Guter Wissenschaftlicher Praxis bekannt ist und ich mich zur Einhaltung dieser Satzung verpflichte.

Berlin, August 2020 Dr. med. Till Althoff